State of Wyoming
Department of Transportation

FINAL REPORT
WY1902F

DEVELOPMENT OF LOAD AND RESISTANCE FACTOR DESIGN PROCEDURES FOR DRIVEN PILES ON SOFT ROCKS IN WYOMING

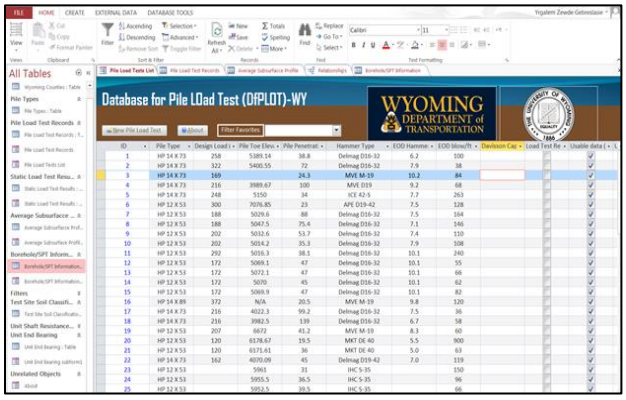

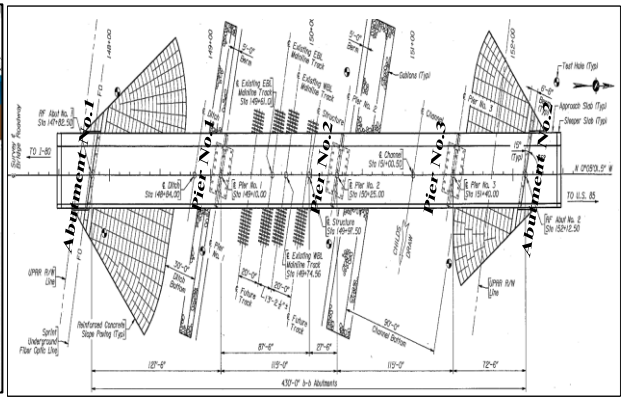

By:
Department of Civil and Architectural Engineering
University of Wyoming
1000 E. University Avenue, Dept. 3295
Laramie, Wyoming 82071
April 2019

DISCLAIMER

Notice

This document is disseminated under the sponsorship of the Wyoming Department of Transportation (WYDOT) in the interest of information exchange. WYDOT assumes no liability for the use of the information contained in this document. WYDOT does not endorse products or manufacturers. Trademarks or manufacturers' names appear in this report only because they are considered essential to the objective of the document.

Quality Assurance Statement

The Wyoming Department of Transportation (WYDOT) provides high-quality information to serve government, industry, and the public in a manner that promotes public understanding. Standards and policies are used to ensure and maximize the quality, objectivity, utility, and integrity of its information. WYDOT periodically reviews quality issues and adjusts its programs and processes to ensure continuous quality improvement

.

Copyright

No copyrighted material, except that which falls under the "fair use" clause, may be incorporated into a report without permission from the copyright owner, if the copyright owner requires such. Prior use of the material in a WYDOT or governmental publication does not necessarily constitute permission to use it in a later publication.

- Courtesy — Acknowledgment or credit will be given by footnote, bibliographic reference, or a statement in the text for use of material contributed or assistance provided, even when a copyright notice is not applicable.
- Caveat for Unpublished Work —Some material may be protected under common law or equity even though no copyright notice is displayed on the material. Credit will be given and permission will be obtained as appropriate.
- Proprietary Information — To avoid restrictions on the availability of reports, proprietary information will not be included in reports, unless it is critical to the understanding of a report and prior approval is received from WYDOT. Reports containing such proprietary information will contain a statement on the Technical Report Documentation Page restricting availability of the report.

Creative Commons:

The report is covered under a Creative Commons, CC-BY-SA license. When drafting an adaptive report or when using information from this report, ensure you adhere to the following:

Attribution — You must give appropriate credit, provide a link to the license, and indicate if changes were made. You may do so in any reasonable manner, but not in any way that suggests the licensor endorses you or your use.

ShareAlike — If you remix, transform, or build upon the material, you must distribute your contributions under the same license as the original.

No additional restrictions — You may not apply legal terms or technological measures that legally restrict others from doing anything the license permits.

You do not have to comply with the license for elements of the material in the public domain or where your use is permitted by an applicable exception or limitation.

No warranties are given. The license may not give you all of the permissions necessary for your intended use. For example, other rights such as publicity, privacy, or moral rights may limit how you use the material.

TECHNICAL REPORT DOCUMENTATION PAGE

1. Report No. WY-1902F	2. Government Accession No.	3. Recipient's Catalog No.
4. Title and Subtitle Development of Load and Resistance Factor Design Procedures for Driven Piles on Soft Rocks in Wyoming		5. Report Date April 2019 6. Performing Organization Code:
7. Author(s) Kam W. Ng (0000-0001-5099-5454), Pramila Adhikari (0000-0003-2155-3467), and Yrgalem Z. Gebreslasie (0000-0001-6378-6483)		8. Performing Organization Report No. RS06216
9. Performing Organization Name and Address Department of Civil and Architectural Engineering University of Wyoming 1000 E. University Avenue, Dept. 3295 Laramie, WY 82071-2000		10. Work Unit No. 11. Contract or Grant No. RS06216
12. Sponsoring Agency Name and Address Wyoming Department of Transportation 5300 Bishop Blvd. Cheyenne, WY 82009-3340 WYDOT Research Center (307) 777-4182		13. Type of Report and Period Final Report – March 22th, 2016 to June 30th 2019 14. Sponsoring Agency Code FHWA & WYDOT
15. Supplementary Notes WYDOT technical contacts: Mark Falk and Todd Sullivan		

16. Abstract

Static Analysis methods originally developed for soils are currently used for estimating pile resistances in Intermediate Geomaterials (IGMs), and structural capacity has been considered as the limiting pile capacity on hard rocks. The application of current Load and Resistance Factor Design (LRFD) for piles in IGMs has resulted in relatively high uncertainties in pile resistance estimation during design and the length to which the piles are driven into IGMs during construction. Moreover, the absence of standard criteria to differentiate the geomaterials creates challenges in the design and construction of driven piles in IGMs. The application of a dynamic analysis method using Wave Equation Analysis Program is constrained by geomaterial input for IGMs and rocks. These current challenges have led to conservative pile resistance estimations. Thus, the overall objectives of this study were to determine efficient static analysis methods, dynamic procedures for construction control, pile setup/relaxation, and resistance factors for the estimation of the axial pile resistances in IGMs, ensuring a prescribed level of reliability to meet LRFD philosophy. To accomplish these objectives, classification criteria of geomaterials were first created to establish a standard quantitative delineation between the soils, IGMs, and hard rocks for the design of driven piles. In addition, a catalog of IGM properties was prepared to facilitate the design of piles in IGMs. Secondly, a new set of design equations were developed and validated for IGMs by utilizing the developed geomaterial classification criteria. Thirdly, wave equation analysis procedures for IGMs were recommended for pile construction control. Fourthly, changes in pile resistances in IGMs with respect to time at the end of driving and beginning of restrike were assessed. Finally, probability based resistance factors were calibrated and recommended based on the efficiency factors for the existing and calibrated static analysis methods. To facilitate the implementation of the recommended LRFD procedures, a pile design example is developed.

17. Key Words Driven piles; Intermediate geomaterials; Load and Resistance Factor Design (LRFD); Geomaterial classification; Static Analysis; Wave Equation	18. Distribution Statement No restrictions. This document is available through the National Transportation Library and the Wyoming State Library.

19. Security Classif. (of this report) Unclassified	20. Security Classif. (of this page) Unclassified	21. No. of Pages: 155	22. Price

Form DOT F 1700.7 (8-72) Reproduction of completed page authorized

SI* (MODERN METRIC) CONVERSION FACTORS

APPROXIMATE CONVERSIONS TO SI UNITS

Symbol	When You Know	Multiply By	To Find	Symbol
		LENGTH		
in	inches	25.4	millimeters	mm
ft	feet	0.305	meters	m
yd	yards	0.914	meters	m
mi	miles	1.61	kilometers	km
		AREA		
in^2	square inches	645.2	square millimeters	mm^2
ft^2	square feet	0.093	square meters	m^2
yd^2	square yard	0.836	square meters	m^2
ac	acres	0.405	hectares	ha
mi^2	square miles	2.59	square kilometers	km^2
		VOLUME		
fl oz	fluid ounces	29.57	milliliters	mL
gal	gallons	3.785	liters	L
ft^3	cubic feet	0.028	cubic meters	m^3
yd^3	cubic yards	0.765	cubic meters	m^3
	NOTE: volumes greater than 1000 L shall be shown in m^3			
		MASS		
oz	ounces	28.35	grams	g
lb	pounds	0.454	kilograms	kg
T	short tons (2000 lb)	0.907	megagrams (or "metric ton")	Mg (or "t")
		TEMPERATURE (exact degrees)		
^oF	Fahrenheit	5 (F-32)/9 or (F-32)/1.8	Celsius	^oC
		ILLUMINATION		
fc	foot-candles	10.76	lux	lx
fl	foot-Lamberts	3.426	$candela/m^2$	cd/m^2
		FORCE and PRESSURE or STRESS		
lbf	poundforce	4.45	newtons	N
lbf/in^2	poundforce per square inch	6.89	kilopascals	kPa

APPROXIMATE CONVERSIONS FROM SI UNITS

Symbol	When You Know	Multiply By	To Find	Symbol
		LENGTH		
mm	millimeters	0.039	inches	in
m	meters	3.28	feet	ft
m	meters	1.09	yards	yd
km	kilometers	0.621	miles	mi
		AREA		
mm^2	square millimeters	0.0016	square inches	in^2
m^2	square meters	10.764	square feet	ft^2
m^2	square meters	1.195	square yards	yd^2
ha	hectares	2.47	acres	ac
km^2	square kilometers	0.386	square miles	mi^2
		VOLUME		
mL	milliliters	0.034	fluid ounces	fl oz
L	liters	0.264	gallons	gal
m^3	cubic meters	35.314	cubic feet	ft^3
m^3	cubic meters	1.307	cubic yards	yd^3
		MASS		
g	grams	0.035	ounces	oz
kg	kilograms	2.202	pounds	lb
Mg (or "t")	megagrams (or "metric ton")	1.103	short tons (2000 lb)	T
		TEMPERATURE (exact degrees)		
^oC	Celsius	1.8C+32	Fahrenheit	^oF
		ILLUMINATION		
lx	lux	0.0929	foot-candles	fc
cd/m^2	$candela/m^2$	0.2919	foot-Lamberts	fl
		FORCE and PRESSURE or STRESS		
N	newtons	0.225	poundforce	lbf
kPa	kilopascals	0.145	poundforce per square inch	lbf/in^2

TABLE OF CONTENTS

LIST OF FIGURES

LIST OF TABLES

LIST OF ACRONYMS

AASHTO - American Association of State Highway and Transportation Officials
BOR- Beginning of Restrike
β_T – Target reliabililty index
CAPWAP- CAse Pile Wave Analysis Program
COV- Coefficient of Variation
DL- Dead Load
FHWA- Federal Highway Administration
DOT- Department of Transportation
EOD- End of Driving
FOSM- First-Order-Second-Moment
FORM- First-Order-Reliability-Model
IGM- Intermediate Geomaterial
LRFD - Load and Resistance Factor Design
LL- Live load
MCS- Monte-Carlo Simulation
$(N_1)_{60}$ – SPT N-value corrected to overburden and 60% hammer energy
PDA- Pile Driving Analyzer
PDF- Probability Density Function
q_u – Unconfined Compression Strength
R- Resistance
SA- Static Analysis
SA*- SPT N Based Geomaterial Input Method in GRLWEAP
SPT- Standard Penetration Test
ST- Soil Type Based Geomaterial Input Method in GRLWEAP
s_u – Undrained shear strength
UCS- Uniaxial/ Unconfined Compressive Strength
WEAP- Wave Equation Analysis Program

CHAPTER 1. INTRODUCTION

1.1 Background

Steel driven piles are typically used to support bridges due to their high driving durability on rock materials and a shallow bedrock stratigraphy in Wyoming. The total axial resistance of these piles consists of a combination of shaft resistance and end bearing. To attain the required resistance, especially in a soft overburden soil, the pile would have to rely on its end bearing on soft rocks or intermediate geomaterial (IGM). Soft rock is not well defined for driven piles in the American Association of State Highway and Transportation Officials (AASHTO) Load and Resistance Factor Design (LRFD) Bridge Design Specifications (2017). IGM is a broader term consisting of soft rocks, dense sand and gravels, and stiff overly-consolidated soil materials, and the term IGM has been used throughout the report. Due to the natural variability of IGM materials, uncertainties in deep foundation design are exacerbated, leading to many construction challenges (Mokwa and Brooks 2008).

The AASHTO (2017) provide the following general recommendations for piles driven in IGM.

(1) Piles driven in IGM shall be treated in the same manner as soil;
(2) There are no well acceptable approaches to differentiate IGM from soils and hard rocks. However, local experience with driving piles in IGM shall be applied to define its quality; and
(3) Piles shall be driven based on locally developed criteria to prevent pile damage. Dynamic analysis methods should be used to evaluate pile drivability, control pile driving, and detect pile damage.

Wyoming Department of Transportation (WYDOT) currently adapts the AASHTO (2017) and applies local experiences to design and construct these pile foundations. A site investigation is normally performed by the Geology Program at every bridge project to determine its subsurface profile and geomaterial properties. Standard Penetration Test (SPT) is the most commonly used in-situ field test in Wyoming. At the same location for SPT test, a drivepoint penetration test is performed by driving a 2-in diameter drivepoint into the ground using a 140-lb hammer at a drop height of 30 in. Hammer blow counts to penetrate the drivepoint 12 inches into the ground are recorded. The main purpose of the drivepoint penetration test is to determine the depth of an adequate bearing layer, such as unweathered bedrock, for the end bearing pile. When a bedrock layer is encountered, rock coring will be performed to determine the Rock Quality Designation (RQD) value, and rock samples will be tested for the uniaxial compressive strength (q_u). The Geology Program has developed a table of typical properties of soil materials for pile capacity estimation. It is a challenge to estimate shaft resistance and end bearing of a pile driven in IGM because locally calibrated unit shaft resistance and end bearing of piles in IGM are currently not available. This leads to uncertainties of pile performance, in terms of resistance, until it can be verified during construction. The current practice of WYDOT uses Wave Equation Analysis Program (WEAP) to establish pile driving criteria for all production piles. Pile Driving Analyzer (PDA) with subsequent signal matching analyses using the CAse Pile Wave Analysis Program (CAPWAP) is used as a construction control method on about 2 percent of the production piles in some bridge projects. PDA/CAPWAP is implemented to determine and verify the required pile capacity at bridge projects expecting high loads and driven into IGM. Pile restrikes at 24

hours after the end of driving (EOD) are normally performed to further ensure that the desired pile resistance is achieved, and pile performance is accepted.

1.2 Problem Statement

The aforementioned background leads to the following general design and construction challenges pertaining to piles driven in IGM:

Design Challenges

- Geotechnical resistance normally governs the design of piles driven in IGM. However, static analysis methods are not available for pile resistance estimation. The AASHTO (2017) recommend that piles driven in IGM shall be designed in the same manner as soil, while piles driven in hard rocks shall be governed by the structural limit. However, pile resistances in IGM are usually under-predicted, and pile-rock-soil interaction is normally not known in a structural analysis (Ng et al. 2015). Furthermore, no clear definition of IGM is available for driven piles, and they are normally differentiated based on local experiences.
- To satisfy the LRFD strength limit state as given by Equation (1) where γ is the load factor, Q is the applied load, φ is the resistance factor and R is the pile resistance, resistance factors were developed for piles driven in soil materials (AASHTO 2017). However, resistance factors for driven piles in IGM materials are currently not available.

$$\sum \gamma_i Q_i \leq \varphi R \quad (1)$$

- The natural variability of IGM creates a high uncertainty in the subsurface condition for pile designs. Also, knowledge on the rock quality is limited to typical properties in terms of rock quality designation (RQD) and uniaxial compressive strength (q_u). Advanced strength parameters required in the characteristic lines method proposed by Serrano and Olalla (2002), based on Hoek and Brown's non-linear failure model, are not readily available for more complex pile analyses. Hannigan et al. (2006) acknowledged that pile-rock contact area, penetration depth, and rock quality are usually not available for the pile resistance estimation during the design state. However, the subsurface investigation normally performed by the Geology Program enables the estimation of pile penetration depth and basic rock properties.

Construction Challenges

- Congruent to the design challenges, total resistance of a pile in IGM is typically determined using dynamic analysis methods during construction. Furthermore, static load test, which is expensive and time consuming, is usually neither performed to verify the pile resistance nor calibrate the dynamic analysis methods. According to Thompson and Thompson (1985), pile load test results should be used for the pile design because strength of weathered rock could govern the pile design, and pile resistance could decrease due to rock relaxation.
- Large discrepancies between estimated and measured pile resistances were identified by Ng et al. (2015). It is not unusual that these piles do not satisfy the LRFD strength limit state at the end of driving (EOD), and occasionally at the beginning of last restrike (BOR). However, it is important to note that WEAP was used to evaluate all production piles while PDA/CAPWAP covered only about 2 percent of the total production piles. When the pile

performance is not attained during construction, possible pile extension and/or additional piles with an enlarged pile cap will be proposed to achieve the required resistance. This could incur additional construction duration and operational cost.

- The high uncertainty in pile performance could incur difficulty in the construction management since foundation construction is the critical path of a bridge project. This uncertainty could result in higher construction bids, higher frequency of claims, and higher design safety for offsetting the challenge in construction management (Mokwa and Brooks 2008).
- Conflicts between owners and contractors could occur. These conflicts could result in change-orders to the original contract for additional claims and time to achieve the required pile performance.

1.3 Goal and Objectives

The overall goal of the research project is to develop locally calibrated LRFD procedures (i.e., design methodologies and resistance factors) for driven piles on soft rocks in Wyoming. Recognizing the design and construction challenges of piles driven on soft rocks, the research project was conducted to accomplish the following objectives:

- To advance the knowledge of design and construction of piles driven in IGM;
- To alleviate the aforementioned design and construction challenges; and
- To advance the current state of practice pertaining to the design and construction of piles in IGM in Wyoming.

1.4 Research Tasks

1.4.1 Task 1: Literature review

This task focused on a literature review pertinent to the design and construction of piles driven in IGM. This task included the following activities:

- Documents, papers, reports, catalogs, manuals, notes, and presentation slides pertinent to the design and construction of driven piles on rocks were reviewed.
- The current state of knowledge and the current state of practice relating to driven piles on rocks were documented and reviewed.
- Current specifications and guidelines adopted by various Departments of Transportation (DOTs), AASHTO, and other agencies pertinent to driven piles on rocks were reviewed;
- Criteria adopted by state DOTs and agencies to differentiate soft and hard rocks were identified.
- Usable driven pile data for subsequent tasks were identified.
- Gaps in the body of knowledge were identified.

1.4.2 Task 2: Usable data collection

High quality and usable data containing subsurface, pile, hammer, installation, and load test information were identified and collected while conducting Task 1. For this, available electronic databases such as PILOT database developed for Iowa DOT (Roling et al. 2011), updated second version of comprehensive Deep Foundation Load Test Database (DFLTD) developed by Federal Highway Administration (FHWA) (Petek et al. 2016), Full Portland State University (PSU) Master database developed for the Oregon DOT (Smith et al. 2010), and Minnesota

DOT/LT2008 developed for Minnesota DOT (Paikowsky et al. 2009) were assessed. The geotechnical reports, including the pile details, geomaterial details, and dynamic tests results, were provided by WYDOT. All usable pile data were stored in an electronic database developed using a commercial program, called Microsoft Office Access.

1.4.3 Task 3: Subsurface and geo-material (soil and rock) assessment

Geotechnical reports and subsurface profiles were assessed to determine properties of overburden soils and underlying soft rock materials necessary for pile resistance estimation in Task 4. Lab or field measured properties were used, if they were reported. If lab and field measured properties were not reported, the geomaterial properties calculated or obtained from correlation table developed by WYDOT were considered. In some of the cases where properties were not available from both of these methods, geomaterial properties were correlated from literature.

1.4.4 Task 4: Pile resistance estimation and statistical analysis

Using the data collected from previous tasks, the geotechnical resistances of driven piles identified as usable data records were estimated using static analysis methods specified in the AASHTO (2017). These static analysis methods are 1) α-method by Tomlinson (1987), 2) β-method by Esrig and Kirby (1979), 3) λ-method by Vijayvergiya and Focht (1972), 4) SPT method by Meyerhof (1976), and 5) Nordlund (1963) method. Also, pile resistances were estimated using WEAP. Estimated resistances were compared with resistances measured by CAPWAP as the static load test results were not available and expressed in terms of resistance bias (ratio of measured to estimated pile resistance). Then the statistical distribution and its associated statistical parameters (i.e., mean resistance bias and coefficient of variation) were determined. These statistical parameters were applied in Task 6 for the development of locally calibrated LRFD resistance factors (φ) using probability-based methods, specifically for driven piles on soft rocks in Wyoming. This study provided the basis for the calibration of static analysis methods conducted in Task 5. Recommendations on the application of static analysis methods were provided in Task 8.

1.4.5 Task 5: Calibration of static analysis methods

The existing static analysis methods were developed based on piles driven in soil materials. In order to improve the pile design in IGM, static analysis methods were calibrated by modifying respective empirical coefficients (e.g., adhesion factor (α) defined in the α-method) and incorporating IGM properties (e.g., uniaxial compressive strength). Calibration of each static analysis method was performed using a regression analysis technique to reestablish the relationship of empirical coefficients specifically for piles driven in IGM. Furthermore, an independent set of usable pile data that were not used in the calibration were used for the verification of calibrated static analysis methods by statistically comparing the estimated and measured resistances.

1.4.6 Task 6: Development of resistance factors

Using the statistical results from Tasks 4 and 5, LRFD resistance factors were determined using three probability-based reliability methods: First-Order Reliability-Model (FORM), First-Order Second Moment (FOSM) method, and Monte-Carlo Simulation (MCS). These reliability methods account for different uncertainties induced by parameters, such as variability of IGM

and deficiency of a design method, that influence the accuracy of resistance estimations while maintaining a common target reliability index to ensure a prescribed margin of safety. The regional LRFD resistance factors specific to the State of Wyoming were developed based on the assumptions made in the reliability methods, recommended numerical values for probabilistic characteristics of loads, as documented by Paikowsky et al. (2004),Allen (2005), and AASHTO (2017), suggested reliability index of 2.33 for commonly used redundant pile groups (i.e., a group of five or more piles). For a non-redundant pile group, a higher reliability index of 3.00 was used to account for the lower redundancy. The reliability indices of 2.33 and 3.00 corresponded to approximate failure probabilities of 1 in 100 and 1 in 1000, respectively. To increase the efficiency of LRFD, and to provide better recommendations, resistance factors using different reliability methods were developed and compared for existing and calibrated static analysis methods, as well as the WEAP. Finally, a set of resistance factors for both design and construction control methods were recommended.

1.4.7 Task 7: Criteria assessment for soft and hard rocks

The criteria adapted by other state DOTs and agencies gathered from the literature review in Task 1 were assessed. Relevant WYDOT guidelines, specifications, and subsurface investigation reports were reviewed. A flowchart along with design charts were recommended to facilitate the classification of IGM from soils and hard rocks.

1.4.8 Task 8: Outcomes and recommendations

Upon getting the outcomes from Tasks 1 through 7, recommendations were made to facilitate the design and construction of driven piles in IGM, in Wyoming. The research outcomes and recommendations are listed below:

- A collection of usable pile data.
- An electronic pile database for pile analyses, LRFD resistance factor development, and future pile data collection.
- A catalog of IGM properties for pile designs.
- Calibrated static analysis methods for the estimation of shaft resistance and end bearing of piles driven in IGM.
- A set of recommended resistance factors for design and construction control methods.
- Recommendations on current WYDOT criteria for the classification of IGM from soils and hard rocks.
- Recommendations of pile design and construction best practices.
- Recommendations for the revision of existing WYDOT pile design and construction specifications and guidelines.

The research outcomes and recommendations will provide WYDOT the basis for the establishment of revised guidelines and specifications pertaining to piles driven in IGM. It is envisioned that the recommendations will satisfy the study objectives, and bring benefits to WYDOT and relevant stakeholders.

1.5 Report Outline

This report consists of eight chapters, which are briefly described below. References are included after Chapter Eight.

- **Chapter 1 - *Introduction:*** This chapter discusses the prevalent challenges during the design and construction of piles in IGMs, introduces the research tasks and objectives accomplished by the research team, and briefly lists the final outcomes and recommendations.
- **Chapter 2 - *Literature Review:*** This chapter presents the background on static and dynamic analysis methods for the determination of pile resistances. Furthermore, it presents the current state of knowledge adopted by different Department of Transportations (DOTs) on IGM classification, and the design and construction of driven piles in IGMs. The review on available databases of driven piles on IGM and the collection of usable pile data from literature is discussed. It also includes the discussion on LRFD and reliability methods for the calibration of resistance factors.
- **Chapter 3 – *Electronic Database (WyoPile):*** This chapter presents the features of electronic database called WyoPile and discusses the user manual of the WyoPile database. It includes an overview of pile and geomaterial data.
- **Chapter 4 – *Geomaterial Classification, and IGM Catalog:*** This chapter presents the methodologies adopted for developing the geomaterial classification criteria. It presents the charts and a flowchart to aid in geomaterial classification. A catalog of IGM properties encountered in Wyoming is presented.
- **Chapter 5 – *Evaluation, Calibration, and Validation of Static Analysis methods along with Economic Impact and Time Dependent Pile Resistance Study:*** This chapter summarizes the evaluation of static analysis methods currently used for pile design in IGMs in terms of resistance biases and presents the findings from economic impact study. It further presents the calibration and validation of static analysis methods. The findings from time-dependent pile resistance study are also discussed.
- **Chapter 6 – *Wave Equation Analysis of Driven Piles in IGM:*** This chapter presents the detailed procedure for conducting bearing graph analysis for piles driven in IGMs using two different approaches of toe quake values. Resistance factors were determined for WEAP and are presented in this chapter.
- **Chapter 7 – *Development of Resistance Factors:*** This chapter presents the procedures and findings of calibration of LRFD resistance factors for steel H-piles driven in IGMs for existing SA methods, and calibrated SA methods. The uncertainties in the determined resistance factors are also presented. This chapter compares the calibrated and existing SA methods based on efficiency factors for final recommendation.
- **Chapter 8 – *Summary, Conclusions, and Recommendations:*** This chapter presents a summary of the research, conclusions, and recommendations for future works.
- **Appendix A – *Design Charts for q_{usi}***: Design charts for q_{usi} are presented for geomaterial classification.
- **Appendix B – *Design Charts for q_{usf}***: Design charts for q_{usf} are presented for geomaterial classification.
- **Appendix C – *LRFD Pile Design Example***: A pile design example is presented to facilitate the implementation of the recommended LRFD procedures.

CHAPTER 2. LITERATURE REVIEW

This chapter presents the findings from the review of bridge design manuals, specifications, and geotechnical manuals of different Departments of Transportation (DOTs) pertaining to the current state of practice for IGMs classification and the design and construction of driven piles in IGMs. Literature review on static analysis methods consisting of α-method, by Tomlinson (1987), β-method, by Esrig and Kirby (1979), λ-method, by Vijayvergiya and Focht (1972), SPT method, by Meyerhof (1976), and Nordlund (1979) method is presented. Review on dynamic analysis methods of driven piles consisting of WEAP, PDA, and CAPWAP are also presented. Finally, the background on LRFD and reliability models for the calibration of resistance factors are presented.

2.1 Introduction

Different terminologies, like soft rocks, weak rocks, indurated soils, and intermediate geomaterials (IGM), are used in practice among the geotechnical and geological professionals to denote the geomaterials that lie on the continuum between soils and rocks. The AASHTO (2017) defines IGM as the material whose strength and compressibility are transitional between rock and soil. The term IGM was first applied by O'Neill et al. (1996). O'Neill et al. (1996) defined cohesionless IGMs as the very dense granular materials whose corrected Standard Penetration Test (SPT) N-values for 60 percent hammer energy efficiency lie between 50 and 100, and cohesive IGMs as the geomaterials whose uniaxial compressive strength (UCS) lies between 10 ksf and 100 ksf. However, this definition of IGM has been limited for the design of drilled shafts (Turner 2006). Classification of IGM for the design of driven piles has not yet been established.

IGM formations occur in an intermediate phase during the transformation from soils to rocks or vice-versa. In one hand, they can be the outcome of the disintegration, weathering, shearing, and tectonization of hard rocks, while on the other they can be the consolidated, cemented soils in the process of lithification and diagenesis. IGMs are complex geomaterials owing to the large variation in their material properties due to difference in their degree of transformation from soils to rocks or vice-versa. They may be weak either of the weak constituent material or the discontinuities present in them (Gannon et al. 1999). IGMs have been treated either as soil or rocks, depending upon whether they are being encountered in problems related to rock mechanics or soil mechanics. However, Johnston I.W. (1994) pointed out that the combined approach of both the soil mechanics and rock mechanics should be applied to IGMs, as they form a central part of the spectrum between soils and rocks. He further emphasized that the extrapolation from either the soil mechanics or rock mechanics in isolation can lead to conservative and uneconomic solutions (Johnston 1994).

2.2 Classification of IGMs

The most essential, preliminary requirement for any geotechnical site characterization is to identify IGMs and determine their engineering properties for pile design. Though many descriptive definitions are available for weak and soft rocks, IGMs lack consistent classification criterion for the design of driven piles. Unconfined Compression Strength (UCS) and the SPT N-values have been commonly used by various authors to define weak rocks. Some of the prevalent criteria for classifying weak rocks and IGMs are summarized in Table 1.

Table 1. Available classification criteria for weak rocks and IGMs.

Source	Geomaterial	Definition
ISRM (1981) (Oliveira 1993)	Low strength rocks	40 ksf $\leq$ UCS $\leq$ 400 ksf
ISSMFE (1989)	Soft rocks	5 ksf $\leq$ UCS $\leq$ 500 ksf
ISO1468-2:2003 (Terente et al. (2015))	Weak rocks	6 ksf $\leq s_u \leq$ 200 ksf
BS5930 (1981) (Clarke and Smith (1992)	Weak rocks	UCS < 100 ksf
O'Neill et al. (1996)	Cohesive IGM	10 ksf $\leq$ UCS $\leq$ 100 ksf
	Cohesionless IGM	50-100 blows/ 0.3 m
Clayton (1995)	a) Very weak	$0 < N_{60} < 80$
	b) Weak	$80 < N_{60} < 200$
	c) Moderately weak and stronger	$N_{60} \geq 200$
Gannon et al. (1999)	Weak rocks	12 ksf $\leq$ UCS $\leq$ 260 ksf 100 < Mass Stiffness Values < 1000

s_u- Undrained shear strength; UCS- Unconfined Compression Strength; N_{60}- SPT N-value corresponding to 60% hammer energy.

2.3 Sampling and Testing of IGMs

IGMs are highly heterogeneous, anisotropic, and display a great variation in the engineering properties because their behaviors are difficult to predicted. Furthermore, the uncertainties in the extent of damage caused in IGMs, due to pile driving process, create more challenges in understanding the pile performance. Determination of pile drivability in IGMs is a challenging issue that influences a successful installation of piles without overstressing or pile damage. The dynamic penetration in weak and weathered rocks is affected by different factors, like intact strength of rocks, spacing and tightness of joints, and porosity (Gannon et al. 1999). Gannon et al. (1999) therefore emphasized a need to relate measurable parameters of IGMs to boreability or drivability. However, measurable strength parameters of IGMs are highly uncertain due to the inherent variability associated with IGMs. This was demonstrated by Rohde and Feng (1990) in which negative correlation was seen from the graph of coefficient of variation (COV) of UCS obtained from 133 rock specimens. This implied that more scatter existed as the strength of the rock decreased. Hence, IGMs may demand different approaches in in-situ testing, collection of undisturbed samples, laboratory testing, and the interpretation of the results relating to pile driving process. As most of the sampling and testing methods have been derived from either soil mechanics or rock mechanics for soils and hard rocks, IGMs may not be truly represented with the existing conventional methods (Oliveira 1993). Rocha (1971) stated that the integral sampling technique might be the effective technique that can better represent weak zones, fractures, and infillings of the core sample giving the overall features of the rock mass.
In-situ tests may prove to be effective for weak rocks as the discontinuity and fracture planes affecting the rock mass behavior are well reflected in in-situ tests. SPT is the widely used in-situ tests which were also used by Clayton (1995) to classify weak rocks. However, Stark et al. (2013) indicated that the penetration of split spoon sampler up to 12 inches was difficult to obtain in IGMs during a SPT test which led to the requirement of extrapolation and individual

judgment for the determination of SPT N-values. To overcome the challenge associated with SPT procedure for IGMs, Stark et al. (2013) modified the procedure to record the penetration rate (penetration of the sampler for every 10 blows) until a total of 100 blows is achieved. Pressuremeter test is another important in-situ test for the determination of the modulus of deformation, a useful parameter in predicting consolidation and settlement of foundations. Akai (1997) stated that the application of pressuremeter test can be extended to soft rocks with few careful considerations during the interpretation of pressuremeter results. Haberfield and Johnston (1993) indicated that various factors like drainage conditions, dilation, radial cracking and fractures influence the pressuremeter results on soft rocks unlike the assumptions made for clays.

2.4 Determination of Axial Pile Resistances

The total axial capacity of a pile is the sum of shaft resistance and end bearing experienced by a pile. Axial pile capacity is determined using various static analysis methods during the design stage for the estimation of pile length. The dynamic methods are used for the verification of designed pile capacity. Along with the verification of pile capacity, dynamic methods can be used for pile construction control, detection of pile damage, evaluation of driving hammer performance, assessment of soil resistance distribution, determination of dynamic soil parameters, and evaluation of time dependent pile capacity. Different dynamic methods are now being routinely used, and have been incorporated into a standard specification for deep pile foundations by the American Society for Testing and Materials (ASTM D4945-2008). The most prevalent dynamic analysis methods are PDA, CAPWAP, and WEAP, which are discussed in Sections 2.4.2 to 2.4.4. The detailed descriptions and analyses of these three dynamic methods can be found in Ng (2011).

2.4.1 Static Analysis Methods

Analytical methods that use soil strength and compressibility properties to determine pile capacity and performance are called static analysis methods (Hannigan et al., 2006). Though their accuracy is inferior to that of the field tests, static analysis methods are still very important during the pile design. They are commonly used to determine the most cost effective pile type and to estimate pile contract lengths in the design phase. Care must be taken to address site variability while using the static analysis methods as they primarily depend on the geomaterial properties for estimating the pile resistance (Abu-Hejleh et al., 2013). Knowledge of the design loads is also necessary to use the methods for appropriate design (Hannigan et al., 2006). The five static analysis methods for the determination of nominal unit shaft resistance and nominal unit end bearing are discussed in subsequent subsections. Total shaft resistance, Q_s (kips), is obtained by multiplying the unit shaft resistance, q_s (ksf), by the shaft area, A_s (ft^2). For H-piles in this study, shaft area of the pile shaft was calculated by multiplying the perimeter of a rectangle (twice the sum of flange width and web depth) enclosing the H-pile with the embedded depth in that layer. Total end bearing Q_p (kips) is obtained by multiplying the unit end bearing, q_p (ksf), by the pile toe area, A_t (ft^2). Pile toe area in this study is calculated using a box area (flange width × web depth) considering a complete plugging of pile.

2.4.1.1 Total stress or α- method (Tomlinson method)

The α-method is suitable for estimating pile resistance in cohesive soils. This classic method is based on a total stress theory, and pile resistance is estimated using undrained shear strength of

soil. The α-method enables us to calculate both the shaft resistance and end bearing. Unit shaft resistance, q_s, is calculated using Equation (2).

$$q_s = \alpha \times s_u \quad (2)$$

where,

s_u = undrained shear strength (ksf), and
α = empirical adhesion factor applied to s_u.

The adhesion factor, α, represents the percentage of the undrained shear strength (s_u) mobilized by the pile-soil adhesion phenomenon (Cherubini & Vessia, 2007). The α factor decreases with increasing s_u, as shown in Figure 1. This factor also depends on pile type, dimension, and embedment depth.

The unit end bearing, q_p, can be calculated using Equation (3).

$$q_p = N_c \times S_u \quad (3)$$

where,

N_c = a dimensionless bearing capacity factor, which is usually taken as nine for deep foundations (Hannigan et al., 2006).

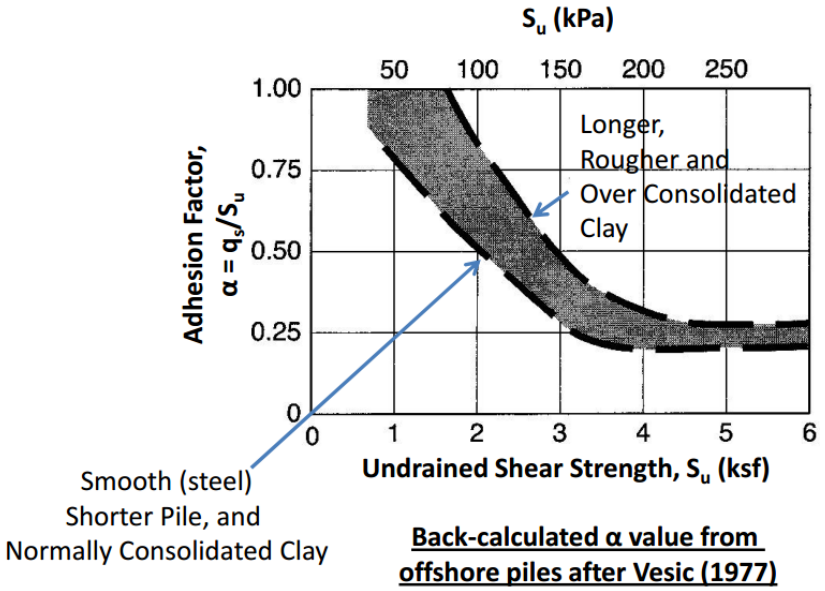

Source: Vesic (1977)

Figure 1. Adhesion factor, α, as function of undrained shear strength, S_u (After Vesic 1977).

2.4.1.2 Effective Stress method (β- method)

The β-method is based on effective stress, and is used to estimate the resistance of piles in cohesionless, cohesive, or layered soils (Hannigan et al., 2006, AASHTO, 2014). Cohesionless soils have fast drainage, and hence, it is reasonable to use the effective stress for calculating the pile resistance. In the case of cohesive soils, the method can be used for normally consolidated

and slightly overconsolidated clays. For heavily overconsolidated clays, the β-method usually overestimates the pile resistance (AASHTO, 2014). In the current research, the β-method has been used for estimating pile resistance in cohesionless geomaterials only. For cohesionless geomaterials, the β factor can be obtained as function of effective friction angle, ϕ', from Table 2 or Figure 2. The β-method has provisions for calculating both the shaft resistance and end bearing. The shaft resistance, q_s, is given by Equation (4).

$$q_s = \beta \times \sigma'_v \quad (4)$$

where,

σ'_v = vertical effective stress (ksf), prior to pile installation, and
β = a factor taken from Figure 2.

Table 2. Approximate range of β coefficient (Fellenius, 1991).

Soil Type	ϕ' (degree)	β
Clay	25 - 30	0.23 - 0.40
Silt	28 - 34	0.27 - 0.50
Sand	32 - 40	0.30 - 0.60
Gravel	35 - 45	0.35 - 0.80

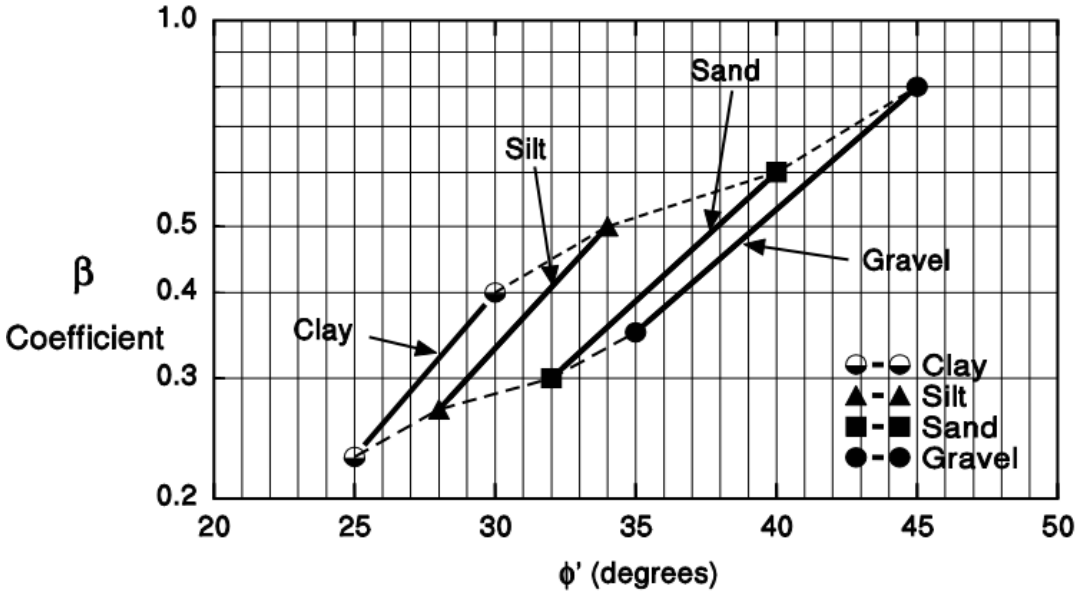

Source: Fellenius (1991)

Figure 2. β coefficient versus effective friction angle, ϕ', for different soil types (After Fellenius, 1991).

The unit end bearing (unit toe resistance), q_p, is given by Equation (5).

$$q_p = N_t \times p_t \quad (5)$$

where,

N_t = the bearing factor, and

p_t = the effective vertical stress at the pile toe.

2.4.1.3 Nordlund method

The Nordlund method is an effective stress analysis used to estimate both shaft resistance and end bearing of piles driven in cohesionless soils (AASHTO, 2014). It was originally developed based on pile load-test results and accounts for the pile taper and soil displacement. According to Hannigan et al. (2006), the Nordlund method overestimates the resistance of piles larger than 24 inches in dimensions.

The nominal unit shaft resistance, q_s, is calculated using Equation (6). Soil friction angle, friction angle between soil and pile, pile taper from the vertical, effective overburden stress, and the volume of soil displaced by the pile affect the shaft resistance of the pile.

$$q_s = K_\delta C_F \sigma'_v \times \frac{\sin(\delta + \omega)}{\cos\omega} \quad (6)$$

where,

K_δ = coefficient of lateral earth pressure at mid-point of soil layer (Table 3 and Table 4),

δ =friction angle between pile and soil,

C_F= correction factor for K_δ when $\delta \neq \phi$ (Figure 3),

σ'_v = effective overburden stress (ksf) at midpoint of soil layer under consideration, and

ω = angle of pile taper from vertical (degrees).

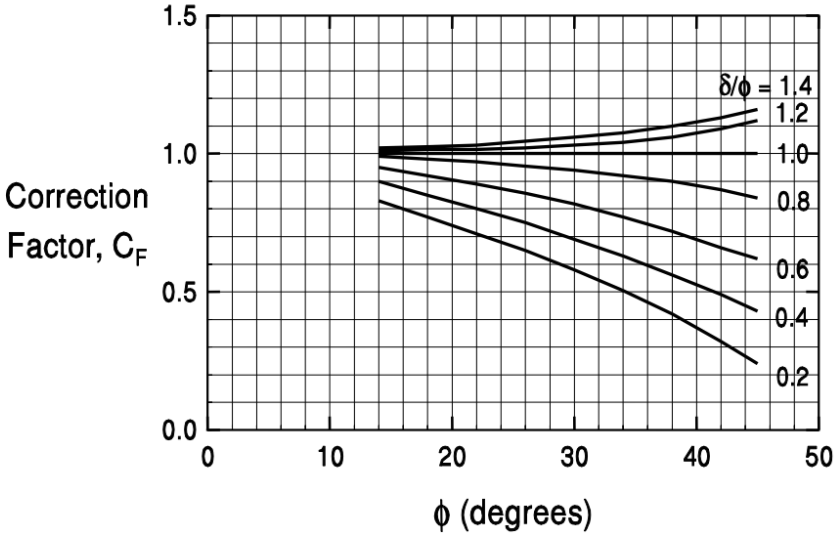

Source: Hannigan et al. (2006)

Figure 3. Correction factor for K_δ when $\delta \neq \phi$ (Hannigan et al., 2006 after Nordlund 1963).

Table 3. Design table for evaluating K_δ for piles when $\omega = 0$ ($V = 0.0093$ to 0.0930 m^3/m or 0.10 to 1.00 ft^3/ft) (Hannigan et al., 2006).

ϕ	Displaced Volume -V, m^3/m, (ft^3/ft)									
	0.0093 (0.10)	0.0186 (0.20)	0.0279 (0.30)	0.0372 (0.40)	0.0465 (0.50)	0.0558 (0.60)	0.0651 (0.70)	0.0744 (0.80)	0.0837 (0.90)	0.0930 (1.00)
25	0.70	0.75	0.77	0.79	0.80	0.82	0.83	0.84	0.84	0.85
26	0.73	0.78	0.82	0.84	0.86	0.87	0.88	0.89	0.90	0.91
27	0.76	0.82	0.86	0.89	0.91	0.92	0.94	0.95	0.96	0.97
28	0.79	0.86	0.90	0.93	0.96	0.98	0.99	1.01	1.02	1.03
29	0.82	0.90	0.95	0.98	1.01	1.03	1.05	1.06	1.08	1.09
30	0.85	0.94	0.99	1.03	1.06	1.08	1.10	1.12	1.14	1.15
31	0.91	1.02	1.08	1.13	1.16	1.19	1.21	1.24	1.25	1.27
32	0.97	1.10	1.17	1.22	1.26	1.30	1.32	1.35	1.37	1.39
33	1.03	1.17	1.26	1.32	1.37	1.40	1.44	1.46	1.49	1.51
34	1.09	1.25	1.35	1.42	1.47	1.51	1.55	1.58	1.61	1.63
35	1.15	1.33	1.44	1.51	1.57	1.62	1.66	1.69	1.72	1.75
36	1.26	1.48	1.61	1.71	1.78	1.84	1.89	1.93	1.97	2.00
37	1.37	1.63	1.79	1.90	1.99	2.05	2.11	2.16	2.21	2.25
38	1.48	1.79	1.97	2.09	2.19	2.27	2.34	2.40	2.45	2.50
39	1.59	1.94	2.14	2.29	2.40	2.49	2.57	2.64	2.70	2.75
40	1.70	2.09	2.32	2.48	2.61	2.71	2.80	2.87	2.94	3.0

Table 4. Design table for evaluating K_δ for piles when $\omega = 0$ (V = 0.093 to 0.930 m^3/m or 1.0 to 10.0 ft^3/ft) (Hannigan et al., 2006).

ϕ	Displaced Volume -V, m^3/m (ft^3/ft)									
	0.093 (1.0)	0.186 (2.0)	0.279 (3.0)	0.372 (4.0)	0.465 (5.0)	0.558 (6.0)	0.651 (7.0)	0.744 (8.0)	0.837 (9.0)	0.930 (10.0)
25	0.85	0.90	0.92	0.94	0.95	0.97	0.98	0.99	0.99	1.00
26	0.91	0.96	1.00	1.02	1.04	1.05	1.06	1.07	1.08	1.09
27	0.97	1.03	1.07	1.10	1.12	1.13	1.15	1.16	1.17	1.18
28	1.03	1.10	1.14	1.17	1.20	1.22	1.23	1.25	1.26	1.27
29	1.09	1.17	1.22	1.25	1.28	1.30	1.32	1.33	1.35	1.36
30	1.15	1.24	1.29	1.33	1.36	1.38	1.40	1.42	1.44	1.45
31	1.27	1.38	1.44	1.49	1.52	1.55	1.57	1.60	1.61	1.63
32	1.39	1.52	1.59	1.64	1.68	1.72	1.74	1.77	1.79	1.81
33	1.51	1.65	1.74	1.80	1.85	1.88	1.92	1.94	1.97	1.99
34	1.63	1.79	1.89	1.96	2.01	2.05	2.09	2.12	2.15	2.17
35	1.75	1.93	2.04	2.11	2.17	2.22	2.26	2.29	2.32	2.35
36	2.00	2.22	2.35	2.45	2.52	2.58	2.63	2.67	2.71	2.74
37	2.25	2.51	2.67	2.78	2.87	2.93	2.99	3.04	3.09	3.13
38	2.50	2.81	2.99	3.11	3.21	3.29	3.36	3.42	3.47	3.52
39	2.75	3.10	3.30	3.45	3.56	3.65	3.73	3.80	3.86	3.91
40	3.00	3.39	3.62	3.78	3.91	4.01	4.10	4.17	4.24	4.30

The unit end bearing, q_p (ksf), is calculated using Equation (7).

$$Q_p = \alpha_t N'_q p_t \leq q_L \quad (7)$$

where,

α_t = dimensionless coefficient from (Figure 4a),
N'_q = dimensionless bearing capacity factor (Figure 4b),
p_t = effective overburden stress at pile tip (ksf) ≤ 3 ksf, and
q_L = limiting unit tip resistance (Figure 5).

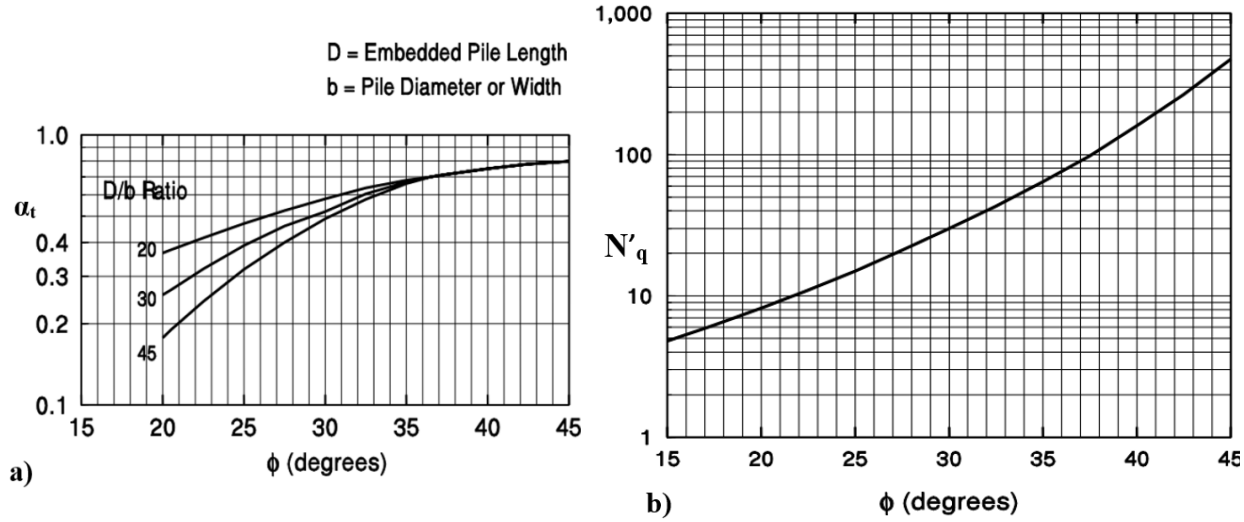

Source: Bowles (1977) Source: Bowles (1977)

Figure 4. a) α_t coefficient, and b) bearing capacity factor N'_q (After Bowles, 1977).

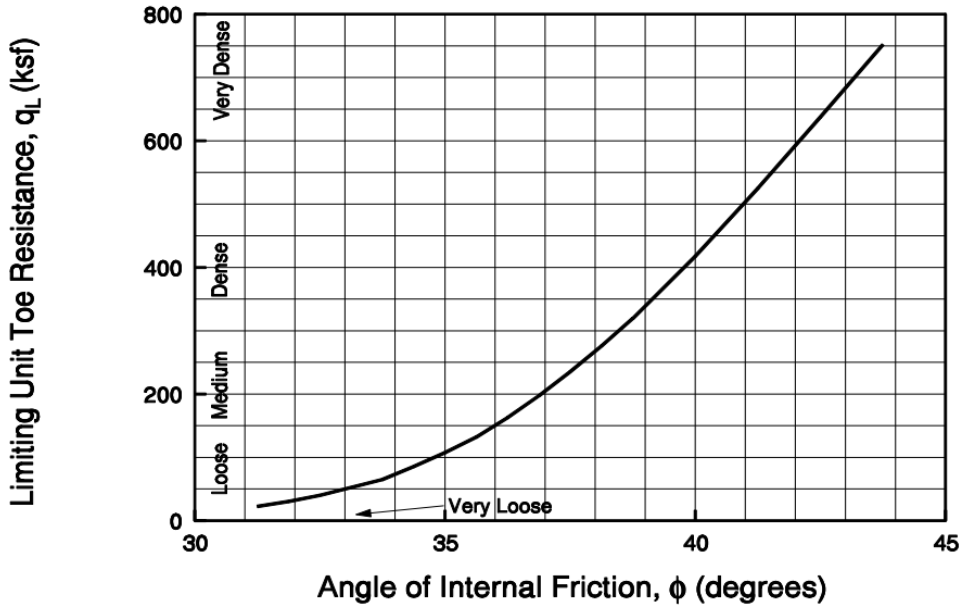

Source: Meyerhof (1976)

Figure 5. Limiting unit toe resistance for cohesionless soils (After Meyerhof 1976).

2.4.1.4 SPT method (Meyerhof 1976)

Laboratory tests are usually difficult to conduct on cohesionless soils, such as sands, because of the difficulty in obtaining good quality (undisturbed) samples. Field tests, such as the standard penetration test (SPT), are more convenient (AASHTO, 2014). SPT, performed during a test boring, approximates the soil resistance to dynamic penetration. Soil samples for lab tests can also be simultaneously collected using split spoon or Shelby tube samplers. Details on SPT and sampling can be found in many geotechnical books. This field test gives more consistent results in cohesionless soils with less large gravels (Kulhawy & Mayne, 1990). The results from SPT are usually reported in blows per foot (SPT N-values).

In geotechnical foundation practice and engineering usage, SPT correlations are used to estimate engineering properties of soils. The correlations have been developed on the basis of 60 percent hammer efficiency (Mayne et al., 2002). Hence, the N-values are corrected to a 60 percent hammer efficiency, depending on the type of hammer used during the test. Further, corrections made include borehole correction, C_b, and rod length correction, C_r. The resulting blow count is designated as N_{60} (Equation (8))

$$N_{60} = C_b C_r \left(\frac{E_m}{60}\right) N \tag{8}$$

where,

E_m = efficiency of the hammer used for the SPT test (%).

The blow counts are further corrected to account over burden stress and the resulting SPT-N values is designated $(N_1)_{60}$ (Equation (9)).

$$(N_1)_{60} = \left(\frac{P_a}{\sigma_{vo}}\right)^{0.5} N_{60} \tag{9}$$

where,

P_a = atmospheric pressure (psf), and

σ_{vo} = vertical overburden stress (psf) at location of blow counts.

The corrected SPT blow counts are used in various correlations to determine engineering properties of soils. The SPT method is an empirical method used to estimate pile resistance in cohesionless soils from SPT N-values. The corrected N-value, $(N_1)_{60}$, is used in the formulas for estimating both shaft resistance and end bearing. The SPT method is quick and easy to use. However, if the aforementioned corrections are not properly applied, the accuracy of the SPT method is highly compromised (Hannigan et al., 2006). Hence, the SPT method should be used only for preliminary design.

The nominal unit shaft resistance, q_s (ksf), can be determined by Equations (10) and (11).

$$q_s = \frac{(\quad)_{60}}{25} \quad \text{for displacement piles} \tag{10}$$

$$q_s = \frac{(\quad)_{60}}{50} \quad \text{for non} - \text{displacement piles} \tag{11}$$

where,

$(\quad)_{60}$ average corrected SPT-blow count along the pile side (blows/ft).

Nominal unit end bearing, q_p (ksf), is calculated using Equation (12)

$$q_p = \frac{0.8(\quad)_{60}\, D_b}{D} \leq q_L \tag{12}$$

where,

$(N_1)_{60}$ = corrected SPT N near pile tip,
D = pile width or diameter (ft),
D_b = depth of penetration in bearing strata (ft), and
q_L = limiting tip resistance (ksf), taken as eight times the value of $(N_1)_{60}$ for sands and six times the value of $(N_1)_{60}$ for non-plastic silt.

2.4.1.5 λ-method

Vijayvergiya and Focht (1972) developed the λ-method for calculating the shaft resistance of piles driven into clays and mixed soils. The pile shaft resistance is expressed as function of passive earth pressure (AASHTO, 2014). The nominal unit shaft resistance is given by Equation (13). The static analysis methods are summarized in Table 5.

$$q_s = \lambda(\sigma'_v + 2s_u) \tag{13}$$

where,

$\sigma_v' + 2s_u$ = passive lateral earth pressure (ksf),
σ_v' = average effective stress,
s_u = average undrained shear strength, and
λ = an empirical dimensionless coefficient taken from Figure 6.

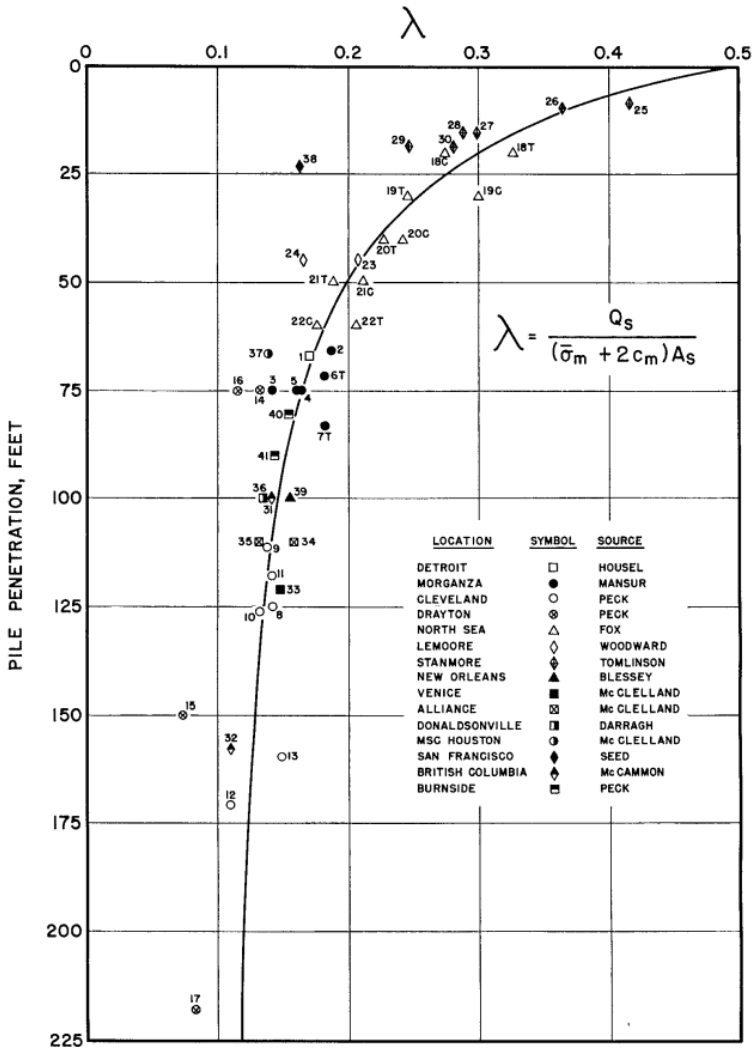

Source: Vijayvergiya and Focht (1972)

Figure 6. λ coefficient for driven pipe piles (After Vijayvergiya and Focht (1972)).

Table 5. Summary of the existing static analysis methods applied in this study.

Static analysis method	Type of applicable geomaterial	Unit shaft resistance (q_s)	Pile shaft area, A_s	Unit end bearing (q_p)	Pile toe area, A_t
α-method	Cohesive	$\alpha \times s_u$	Perimeter[1] × Embedded depth	$N_c \times S_u$	Flange width × Web depth
λ-method	Cohesive or mixed	$\lambda(\sigma'_v + 2s_u)$		NA	
β-method	Cohesionless	$\beta \times \sigma_v'$		$N_t \times p_t$	
SPT	Cohesionless	$(\tilde{N}_1)_{60}/50$		$0.8(N_1)_{60}\, D_b/D$	
Nordlund	Cohesionless	$K_\delta C_F \sigma'_v \sin(\delta)$		$\alpha_t\, N'_q\, p_t$	

[1]–(2×(flange width + web depth)); NA–not applicable, for other symbols refer to respective sections of the methods.

2.4.2 Pile Driving Analyzer (PDA)

Professor G.G. Goble and his students developed Pile Driving Analyzer (PDA), a data acquisition system, in the 1960s, at the Case Western Reserve University (Case). The Case method is used by PDA to 1) estimate pile capacity, 2) investigate the development of soil resistances as a function of time, 3) evaluate pile data quality, 4) assess the soil resistance distribution, 5) determine the pile integrity, and 6) evaluate the driving system performance. The measurement of pile strains and accelerations used in the Case method is fulfilled by a pair of transducers and accelerometers fitted near the pile top. PDA converts the strain and acceleration signals generated at every hammer impact on the test pile during pile driving to force and velocity records, respectively, as a function of time. This PDA force and velocity records can be fed into the CAPWAP to determine the static shaft resistance and end bearing, the load settlement curve, and the dynamic soil parameters (i.e., quakes and damping factors).

In the Case method, the dynamic soil resistance is treated as a linear function of a viscous damping coefficient and a pile toe velocity. Based on this assumption, PDA estimates the pile capacity by using the maximum static resistance (RMX) and by searching for time t_1 in the force and velocity records that gives the largest value of static soil resistance (RSP). PDA estimates the shaft resistance (SFR) and subtracts the SFR from the RMX to determine the end bearing. Thus, the soil resistance distribution along the embedded pile length is estimated. PDA evaluates the driving system performance by computing the maximum hammer energy (EMX), which was used in calculating the energy transferred ratio (ETR), and by estimating the stroke (STK) of the open-ended diesel hammers used in the field tests. Besides evaluating the hammer performance, PDA monitors the pile integrity during driving by calculating and comparing the maximum compressive and tensile stresses with the allowable stresses given by the users. PDA also assesses the pile quality using the term BTA, derived by Rausche and Goble (1979), to describe the severity of pile damage.

2.4.3 Case Pile Wave Analysis Program (CAPWAP)

CAPWAP (Pile Dynamics, Inc. 2000) is a rigorous, numerical modeling technique developed by Goble and his students in the 1970s. PDA records are used as input data for more accurate estimations of pile capacity, soil resistance distribution, and dynamic soil properties. CAPWAP adopted the Smith (1962) soil-pile model using the wave equation algorithm in the analysis to perform a signals-matching process with the combination of several analytical techniques, as described by Pile Dynamics, Inc. (2000), Ng (2011) and AbdelSalam et al. (2012). Pile is modeled as a series of lumped masses connected with linear elastic springs and linear viscous dampers, whereas soil is modeled as a series of elastic-plastic springs and linear viscous dampers. The series of lumped masses of pile are linked to a series of soil models. Soil elastic-plastic springs is defined by the soil static resistances (Rs) and soil quakes (q), and the viscous dampers of a soil model are defined by the damping factors. CAPWAP is called a signal matching technique as the soil static resistance at each soil segment, soil quake, the Smith's damping factor (Js) and the Case damping factor (Jc) are adjusted until the computed signal matches the measured signal from PDA. The summation of all adjusted soil resistances along the pile shaft provides the soil shaft resistance, and the total pile capacity is determined by adding the shaft resistance with the soil resistance, adjusted at the pile toe. The soil quakes and soil damping factors for the soil segments, along the shaft and the soil segment at the toe, are also obtained from CAPWAP.

2.4.4 Wave Equation Analysis Program

Wave equation has been long applied to simulate a complex pile driving process by mathematical modeling of one-dimensional propagation of the wave in a pile. Smith (1960) provided the solution of the wave equation using a finite difference scheme. Using the mathematical model by Smith (1951; 1960), a computer program called WEAP was developed by Goble et al. (1976) and Hirsch et al. (1976) for dynamic analysis of piles during driving. The program models the hammer, driving system, pile, and soil (geomaterial) through a combination of lumped masses, springs, and dashpots. WEAP is a widely used dynamic analysis method today for the drivability analysis, static pile resistance estimation, determination of induced stresses in the pile, and assurance of pile integrity. Unlike CAPWAP, which uses PDA records, WEAP models the different hammer driving system with entirely different combinations of masses, springs, and/or dampers. The WEAP program (GRLWEAP^{TM}) provides a database of various hammer types that allows a more accurate and convenient hammer modeling. WEAP analyses can be performed at end of driving (EOD) as well as several re-strikes. Drivability, bearing graph, and inspector chart are the main outputs of WEAP. However, our study focused only on the bearing graph analysis.

2.5 Current State DOTs' Practices on Driven Piles IN IGMs

2.5.1 Illinois Department of Transportation (IDOT)

According to IDOT (2012), the common types of driven piles used by IDOT are steel H-piles, metal shell, precast concrete, and timber. IDOT has some separate provisions for the design of piles in rocks, though they do not specifically address IGMs. IDOT (2012) states that if the estimated pile tip elevation is within 20 feet of the bedrock, then it is desirable to extend H-piles to the bedrock, as they are comparatively easy to drive in rocks and offer economic pile design.

According to IDOT (2009), modified IDOT (K-IDOT) static method and Washington State DOT(WSDOT) formula, based on the study conducted by (Long et al. 2009), are used for static and dynamic analysis of driven piles. The calculation of pile capacity in rocks has been incorporated by providing the values of various factors in the design equation for rocks. For non-displacement piles (such as steel H-piles), the nominal required pile capacity (RN) would be taken the lesser of the following two Equations (14) and (15).

(i) For plugged condition

$$R_N = (F_S\, q_S A_{SAp} + F_P\, q_P A_{Pp}) \times (I_G) \quad (14)$$

(ii) For unplugged condition

$$R_N = (F_S\, q_S A_{SAu} + F_P\, q_P A_{Pu}) \times (I_G) \quad (15)$$

where,

F_S = the pile type correction factor for side resistance, which is taken as 0.3 for cohesionless soils, 1.5 for cohesive soils, and 1.0 for rock;

F_P = the pile type correction factor for tip resistance, which is taken as 0.3 for cohesionless soils, 1.0 for cohesive soils, and 1.0 for rock,

A_{SAu} = The unplugged surface area = (4 x flange width + 2 x member depth) x pile length,

A_{SAp} = The plugged surface area = (2 x flange width + 2 x member depth) x pile length,
A_{Pu} = The cross-sectional area of steel member,
A_{Pp} = The flange width x member depth, and
I_G = The bias factor ratio which relates the Modified IDOT static method to the construction verification method used.

The q_S and q_P are the nominal unit side resistance and the nominal unit end bearing, respectively. The values of q_S and q_P have been defined for various rock types as presented in Table 6.

Table 6. Nominal unit side and tip resistance for different rock types.

Rock types	Nominal unit side resistance (q_S)	Nominal unit end bearing (q_p)
Shale	12 ksf	120 ksf
Sandstone	20 ksf	200 ksf
Limestone/Dolomite	24 ksf	240 ksf

The estimated length of the pile includes the penetration of the pile in the rock. The penetration into rock depends upon the factors like the required resistance, type of rock, and the strength of rock (IDOT 2012). The expected penetration has been given as 2.5 to 10 ft. in shale, 1.5 to 6 ft. in sandstone, and 0.5 to 3 ft. in limestone (IDOT 2012).

WSDOT method, developed by Allen (2005) for the Washington State DOT, is being practiced in IDOT for the pile capacity verification at the EOD. According to WSDOT, the ultimate capacity, R_N (in kips) is calculated by Equation (16)

$$R_N = 6.6\ F_{eff}\ WH\ \ln(10N) \quad (16)$$

where,
F_{eff} = the hammer efficiency,
W = the weight of hammer (in kips),
H = the drop of hammer (in ft), and
N = the average pile penetration resistance (blows/ in).

A study was conducted by Long and Anderson (2014) to improve the design and construction practices for driven piles in the state of Illinois. Based on their study, they recommended different hammer efficiency values based on pile type and geomaterial for single-acting diesel hammers. They proposed different hammer efficiency values for rock and shale at EOD and BOR conditions.

2.5.2 Colorado Department of Transportation (CDOT)

Weak rocks consisting of claystone, siltstone, sandstone, and interbedded sandstone-claystone are encountered in Colorado, due to the two common geologic formations, Pierre and the Denver formations (Abu-Hejleh et al. 2005). Weak sedimentary bedrock, classified as soft rock, is often found along the front range where significant penetration of H-piles can be achieved (CDOT 2018). If significant penetration cannot be achieved, then the bedrock is classified as hard rock (CDOT 2018). CDOT Bridge Design Manual (2018) states that if the pile penetration in the

bedrock is greater than or equal to 3 ft, then the pile shall be designed following "Piles Driven to Soft Rock" provision in AASHTO. However, if the penetration in bedrock is less than 3 ft, then the piles are designed following AASHTO provision for "Piles Driven to Hard Rock".

2.5.3 Florida Department of Transportation (FDOT)

In order to design the driven piles in Florida, the computer program FB-Deep (Florida Bridge Deep Foundations) is used for the axial load capacity, and the computer program FB-Pier is used for lateral design capacity and pile group settlement (FDOT 2016). These computer programs are provided by the Bridge Software Institute at the University of Florida. Few commonly encountered IGMs, like limestone, limerock, chalk, and very shelly sands, have been included in the design program. FB-Deep uses in-situ tests of either SPT or CPT methods for determining static axial pile capacity of driven piles. The introduction and summary of design methodologies used in FB-Deep can be referred from Lai (2012). Dynamic analysis methods used in FDOT consist of PDA, CAPWAP, WEAP, and Embedded Data Collector (EDC) system.
It has been stated in FDOT (2016) that if the foundation is bearing on rock or IGM, then the confirmation should be made regarding the existence of sufficient depth of bearing layer to prevent punching failure into the weaker stratum.

2.5.4 Minnesota Department of Transportation (MnDOT)

Driven piles constitute about 85 percent of the bridge foundations at MnDOT, with steel H piles comprising the major portion of them (Paikowsky et al. 2009). MnDOT does not have specific provision for the pile design in IGMs or hard rocks. It follows the limit of structural capacity, as per AASHTO, when the piles are driven into hard rocks. According to MnDOT (2016), when the piles are driven into rocks and the pile capacity is controlled by end-bearing, then the nominal pile capacity should be based on the structural capacity of the pile.

2.5.5 Montana Department of Transportation (MDT)

MDT (2008) has a section describing "Piles in Intermediate Geomaterials". Weak shale, weak sandstone, mudstone, claystone, sandstone, and dense sand and gravel are the IGMs found in Montana State. MDT (2008) acknowledges that the classification of IGMs based on material properties has not been established. However, it classifies IGMs as the geomaterials which have uniaxial compressive strength in the range of 12.5 ksf to 260 ksf, and a stiffness modulus in the range of 2.1 ksf to 21,000 ksf.

Regarding the design of driven piles into IGMs, MDT (2008) states that applying the same methods developed for soils in IGMs does not give reliable estimation of pile capacity and design depth. Thus, it emphasizes the use of CAPWAP signal matching test, including a dynamic wave equation analysis during pile installation to confirm that the designed capacity is attained. For the piles driven to rock, load capacity is determined based on driving observations, local experience, and load tests due to the uncertainties in the contact area of piles to rocks, penetration depth into rock, and the rock quality (MDT 2008).

2.5.6 Maine Department of Transportation (MaineDOT)

No specific methods for the determination of pile capacity driven in IGMs were found at the Maine DOT (2014). Ten feet coring was recommended, if the piles were bearing on rocks, to ensure that the bearing layer was not terminated in boulders, and RQD calculation was based on

the 10 ft core. Sandford and Stuart (2014) assessed two methods, Canadian Geotechnical Method (CGM), developed by Canadian Geotechnical Society, in 1985, and the Proposed Intact Rock Method (IRM), equivalent to Rowe and Armitage (1987) equation, for predicting end bearing in steel H-piles driven into rocks. Sanford and Stuart (2014) concluded that the proposed IRM was significantly more reliable than the CGM method.

2.5.7 North Carolina Department of Transportation (NCDOT)

Though NCDOT does not have criteria to classify IGMs for piles, it defines piles driven to rocks based on drivability. Piles driven to rocks are defined as those having a pile drivability of 5 blows per 0.25 inch of movement (NCDOT 2014).

2.5.8 Oregon Department of Transportation (ODOT)

For pile design, ODOT follows AASHTO specifications, along with the Federal Highway Administration (FHWA) publication "Design and Construction of Driven Pile Foundations", by Hannigan et al. (2006) (ODOT 2015).

2.5.9 Washington State Department of Transportation (WSDOT)

No specific provision for determination of axial pile capacity on rocks was found in the "Specifications and Geotechnical Design Manual", of WSDOT. Section 8.12.2 of WSDOT Geotechnical Design Manual M46-03.09 states that the geotechnical design of driven pile foundations, and all related considerations, shall be conducted as specified in the recent version of AASHTO LRFD Bridge Design Specifications Article 10.7 (WSDOT 2015).

2.5.10 **Iowa Department of Transportation (IADOT)**

Based upon the outcome of the three research projects sponsored by the Iowa Highway Research Board, "Development of LRFD Procedures for Bridge Pile Foundations in Iowa- Volume IV: Design Guide and Track Examples" was developed to incorporate the regional LRFD in the practice of Iowa (Green et al. 2012). From the extensive research, Iowa "Blue Book" method was recommended to be used for design of steel H-piles. IADOT does not have any design criteria for piles driven into IGMs. However, it has categorized bedrock into two categories based on uncorrected SPT, one in the range 100-200, and another greater than 200. Iowa DOT LRFD Bridge Design Manual gives the estimated nominal resistance values for end bearing pile in bedrock. The penetration depth required for the full mobilization of end bearing in H-piles has also been mentioned for commonly encountered rock types, like broken limestone, shale, sandstone, and siltstone.

2.5.11 Pennsylvania Department of Transportation (PennDOT)

PennDOT has defined soft and weak rocks as the rocks with uniaxial compressive strength less than 500 tsf (PennDOT 2015). PennDOT (2015) refers to the AASHTO provision for the determination of the bearing capacity of driven piles in weak rock. It further recommends assessing whether geotechnical or structural resistance governs the limiting resistance.

2.5.12 Wyoming Department of Transportation (WYDOT)

WYDOT currently adapts the AASHTO Specifications (2017), and applies local experiences to design and construct the driven pile foundations. The current practice of WYDOT uses WEAP to establish pile driving criteria for all production piles. PDA with subsequent signal matching

analyses using the CAPWAP is used as a construction control method on about 2 percent of the production piles in some bridge projects. PDA/CAPWAP is implemented to determine and verify the required pile capacity at bridge projects expecting high loads and soft rock bearing. Pile restrikes at 24 hours after the end of driving (EOD) are normally performed to further ensure that the desired pile resistance is achieved, and pile performance is accepted.

2.5.13 Summary of Current Practices for IGM classification in the United States and Canada

A review was conducted to learn about the current state of knowledge in characterizing and defining geomaterials and to investigate the existing design and construction of driven piles in IGMs. The review included bridge design manuals, geotechnical manuals, and specifications by 46 DOTs in the United States, as shown in Figure 7. The Canadian Foundation Engineering Manual (CFEM) was also included in the review. Among the 46 states in the United States only six, Montana, Pennsylvania, North Carolina, South Carolina, Tennessee, and Iowa, were found to have criteria for defining IGMs or hard rocks for driven piles. Two states, Montana and Pennsylvania, defined IGMs based on the UCS. MDOT (2008) defined IGMs based on a synthesis of literature as geomaterials with UCS ranging between 12.5 ksf and 260 ksf, and elastic modulus ranging between 2.1 ksf and 21,000 ksf (Mokwa and Brooks 2009). MDOT acknowledged that the classification of IGM based on material properties has yet been standardized. Furthermore, the determination of IGM elastic modulus needs to be complemented by its strain range. PennDOT (2015) considered IGMs as geomaterials with UCS less than 1,000 ksf. Although
NCDOT (2014) did not have criteria for defining IGMs, it was the only DOT that defined rock based on a pile drivability analysis. They defined rocks as a geomaterial if it experienced blow count exceeding 240 blows per foot (bpf) with an approved hammer. The South Carolina DOT (2010) stated that the nominal capacity of piles driven in rocks with rock quality designation (RQD) greater than 10percent was limited by its structural capacity. The Tennessee DOT (2016) defined competent bedrock as “rock drilled within a 10 ft core run without encountering more than three instances of discontinuities, weathered seams greater than 2 in or a single discontinuity greater than 6 in.” IADOT (2013) presented the nominal unit toe resistance of driven piles for two bedrock categorizes: one with N_{60} values ranging between 100 and 200 and the other with N_{60} values exceeding 200. Utah, Colorado, Indiana, Kentucky, and Connecticut have criteria for differentiating weak rocks regardless of the foundation types.

Illinois, Iowa, and Florida DOTs have some provisions for determining pile capacity and embedding depth for region-specific rock types. The remaining DOTs follow AASHTO specifications or Federal Highway Administration (FHWA) publications on pile designs. The CDOT (2018) adapts the AASHTO design provision of “Piles Driven to Hard Rocks”, if the pile penetrates less than 3 ft into the bedrock and “Piles Driven to Soft Rocks”, if the pile penetrates 3 ft or more into the bedrock. The Indiana DOT (2013) limits the maximum nominal geotechnical resistance in hard rocks to 0.65 times the product of area and yield strength of the steel.

CFEM (2006) defined rock as a “natural aggregate of minerals that cannot be readily broken by hand and that will not disintegrate on a first wetting and drying cycle” (Becker and Moore 2006). Classification of rocks has been made into seven categories, from extremely weak to extremely

strong, based on UCS, point load index, and field estimates of strength using a geological hammer, pocket knife, and thumbnail. Geologically defined rocks are treated as a soil mass in a foundation design if they are weakly cemented with UCS, less than 20 ksf, closely spaced discontinuities, and heavy fragmentation (Becker and Moore 2006). The pressuremeter test method was recommended by CFEM (2006) to determine the bearing pressure for the design of foundations in very weak to weak rocks having UCS ranging from 20 to 500 ksf (Becker and Moore 2006).

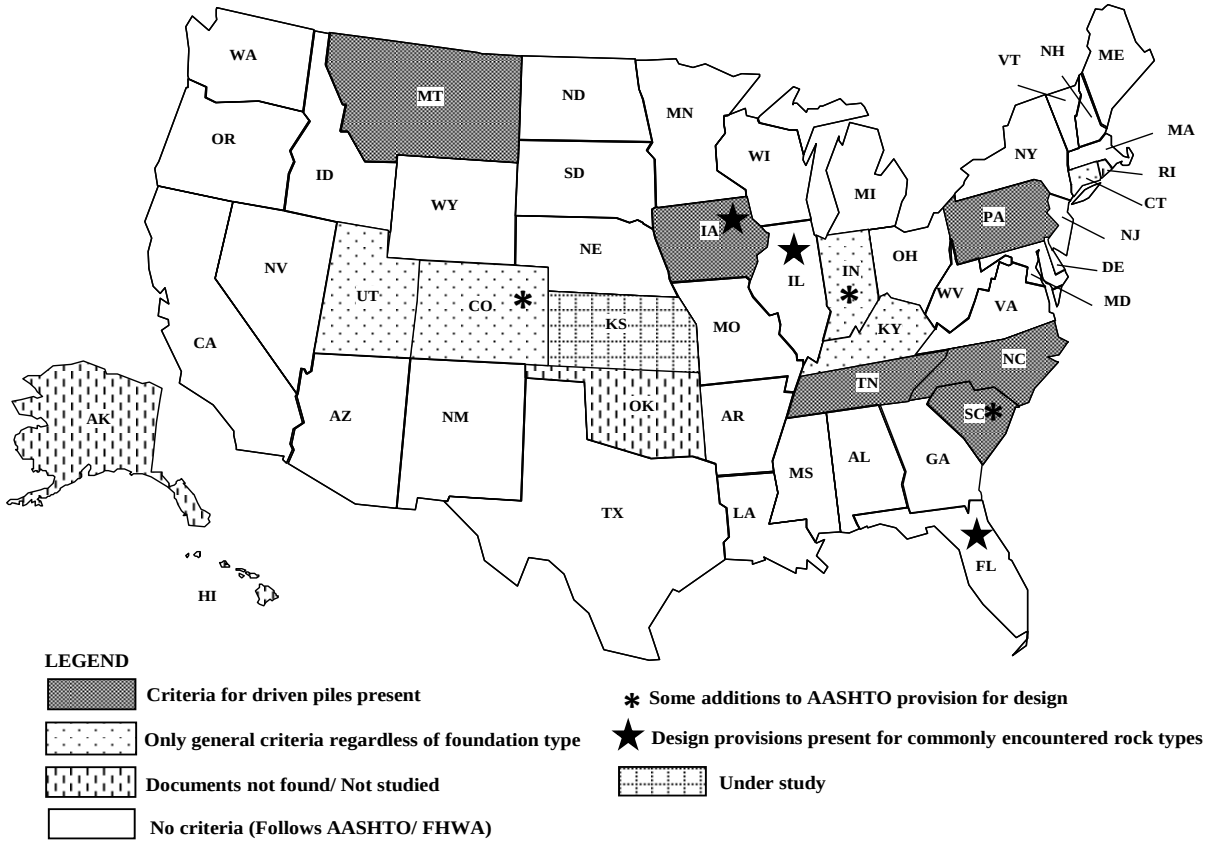

Source: Adhikari (2019)

Figure 7. Summary of DOT practices in defining IGMs and hard rocks along with the design and construction of driven piles in IGMs and hard rocks.

2.6 Collection of Usable Pile Data from Electronic Database and Literature

An electronic database is a systematic organization of information, which provides users with efficient data retrieval by creating queries and filters, along with a user-friendly interface for incorporating additional data. The database can serve a wide range of users, including management personnel, planners, design engineers, and research professionals (Kalavar and Ealy 2000). Abu-Hejleh et al. (2015) emphasized the necessity of high-quality foundation load test databases for reliability calibration that can establish accurate and economical design and construction control methods. FHWA developed a comprehensive Deep Foundation Load Test Database (DFLTD), which stored up to 1,500 load test records mainly from the United States (Kalavar and Ealy 2000). Many load tests, which were documented in the form of databases by

the Florida Department of Transportation (FDOT), were also contained in the DFLTD (Abu-Hejleh et al. 2015). However, no record of piles driven in IGM was found in the DFLTD. Later, FHWA updated the DFLTD by including LTs on large diameter open-end piles and introduced the second version of FHWA DFLTD (DFLTD v.2) (Petek et al. 2016). DFLTD v.2 included three projects with four LTs on open-ended steel pipe piles on IGM. However, all three projects lacked either subsurface exploration details, static load test results, or dynamic load test results. Furthermore, subsurface information was confined only to the Standard Penetration Test (SPT) N-values in DFLTD v.2. Paikowsky et al. (2004) developed three databases, namely, Drilled Shaft Database, Driven Pile Database, and PD/LT2000, which mainly contains driven piles tested for load failure. There were 15 driven concrete piles bearing on rock in the Driven Pile Database. Regional databases on driven piles have been established by different DOTs to promote the local calibration of LRFD procedures with respect to local geology and design practice. DOTs have often included the relevant data from these DFLTD and databases, in NCHRP 507 by Paikowsky et al. (2004), during the development of their regional databases. Nevertheless, there has been little compilation of usable data for driven piles in IGM from these regional databases. The Pile-Load Tests (PILOT), by Roling et al. (2011), consisted of 274 pile load tests in Iowa but contains no pile data on IGM. The ull Portland State University (PSU) master database, developed for the Oregon DOT, had 322 pile records, including records from DFLTD and NCHRP 507 (Smith et al. 2010), but no information was found for piles driven in IGM. The Minnesota DOT developed a foundation load test database, called the Minnesota DOT/LT2008, which included 166 load tests on H-piles, 104 tests on closed end piles (Paikowsky et al. 2009), and a considerable number of H-piles bearing on rock and till. Though pile data bearing on rock were found in the Minnesota DOT/LT2008 and Driven Pile Database, it was difficult to distinguish IGMs from rocks. Some of the possible reasons might be the lack of proper characterization of IGMs from soils and rocks for driven piles and the absence of measured geomaterial properties in these databases.

The current literature available on driven piles in IGMs is not adequate to establish trustworthy design methodologies. Furthermore, the absence of layer-wise CAPWAP results in the literature (Mokwa and Brooks 2009; Long and Horsfall 2017) has been a major obstacle for assessing uncertainties in shaft resistance estimation in IGM. Mokwa and Brooks (2009) compiled information on 21 piles driven in IGMs for eight bridge projects from the MDOT. Out of 21 piles, 13 piles were driven into IGMs, like sandstone, claystone, and shale, and the remaining eight piles were driven into dense sand and gravel. Computer programs DRIVEN and GRLWEAP, the driving formulas WSDOT Gates and FHWA-Gates, and an empirical method used by the Colorado DOT were investigated for their pile resistance estimations. Large variations were observed between predicted and measured pile resistances in IGM using the CAPWAP (Mokwa and Brooks 2009). The importance of separating shaft resistance calculations for IGMs and soil was emphasized (Mokwa and Brooks 2009). Brooks (2008) acknowledged that the study from 21 piles was not enough to develop reliable pile resistance estimation methods. Mokwa and Brooks (2009) recommended that further research is needed on the following: develop undisturbed sampling methods for IGMs, establish correlations between in-situ measurements and design parameters, and better understand pile behaviors in IGMs.

Long and Horsfall (2017) also conducted a study on the resistances of steel H-piles in IGM based on the results of seven static load tests and approximately 208 dynamic load tests. Tests were

conducted along the interchange of US 41- STH 29 and US 41- IH43 flyovers located in Brown County, Wisconsin (Long and Horsfall 2017). Most of these piles were HP 14×73 and a few HP 12×53. The IGMs in this study only consisted of dense soils such as gravels, boulders, sand, stiff clays, and silts. Equations were developed to predict shaft resistance and end bearing. Although the equations were based on a reasonable number of dynamic load tests, the tests did not incorporate a wide range of IGMs, such as IGM-rocks.

2.7 LRFD and Calibration of Resistance Factors

2.7.1 Sources of uncertainties in geotechnical engineering

Phoon and Kulhawy (1999) categorized the sources of uncertainties into inherent variability, measurement errors, and transformation models, whereas, Baecher and Christian (2003) grouped these uncertainties into natural variability, knowledge uncertainty, and model uncertainties. Hacking (1975) referred the term aleatory to the uncertainties due to random physical process, and the term epistemic to the uncertainties due to lack of knowledge (Baecher and Christian 2003). The inherent variability is attributed to the geological processes that occur within different time that causes variation in the geomaterial properties in vertical and horizontal directions. Measurement errors are induced in the field due to the errors in the equipment or procedures, or random testing errors (Phoon and Kulhway 1999). Statistical errors, which arise due to inadequate number of observations in statistically characterizing a soil property, are also included in the measurement errors (Kulhawy 1996). Model uncertainties are the uncertainties created during the transformation of in-situ data into design parameters with the application of some correlations. Model uncertainties even include the models (empirical correlations) employed for design.

2.7.2 Introduction to LRFD

A single parameter, called the factor of safety (FS), is used in Allowable Stress Design (ASD) philosophy to address all possible uncertainties encountered in the determination of loads and resistances. The selection of FS depends on personal judgment based on the level of confidence and experience of engineers leading to inconsistency in design. Though the FS can be adjusted according to the levels of control in analysis and construction, these factors of safety are not indicative of the conservatism associated with the methods and economic implications on design (Paikowsky et al. 2004). Thus, to overcome these shortcomings of ASD, LRFD design philosophy has been developed since the mid-1950s to quantify various uncertainties from different sources using probabilistic approaches to attain a consistent level of reliability (or probability of failure). The probabilistic approaches are used to determine the load and resistance factors that are used during the design to ensure a prescribed level of reliability. These load and resistance factors are multiplied with the nominal loads and nominal resistances to get the factored loads and factored resistances. Nominal resistances are the resistances that are directly calculated using some design methods for specific piles. Therefore, the basic principle of LRFD as shown by Equation (17), is that the factored resistance should always exceed the factored loads.

$$\sum \eta_i \gamma_i Q_{ni} \leq \varphi R_n \tag{17}$$

where,

Q_{ni}= a specific nominal load

η= load modifier relating to ductility, redundancy, and operational importance of nominal load Q_{ni}

γ_i= load factor to be applied for specific nominal load Q_{ni}

φ= the resistance factor, and

R_n= nominal resistance available (either ultimate resistance or resistance at certain deformation)

The advantage of probabilistic approach in dealing with uncertainties can be illustrated in Figure 8. Load (Q) and resistance (R) are treated as the random variables and Probability density Functions (PDFs) of these random variables show the variation or uncertainties associated with them. The narrower curve of load indicates that the uncertainties related with load are comparatively lesser than the uncertainties related with the resistance. The region of failure is indicated by the region where 2 PDFs overlap (R < Q). If we consider load and resistance as the deterministic or fixed values as represented only by their means, $\overline{Q}$ and $\overline{R}$ for load and resistance respectively, then the mean FS is given by $\overline{FS}$= $\overline{R}$/ $\overline{Q}$. However, if we consider load and resistance as random variables and use PDFs to indicate their variation, then the FS associated with nominal loads and resistances is given by FS_n= R_n/Q_n. FS_n is smaller than $\overline{FS}$ for the case, as shown in Figure 8, which indicates that the prescribed FS is not achieved. If the resistance has a greater variation with the same mean value $\overline{R}$, then the PDF of R is shown by the dotted line in Figure 8. As the mean value of resistance remains the same, there will be no change in the mean FS. However, the probability of failure will be increased as shown by the increase in the overlapping area between the PDF shown by dotted curve and the PDF of load.

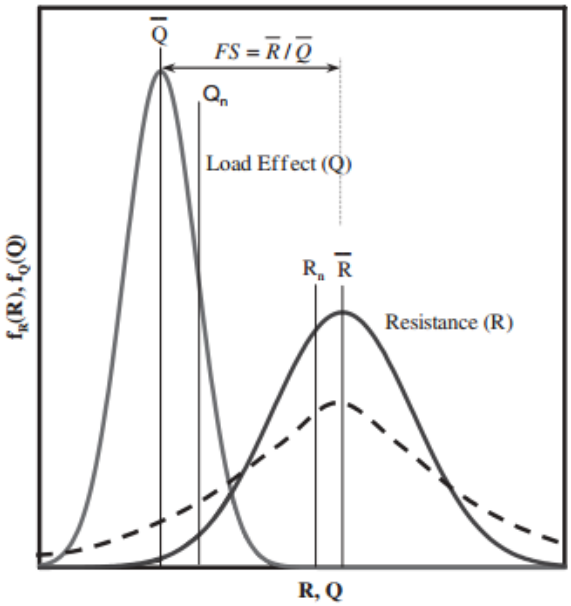

Source: Paikowsky et al. (2004)

Figure 8. Probability density function (PDFs) of load and resistances (Adopted from Paikowsky et al. (2004)).

2.7.3 Concept of reliability index

Reliability is defined as the probability of performance or limit state function, g(**X**) being greater than zero. **X** indicates the vector of random variables which are involved in defining the safety margin (failure or safe) of a system. The limit state equation in our study is given by Equation (18).

$$g = R - Q \tag{18}$$

where,

g = a random variable representing margin of safety.

The reliability is given by Equation (19).

$$\text{Reliability} = 1 - p_f = P(g(\mathbf{X})>0) = \int_{g(x)>0} f_x(\mathbf{x})d\mathbf{x} \tag{19}$$

where,

p_f = probability of failure, and

$f_x(\mathbf{x})$ = the joint PDF of **X.**

Thus, two main parameters required for the computation of reliability are the joint probability density of all the random variables defining the state of a system, and the limit state function. The reliability of the system can be measured by a reliability index, β, which is defined as the number of standard deviations from the failure surface (g=0) to the mean (μ_g) in the PDF of g.

It is expressed by the Equation (20) and illustrated in Figure 9.

$$\beta = \frac{\mu_g}{\sigma_g} \tag{20}$$

where,

σ_g = standard deviation of g.

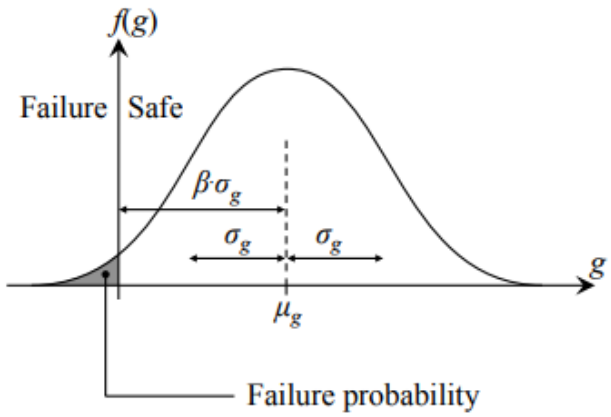

Source: Withiam et al. (1998)

Figure 9. Probability density function of g (g= R-Q) indicating margin of safety and the reliability index, β.

If the PDF of g is normally distributed, then

$$p_f = P(g(\mathbf{X})<0) = P(g(R,Q)<0) = \Phi\left(\frac{0-\mu_g}{\sigma_g}\right) = \Phi(-\beta) \quad (21)$$

where,

Φ = standard normal cumulative distribution function (CDF).

However, the approximate relationship between probability of failure and reliability index, as presented by Rosenbleuth and Esteva (1972) is given by Equation (22).

$$p_f = 460\, e^{-4.3\beta} \quad (22)$$

2.7.4 Calibration of resistance factors using reliability theory

FHWA mandated the application of the LRFD in bridges initiated after October 1, 2007, in the United States. However, state DOTs were reluctant in adopting the LRFD due to the increased cost of foundations resulting from conservative resistance factors. Therefore, with an objective of implementing the LRFD, FHWA permitted the regional calibration of resistance factors to account for local soil conditions, and design and construction practices.

Du (2005) pointed out that the calculation of reliability by direct integration, as shown in Equation (2.18), is difficult due to various reasons. Firstly, a multidimensional integration is required due to a number of random variables involved in a limit state function. Secondly, the integrand $f_x(\mathbf{x})$ is the joint pdf of **X,** which is generally a non-linear multidimensional function. Thirdly, the integration boundary can also be a multidimensional and a non-linear function. Therefore, to facilitate the calculation of probability of failure, various approximation methods as First-Order-Second-Moment (FOSM), First-Order-Reliability-Model (FORM), and *Monte-Carlo Simulation (MCS) are being used.*

2.7.5 First-Order-Second-Moment (FOSM)

FOSM is one of the analytical methods originally used by Cornell (1969) to calculate the reliability index. FOSM requires first and second moments (i.e. mean and standard deviation) of the random variables and linearized form of the performance (limit-state) function. Thus, non-linear limit state function is expanded using Taylor's series, and only the first order terms are retained. Taylor's series is used for the approximation of the non-linear function as the sum of terms involving derivatives of that function at a single point. As only the first order terms of Taylor's series expansion are retained in FOSM, the process is called the linearization of the function at the point considered. In FOSM, linearization is carried out at the mean values of the random variables involved in the limit state function. This linearization or approximation is utilized for obtaining the moments (mean and standard deviation) of the limit state function. The mean and standard deviation of the approximated limit state function are accurate, if the function is linear. The main drawback of the FOSM is that the method will produce different reliability indices for equivalent limit state functions which is known as the invariance problem of the method. This is because of the difference in gradients of the equivalent limit state functions at the mean values. In this study, the limit state function as given by Equation (18), is a linear

function involving load (Q) and resistance (R), and the resistance factor is determined using closed form Equation (23).

$$\varphi = \frac{\left(\frac{\gamma_D Q_D}{Q_L}+\gamma_L\right)\lambda_R\sqrt{\frac{1+\mathrm{COV}_{QD}^2+\mathrm{COV}_{QL}^2}{1+\mathrm{COV}_R^2}}}{\left(\frac{\lambda_D Q_D}{Q_L}+\lambda_L\right)\exp\left(\beta_T\times\sqrt{\ln\left(\left(1+\mathrm{COV}_R^2\right)\left(1+\mathrm{COV}_{QD}^2+\mathrm{COV}_{QL}^2\right)\right)}\right)} \quad (23)$$

where,

γ_D = dead load factor;
γ_L= live load factor;
Q_D/Q_L= dead load to live load ratio;
COV_{QD} = coefficient of variation of dead load,
COV_{QL} = coefficient of variation of live load,
COV_R= coefficient of variation of resistance,
λ_D= mean dead load bias,
λ_L = mean live load bias,
λ_R= mean resistance bias, and
β_T= target reliability index.

The statistical summaries of the loads presented in Table 7, and the target reliability indices of 2.33 and 3 were referred from Paikowsky et al. (2004).

Table 7. Statistical parameters of dead and live loads (Paikowsky et al. 2004).

Statistical Parameters	Dead Load	Live Load
Mean bias	λ_D= 1.05	λ_L= 1.15
Load factor	γ_D= 1.25	1.75
Coefficient of variation	COV_{QD}= 0.1	COV_{QL}= 0.2

2.7.6 First-Order-Reliability-Model (FORM)

FORM utilizes the Hasofer and Lind (1974) definition of reliability index, as the minimum distance from the linearized failure surface to the origin of reduced random variables. Since the linearization of the non-linear failure surface (limit state function) is carried out at points on the failure surface instead of the mean values as in FOSM, the invariance problem is overcome by FORM. There are several points on the failure surface. However, the interest is to locate a point called the most probable point (MPP), which is at a minimum distance from the origin of the reduced random variables. This minimum distance is the measure of the reliability as a reliability index. Thus, the major task in FORM is to locate the MPP. To locate MPP, the variables are first transformed into standard normal variables (having zero mean and unit standard deviation). For non-normal distribution functions, while transforming the variables into standard normal variables, the probability density functions and the cumulative distributions of both the actual distribution and the standard normal distributions are kept equal. Then, the point on the failure surface is located by using optimization techniques such that it lies at the shortest distance from the origin. Iteration is generally adopted for locating MPP, and the shortest distance from the

origin of the standard normal variates to the MPP is the reliability index. The procedure for determining resistance factor from FORM utilizing Rackwitz and Fiessler (1978) algorithm has been illustrated in the flowchart as shown in Figure 10. The random variables involved in the limit state function for this study were pile resistance (R), dead load (DL), and live load (LL). For the calculation of reliability index, β, the statistical parameters should correspond to the statistics of measured R, DL, and LL. Therefore, to obtain the statistical parameters for measured R, DL, and LL, biases were first calculated that are the ratio of the measured to estimated values. Multiplying the nominal values of R, DL, and LL with the statistical summaries of bias to obtain the statistics of measured R, DL, and LL is termed as scaling of the bias (Allen et al. 2005).

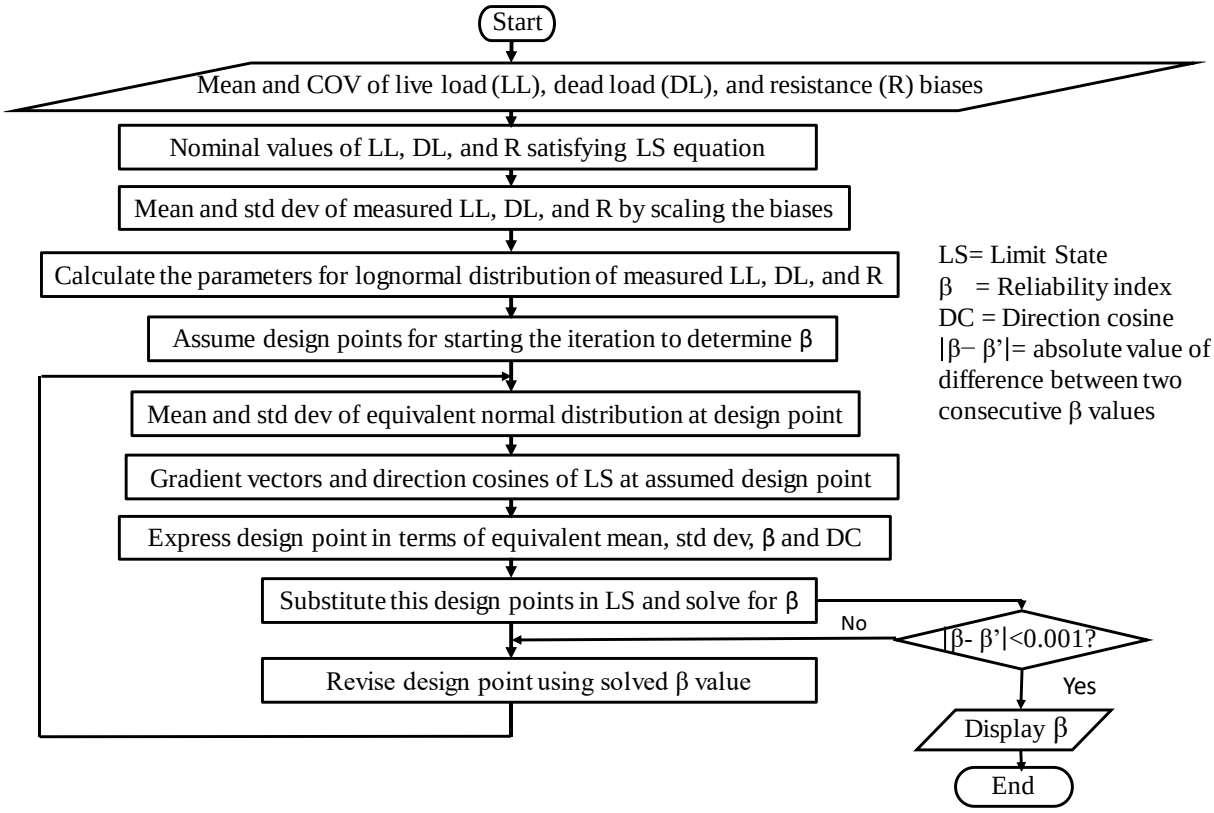

Source: Adhikari (2019)

Figure 10. Stepwise process for determining resistance factor from FORM.

2.7.7 Monte Carlo Simulation (MCS)

MCS is a technique to generate the random numbers, as per the distribution of the random variables, to facilitate the direct calculation of the probability of failure. According to Allen (2005), MCS does not require the location of the design point, rather the data need to be fit in the region of the design point. The accuracy of MCS depends upon the number of simulations chosen to generate a random variable. In MCS, the best distributions of the load and resistance biases are obtained. Then the parameters of the best fit distributions are determined. Random numbers (biases of loads and resistances) are generated based on the parameters of the best fit distributions. These randomly generated load and resistance biases were scaled by multiplying to the nominal values of load and resistance satisfying the limit state equation. Resistance factor comes into calculation during this scaling process. A resistance factor is assumed, and the

measured load and resistance values are generated. Limit state function is calculated for each generated load and resistance values. Then the probability of failure is calculated as the number of failures divided by the number of simulations. The resistance factor was changed until the desired probability of failures of 0.01 and 0.001 corresponding to reliability indices of 2.33 and 3.00 were obtained. The procedure for determining resistance factor from MCS has been illustrated in the flowchart, as shown in Figure 11.

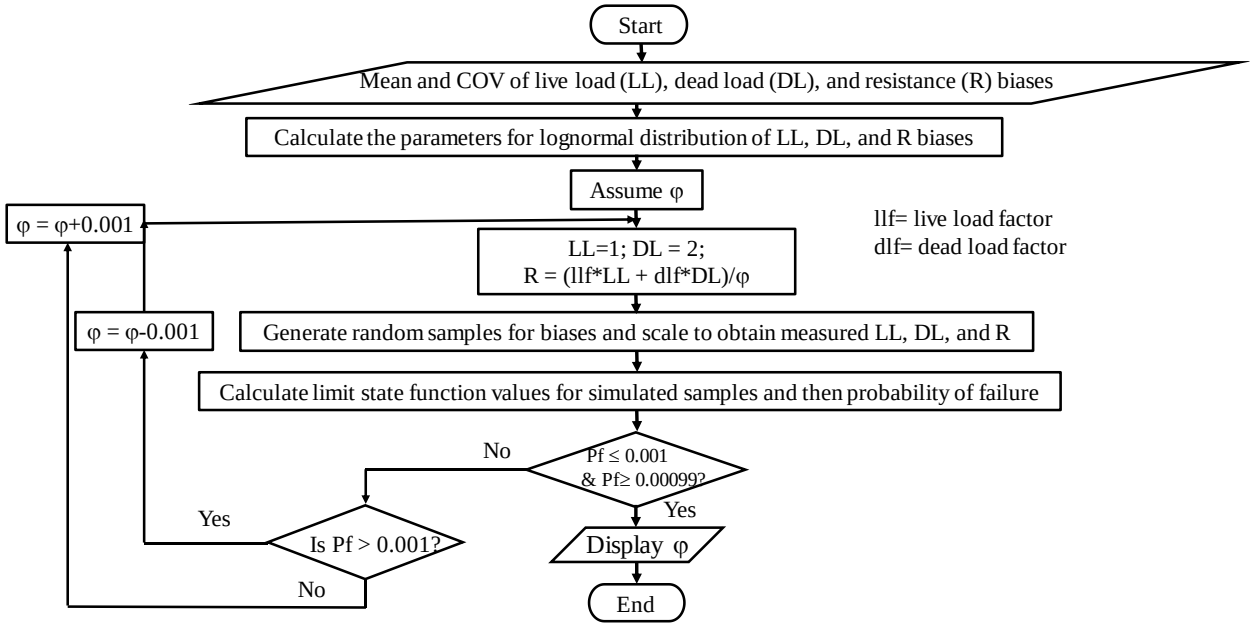

Source: Adhikari (2019)

Figure 11. Stepwise process for determining resistance factor from MCS for reliability index of 3.00.

CHAPTER 3. ELECTRONIC DATABASE (WYOPILE)

3.1 Introduction

An electronic database, WyoPile, presented in this chapter, was created with the objectives of alleviating existing design and construction challenges, advancing the knowledge associated with driving piles in IGMs, and calibrating the reliability-based resistance factors based on the geology of Wyoming. This is a high-quality database that contains the necessary information on projects, subsurface profiles, piles, hammers, and load tests required for reliability calibration. Historical reports on the dynamic load test of the piles and construction plans were provided to the research team by WYDOT. These reports and technical documents were uploaded into the database as electronic attachments for easy reference. Furthermore, user-friendly features that allow for convenient filtering, sorting, searching, querying, and updating make the database more attractive. The WyoPile database consists of 45 piles from 17 bridge projects and 1 building project from 9 Wyoming counties. The location of all the test piles is shown in Figure 12. The presence of the layer-wise CAPWAP result for each pile is one of the appealing features of the database that enables users to determine shaft resistances contributed from individual soil and IGM layers. The database contains a range of strength parameters for different geomaterials, which can eventually be utilized for geomaterial classification and preparation of a catalog of IGM properties for pile design. Additionally, the WyoPile database simplifies grouping of the similar geomaterials, retrieval of subsurface profiles, and parameters required as input for static analysis.

3.2 Overview of Data in WyoPile

WyoPile houses quality information required for static and dynamic analysis of piles driven in IGM throughout Wyoming. Static analysis uses the geomaterial profile along with the strength properties (cohesion, internal friction angle, q_u), unit weights, and pile dimensions. Along with this information, the dynamic analysis further requires information on the pile driving hammer, driving system, and penetration resistance (hammer blows counted during pile driving process). Dynamic load test results consist of blow counts and stroke heights of the hammer observed at the EOD and BOR. In addition, pile resistances measured from the signal matching technique using the Pile Driving Analyzer (PDA) and CAPWAP are recorded. Pile resistances determined from CAPWAP are considered as the next most accurate construction control method after static load test, and they were used to evaluate the reliability of static analysis methods in term of resistance bias (ratio of CAPWAP resistance to predicted resistance). Resistance bias is the main parameter used for calibration of resistance factors. Thus, if all the information required for static and dynamic analysis were present, along with the corresponding CAPWAP results, then the pile was characterized as a “usable” pile; otherwise, it was characterized as “nonusable” pile. Of the 45 piles, 10 were identified as “nonusable” piles and the remaining 35 were considered usable. The dynamic results obtained during the EOD and BOR can be valuable for understanding time dependent pile resistances of IGM. Table 8 summarizes the pile, subsurface, driving and hammer data of the 35 usable piles.

IGMs were categorized into IGM-soil and IGM-rock to reduce the large variabilities associated with IGM material. IGM-soil consists of disintegrated geomaterials that are stiffer than soils, whereas, IGM-rock consists of geomaterials that are geologically defined as rocks (solid

aggregation of minerals). The details on geomaterial classification are presented in chapter 4. IGMs at the bridge sites were dense sand and gravel, low plasticity silts, sandstone, siltstone, claystone, shale, and breccia. The distribution of the piles, according to the geomaterials in the bearing layer, is shown in Figure 13. The total length of the embedded pile along with the pile length embedded in the IGMs is also included in Table 8. Three piles with IDs 8, 17, and 41 had zero embedment length in IGMs.

All 35 usable piles were steel H-piles with 9 piles having a yield strength of 36 ksi and the remaining 26 piles having a yield strength of 50 ksi. The embedment length ranged from 19.5 ft to 139 ft with 23 pile lengths within 49 ft. The most common pile types were HP 14×73 and HP 12×53, and the commonly used pile driving hammers in Wyoming were Delmag D16-32 and ICE 42-S. The distribution of the hammer types is presented in Figure 14.

3.3 WyoPile Structure

The WyoPile database was built in Microsoft Office Access® by integrating information entered through various tables and forms. The layout of the database was adopted from the PILOT database (Roling et al. 2011). The "Pile Load Tests List", shown in Figure 15, constitutes the main form displayed in the home page after the database is launched. The main form presents the information on the piles in a tabular format, facilitates the addition of new pile LTs through a separate tab, called "New Pile Load Test", allows for acquisition of details, and offers filtering options. “Pile Load Test Records” stores information in a table format and the fields of the table are described in subsection 3.3.1. Another form, called "Pile Load Test Record Form (PLTRF)", is shown in Figure 16, which was created to complement the main form for organized and user-friendly access to pile details. PLTRF can be prompted by clicking the unique cataloging number called "ID", which is automatically assigned by Microsoft Office Access® to each pile record in the main form. The upper part of PLTRF summarizes the general information of the pile, such as name and geographical location of the project site, pile location in the bridge structure, pile size, drive date, LRFD pile load, the hammer used, and the top and bottom elevations of the pile. The details of the PLTRF were systematically arranged in six tabs at the lower part of PLTRF (Figure 16), which are described from subsection 3.3.2 through 3.3.6.

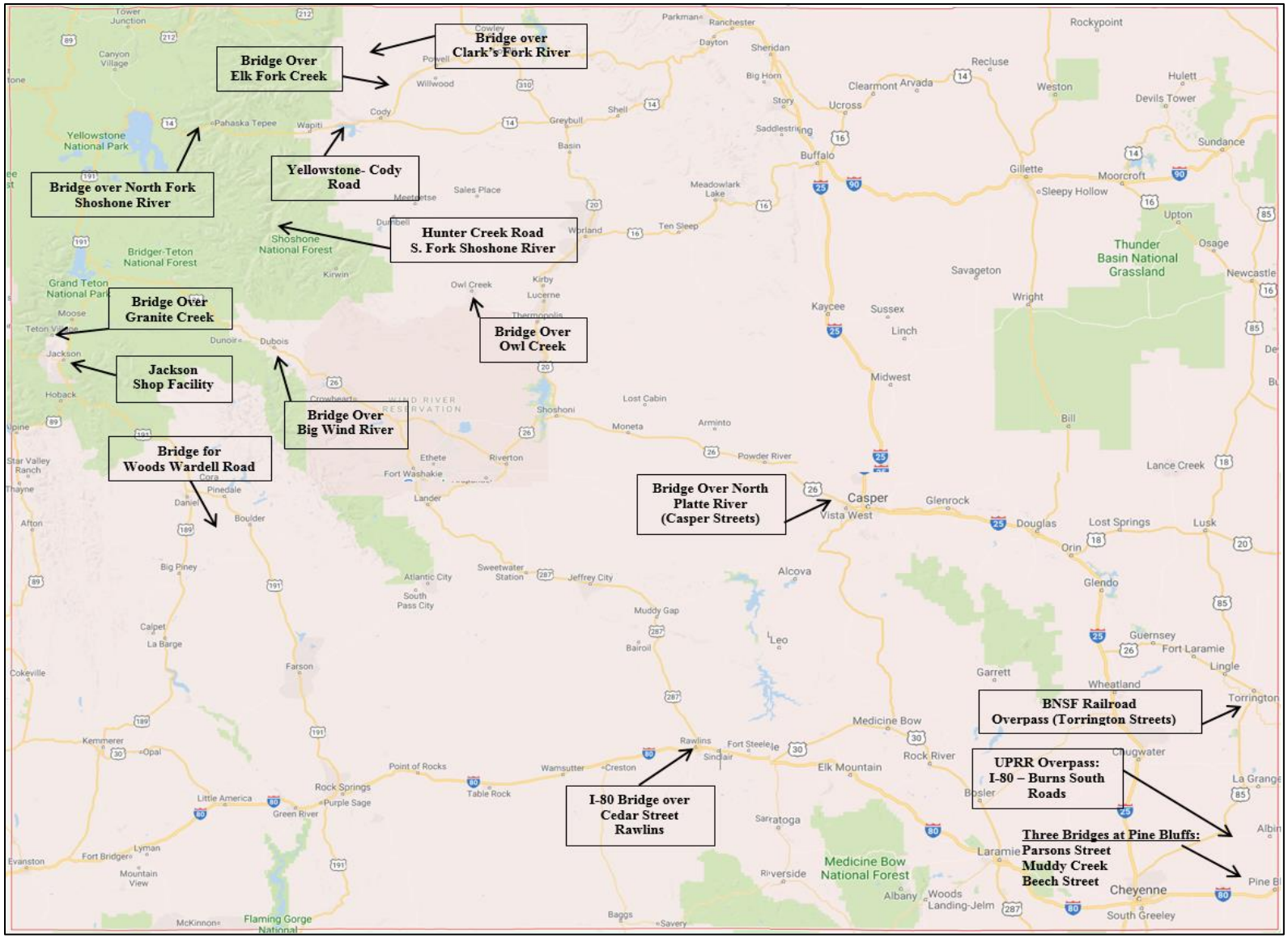

Source: Google Maps

Figure 12. Wyoming map with the location of the test piles (https://www.google.com/maps/place/WY).

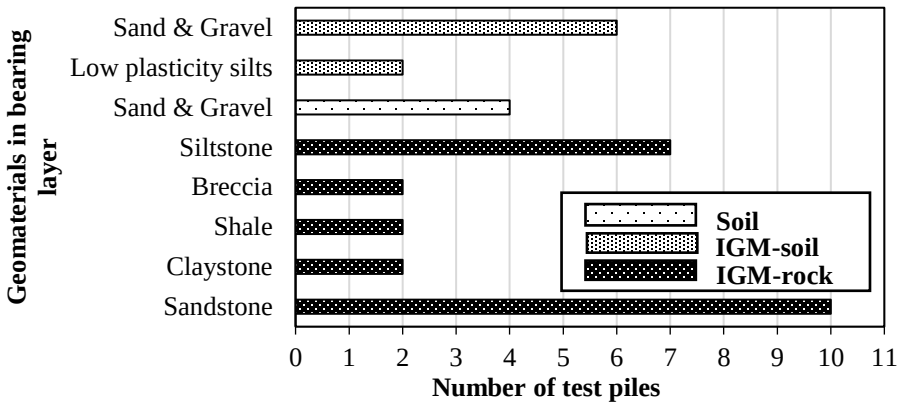

Source: Adhikari (2019)

Figure 13. Distribution of the 35 usable piles by the geomaterials in the bearing layer.

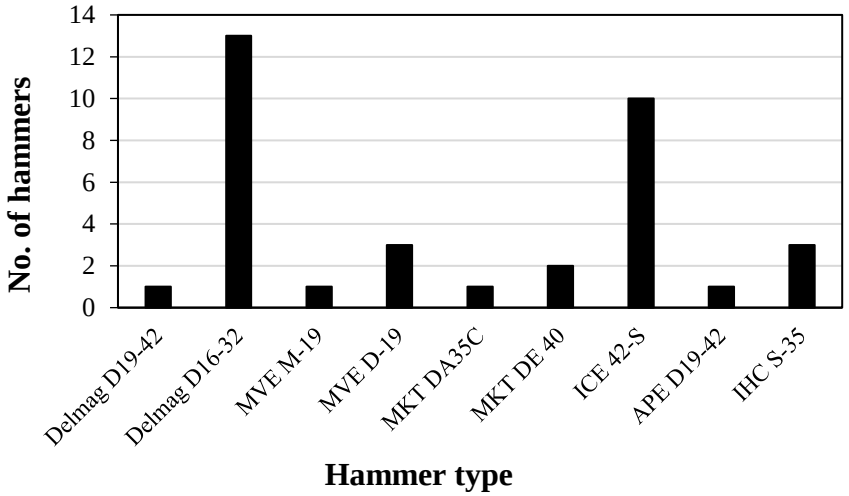

Source: Gebreslasie (2018)

Figure 14. Hammer types used for pile installation and dynamic load testing.

Table 8. Summary of the 35 usable pile, subsurface, hammer, and driving information.

Project	Pile ID	County	Pile Location	Steel H-Pile Size	Bearing Layer [SPT N] / (S_u in ksf)	Overburden Geomaterial	L_{EMB} EOD (BOR) (ft)	L_{IGM} (ft)	Driving Hammer Used	EOD Blow Counts (bpf)	BOR Blow Counts (bpf)
Burns South	1	Laramie	Pi-3 P-1	14×73	Sandstone [300] / (5.30)	S+G and sandstone	37.6 (38.6)	37.6	Delmag D16-32	100	108
	2	Laramie	A-1 P-1	14×73	Sandstone [200] / (2.59)	Sand/ S+G	68.3	28.25	Delmag D16-32	452	600
Casper Street	3	Natrona	A-2 P-1	14×73	Sandstone [627] / (NA)	Sand	24.1	2.08	MVE D-19	84	84
	16	Natrona	Pi-1 P-17	14×89	Shale [NA] / (167)	S+G	20.5	20.5	MVE D-19	118	288
BNSF Torrington	4	Goshen	A-2 P-1	14×73	Claystone [70] / (2)	Sand	100	1.8	MVE D-19	68	120
	17	Goshen	A-1 P-1	14×73	Sand [25] / (1.04)	Sand	99.2 (99.3)	0	Delmag D16-32	36	48
	18	Goshen	A-1 P-9	14×73	Claystone [NA] / (0.5)	Sand	139	7.5	Delmag D16-32	58	72
Owl Creek	5	Hot Springs	B-2 P-5	14×73	Shale [NA] / (4)	Sand/ Shale	27 (27.1)	13.5	ICE 42-S	263	360
Woods Wardell	6	Sublette	Pi-2 P-1	12×53	Claystone [59] / (38)	Claystone	23	23	APE D19-42	128	156
PB Parson	7	Laramie	A-1 P-5	12×53	Siltstone [116]/ (22.55)	Silts	87.9 (88)	69.3	Delmag D16-32	164	216
	8	Laramie	A-2 P-1	12×53	Sand [72] / (4.68)	Silty Sand	75.2 (75.4)	0	Delmag D16-32	146	137
PB Muddy Creek	9	Laramie	A-2 P-1	12×53	Silts [19] / (3.59)	Silty Sand	53.6	25.3	Delmag D16-32	109	NA
	10	Laramie	B-2 P-1	12×53	Silts [66.5] / (2.69)	Sandy Silt	35.3	20.8	Delmag D16-32	108	NA
	11	Laramie	B-3 P-10	12×53	Siltstone [115] / (3.59)	Sandy Silt	38	0.7	Delmag D16-32	240	NA
PB Beech Street	12	Laramie	A-1 P-1	12×53	Siltstone [55] / (9.5)	Sandy Silt	46.7	28.6	Delmag D16-32	55	84
	13	Laramie	A-1 P-5	12×53	Siltstone [55] / (9.5)	Sandy Silt	46.9 (47)	28.3	Delmag D16-32	66	156
	14	Laramie	A-2 P-1	12×53	Siltstone [32] / (9.5)	Sandy Silt	44.7 (45)	0*	Delmag D16-32	62	96
	15	Laramie	A-2 P-3	12×53	Siltstone [32] / (9.5)	Sandy Silt	46.4 (46.6)	0*	Delmag D16-32	82	96

Table 8. Summary of the 35 usable pile, subsurface, hammer, and driving information (continue).

Project	Pile ID	County	Pile Location	Steel H-Pile Size	Bearing Layer [SPT N] / (S_u in ksf)	Overburden Geomaterial	L_{EMB} EOD (BOR) (ft)	L_{IGM} (ft)	Driving Hammer Used	EOD Blow Counts (bpf)	BOR Blow Counts (bpf)
Cedar Street	19	Carbon	A-2 P-5	12×53	Sandstone [58] / (3.26)	Silty Sand	41.2	3.2	MVE M-19	60	84
Hunter Creek	20	Park	A-2 P-3	12×53	S+G [150] / (NA)	S+G	19.5	19.5	MKT DE 40	850	NA
	21	Park	A-1 P-2	12×53	S+G [133] / (NA)	S+G	36	35.9	MKT DE 40	63	NA
Clark's Fork	22	Park	A-2 P-1	14×53	S+G [240] / (NA)	S+G	45	39.9	Delmag D19-42	119	200
Jackson Shop	23	Teton	Column	12×53[1]	S+G [200] / (NA)	Clay	31	2.0	IHC S-35	NA	600
	24	Teton	Column	12×53[1]	Sand [200] / (NA)	Clay	36	6.5	IHC S-35	NA	108
	25	Teton	Column	12×53[1]	S+G [166] / (NA)	Clay	39	9.5	IHC S-35	NA	84
NF (Hanging)	26	Park	A-2 P-6	14×73	Sandstone [165] / (NA)	S+G/ Breccia	69	69.0	ICE 42-S	193	NA
NF (Pahaska)	27	Park	A-1 P-3	14×73[1]	Sandstone [448] / (NA)	S+G	41	39.5	ICE 42-S	114	NA
	28	Park	A-2 P-3	14×73[1]	Sandstone [381] / (NA)	S+G	32	32.0	ICE 42-S	1125	NA
Wind River	30	Fremont	A-1 P-4	12×53[1]	Sandstone [38] / (NA)	Sand	85	49.0	ICE 42-S	NA	132
	35	Fremont	A-2 P-2	12×53[1]	Sandstone [35] / (NA)	Sand	88	48.0	ICE 42-S	NA	216
	36	Fremont	A-2 P-3	12×53[1]	Sandstone [35] / (NA)	Sand	85.5	45.5	ICE 42-S	NA	120
Yellowstone	39	Park	A-2 P-6	14×73	Breccia [73] / (2.69)	Sand	59	17.4	ICE 42-S	132	120
	40	Park	A-2 P-1	10×42[1]	Breccia [73] / (2.69)	Sand	45	25.1	ICE 42-S	NA	18
Granite Creek	41	Teton	A-2 P-1	14×73	Sand [42] / (NA)	Sand	40	0.0	MKT DA35C	29	NA
Elk Fork Creek	43	Park	A-2 P-5	14×73	S+G [300] / (NA)	S+G	40	40.0	ICE 42S	49	NA

A-Abutment; APE-American Pile driving Equipment; B-Bent; ICE-International Construction Equipment; IHC-International Harvester Company; L_{EMB}-Embedded pile length; L_{IGM}- Embedded pile length in IGM; MKT-name of pile manufacturing company; MVE-Mississippi Valley Equipment; [N] - SPT- N values; PB-Pine Bluffs; NF-North Fork; NA-not available; (S_u)- Undrained shear strength; S+G-Dense sand and gravel; P-Pile; Pi-Pier; bpf-Hammer blows per foot; EOD-End of driving; BOR-Beginning of restrike; [1]- pile having a yield strength of 250 MPa (36 ksi); *-IGM (Siltstone) lies at the distance within two times the pile diameter from pile tip.

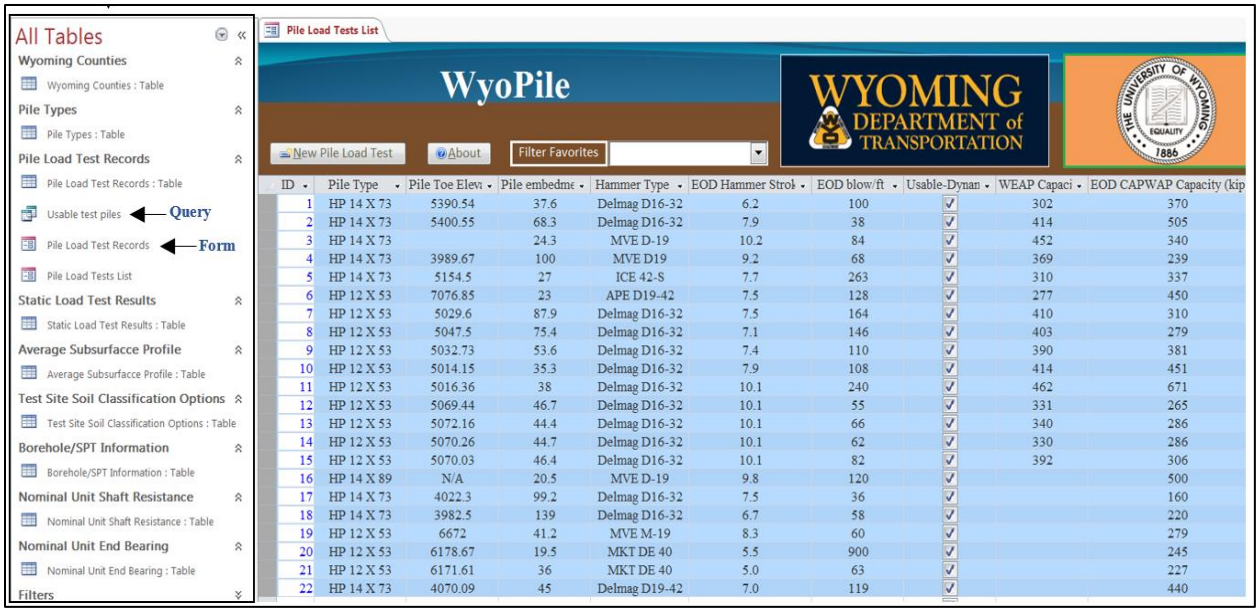

Source: Gebreslasie (2018)

Figure 15. Partial screenshot of the "Pile Load Tests List" main form.

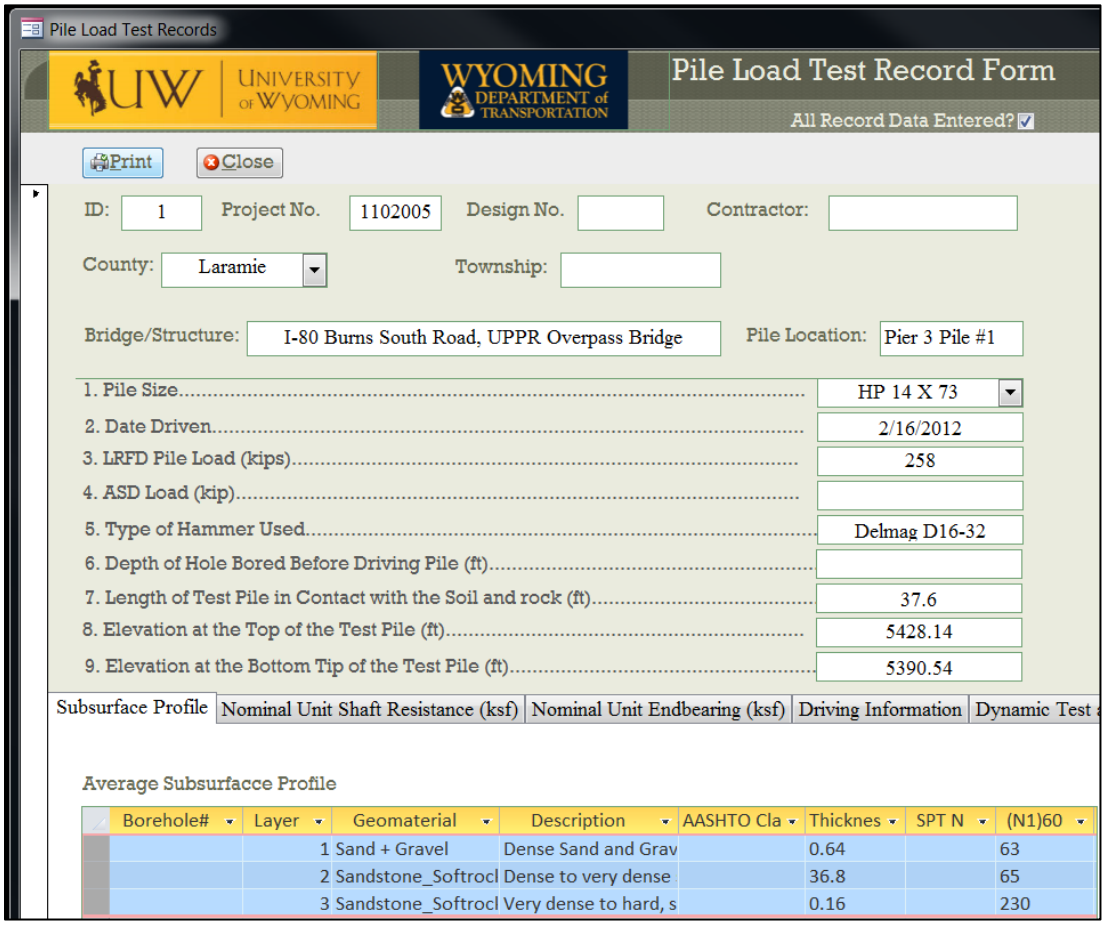

Source: Gebreslasie (2018)

Figure 16. Pile Load Test Record Form (PLTRF) for the first pile (ID 1).

3.3.1 Fields in the "Pile Load Test Records" table

Figure 17 shows the screenshot of some fields in the "Pile Load Test Records". The descriptions of all the fields in "Pile Load Test Records" are presented below.

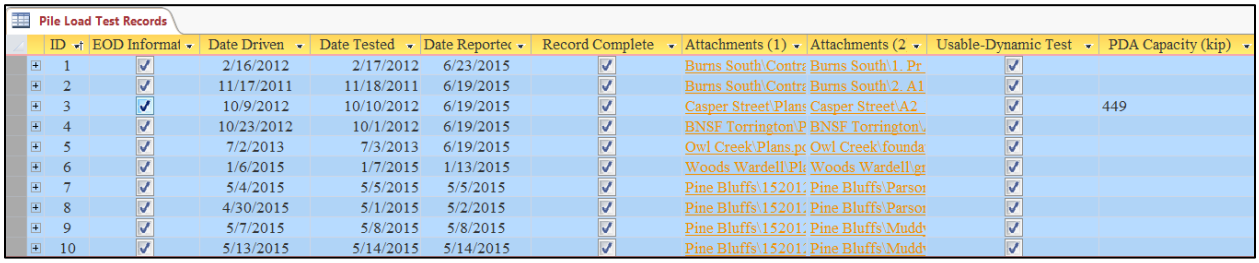

Pile Load Test Records

ID	EOD Informat	Date Driven	Date Tested	Date Reporte	Record Complete	Attachments (1)	Attachments (2	Usable-Dynamic Test	PDA Capacity (kip)
1	☑	2/16/2012	2/17/2012	6/23/2015	☑	Burns South\Contra	Burns South\1_Pr	☑	
2	☑	11/17/2011	11/18/2011	6/19/2015	☑	Burns South\Contra	Burns South\2_A1	☑	
3	☑	10/9/2012	10/10/2012	6/19/2015	☑	Casper Street\Plans	Casper Street\A2_	☑	449
4	☑	10/23/2012	10/1/2012	6/19/2015	☑	BNSF Torrington\P	BNSF Torrington\	☑	
5	☑	7/2/2013	7/3/2013	6/19/2015	☑	Owl Creek\Plans.pc	Owl Creek\founda	☑	
6	☑	1/6/2015	1/7/2015	1/13/2015	☑	Woods Wardell\Pla	Woods Wardell\gi	☑	
7	☑	5/4/2015	5/5/2015	5/5/2015	☑	Pine Bluffs\15201	Pine Bluffs\Parso	☑	
8	☑	4/30/2015	5/1/2015	5/2/2015	☑	Pine Bluffs\15201	Pine Bluffs\Parso	☑	
9	☑	5/7/2015	5/8/2015	5/8/2015	☑	Pine Bluffs\15201	Pine Bluffs\Mudd	☑	
10	☑	5/13/2015	5/14/2015	5/14/2015	☑	Pine Bluffs\15201	Pine Bluffs\Mudd	☑	

Source: Gebreslasie (2018)

Figure 17. Screenshot of the "Pile Load Test Records" table.

- **ID:** A unique cataloging number (Primary Key) automatically assigned by Microsoft Office Access® to each record within WyoPile.
- **Contractor:** The name of the contracting company responsible for the construction of the specified bridge project including driving of the test pile.
- **County:** This database field utilizes a drop-down menu for simple selection of the Wyoming County in which the specified bridge construction project is located.
- **Township:** This field allows one to manually enter the name of the township corresponding to the location of the specified Wyoming bridge construction project.
- **Bridge/Structure:** This field allows one to manually enter the name of the bridge or other structure of which the pile is a part.
- **Pile Location:** This field allows one to manually enter a short description of the test pile location in relation to the features of the bridge under construction (at abutments or at piers).
- **Pile Type:** This field utilizes a drop-down menu for simple selection of the test pile type and size. Steel H-Piles (from 10×42, 10×57, 12×53, 12×74, 14×73, 14×89, and Steel H – a generic option that may be utilized for instances where the exact Steel H pile size is unknown), Monotube Piles, Steel Pipe Piles (10", 12", 16", and 18" outside diameter), and Timber Piles (18', 20', 25', 30', 34', 35', 40', 45', 50', 55', and 60' length or Timber – a generic option that may be utilized for instances where the exact timber pile length is unknown).
- **Tested By:** Manually entered text names of those people/company who were responsible for the load test on the specified pile.
- **Date Tested:** Date on which the pile load test for the specified pile was conducted (formatted to accept date entries).
- **Date Reported:** Date on which the pile load test results for the specified pile were reported to the WYDOT.
- **Date Driven:** The date on which the specified test pile was driven.
- **LRFD Pile Load (kip):** This database field specifies the total sum of all design loads for which any given pile in the structure is anticipated to support based on the superstructure loading evaluation. In other words, the given pile must possess a bearing capacity equal to or greater than this value to ensure the safety of the structure.

- **Type of Hammer Used:** This database field contains information about the type of hammer used for driving the test pile. Examples of possible entries into this database field include: MVE M-19, IHC S-35, and Delmag D16-32
- **Initial borehole depth (ft):** The depth, in feet, of the hole bored to initiate pile driving of the specified test pile. (A value of zero in this field indicates that no hole was bored prior to driving.)
- **Pile embedment at EOD (ft):** The length, in feet, of the test pile in direct contact with the soil.
- **Pile Toe Elevation (ft):** The elevation, in feet, at which the toe of the driven test pile resides with reference to the mean sea level datum.
- **Attachments:** Six hyperlink database fields were created so that important information related to each pile load test could be easily accessed. The hyperlinked text descriptions found within these database fields maintain a direct path to the file of interest.
- **Record complete?:** This yes/no database field was created mostly for the one(s) responsible for the data entry procedures, so that an easy distinction could be made between those records still requiring data to be entered and those that had been termed complete. When all available information has been entered for a specific record, this field receives a check mark.
- **Usable dynamic test:** This database field receives a checkmark when the PDA device is used to monitor the installation of the test pile, which must be instrumented with accelerometers and strain transducers near the pile head, and assess its bearing capacity at either the EOD or BOR conditions; otherwise, this database field is left unchecked.
- **EOD Date/Time:** In this database field, which has been formatted to accept dated entries of the form: Month/Day/Year Time-of-Day (e.g., 1/9/2015 11:15:45AM), the date and time at which the EOD condition was achieved is input.
- **EOD PDA Capacity (kips):** The maximum static pile capacity estimate, in units of kips, provided by PDA at the EOD (i.e., RMX).
- **First Restrike Date/Time:** In this database field, which has been formatted to accept dated entries of the form: Month/Day/Year Time-of-Day (e.g., 1/9/2015 11:15:45AM), the date and time corresponding to the beginning of the first restrike are added.
- **First Restrike PDA Capacity (kips):** This field represents the maximum static pile capacity estimate, in units of kips, provided by PDA at the beginning of the first restrike (i.e., RMX).
- **Second Restrike Date/Time:** In this database field, which has been formatted to accept dated entries of the form: Month/Day/Year Time-of-Day (e.g., 1/9/2015 11:15:45AM), the date and time corresponding to the beginning of the second restrike are inserted.
- **Second Restrike PDA Capacity (kips):** This field represents the maximum static pile capacity estimate, in units of kips, provided by PDA at the beginning of the second restrike (i.e., RMX).

3.3.2 Subsurface Profile

This is the first tab of the PLTRF which summarizes information on the detailed layer-wise description of the geomaterials, along with their parameters at the pile location. The geomaterial information displayed on this tab is called from the information entered in different fields of the "Average Subsurface Profile" source table. The tab (or the source table) stores information on

material description, thickness, average SPT blow count, unit weight, cohesion, friction angle, uniaxial compressive strength, and rock quality designation (RQD).

3.3.3 Nominal Unit Shaft Resistance (ksf)

This second tab of the PLTRF as shown in Figure 18 stores layer-wise nominal unit shaft resistances of the pile as estimated using the five SA methods (α-, β-, SPT, λ- and Nordlund), and the measured shaft resistance using CAPWAP.

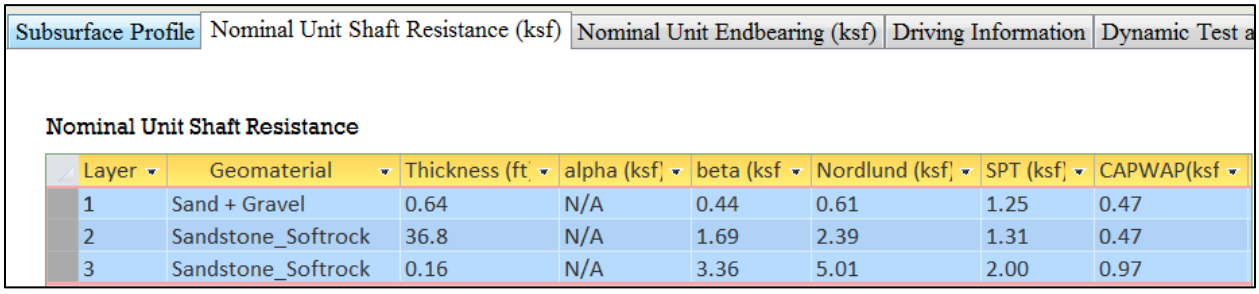

Source: Gebreslasie (2018)

Figure 18. Screenshot of the "Nominal Unit Shaft Resistance" tab of the PLTRF.

3.3.4 Nominal Unit End Bearing (ksf)

This tab of the PLTRF as shown in Figure 19 provides nominal unit end bearing of the pile as estimated by the four SA methods (α-, β-, SPT, and Nordlund), and the measured shaft resistance using CAPWAP.

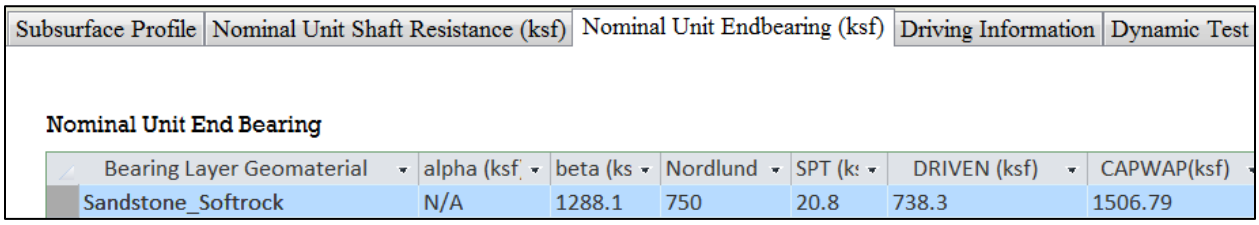

Source: Gebreslasie (2018)

Figure 19. Screenshot of the "Nominal Unit End Bearing" tab of the PLTRF.

3.3.5 Driving Information

This tab holds the driving system information, such as the weight of hammer ram, cushion thickness, hammer strokes at EOD and BOR, transferred hammer energy, and driven pile length, which is necessary for conducting drivability analysis and bearing graph analysis using the WEAP (Figure 20).

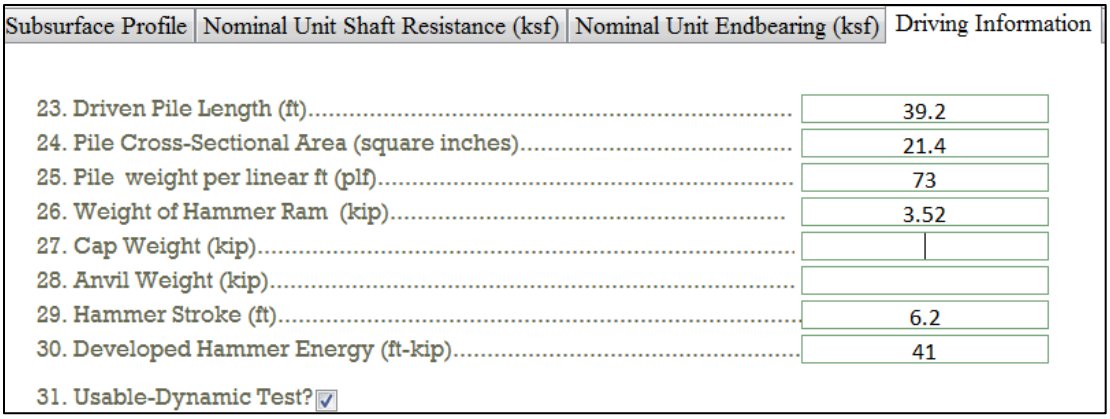

Source: Gebreslasie (2018)

Figure 20. Screenshot of the "Driving Information" tab of the PLTRF.

3.3.6 Dynamic Test and Analysis Results:

This tab stores information on observed blow counts at EOD and restrikes required for the bearing graph analysis from WEAP. It further houses information on the predicted resistance using WEAP, resistances (total, shaft, and end bearing) measured using CAPWAP and PDA, and dates of driving and restrikes (Figure 21).

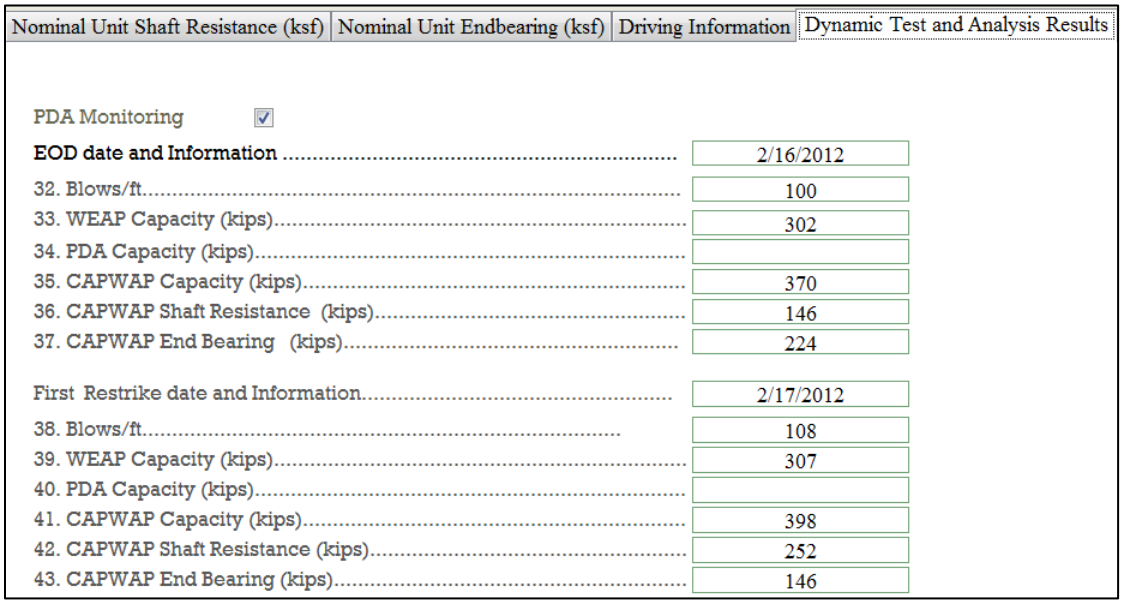

Source: Gebreslasie (2018)

Figure 21. Screenshot of the "Dynamic Test and Analysis Results" tab of the PLTRF.

3.3.7 Static Load Test Results:

This tab was built in PLTRF to facilitate the addition of SLT results conducted on future piles. It stores information on the load, displacement, and measured pile capacity in accordance with Davisson's failure criterion (Davisson 1972), as shown in Figure 22.

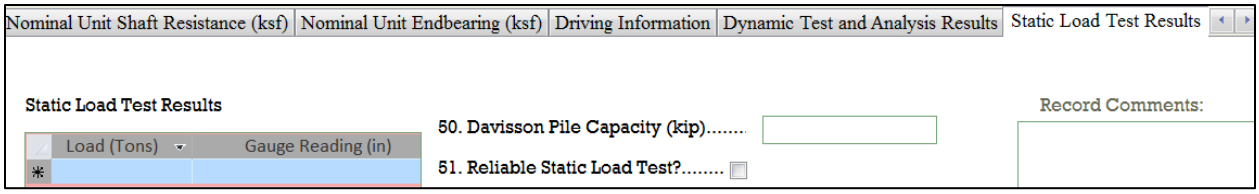

Source: Gebreslasie (2018)

Figure 22. Screenshot of the "Static Load Test Results" tab of the PLTRF.

3.4 Disclaimer

WyoPile was established as part of a research project, "Development of Load and Resistance Factor Design Procedures for Driven Piles on Soft Rocks in Wyoming", funded by the Wyoming Department of Transportation (WYDOT). Neither WYDOT nor the research team of this report make any warranty, expressly or implicitly, or assumes any legal liability or responsibility for the accuracy, completeness, or usefulness of any information contained in WyoPile. If a problem arises during the usage of WyoPile or if more knowledge is required, contact those currently maintaining the database at the WYDOT.

CHAPTER 4. GEOMATERIAL CLASSIFICATION CRITERIA ALONG WITH THE IGM CATALOG OF WYOMING

4.1 Introduction

Static analysis (SA) methods are commonly used to estimate axial pile capacity (resistance) and pile length during the design stage for preparing bidding documents. Due to the absence of readily available SA methods for estimating axial pile resistances in intermediate geomaterials (IGMs), existing SA methods with empirically developed design coefficients for soils are being applied to IGMs, whose strength and compressibility lie in between soils and hard rocks. Being empirical in formulation, the reliability of SA methods in pile length and capacity estimation is highly dependent upon the similarity of the geomaterials and the piles being used. However, IGMs exhibit high variability in density, hardness, and strength deviating from soil-like to rock-like behavior. The structural limit state, based on the buckling failure mode, governs the axial capacity (compressive resistance) of piles driven in hard rocks, while the geotechnical capacity, based on the geomaterial properties, governs the strength limit state design of piles in soils (AASHTO 2017). Thus, by treating IGMs as soils in SA, it can result in unreliable pile estimations. A recent research study by Ng and Sullivan (2017b), using 15 steel H-piles driven in IGM in Wyoming, concluded that existing SA methods resulted in inconsistent and conservative estimation of pile resistances in IGMs. Such conservative estimations often lead to construction challenges and management issues due to early pile refusal, pile overrun, and pile overstresses. Though a static load test program provides the most reliable estimation of pile capacity, it is not always economically justifiable. Thus, there is a need to improve pile resistance estimation in IGMs during the design stage. However, prior to the development of SA methods for IGMs, it is critical to first develop geomaterial classification criteria that enable systematic identification of IGMs from soils and hard rocks. The proposed geomaterial classification criteria will provide the foundation for future improvement and recalibration of SA methods for IGMs. It is expected that the combination of proposed geomaterial classification criteria and subsequent development of improved SA methods will alleviate the existing construction challenges associated with driven piles in IGMs.

IGMs have been generally defined, in AASHTO (2017), as materials having strength and compressibility in between soils and hard rocks. Past research studies have proposed different criteria for defining IGMs in terms of UCS and SPT N-value. Different values of UCS, given by Clarke and Smith (1992), the International Society of Rock Mechanics (de Freitas 1993), Johnston (1989), the Geological Society of London (de Freitas 1993), Gannon et al. (1999), and Akai (1997) have reflected the disparity associated with defining IGMs (Brooks 2008). For drilled shafts, IGMs have been classified as either cohesive materials with UCS values ranging between 10 to 100 ksf or cohesionless materials with SPT N-values corresponding to 60 percent hammer efficiency (N_{60}) lying between 50 and 100 (O'Neil and Reese 1999). Criteria proposed by various researchers are in less agreement as they have been introduced for different applications, such as tunneling, rippability, and geologic genesis (Santi and Doyle, 1997). There is currently no established definition to separate IGMs from hard rocks and soils for the design of driven piles. Local and regional experience is recommended by AASHTO (2017) for identifying IGMs and hard rocks. Thus, establishing criteria for classifying geomaterials, in terms of engineering parameters, is a first step towards overcoming existing design and construction challenges of driven piles in IGMs.

This chapter presents development of geomaterial classification criteria for driven piles using 28 historical driven pile datasets for bridge projects in Wyoming. Geomaterial descriptions, geomaterial properties, pile information, and the pile capacity from the CAPWAP program were used for developing the classification criteria. IGMs were categorized into IGM-soils and IGM-rocks to reduce the variation in material properties of IGMs, which ranged from hard soils to soft rocks. The term IGM-soils was used to indicate harder and stiffer soils while the term IGM-rocks was used to indicate rocks (solid aggregate of minerals) those were weaker and softer than hard rocks. A flowchart and design charts are presented to facilitate the classification of geomaterials into soils, IGM-soils, IGM-rocks, and hard rocks. The proposed classification aims to reduce current uncertainties associated with pile capacity estimation. Although the proposed criteria were developed based upon Wyoming data for steel H-piles, the methodologies described in this chapter can be adapted for other pile types to improve axial pile resistance estimations and to overcome construction challenges associated with piles in IGMs. Utilizing the developed geomaterial classification, a catalog (consisting of the geomaterial properties and respective pile resistances) is also presented that could aid designers in preliminary approximations.

4.2 Methodology

To develop the classification criteria, the geomaterials were first categorized into soil-based and rock-based geomaterials, based upon the geological description of the geomaterials given in the WYDOT geotechnical reports that reflect the local practice in the geomaterial identification. It is important to note that in the first classification step, soil-based geomaterials include both soils and IGM-soils, while rock-based geomaterials include both IGM-rocks and hard rocks. Next, two tasks were undertaken to define the borderline between soil and IGM-soil and the borderline between IGM-rock and hard rock.

Soil-based geomaterials were divided into cohesionless or cohesive geomaterials. Cohesionless geomaterials consisted of sands and gravels, which were classified as GW, SW, SP, GP, GM, SM, and SP-SM in accordance with the Unified Soil Classification System (USCS). Cohesive geomaterials comprised only of low plasticity silts (ML) as there was not enough data in clay and high plasticity silts. The Nordlund (1963) method and β-method by Esrig and Kirby (1979) were used for estimating unit shaft resistances in cohesionless geomaterials. Unit weight (γ) and internal friction angle (ϕ) are the two main geomaterial properties required for the estimation of unit shaft resistances in both β- and Nordlund methods. These geomaterial properties obtained from WYDOT reports were either laboratory measured or taken from tables developed by WYDOT based on historical test data. The β coefficients used in the β-method for the determination of unit shaft resistance were referred from Fellenius (1991) with a maximum friction angle of 45°. As the friction angles of soil-based geomaterials corresponding to dense sand and gravels were within 45°, Fellenius (1991) chart was adequate. For the Nordlund method, several charts were referred from Hannigan et al. (2006) to determine the lateral earth pressure (K_δ), correction factor (C_F) for K_δ, and ratio of friction angle between pile and soil to soil friction (δ/ϕ). However, extrapolation was done to determine K_δ of geomaterials exceeding 40°. Extrapolation was not needed on other coefficients. Cohesionless IGM-soils were differentiated from cohesionless soils based on the performance of SA methods consisting of the Nordlund and the β-method, using the coefficient of variation (COV) of resistance biases (ratio

of CAPWAP to predicted pile resistances). Cohesive IGM-soils were differentiated based on unit shaft resistances measured from CAPWAP.

Since SA methods are not available for predicting pile capacity in hard rocks, the same approach could not be used for differentiating IGM-rocks from rock-based geomaterials. When piles are driven into hard rocks, the pile material is likely to fail prior to the failure of the hard rock. Thus, the axial pile capacity in hard rocks will be governed by its structural compressive strength. This design philosophy was utilized in developing a criterion to differentiate IGM-rock and hard rock.

4.3 Classification for Cohesionless IGM-Soils from Soil-based Geomaterials

The $(N_1)_{60}$ values for the cohesionless geomaterials ranged from 10 to 439. Uncorrected SPT N-value as high as 448 was reported by WYDOT for dense to very dense sandy gravel with cobbles and boulders. $(N_1)_{60}$ and was chosen to classify cohesionless IGM-soils from soil-based geomaterials since SPT is the most widely used in-situ test method. The classification approach was established by comparing uncertainties in COV of shaft resistance biases as a function of $(N_1)_{60}$ for two SA methods, the Nordlund method and the β-method. The shaft resistance biases from both the SA methods is presented in Table 9. The uncertainties were measured for shaft resistance estimations to have considerable data for analysis. A driven pile could be installed into multi-geomaterial layers with different $(N_1)_{60}$ values to yield different unit shaft resistances. A total of 35 unit shaft resistance values from each SA method were determined for the classification study by considering all cohesionless soil-based geomaterial layers along the shaft of 28 driven piles.

Shaft layers with $(N_1)_{60}$ values ranging from 10 to 439 were reduced by excluding the shaft layer with the maximum $(N_1)_{60}$ value from each analysis cycle to produce next datasets for subsequent analyses. The COVs of resistance biases were then determined for the different datasets for both Nordlund and β-methods, and compared to the respective maximum $(N_1)_{60}$ values. These values are plotted in Figure 23. To clarify the analysis process, we considered a dataset that initially consisted of 35 shaft layers with the maximum $(N_1)_{60}$ of 439 in the first analysis cycle. The COV of resistance biases from β-method for the 35 layers was calculated as 1.96 and plotted against the maximum $(N_1)_{60}$ of 439 in Figure 23. In the second analysis cycle, the geomaterial layer having $(N_1)_{60}$ of 439 was eliminated from the previous dataset to form a new usable dataset consisting of the remaining 34 shaft layers with a maximum $(N_1)_{60}$ of 262. The COV of resistance biases for the remaining shaft resistances was 1.97 and plotted against the maximum $(N_1)_{60}$ of 262 in Figure 23. Similarly, the analysis was repeated in subsequent cycles until the maximum $(N_1)_{60}$ of the dataset reached 29 for both SA methods, because the boundary between soils and IGM-soils was unlikely to occur below $(N_1)_{60}$ of 29. For the Nordlund method, the higher COV group was around 1.85, while the lower COV group was around 0.8. Likewise, the higher and lower COV groups for the β-method were about 2 and 0.85, respectively. In both methods, the lower COV groups were obtained from datasets with $(N_1)_{60}$ values less than 49, while the higher COV groups were obtained from datasets with $(N_1)_{60}$ values greater than 55. As friction angles and unit weights used for shaft resistance estimation were not correlated from N-values, the higher COV reflects the limitation of current SA methods developed based on soil database in the shaft resistance estimation in cohesionless IGM-soil with $(N_1)_{60}$ greater than 49 to 55. Understanding the priority of geometerial classifications for the future development of SA

methods for IGM, $(N_1)_{60}$ of 50 was recommended as the boundary separating cohesionless soils and IGM-soils for the cohesionless soil-based geomaterials.

Table 9. Estimated and measured unit shaft resistances of 35 geomaterial layers.

Pile ID	Layer	$(N_1)_{60}$	ϕ (deg)	$(q_s)_\beta$	$(q_s)_N$	$(q_s)_C$	$(q_s)_C/(q_s)_\beta$	$(q_s)_C/(q_s)_N$
1	1	63	33	0.44	0.61	0.69	1.57	1.13
2	1	22	29	0.49	0.53	0.19	0.39	0.36
2	2	16	29	1.04	1.14	0.25	0.24	0.22
2	3	35	33	1.39	1.75	0.25	0.18	0.14
3	0	12	30	0.51	0.54	0.45	0.88	0.83
4	1	12	30	2.20	2.68	0.32	0.15	0.12
5	1	16	32	0.21	0.30	0.42	2.00	1.40
8	2	13	36	1.63	2.01	0.54	0.33	0.27
8	3	29	37	3.18	4.05	0.99	0.31	0.24
9	1	10	38	0.70	0.88	0.44	0.63	0.50
10	1	34	34	0.45	0.55	0.53	1.18	0.96
14	1	27	36	0.57	0.69	0.26	0.46	0.38
14	2	11	33	1.29	1.64	1.13	0.88	0.69
15	1	26	36	0.61	0.75	0.42	0.69	0.56
15	2	10	33	1.35	1.72	1.26	0.93	0.73
16	1	55	32	0.24	0.34	2.52	10.5	7.41
17	1	11	29	0.74	0.85	0.13	0.18	0.15
17	2	12	32	2.34	2.82	0.33	0.14	0.12
18	1	11	29	2.06	0.81	0.062	0.03	0.08
18	2	11	32	2.65	3.20	0.31	0.12	0.10
19	1	44	29	0.50	0.60	0.22	0.44	0.37
19	2	29	29	1.19	1.38	1.52	1.28	1.10
20	1	210	34	0.34	0.42	0.77	2.26	1.83
21	1	59	34	0.71	0.96	0.35	0.49	0.36
22	1	20	30	0.26	0.29	0.16	0.62	0.55
22	2	123	33	0.93	1.26	0.44	0.47	0.35
26	1	82	43	1.29	1.99	0.18	0.14	0.09
27	1	79	30	0.56	0.64	0.25	0.45	0.39
27	2	439	45	2.73	2.73	1.74	0.64	0.64
28	1	49	35	0.62	0.79	0.23	0.37	0.29
28	2	71	45	2.15	2.15	1.93	0.90	0.90
39	1	20	32	0.82	1.12	0.35	0.43	0.31
41	1	34	36	1.00	1.32	0.31	0.31	0.23
43	1	143	45	1.71	3.60	0.34	0.20	0.09
43	2	262	45	3.01	5.44	1.56	0.52	0.29

ϕ- internal angle of friction; $(q_s)_\beta$- unit shaft resistance estimated from the β-method; $(q_s)_N$- unit shaft resistance estimated from the Nordlund method; and $(q_s)_C$- unit shaft resistance measured from CAPWAP.

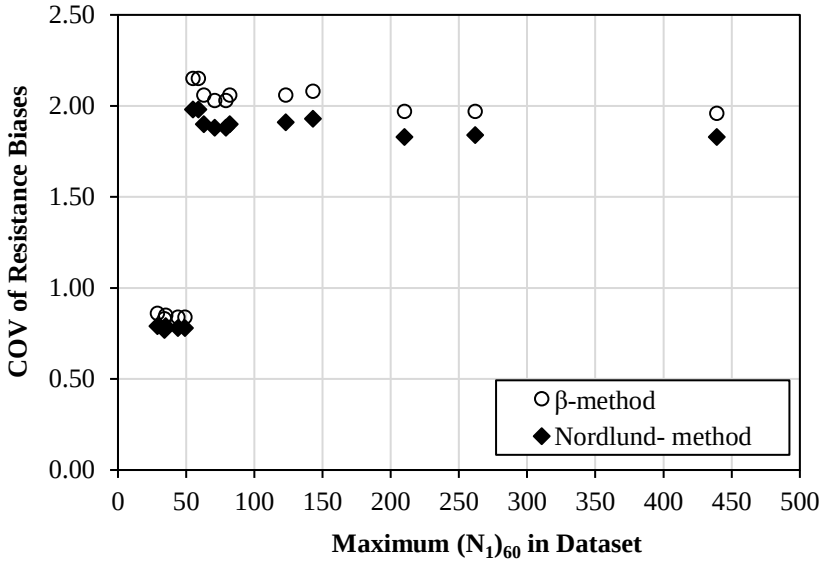

Source: Adhikari (2019)

Figure 23. Comparison of COV and maximum $(N_1)_{60}$ for both the β-method and the Nordlund method.

4.4 Classification for Cohesive IGM-Soils from Soil-based Geomaterials

To classify cohesive soils from cohesive soil-based geomaterials, the unit shaft resistances obtained from the CAPWAP analysis were plotted against their respective undrained shear strength (s_u) values, as shown in Figure 24. It is observed that geomaterials with s_u less than 2.7 ksf have unit shaft resistance less than 1 ksf. Likewise, geomaterials with s_u greater than 2.7 ksf exhibited unit shaft resistances greater than 1 ksf. Hence, an s_u value of 2.7 ksf is recommended to separate cohesive soils from cohesive IGM-soils.

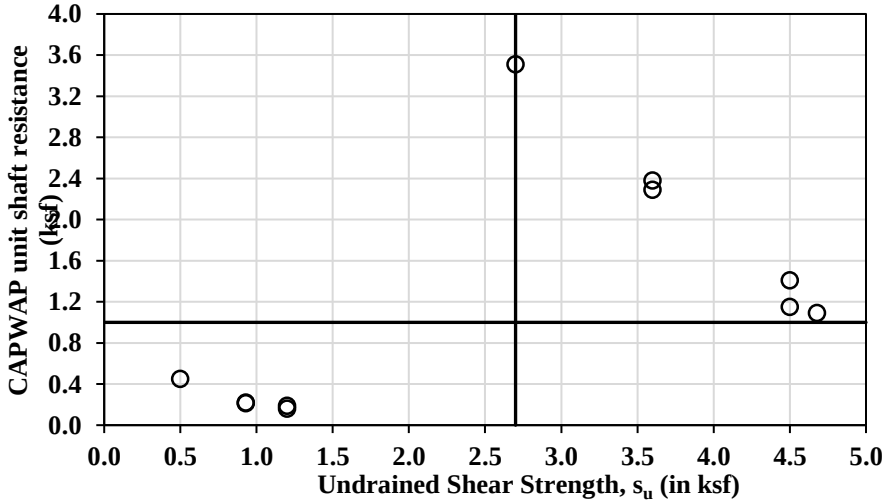

Source: Adhikari (2019)

Figure 24. Comparison of S_u and unit side resistances from CAPWAP.

4.5 Classification for IGM-Rocks from Hard Rocks

The terminology "IGM-Rocks" is adopted to identify geomaterials that have been defined geologically as rocks but are not strong enough to induce failure of the pile material before the bearing failure of the geomaterial. The nominal pile capacity in hard rock shall not exceed the nominal structural compressive strength of the pile (P_n), which depends upon the mode of buckling, either flexural, torsional, or flexural-torsional buckling. Flexural buckling was selected for steel H-piles, while the torsional buckling was neglected due to torsional constraints from the surrounding geomaterial. The P_n of each pile can be determined by Equations (24) through (27) (AASHTO 2017).

$$P_n = \left[0.658^{\left(\frac{P_o}{P_e}\right)}\right] P_o \qquad \text{if } \frac{P_e}{P_o} \geq 0.44 \tag{24}$$

$$P_n = 0.877 P_e \qquad \text{if } \frac{P_e}{P_o} < 0.44 \tag{25}$$

$$P_e = \frac{\pi^2 E}{\left(\frac{KL}{r_s}\right)^2} A_g \tag{26}$$

$$P_o = Q F_y A_g \tag{27}$$

where,

P_e = the elastic critical buckling resistance,
A_g = the gross cross-sectional area of the pile,
K = the effective length factor in the plane of buckling,
L = the unbraced length in the plane of buckling,
r_s = the radius of gyration about the axis normal to the plane of buckling,
P_o = the equivalent nominal yield resistance,
Q = the slender element reduction factor which is equal to 1 for piles without slender elements, and
F_y = the specified minimum yield strength of a steel pile.

The contribution of the surrounding soil to the bracing of a driven pile has yet been fully investigated. However, in this study, piles were assumed fully embedded in the soil, and the unbraced length (L) was assumed zero following the design procedures by Hartle et al. (2003). Furthermore, Tscheotarioff (1973) indicated that the surrounding soil provides an adequate lateral support against buckling. However, nonzero unbraced length in fully embedded soils can be investigated in the future by considering depth to fixity, in addition to laterally unsupported length for unbraced length determination. Rigorous P-Δ analysis can be performed to determine the axial compressive strength in the structural limit state of piles (AASHTO 2017), which can be incorporated into the proposed framework for IGM-rock classification. In the current study, factored compressive strength was considered to account for the assumed zero unbraced length of fully embedded piles, and Equation (24) is adopted for the determination of P_n ,since the ratio $\frac{P_e}{P_o}$ is greater than 0.44. With zero unbraced length in Equation (26), P_e becomes infinitely large and the ratio $\frac{P_o}{P_e}$ approaches zero leading P_n of the H-pile, without slender elements (i.e., Q = 1), to depend on the yield strength of the steel and cross-sectional area of the pile.

The strength limit state governing the axial pile capacity changes from geotechnical factor (depending upon geomaterial properties) to structural factor (depending upon structural compressive strength) when the geomaterials change from IGM-rocks to hard rocks. Therefore, the boundary differentiating IGM-rocks from hard rocks was established by limiting the factored geotechnical resistance to the factored compressive strength of a pile. For the Load and Resistance Factor Design (LRFD) limit state criterion, the factored load is equated to the factored resistance, so that the maximum factored load that a pile driven into hard rocks can sustain is the factored compressive strength of the pile.

Toe resistance (R_P) also contributes to the total resistance of a pile driven into hard rocks. The percent contribution, depending on the shaft resistance of geomaterials along the pile, was considered in the determination of the boundary based on UCS values, which can be conveniently determined in a laboratory and are widely used for describing rock compressive strength. The calculation procedure to determine the boundary UCS is described as follows:

1. Factored toe resistance ($\varphi_P R_P$) is obtained by considering factored pile compressive strength distributed to the pile tip as

$$\varphi_P R_P = \text{percent toe resistance} \times \text{factored pile compressive strength} \quad (28)$$

$$\varphi_P R_P = \text{percent toe resistance} \times 0.6 P_n \quad (29)$$

where,

R_P = the toe resistance,

φ_P = the resistance factor corresponding to toe resistance, and

0.6 = the resistance factor used for the axial capacity of H-piles in compression without bending.

2. The factored unit toe resistance ($\varphi_P q_p$) of a pile on hard rocks is expressed as $\frac{\varphi_P R_P}{\text{Box toe area}}$. Box toe area is reasonably suggested because plugging was determined in nine of the 11 pile cases from the CAPWAP analysis.

3. Since the structural compressive strength of a pile is considered as the maximum load, the factored unit toe resistance, obtained in step 2 using the method described in step 1, is the distributed load at the pile toe. This step consists of determining the factored unit toe resistance considering the geotechnical resistance. For geotechnical axial resistance, the factored unit toe resistance ($\varphi_P q_p$) was determined using equations, recommended for drilled shafts, in terms of UCS of rocks. For intact rock, the unit toe resistance (q_p) was recommended by Rome and Armitage (1987) as 2.5 times UCS ($2.5 \times q_u$). The determination of q_p based on 2.5 times of UCS is also justifiable for driven piles, due to the effect of confinement from surrounding rocks to the compressive strength. For fractured rock masses, Carter and Kulhawy (1988) substituted the minor principal stress (confinement) in the Hoek-Brown (1988) strength criterion with $q_u\sqrt{s}$, where s is the fractured rock mass parameter, and recommended Equation (31) for the determination of q_p. Though Equation (31) was developed for shallow foundation on rock, it could be extended to driven piles as similarly applied to drilled shafts (AASHTO 2017). Fractured rocks underneath the driven pile tip are expected to experience the same general shear failure mode. Equation (31) yields the lower bound of the unit toe resistance as the vertical stress

was assumed zero outside the foundation footprint. Since both q_p equations were developed based on the strength parameters of rocks, regardless of the foundation types, these equations were used to determine $\varphi_p q_p$ as follows:

$$\varphi_p q_p = 2.5 \times q_u \times 0.5 \text{ (for intact rocks with RMR} \geq 85) \quad (30)$$

$$\varphi_p q_p = \left[\sqrt{s} + \sqrt{(m\sqrt{s} + s)}\right] q_u \times 0.5 \quad (31)$$

where,

q_u = the UCS defining hard rocks,

RMR = the rock mass rating, and s and m are the fractured rock mass parameters depending on the RMR values (Hoek and Brown 1988).

Thus, the influence of spacing and weathering of discontinuities, along with rock lithology, was accounted for in the determination of toe resistance of fractured rock masses. An RMR value of 85 has been proposed to represent the very good quality rock mass with unweathered joint spacings from three to 10 ft (Hoek and Brown 1988). These joint spacings are at least three times the maximum steel H-pile dimension of 14 in and the bearing failure zone can lie within the joint spacings. Thus, rocks with RMR $\geq$ 85 can be treated as intact. This joint spacing criterion is also in agreement with CFEM (2006) in which the rock mass is considered sound if the joint spacing is greater than one foot for the determination of pile resistance. To account for the uncertainties associated with the q_p estimations using Equations (30) and (31), the resistance factor (φ_p) of 0.5, recommended by AASHTO (2017), for drilled shafts has been assumed for the driven piles in this study. The resistance factor of 0.5 is higher compared to the resistance factors used in existing SA methods for driven piles. However, the resistance factor is lower than that for the CAPWAP and static load tests. Future studies could be performed to revise this φ_p value for specific pile data sets. To define the boundary between IGM-rock governed by the geotechnical resistance and hard rock governed by the structural capacity, the limiting q_u values were back-calculated so that the limiting q_u in Equation (30) was replaced by q_{usi} for intact rocks, while q_u in Equation (31) was replaced by q_{usf} for fractured rock masses.

4. Combining Steps 1 through 3, the back-calculated q_{usi} for intact rocks and the q_{usf} for fractured rock masses are given by Equation (32) and Equation (33), respectively, to differentiate IGM-rock from hard rocks:

$$q_{usi} = \frac{\text{percent toe resistance} \times P_n \times 0.6}{2.5 \times 0.5 \times \text{Box toe area}} \text{ (for intact rocks with RMR} \geq 85) \quad (32)$$

$$q_{usf} = \frac{\text{percent toe resistance} \times P_n \times 0.6}{\left[\sqrt{s} + \sqrt{(m\sqrt{s}+s)}\right] \times 0.5 \times \text{Box toe area}} \text{ (for fractured rock masses with RMR} < 85) \quad (33)$$

Equation (32) and Equation (33) show that both q_{usi} and q_{usf} values depend on the pile size, the nominal compressive strength of piles, and the percent toe resistance. The q_{usf} values also depend upon the fractured rock mass parameters (s and m) with respect to the RMR value. To facilitate the implementation of the proposed classification criteria, the q_{usi} values for three Grade 50, HP14×89, HP14×73, and HP12×53, are plotted against the percent toe resistances in

Figure 25. The q_{usi} value increases as the percentage toe resistance increases. A stronger steel H-pile with a higher compressive capacity (P_n) requires a higher q_{usi} value for differentiating IGM-rock from hard rock. The difference of the box toe areas and P_n of Grade 50 HP14×73 and HP12×53 piles are minimal as shown by the overlapping of q_{usi} values in Figure 25. The q_{usi} charts for Grade 50 HP14×89, HP14×73, HP12×74, HP12×53, and HP10×42 are included in Appendix A.

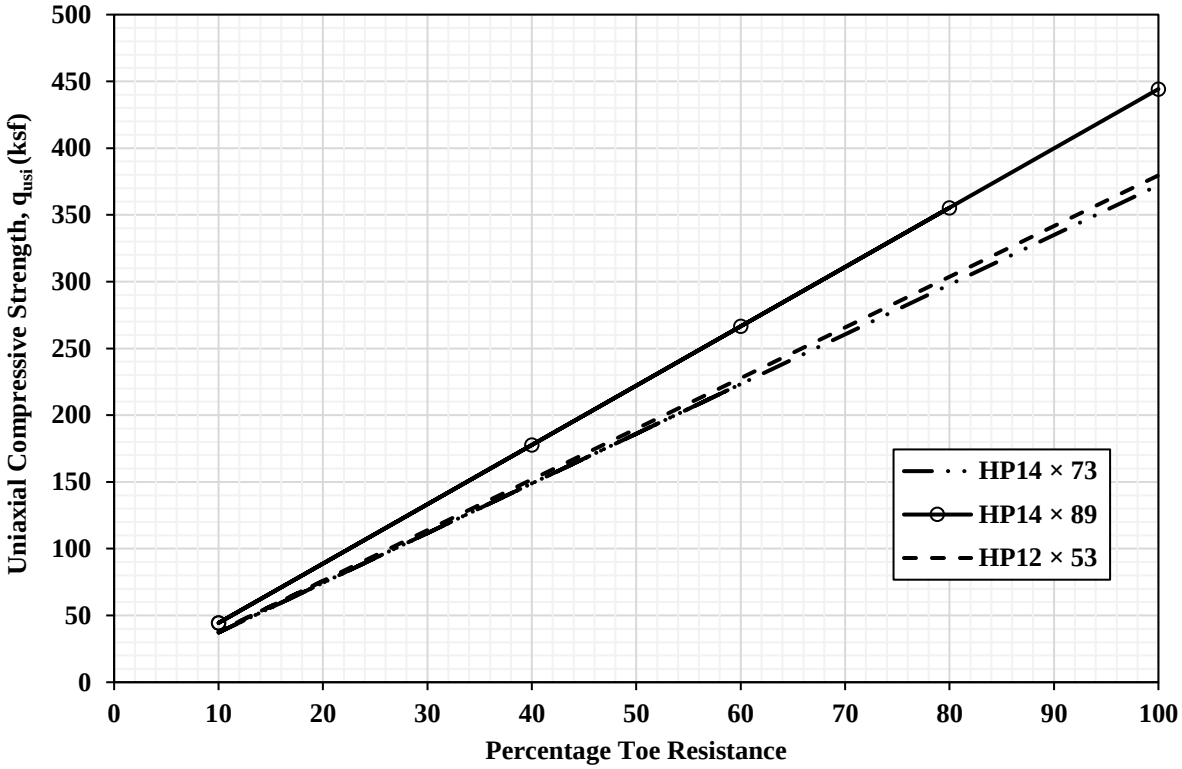

Source: Adhikari (2019)

Figure 25. Calculated q_{usi} values for intact IGM-rocks or hard rocks for three Grade 50 steel H-piles as a function of percent toe resistances.

Grade 50 HP14×73 was selected to illustrate the relationship between back-calculated q_{usf} values, RMR, and percent toe resistance (Figure 26). Since q_{usf} values depend on the rock mass parameters (s and m), Figure 26(a) presents argillaceous rock types, and Figure 26(b) present arenaceous rock types for the pile type selected. The enlarged chart for application purpose is included in Appendix. The results show that q_{usf} values increase with a decrease in RMR. High q_{usf} values are observed for fractured rocks with RMR less than 65. This observation implies that the pile capacity in moderately to heavily weathered rocks, with RMR less than 65, is unlikely to be governed by the pile compressive strength. Similar to q_{usi}, a higher q_{usf} value is observed for a pile with a higher percent toe resistance. The charts showing q_{usf} values for other pile types are included in Appendix B.

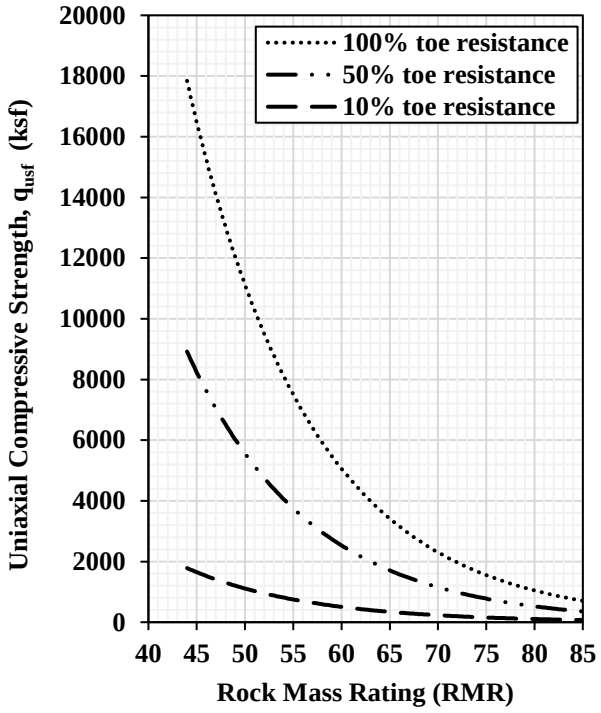

(a) Argillaceous Rocks

Source: Adhikari (2019)

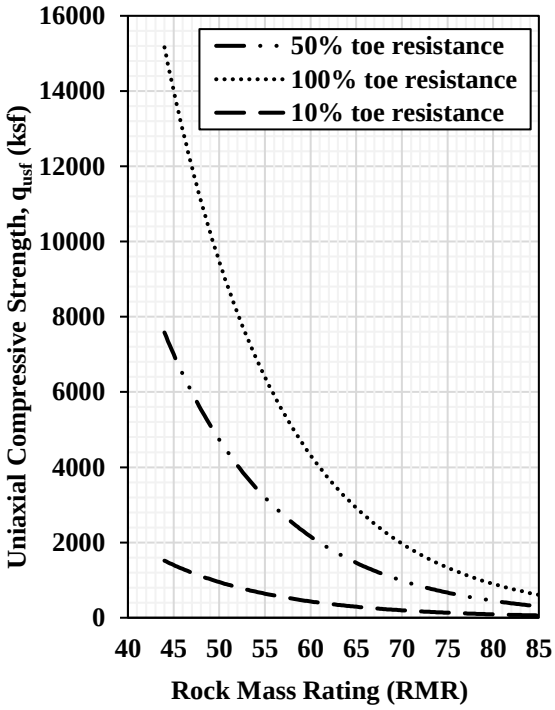

(b) Aranaceous Rocks

Source: Adhikari (2019)

Figure 26. Calculated q_{usf} values for two rock masses and Grade 50 HP14×73 steel pile as a function of RMR and percent toe resistances.

4.6 Estimation of Percent End Bearing

It is evident from Section 4.5 that the boundary uniaxial compressive strength values depend upon the percentage end bearing. A regression analysis based on 25 piles at the EOD revealed that the percentage end bearing can be related to embedded pile length and $\ln[(N_1)'_{60}]$, where $(N_1)'_{60}$ value is the weighted average of $(N_1)_{60}$ values of all overburden geomaterials. The data is presented in Table 10. Three piles among 28 piles at the EOD were excluded as SPT N-values were missing in some of the geomaterial layers. The scatterplot matrix produced in statistical program R consisting of end bearing, square of pile length, and $\ln((N_1)'_{60})$ is presented in Figure 27. The regression analysis was conducted between the $(N_1)'_{60}$, embedded pile length, and the percentage end bearing. Linear model is the best fit model between the percentage end bearing, square of pile length, and $\ln((N_1)'_{60})$ values with a coefficient of determination (R^2) of 0.56 and an adjusted R^2 of 0.52. The regression model for the percentage end bearing is given by

$$\text{Percentage end bearing} = 13.62 - 0.003\,(\text{embedded pile length})^2 + 12.78\ln((N_1)'_{60}) \quad (34)$$

Diagnostic plots of residuals were generated to assess the fitted model. After observing the diagnostic plot, one point was excluded as it showed high residual. The regression analysis was then conducted on the remaining 24 data points. A linear fit model, given by Equation (35), is the

best fit for the expected percentage end bearing in terms of pile length and $(N_1)'_{60}$ values with an R^2 of 0.70 and an adjusted R^2 of 0.67.

Percentage end bearing = $13.61 - 0.004$ (embedded pile length)^2 + $12.80 \ln ((N_1)'_{60})$

Table 10. Percentage toe resistances, weighted average $(N_1)_{60}$ values of overburden geomaterials, and pile length of 25 piles at EOD

Percentage toe resistance	Weighted average $(N_1)_{60}$ values of overburden geomaterial	Embedded pile length (ft)
60.54	65.67	37.6
79.8	28.09	68.3
44.12	59.26	24.1
37.66	12.00	20.5
15	11.00	99.2
61.12	21.39	27.0
53.41	39.38	23.0
17.78	25.03	87.9
28.47	23.71	75.2
26.27	11.89	53.6
31.06	49.95	35.3
46.22	25.89	38.0
45.47	14.81	46.7
36.73	14.78	46.9
50.78	18.14	44.7
47.54	17.39	46.4
46.59	20.16	41.2
75.51	210.00	19.5
77.97	59.00	35.9
80.68	111.35	45.0
48.38	112.66	69.0
71.56	183.31	41.0
75.57	55.74	32.0
59.54	34.00	40.0
82.71	135.15	40.0

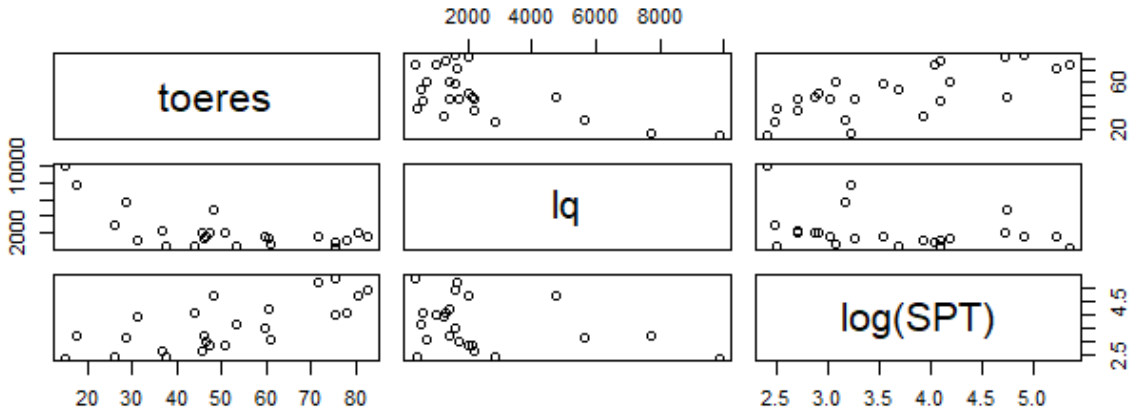

Figure 27. Scatterplot matrix between toe resistance, square of pile length (lq), and natural logarithm of weighted $(N_1)_{60}$ values of overburden geomaterials

4.7 Catalog of Wyoming IGM Properties

IGMs are often difficult to be sampled due to their underlying transitional behavior between soils and rocks. The existing correlations to determine geomaterial design parameters, such as undrained shear strength, internal friction angle, and unconfined compression strength from in-situ tests, were developed for soils. In the absence of established correlations to relate in-situ tests to the IGM properties, a catalog of site specific IGM properties and unit pile resistances can provide initial approximations for designers. Thus, the mean and range of geomaterial properties and CAPWAP measured unit pile resistances are summarized in Table 11 and Table 12 for shaft resistances and end bearing, respectively. The proposed geomaterial classification was utilized for categorizing the geomaterial properties. The geomaterial properties and unit pile resistances from nine additional piles obtained from WYDOT were also included along with the historical records from 28 driven piles to develop the catalog. These 37 piles are the piles with EOD records.

The catalog is based only on the measured geomaterial properties. Though 17 cohesive soils were observed in total, only 14 were used in catalog (Table 11) as three of the soils exhibited relatively high unit shaft resistances of 1.82, 1.33, and 2.38 ksf. The mean and range of the geomaterial properties are not based on the total number of observations for all geomaterials due to the unavailability of properties, rather they are calculated based on the available data.

Table 11. Catalog of geomaterial properties along the pile shafts of 37 piles and CAPWAP measured shaft resistances.

Soil							
Geomaterial	**n**	**q_s (ksf)**		**s_u (ksf)**		**$(N_1)_{60}$**	
		Mean	**Range**	**Mean**	**Range**	**Mean**	**Range**
Cohesionless	23	0.5	0.1-1.5	NA	NA	18	9-35
Cohesive	14	0.2	0.1-0.5	NA	NA	27	7-63
IGM-soil							
Geomaterial	**n**	**q_s (ksf)**		**S_u (ksf)**		**$(N_1)_{60}$**	
		Mean	**Range**	**Mean**	**Range**	**Mean**	**Range**
Cohesionless	11	1	0.18-2.52	NA	NA	132	55-439
Cohesive	8	1.63	1.09-3.59	NA	NA	26	7-61
IGM-rock							
Geomaterial	**n**	**q_s (ksf)**		**q_u (ksf)**		**$(N_1)_{60}$**	
		Mean	**Range**	**Mean**	**Range**	**Mean**	**Range**
Sandstone	6	1.5	0.5-2.7	155.57[1]	1.2-459[1]	178	22-579
Siltstone	8	2.8	1.5-4.6	74.06[2]	45.2-80.8[2]	68[*]	43-VH
Claystone	5	1.9	0.5-3.3	75[3]	75[3]	47[#]	29-VH
Shale	3	2.6	0.5-4.5	8.08[3]	8.08[3]	19	9-29
Breccia	2	0.9	0.6-1.2	NA	NA	154	154

q_s- CAPWAP measured unit shaft resistance; s_u- Undrained shear strength; q_u- Uniaxial compression strength; $(N_1)_{60}$- SPT N-value corrected for overburden and 60% hammer energy; [*]- Mean calculated based on 4 observations as remaining 4 had very high SPT N-values; [#]- Mean based on 2 observations as remaining available had very high SPT N- values; n- No. of observations of geomaterial; VH- Very high equivalent SPT N-values exceeding 500; 1- based on three observed values; 2- based on six observed values.3- based on single observed value.

Table 12. Catalog of geomaterial properties along the bearing layers of 37 piles and CAPWAP measured end bearing.

Soil							
Geomaterial	**n**	**q_p (ksf)**		**s_u (ksf)**		**$(N_1)_{60}$**	
		Mean	**Range**	**Mean**	**Range**	**Mean**	**Range**
Cohesionless	3	54	17-81	NA	NA	25	11-34
IGM-soil							
Geomaterial	**n**	**q_p (ksf)**		**S_u (ksf)**		**$(N_1)_{60}$**	
		Mean	**Range**	**Mean**	**Range**	**Mean**	**Range**
Cohesionless	4	217	177-261	NA	NA	164	59-262
Cohesive	5	138	77-223	NA	NA	33	14-61
IGM-rock							
Geomaterial	**n**	**q_p (ksf)**		**q_u (ksf)**		**$(N_1)_{60}$**	
		Mean	**Range**	**Mean**	**Range**	**Mean**	**Range**
Sandstone	7	189	106-292	155.57[1]	1.2-459[1]	231	36-579
Siltstone	12	261	56-551	74.06[2]	45.2-80.8[2]	58[*]	32-VH
Claystone	3	106	25-245	75[3]	75[3]	66[#]	66
Shale	2	152	149-153	8.08[3]	8.08[3]	9	9
Breccia	1	132	NA	NA	NA	17	NA

q_p- CAPWAP measured unit end bearing; s_u- Undrained shear strength; q_u- Uniaxial compression strength; $(N_1)_{60}$- SPT N-value corrected for overburden and 60% hammer energy; n- No. of observations of geomaterial; [*]- Mean calculated based on 8 observations as remaining 4 had very high SPT N-values; [#]- Based on single available value; VH- Very high equivalent SPT N-values exceeding 500; 1- based on three observed values; 2- based on six observed values.3- based on single observed value.

4.8 Recommendations

A classification flowchart is presented in Figure 28 and summarizesthe proposed geomaterial classification methodology to characterize geomaterials. Soil-based and rock-based geomaterials are differentiated based on the geological description. The soil-based geomaterials are further classified into cohesionless and cohesive geomaterials depending upon the USCS soil classification system. IGM-soils are classified as either cohesionless soil-based geomaterials having $(N_1)_{60}$ greater than 50 or cohesive soil-based geomaterials having s_u greater than 130 kPa (2.7 ksf).

The systematic procedure described in the following steps is recommended for classifying IGM-rocks and hard rocks:

1. The UCS value of rock samples, $(q_u)_{obs}$, will be determined from the uniaxial compressive test, and the RQD of the rock core will be determined from the site investigation.
2. Determine all five factors that contribute to the RMR calculation. These factors are UCS or point load strength index, RQD, joint spacing, joint condition, and ground water condition. A modified RMR calculation is recommended since all the factors required for the RMR calculation are difficult to obtain from a site investigation. The modified RMR calculation involves the observed values of RQD and $(q_u)_{obs}$ from Step 1 while using the maximum relative ratings for the remaining factors. Maximum relative ratings will yield a higher RMR value and a lower, or more conservative, limiting value for q_{usf}.
3. For intact rocks, with RMR greater than or equal 85, $(q_u)_{obs}$ will be compared to q_{usi} determined from Figure 25. For rock masses with RMR less than 85, $(q_u)_{obs}$ will be compared to q_{usf} determined from Figure 26.
4. If $(q_u)_{obs}$ is greater than or equal to either q_{usi} or q_{usf}, the rock-based geomaterial is classified as a hard rock. Otherwise, it is classified as IGM-rock.

The q_{usi} and q_{usf} charts presented in this chapter and Appendices are limited only to some steel H-piles. However, Equations (32) and (33) can be used to determine the required q_{usi} and q_{usf} for other steel H-piles. The q_u charts should be cautiously used for piles subjected to scour or different field conditions resulting in unbraced pile lengths. The proposed methodology can also be applied for developing geomaterial classification criteria for other pile types using the corresponding nominal compressive strength of the pile.

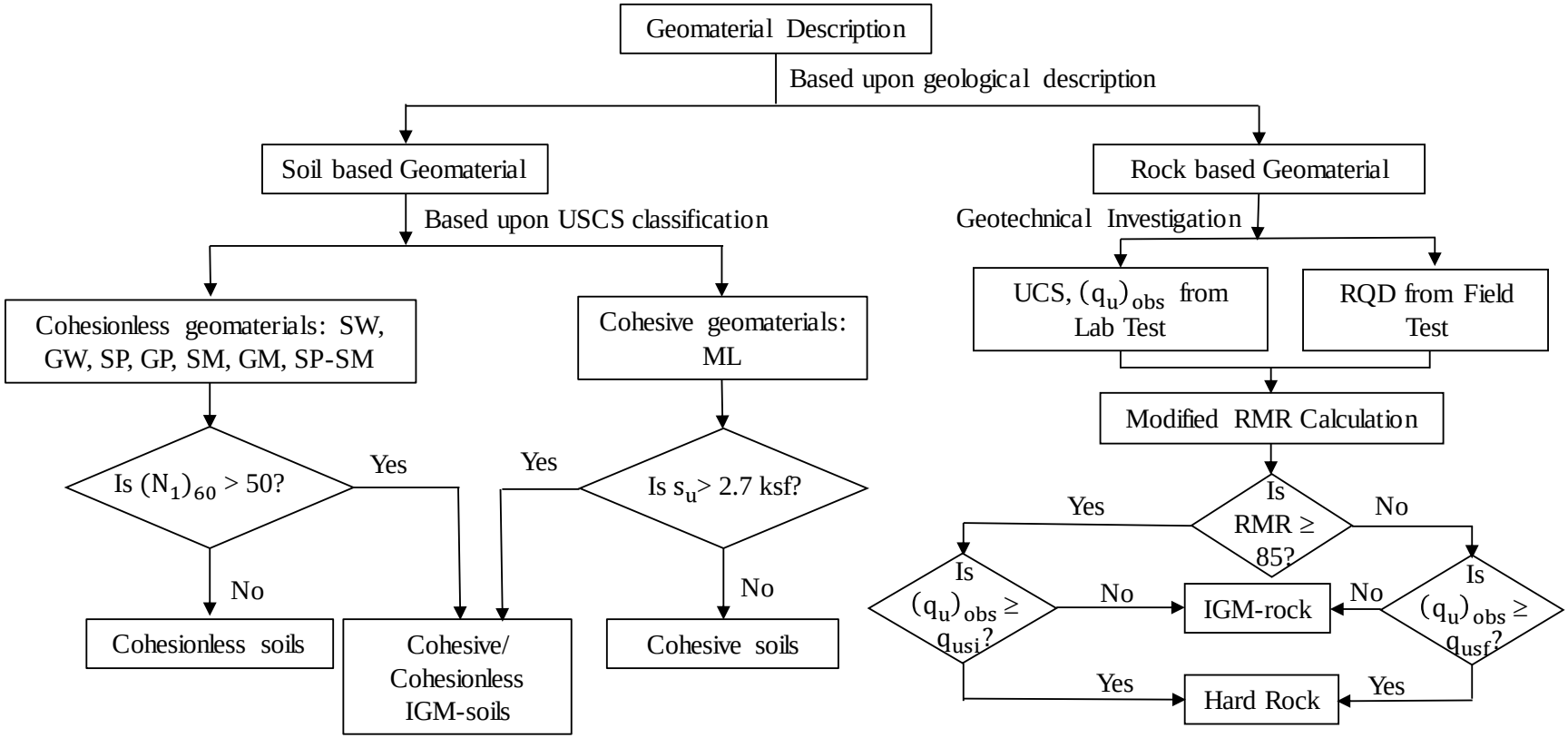

Source: Adhikari (2019)

Figure 28. Proposed flowchart for geomaterial classification.

4.9 Conclusions

The development of geomaterial classification criteria provides the basis for improving pile resistance estimations in IGM and reducing existing pile design and construction challenges in IGMs. This chapter develops geomaterial classification criteria for steel H-piles. The following conclusions can be drawn from this study:

- An extensive literature review found inconsistency in the definitions of IGMs and hard rocks for driven piles.
- Based on the performance of the β-method and Nordlund method in predicting the pile resistances, the criterion using $(N_1)_{60}$ of 50 was established for differentiating cohesionless soils from IGM-soils. Cohesionless soil-based geomaterials having $(N_1)_{60}$ greater than 50 are classified as IGM-soils.
- The classification criterion to differentiate cohesive soils and IGM-soils is established based on the unit CAPWAP shaft resistance of 1 ksf that corresponds to a s_u value of 2.7 ksf. Hence, cohesive soil-based geomaterials with $s_u$values greater than 2.7 ksf are classified as IGM-soils. However, as this criterion was developed based on few data points, this needs to be assessed when more data become available.
- IGM-rocks were differentiated from hard rocks based on boundary UCS values back-calculated by equating the geotechnical resistance to the compressive strength of the pile. As intact rocks and fractured rock masses have different geotechnical resistances, RMR was used for differentiating them. A modified procedure utilizing only UCS and RQD values was proposed for RMR calculation. Thus, factors affecting the boundary UCS in the case of intact rocks were compressive strength and percentage toe resistance. In addition to these factors, rock mass parameters (m and s) and RMR were required for the fractured rocks. In summary, UCS, RQD, compressive strength, and percentage toe resistance were required parameters for the classification of IGM-rocks.
- A systematic procedure to differentiate IGMs from soil-based materials and hard rocks is proposed in this study. A classification flowchart is developed to summarize the established criteria and to facilitate the geomaterial classification process.

CHAPTER 5. EVALUATION, CALIBRATION, AND VALIDATION OF STATIC ANALYSIS METHODS ALONG WITH ECONOMIC IMPACT AND TIME DEPENDENT PILE RESISTANCE STUDY

5.1 Introduction

Five static analysis (SA) methods were used to estimate unit resistances of test piles. The static analysis methods include the α- method by Tomlinson (1980), β-method by Esrig and Kirby (1979), λ-method by Vijayvergiya and Focht (1972), SPT method by Meyerhof (1976), and Nordlund (1963) method, as recommended in the AASHTO (2017). Detailed background of each method is discussed in section 2.4.1 of chapter 2. In this chapter, unit shaft resistances or end bearings estimated using each static analysis method are presented and compared to corresponding CAPWAP-measured unit resistances. An economic impact study was conducted to demonstrate the additional cost that incurred during construction, due to existing inefficient SA methods. The time dependent pile resistance characteristics of different geomaterials were studied using the CAPWAP EOD and BOR results.

The prevalent inconsistency and inefficiency of the static analysis methods in the determination of pile resistances in IGMs were evident by the high coefficient of variations (COVs) of the resistance biases and the mean resistance biases deviating from unity. High discrepancy in the pile length was observed during construction due to inefficient design methods. Thus, with the objective of improving the efficiency of static methods and to alleviate the construction challenges, the design coefficients used in the α- method and the β-method were calibrated using historical pile load test data from 28 piles. The α- and the β-methods were chosen to encompass both the cohesive and cohesionless IGMs, and both methods allow the determination of both shaft resistance and end bearing. The adhesion factor, α, and the bearing capacity factor, N_c, are the design coefficients used in α-method for the determination of shaft resistance and end bearing, respectively. Similarly, the β coefficient and the bearing capacity factor, N_t, are the design coefficients used in β-method for the determination of shaft resistance and end bearing, respectively. The design coefficients were calibrated against the IGM material properties consisting of undrained shear strength (s_u), unconfined compressive strength (q_u), and angle of internal friction (ϕ). The geomaterial classification system developed in chapter 4 classifying IGMs into IGM-soils and IGM-rocks was incorporated in the calibration to channelize the uncertainties in the resistance estimation as per the geomaterial. This chapter presents the regression analyses on the calibration of design coefficients. Further, the performance of static analysis methods with these calibrated design coefficients was assessed using additional independent set of pile data those were not used for calibration. Thus, this chapter presents the details on these additional pile data and bridge projects along with the outcomes of validation.

5.2 Evaluation of Existing Static Analysis Methods

Soils, IGM-soils, and the constituents of IGM-rocks were segregated as being cohesive or cohesionless for the application of the respective static analysis methods. The α-method was applied for clay, low plasticity silts, shale, claystone, siltstone, and breccia. The β-method, the Nordlund method, and the SPT method were used for dense sand and gravels, sandy silts, low plasticity silts, sandstones, and siltstones. The λ-method, being applicable for shaft resistance only, was used for the assessment of shaft resistances in sand and gravels, sandy silts, sandstones, claystones, shales, siltstones, and breccia. The resistance bias less than unity implies

overestimation while the resistance bias greater than unity implies underestimation of pile resistance.

5.2.1 Evaluation of static analysis methods for shaft resistance estimation

5.2.1.1 α-method

The unit shaft resistances from the α-method and the CAPWAP for test piles at EOD is presented in Table 13, Table 14, and Table 15 for soils, IGM-soils, and IGM-rocks respectively.

Table 13. Estimated unit shaft resistance by α-method and measured unit shaft resistance from CAPWAP at the EOD in soil.

Pile ID	Layer	Geomaterial	Estimated q_s using α-method (ksf)	Measured q_s from CAPWAP (ksf)	Resistance bias
3	1	Silty-gravelly sand + isolated clay layers	0.45	0.45	1.0
7	1	sandy silt with intermittent clays	0.88	0.22	0.25
8	1	sandy silt with intermittent clays	0.88	0.215	0.24
11	2	sandy silt	1.30	2.38	1.83
12	1	dense sandy silt + minor gravel	1.14	0.16	0.14
13	1	dense sandy silt + minor gravel	1.14	0.19	0.17

Table 14. Estimated unit shaft resistance by α-method and measured unit shaft resistance from CAPWAP at the EOD in IGM soil.

Pile ID	Layer	Geomaterial	q_s estimated using α-method (ksf)	Measured q_s from CAPWAP (ksf)	Resistance bias
7	2	Sandy Silt	0.93	0.31	0.33
7	3	Silty sand+ Sandy silt	1.17	1.09	0.93
9	2	Sandy Silt	1.04	2.29	2.20
10	2	Sandy Silt +Gravel	1.35	3.51	2.60
12	2	Sandy Silt +Gravel	1.13	1.15	1.02
13	2	Sandy Silt +Gravel	1.13	1.41	1.25

Table 15. Estimated unit shaft resistance by α-method and measured unit shaft resistance from CAPWAP at the EOD in IGM rock.

Pile ID	Layer	Geomaterial	q_s estimated using α-method (ksf)	Measured q_s from CAPWAP (ksf)	Resistance bias
4	2	Claystone	1.36	0.54	0.40
5	2	Shale	3.57	2.67	0.75
5	3	Shale	4.04	0.51	0.13
6	2	Claystone	0.60	1.89	3.15
6	3	Claystone	7.60	3.30	0.43
7	4	Siltstone	5.65	1.65	0.29
11	3	Siltstone	0.79	3.90	4.94
12	3	Siltstone	1.90	1.54	0.81
13	3	Siltstone	1.90	1.86	0.98
16	2	Shale	33.4	4.51	0.14
18	3	Claystone	2.00	0.53	1.06
39	2	Claystone	2.30	1.18	0.51

q_s–unit shaft resistance.

5.2.1.2 λ-method

The unit shaft resistances from the λ-method and the CAPWAP for test piles at EOD is presented in Table 16, Table 17, and Table 18 for soils, IGM-soils, and IGM-rocks respectively.

Table 16. Estimated unit shaft resistance by λ-method and measured unit shaft resistance from CAPWAP at the EOD in soils.

Pile ID	Layer	Geomaterial	q_s estimated using λ-method (ksf)	Measured q_s from CAPWAP (ksf)	Resistance bias
2	1	Sand	0.43	0.19	0.44
2	2	Silty sand	1.68	0.25	0.15
2	3	Sand + gravel	2.49	0.25	0.10
3	0	Sand	1.03	0.45	0.44
3	1	Silty to gravelly sand	1.40	0.45	0.32
4	1	Sand with gravel	1.1	0.32	0.29
5	1	Silty sand + gravel	0.65	0.42	0.65
7	1	Sandy silt with intermittent clays	0.91	0.22	0.24
8	1	Sandy silt with intermittent clays	0.89	0.215	0.24
8	2	Sandy Silt	3.38	0.54	0.16
8	3	Sandy Silt	3.32	0.99	0.30
9	1	Sandy silt with intermittent clays	1.09	0.44	0.40
11	2	Sandy Silt	1.07	2.38	2.22
12	1	Dense sandy Silt + minor gravel	1.06	0.16	0.15
13	1	Dense sandy Silt + minor gravel	1.07	0.19	0.18
14	1	Dense sandy Silt + minor gravel	1.09	0.26	0.24
14	2	Sandy Silt + Gravel	3.47	1.13	0.33
15	1	Dense sandy Silt + minor gravel	1.12	0.42	0.38
15	2	Sandy Silt + Gravel	1.74	1.26	0.72
17	1	Sand	0.74	0.13	0.18
17	2	Sand + gravelly sand	1.31	0.33	0.25
18	1	Sand	0.72	0.062	0.09
18	2	Sand + gravelly sand	1.35	0.31	0.23
19	1	Silty Sand	1.45	0.22	0.15
19	2	Silty Sand	2.18	1.52	0.70
22	1	Sand + gravel +cobbles +boulders	0.37	0.16	0.43
27	1	Sand + gravel +cobbles +boulders	0.47	0.25	0.53
39	1	Sand + gravel + boulders	0.57	0.35	0.61

q_s–unit shaft resistance.

Table 17. Estimated unit shaft resistance by λ-method and measured unit shaft resistance from CAPWAP at the EOD in IGM soil.

Pile ID	Layer	Geomaterial	q_s estimated using λ-method (ksf)	Measured q_s from CAPWAP (ksf)	Resistance bias
1	1	Sand + gravel	1.27	0.69	0.54
7	2	Sandy Silt	3.74	0.31	0.08
7	3	Silty sand+ Sandy silt	3.25	1.09	0.34
9	2	Sandy Silt	2.85	2.29	0.80
10	2	Sandy Silt	2.08	3.51	1.69
12	2	Sandy Silt + Gravel	3.20	1.15	0.36
13	2	Sandy Silt + Gravel	3.09	1.41	0.46
16	1	Sand + gravel	1.06	2.52	2.38
22	2	Sand + gravel +cobbles +boulders	0.65	0.44	0.68
26	1	Sand + gravel +cobbles +boulders	0.42	0.18	0.43
28	1	Gravel +cobbles +boulders	0.42	0.23	0.55

q_s–unit shaft resistance.

Table 18. Estimated unit shaft resistance by λ-method and measured unit shaft resistance from CAPWAP at the EOD in IGM rock.

Pile ID	Layer	Geomaterial	q_s estimated using λ-method (ksf)	Measured q_s from CAPWAP (ksf)	Resistance bias
1	2	Sandstone	2.46	0.69	0.28
1	3	Sandstone	8.10	1.43	0.18
2	4	Sandstone	3.17	0.49	0.15
3	2	Sandstone	7.75	2.74	0.35
4	2	Claystone	6.63	0.54	0.08
5	2	Shale	3.11	2.67	0.86
5	3	Shale	4.84	0.51	0.11
6	2	Claystone	3.68	1.89	0.51
6	3	Claystone	1.79	3.30	1.84
7	4	Siltstone	26.42	1.65	0.06
11	3	Siltstone	5.08	3.90	0.77
12	3	Siltstone	12.19	1.54	0.13
13	3	Siltstone	12.21	1.86	0.15
16	2	Shale	167.69	4.51	0.03
18	3	Claystone	5.65	0.53	0.09
19	3	Sandstone	5.11	1.62	0.32
26	2	Breccia	1.24	0.63	0.51
26	3	Sandstone	1.61	1.96	1.22
39	2	Claystone	3.20	1.18	0.37

q_s–unit shaft resistance.

5.2.1.3 β-method, Nordlund method, and SPT method

As the β-, Nordlund, and SPT methods are applicable for cohesionless geomaterials, the unit shaft resistances calculated from the three methods are presented jointly. The estimated unit shaft resistances, CAPWAP measured unit shaft resistances, and the resistance biases are presented in

Table 19, Table 20, and Table 21 for soils, IGM-soils, and IGM-rocks respectively. There were 29 soil layers, 16 IGM-soil layers, and 13 IGM-rock layers.

Table 19. Estimated unit shaft resistance by β-, Nordlund, and SPT methods and the measured unit shaft resistance from CAPWAP at the EOD in soil.

Pile ID	Layer	Geomaterial	$q_{s\beta}$ (ksf)	q_{sN} (ksf)	q_{ss} (ksf)	q_{sC} (ksf)	RB (β)	RB (Nord.)	RB (SPT)
2	1	Sand	0.49	0.53	0.44	0.19	0.39	0.36	0.43
2	2	Silty sand	1.04	1.14	0.32	0.25	0.24	0.22	0.78
2	3	Sand + gravel	1.39	1.75	0.71	0.25	0.18	0.14	0.35
3	0	Sand	0.51	0.54	0.23	0.45	0.88	0.83	1.96
3	1	Silty to gravelly sand	0.93	1.00	0.17	0.45	0.48	0.45	2.65
4	1	Sand with gravel	2.2	2.68	0.25	0.32	0.15	0.12	1.28
5	1	Silty sand + gravel	0.21	0.30	0.32	0.42	2.00	1.40	1.31
7	1	Sandy silt with intermittent clays	0.53	0.65	0.48	0.22	0.42	0.34	0.46
8	1	Sandy silt with intermittent clays	0.60	0.75	0.46	0.22	0.36	0.29	0.47
8	2	Sandy Silt	1.63	2.01	0.26	0.54	0.33	0.27	2.08
8	3	Sandy Silt	3.18	4.05	0.59	0.99	0.31	0.24	1.68
9	1	Sandy silt with intermittent clays	0.70	0.88	0.20	0.44	0.63	0.50	2.20
10	1	Silty sand + gravel	0.45	0.55	0.69	0.53	1.18	0.96	0.77
11	2	Sandy Silt	1.02	0.96	0.48	2.38	2.33	2.48	4.96
12	1	Dense sandy silt + minor gravel	0.51	0.63	0.51	0.16	0.31	0.25	0.31
13	1	Dense sandy silt + minor gravel	0.52	0.65	0.51	0.19	0.37	0.29	0.37
14	1	Dense sandy silt + minor gravel	0.57	0.69	0.54	0.26	0.46	0.38	0.48
14	2	Sandy Silt + Gravel	1.29	1.64	0.21	1.13	0.88	0.69	5.38
15	1	Dense sandy silt + minor gravel	0.61	0.75	0.52	0.42	0.69	0.56	0.81
15	2	Sandy Silt + Gravel	1.35	1.72	0.21	1.26	0.93	0.73	6.00
17	1	Sand	0.74	0.85	0.22	0.13	0.18	0.15	0.59
17	2	Sand + gravelly sand	2.34	2.82	0.24	0.33	0.14	0.12	1.38
18	1	Sand	2.06	0.81	0.23	0.062	0.03	0.08	0.27
18	2	Sand + gravelly sand	2.65	3.20	0.22	0.31	0.12	0.10	1.41
19	1	Silty sand	0.50	0.60	0.56	0.22	0.44	0.37	0.39
19	2	Silty sand	1.19	1.38	0.25	1.52	1.28	1.10	6.08
22	1	Sand + gravel +cobbles+ boulders	0.26	0.29	0.39	0.16	0.62	0.55	0.41
39	1	Sand + gravel + boulders	0.82	1.12	0.40	0.35	0.43	0.31	0.88
41	1	Silty sand + gravel +cobbles+ boulders	1.00	1.32	0.68	0.31	0.31	0.23	0.46

$q_{s\beta}$- unit shaft resistance from β-method; q_{sN}- unit shaft resistance from Nordlund method; q_{ss}- unit shaft resistance from SPT-method; q_{sC}- unit shaft resistance from CAPWAP; RB- Resistance bias; Nord.- Nordlund method.

Table 20. Estimated unit shaft resistance by β-, Nordlund, and SPT with the measured unit shaft resistance from CAPWAP at the EOD in IGM-soil.

Pile ID	Layer	Geomaterial	$q_{s\beta}$ (ksf)	q_{sN} (ksf)	q_{ss} (ksf)	q_{sC} (ksf)	RB (β)	RB (Nord.)	RB (SPT)
1	1	Sand + gravel	0.44	0.61	1.25	0.69	1.57	1.13	0.55
7*	2	Sandy Silt	1.17	1.49	0.14	0.31	0.26	0.21	2.21
7*	3	Silty sand+ Sandy silt	3.33	4.27	0.58	1.09	0.33	0.26	1.88
9*	2	Sandy Silt	2.23	2.84	0.28	2.29	1.03	0.81	8.18
10*	2	Sandy Silt	1.54	2.31	1.22	3.51	2.28	1.52	2.88
12*	2	Sandy silt + gravel	1.15	1.50	0.14	1.15	1.00	0.77	8.21
13*	2	Sandy silt + gravel	1.01	1.52	0.14	1.41	1.40	0.93	10.07
16	1	Sand + gravel	0.24	0.34	1.10	2.52	10.50	7.41	2.29
20	1	Sand+ gravel + cobbles + boulders	0.34	0.42	2.00	0.77	2.26	1.83	0.39
21	1	Sand+ gravel + cobbles + boulders	0.71	0.96	1.18	0.35	0.49	0.36	0.30
22	2	Sand+ gravel + cobbles + boulders	0.93	1.26	2.00	0.44	0.47	0.35	0.22
26	1	Sand+ gravel + cobbles + boulders	1.29	1.99	1.64	0.18	0.14	0.09	0.11
27	1	Sand+ gravel + cobbles + boulders	0.56	0.64	1.58	0.25	0.45	0.39	0.16
28	1	Sand+ gravel + cobbles + boulders	0.62	0.79	0.98	0.23	0.37	0.29	0.23
43	1	Sand + cobbles	1.71	3.60	2.00	0.34	0.20	0.09	0.17
43	2	Sand+ gravel	3.01	5.44	2.00	1.56	0.52	0.29	0.78

$q_{s\beta}$- unit shaft resistance from β-method; q_{sN}- unit shaft resistance from Nordlund method; q_{ss}- unit shaft resistance from SPT-method; q_{sC}- unit shaft resistance from CAPWAP; RB- Resistance bias; Nord.- Nordlund method.

Table 21. Estimated unit shaft resistance by β-, Nordlund, and SPT with the measured unit shaft resistance from CAPWAP at the EOD in IGM-rock.

Pile ID	Layer	Geomaterial	$q_{s\beta}$ (ksf)	q_{sN} (ksf)	q_{ss} (ksf)	q_{sC} (ksf)	RB (β)	RB (Nordlund)	RB (SPT)
1	2	Sandstone	1.69	2.39	1.31	0.69	0.41	0.29	0.53
1	3	Sandstone	3.36	5.01	2.00	1.43	0.43	0.29	0.72
2	4	Sandstone	2.88	3.68	0.71	0.49	0.17	0.13	0.69
3	2	Sandstone	3.08	4.97	2	2.74	0.89	0.55	1.37
7	4	Siltstone	5.90	7.90	1.32	1.65	0.28	0.21	1.25
11	3	Siltstone	1.77	4.50	2.00	3.90	2.20	0.87	1.95
12	3	Siltstone	2.73	3.83	0.86	1.54	0.56	0.40	1.79
13	3	Siltstone	2.75	3.86	0.86	1.86	0.68	0.48	2.16
19	3	Sandstone	3.40	5.08	0.61	1.62	0.48	0.32	2.66
26	2	Sandstone	2.67	4.12	3.08	0.63	0.24	0.15	0.20
26	3	Sandstone	3.56	5.49	2.67	1.96	0.55	0.36	0.73
27	2	Sandstone	2.73	3.88	2.00	1.74	0.64	0.45	0.87
28	2	Sandstone	2.15	3.06	1.41	1.93	0.90	0.63	1.37

$q_{s\beta}$- unit shaft resistance from β-method; q_{sN}- unit shaft resistance from Nordlund method; q_{ss}- unit shaft resistance from SPT-method; q_{sC}- unit shaft resistance from CAPWAP; RB- Resistance bias.

5.2.2 Evaluation of static analysis methods for end bearing estimation

5.2.2.1 α-method

The unit end bearings from the α-method and the CAPWAP for test piles at EOD is presented in Table 22, and Table 23 for IGM-soils, and IGM-rocks respectively. There was no test pile bearing on cohesive soil.

Table 22. Summary of estimated unit end bearing by α-method and measured unit end bearing from CAPWAP at the EOD in IGM soil.

Pile ID	Bearing Layer	q_p estimated using α-method (ksf)	Measured q_p from CAPWAP (ksf)	Resistance bias
9	Sandy Silt	32.4	101.49	3.1
10	Sandy Silt +Gravel	24.3	142.08	5.8

Table 23. Estimated unit end bearing by α-method and measured unit end bearing from CAPWAP at the EOD in IGM rock.

Pile ID	Bearing Layer	q_p estimated using α-method (ksf)	Measured q_p from CAPWAP (ksf)	Resistance bias
4	Claystone	18	48.6	2.7
5	Shale	36.36	149.44	4.1
6	Claystone	342	243.9	0.7
7	Siltstone	203.4	55.92	0.3
11	Siltstone	32.4	314.61	9.7
12	Siltstone	85.5	122.29	1.4
13	Siltstone	85.5	106.56	1.2
14	Siltstone	85.5	147.36	1.72
15	Siltstone	85.5	147.46	1.72
16	Shale	1503	153.76	0.1
18	Claystone	4.5	25.39	5.64
39	Claystone	24.3	132.35	5.45

5.2.2.2 β-method, Nordlund method, and SPT method

The estimated unit end bearings from β-, Nordlund, and SPT methods, and the measured unit end bearing from CAPWAP are presented jointly along with their respective resistance bias for test piles at EOD for soils, IGM-soils, and IGM-rocks in **Error! Reference source not found.**, Table 25, and Table 26, respectively.

Table 24. Estimated unit end bearing by β-, Nordlund, and SPT methods and measured unit end bearing from CAPWAP at the EOD in soil.

Pile ID	Bearing layer geomaterial	$q_{p\beta}$ (ksf)	q_{pN} (ksf)	q_{ps} (ksf)	q_{pC} (ksf)	RB (β)	RB (Nord.)	RB (SPT)
8	Sandy Silt	344.84	194.4	266.5	80.68	0.23	0.42	0.30
17	Sand + gravelly sand	317.5	50	140.14	17.41	0.05	0.35	0.12
41	Silty sand+ gravel + cobbles + boulders	322.13	150	321.71	63.11	0.20	0.42	0.20

$q_{p\beta}$- unit end bearing from β-method; q_{pN}- unit end bearing from Nordlund method; q_{ps}- unit end bearing from SPT-method; q_{pC}- unit end bearing from CAPWAP; RB- Resistance bias; Nord.- Nordlund method.

Table 25. Estimated unit end bearing by β-, Nordlund, and SPT methods and measured unit end bearing from CAPWAP at the EOD in IGM-soil.

Pile ID	Bearing layer geomaterial	$q_{p\beta}$ (ksf)	q_{pN} (ksf)	q_{ps} (ksf)	q_{pC} (ksf)	RB (β)	RB (Nord.)	RB (SPT)
9	Sandy Silt	293.74	266.4	221.42	101.49	0.35	0.38	0.46
10	Sandy Silt +Gravel	989	425	389.52	142.08	0.14	0.33	0.36
20	Sand+ gravel + cobbles + boulders	68	51.22	1768.95	185	2.72	3.61	0.10
21	Sand+ gravel + cobbles + boulders	141	75	1077.10	177	1.26	2.36	0.16
22	Sand+ gravel + cobbles + boulders	156.7	50	1701.17	260.82	1.66	5.22	0.15
43	Sandy Silt +Gravel	867.60	750	1241.35	246.33	0.28	0.33	0.20

$q_{p\beta}$- unit end bearing from β-method; q_{pN}- unit end bearing from Nordlund method; q_{ps}- unit end bearing from SPT-method; q_{pC}- unit end bearing from CAPWAP; RB- Resistance bias; Nord.- Nordlund method.

Table 26. Estimated unit end bearing by β-, Nordlund, and SPT methods and measured unit end bearing from CAPWAP at the EOD in IGM-rock.

Pile ID	Bearing layer geomaterial	$q_{p\beta}$ (ksf)	q_{pN} (ksf)	q_{ps} (ksf)	q_{pC} (ksf)	RB (β)	RB (Nordlund)	RB (SPT)
1	Sandstone	840	337.5	540.1	162.5	0.19	0.48	0.30
2	Sandstone	640.8	360	1171	292.35	0.46	0.81	0.25
3	Sandstone	896	750	882	106.28	0.12	0.14	0.12
7	Siltstone	399.41	369.6	308.21	55.92	0.14	0.15	0.18
11	Siltstone	749	750	882.6	314.61	0.42	0.42	0.36
12	Siltstone	513.9	315	72.4	122.29	0.24	0.39	1.69
13	Siltstone	514.6	261	65.86	106.56	0.21	0.41	1.62
14	Siltstone	495.6	281	20.30	147.36	0.30	0.52	7.26
15	Siltstone	515.4	281	19.91	147.46	0.29	0.52	7.41
19	Sandstone	866.1	337.5	178.82	130	0.15	0.39	0.73
26	Sandstone	207.5	675	1069.03	144.39	0.70	0.21	0.14
27	Sandstone	1161.97	750	3429.14	270.31	0.23	0.36	0.08
28	Sandstone	921.55	750	2537.41	216.71	0.24	0.29	0.09

$q_{p\beta}$- unit end bearing from β-method; q_{pN}- unit end bearing from Nordlund method; q_{ps}- unit end bearing from SPT-method; q_{pC}- unit end bearing from CAPWAP; RB- Resistance bias.

5.2.3 Summary of the evaluation of static analysis methods

Resistance bias, expressed as the ratio of CAPWAP measured to estimated pile resistance, was taken as the main variable to assess the static analysis methods. The statistical summaries in terms of mean ($\bar{x}$) and coefficient of variation (COV), calculated as a ratio of sample standard deviation to mean, of these resistance biases were calculated as shown in Table 27. Sample sizes of SA methods for shaft resistance estimation ranged from 6 to 29, while sample sizes of SA methods in end bearing estimation ranged from zero to 13. A maximum sample size of 29 corresponded to β-, Nordlund, and SPT methods in soils for shaft resistance estimation. The COV is an indication of how consistently SA method estimates the pile resistance. In estimating shaft resistance, the SPT-method, among all the SA methods, had the highest mean bias of 2.41 in IGM-soils and the Nordlund method had the lowest mean bias of 0.39 in IGM-rocks. In estimating end bearing, the SPT-method had the lowest $\bar{x}$ of 0.24 in IGM-soils and the α-method had the highest $\bar{x}$ of 2.90 in IGM-rocks. The COV of resistance biases for shaft resistance estimation ranged from 0.52 to 1.73 while for end bearing estimation ranged from 0.46 to 1.69.

Table 27. Statistical summaries of resistance biases for three geomaterials, five SA methods, shaft resistance, and end bearing.

Geomaterial	SA method	Statistical summaries					
		For shaft resistance estimation			For end bearing estimation		
		Sample Size (N)	Sample mean ($\bar{x}$)	COV	Sample Size (N)	Sample mean ($\bar{x}$)	COV
Soil	α–method	6	0.61	1.13	0	Very small sample size	
	β–method	29	0.59	0.91	2		
	Nordlund	29	0.5	0.99	2		
	SPT	29	1.61	1.09	2		
	λ-method	28	0.40	1.01	Not applicable for end bearing		
IGM-soil	α–method	6	1.39	0.61	2	Very small sample size	
	β–method	16	1.45	1.73	6	1.07	0.95
	Nordlund	16	1.05	1.70	6	2.04	1.01
	SPT	16	2.41	1.38	6	0.24	0.59
	λ-method	11	0.76	0.90	Not applicable for end bearing		
IGM-rock	α–method	12	1.13	1.28	12	2.90	0.98
	β–method	13	0.65	0.80	13	0.28	0.57
	Nordlund	13	0.39	0.52	13	0.39	0.46
	SPT	13	1.25	0.58	13	1.56	1.69
	λ-method	19	0.42	1.11	Not applicable for end bearing		

COV-Coefficient of variation.

5.3 Economic Impacts of Current Pile Design Practice

The Venn diagram shown in Figure 29 represents the number of usable piles in IGM used in the economic study for the EOD and BOR conditions. As three test piles were bearing on soils, they were excluded in the economic impact study of current pile design practice on IGM. Three

different subsets consisting of EOD, BOR, and EOD ∩ BOR were recognized out of the universal set, U, as shown in Figure 29.

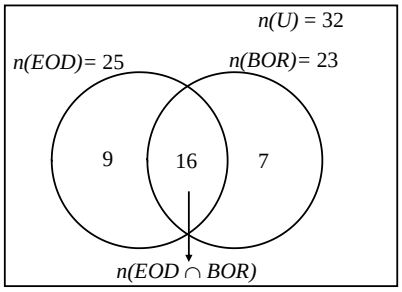

n(U) = Total no. of usable piles in IGM
n(EOD) = No. of usable piles in IGM with EOD records
n(BOR) = No. of usable piles in IGM with BOR records
n(EOD ∩ BOR) = No. of usable piles in IGM with both EOD and BOR records

Source: Adhikari (2019)

Figure 29. Venn diagram representing the number of usable piles at EOD and BOR for static analysis.

The scope of the economic impact study of current pile design practice was limited to determining the discrepancy in the number of piles observed during construction for each project. As pile lengths varied with projects, the differences in the number of piles were converted to an equivalent weight of steel, which was then normalized by the structural load for comparison. First, the load carried by the structure was calculated to determine the number of piles from the SA and CAPWAP methods. The total load per bridge structure (abutment/pier/bent) was obtained by multiplying the number of installed piles as reported in the drawings with the load (factored load for LRFD and ultimate load for allowable stress design (ASD)). Different design philosophies, LRFD and ASD, were used in the projects as they were conducted over different years, from 1993 to 2015. Next, factored pile resistances (φR) or resistances (R) were determined using the SA and CAPWAP at both the EOD and BOR conditions depending upon LRFD or ASD philosophy used. Embedded pile depths (L_{EMB}) reported in CAPWAP (Table 8) were used to estimate the pile resistances using SA to ensure a consistent comparison. Only the Nordlund and α-methods, with corresponding resistance factors of 0.45 and 0.35 recommended in the AASHTO (2017), were applied for cohesionless and cohesive geomaterials, respectively. These two methods were chosen as both were applicable for the shaft resistance and end bearing estimation and have relatively higher resistance factors. Finally, the numbers of piles to sustain the structural load were calculated by dividing the structure load with the factored pile resistances from SA and CAPWAP. Next, the difference in the number of piles between CAPWAP and SA (i.e., n2-n1) was calculated for each project, as summarized in Table 28 and Table 29 for EOD and BOR conditions, respectively. A positive difference indicates that the pile resistance was overestimated by SA leading to underestimation of the number of piles. The number of piles was reported with decimal places to avoid rounding errors in the calculation of steel weight due to the discrepancy in the pile numbers between CAPWAP and SA.

The economic value associated with the discrepancy observed during construction at the EOD owing to the inefficient SA methods is presented in terms of steel weight per load in the last column of Table 28. For example, the discrepancy observed during construction of a bent structure in the Owl Creek project is -9.50 lb oer kip load. A negative sign indicated that the number of piles was overestimated by SA methods due to underestimation in the pile resistance. As the bent structure load was 1,240 kips, 11.78 kips of steel would be overestimated during the

design phase and the required capacity would be attained with a fewer number of piles. Table 28 shows that SA overestimated the pile resistances in 17 of the 25 cases, leading to fewer piles allocated in the design phase for bidding. If a targeted pile resistance based on the allocated number of piles cannot be attained using a construction control method, such as CAPWAP, the pile penetrations will either be extended further, or the number of piles will be increased, which will eventually create cost overruns. Table 29 presents the difference in the number of piles as determined from SA and CAPWAP at the BOR conditions from 23 projects. The increase in the pile embedment depth during restrike as indicated in Table 8 was considered in the analysis. SA overestimated the number of piles in five of the 23 projects.

Table 28. Summary of economic impact study for the SA methods and CAPWAP at EOD.

Project	Structure	γQ/Q per structure (kips)	φR/R from SA (kips)	φR/R from CAPWAP (kips)	No. of pile from SA (n1)	No. of pile from CAPWAP (n2)	Diff. in No. of pile (n2-n1)	Difference in steel weight per unit load (lb/kips)
Burns South	Pier	5418	398.94	240.50	13.58	22.53	8.95	4.533
	Abutment	1290	504.13	328.25	2.56	3.93	1.37	5.299
Casper Street	Abutment	2366	536.06	221.00	4.41	10.71	6.29	4.679
	Pier	7812	784.03	325.00	9.96	24.04	14.07	3.287
BNSF Torrington	Abutment	1944	569.34	155.35	3.41	12.51	9.10	34.169*
	Abutment	1944	785.41	143.00	2.48	13.59	11.12	58.039*
Owl Creek	Bent	1240	106.57	219.05	11.64	5.66	-5.97	-9.497
Woods W.	Pier	4200	201.36	292.50	20.86	14.36	-6.50	-1.886
PB Parson	Abutment	940	651.18	201.37	1.44	4.67	3.22	15.981
PB Muddy Creek	Abutment	1212	290.63	247.39	4.17	4.90	0.73	1.708
	Bent 2	1010	277.15	292.96	3.83	3.45	-0.39	-0.364
	Bent 3	1460	401.72	435.96	3.63	3.35	-0.29	-0.394
PB Beech Street	Abutment	860	238.66	172.25	3.60	4.99	1.39	3.999
	Abutment	860	215.42	185.84	3.99	4.63	0.64	1.837
	Abutment	860	221.43	185.84	3.88	4.63	0.74	2.049
	Abutment	860	229.78	198.64	3.74	4.33	0.59	1.678
Cedar Street	Abutment	1035	245.59	181.35	4.21	5.71	1.49	3.149
Hunter Creek	Abutment	960	37.30	159.25	25.74	6.03	-19.71	-21.221
	Abutment	960	94.93	147.55	10.11	6.51	-3.61	-7.148
Clark's Fork	Abutment	1296[1]	140.48	286.00	9.23	4.53	-4.69	-11.898
NF (Hanging)	Abutment	2160[1]	913.58	263.84	2.36	8.19	5.82	13.578
NF (Pahaska)	Abutment	1780[1]	602.66	333.91	2.95	5.33	2.38	3.997
	Abutment	1780[1]	566.27	250.25	3.14	7.11	3.97	5.209
Yellowstone	Abutment	1880[1]	176.20	237.25	10.67	7.92	-2.75	-6.290
Elk Fork Creek	Abutment	1610[1]	774.98	263.25	2.08	6.12	4.04	7.324
							Average (A)	4.473
							Standard Deviation (SD)	15.096
							A + 2 × SD	34.665
							Average excluding two abutments from BNSF project (potential outliers)	0.853

PB-Pine Bluff; NF-North Fork; W-Wardell; γQ-Factored load for LRFD; Q- Ultimate load for ASD; n-Number of piles; Diff.-Difference; φR-Factored pile resistance for LRFD; R- Resistance for ASD; *- Potential outlier; [1]- Ultimate load for Allowable Stress Design; and No.-Number.

Table 29. Summary of economic impact study for the SA methods and CAPWAP at BOR.

Project	Structure	γQ/Q per structure (kips) Q	φR/R from SA (kips)	φR/R from CAPWAP (kips)	No. of pile from SA (n1)	No. of pile from CAPWAP (n2)	Diff. in No. of pile (n2-n1)	Difference in steel weight per unit load (lb/kips)
Burns South	Pier	5418	409.54	258.70	13.23	20.94	7.71	4.012
	Abutment	1290	504.13	390.00	2.56	3.31	0.75	2.894
Casper Street	Abutment	2366	536.06	247.00	4.41	9.58	5.17	3.841
	Pier	7812	784.03	287.95	9.96	27.13	17.17	4.009
BNSF Torrington	Abutment	1944	569.34	175.50	3.41	11.08	7.66	28.774*
	Abutment	1944	785.41	169.00	2.48	11.50	9.03	47.122*
Owl Creek	Bent	1240	107.23	235.95	11.56	5.26	-6.31	-10.064
Woods W.	Pier	4200	201.36	325.00	20.86	12.92	-7.93	-2.303
PB Parson	Abutment	940	652.60	211.90	1.44	4.44	3.00	14.864
PB Beech Street	Abutment	860	238.66	188.50	3.60	4.56	0.96	2.760
	Abutment	860	216.11	221.00	3.98	3.89	-0.09	-0.255
	Abutment	860	222.31	198.90	3.87	4.32	0.46	1.263
	Abutment	860	230.39	208.65	3.73	4.12	0.39	1.117
Cedar Street	Abutment	1035	245.59	211.90	4.21	4.88	0.67	1.414
Clark's Fork	Abutment	1296[1]	140.48	266.50	9.23	4.86	-4.36	-11.058
Jackson Shop	Column	280[1]	375.86	286.00	0.74	0.98	0.23	1.373
	Column	280[1]	421.04	269.75	0.67	1.04	0.37	2.542
	Column	280[1]	460.03	227.50	0.61	1.23	0.62	4.592
Wind River	Abutment	1140[1]	182.98	97.50	6.23	11.69	5.46	21.585
	Abutment	1140[1]	186.91	117.00	6.10	9.74	3.64	14.910
	Abutment	1140[1]	176.52	100.75	6.46	11.32	4.86	19.307
Yellowstone	Abutment	1880[1]	176.20	211.25	10.67	8.90	-1.77	-4.056
	Abutment	4501	119.13	78.00	3.78	5.77	1.99	8.365
Average (A)								6.756
Standard Deviation (SD)								12.918
A + (2 × SD)								32.592
Average excluding two abutments from BNSF project (potential outliers)								3.862

PB- Pine Bluff; W- Wardell; Q- Factored load for LRFD or ultimate load for ASD; n- Number of piles; Diff.-Difference; R- Factored pile resistance; SD – Standard Deviation; *- Potential outlier; [1]- Ultimate load for Allowable Stress Design; and No.-Number.

It is important to note that the difference in steel weight per unit load for the BNSF Torrington project seemed very high, or approximately greater than the average value by twice the standard deviation, as shown in Table 28 and Table 29. The pile lengths at the two abutments were 100 ft and 139 ft, which were relatively longer than rest of the piles. One of the possible reasons might be the overestimation of shaft resistances in the longer piles. Excluding the results of the BNSF Torrington project reduced the average differences in the steel weight per unit load to 0.85 lb/kip and 3.86 lb/kip for both the EOD and BOR conditions, respectively. The economic impact study at EOD concluded that the overestimation of pile resistances at the design phase led to an

average cost overrun. This can be interpreted as 0.14 in overrun of HP14×73 pile per kip load. Similarly, the economic impact study at BOR concluded an average cost overrun. This is equivalent to a 0.63 in overrun of HP14×73 pile per kip load. The effect of restrike on economic analysis was assessed based on the 14 projects having both the EOD and the BOR records excluding the BNSF Torrington project. The average difference in steel decreased from 01.21 lb/kip at the EOD to 0.60 lb/kip. This decrease is attributed to the increase in the pile resistance at the BOR owing to short-term pile setup.

5.4 Calibration of Static Analysis Methods

5.4.1 Calibration of design coefficients for IGM-Soils

The calibration of the design coefficients of α- and the β-methods required for the determination of shaft resistance and end bearing in IGM-soils was described in the following subsections.

5.4.1.1 Calibration of the adhesion factor, α- coefficient

The unit shaft resistance (q_s) of a pile in cohesive IGM-soils can be estimated by the α- method using Equation (36).

$$q_s = \alpha \times s_u \tag{36}$$

where,

s_u is the undrained shear strength.

There were a total of six IGM-soils layers with their corresponding s_u values. To calibrate the α-coefficient for the determination of shaft resistance in IGM-soils, first, the CAPWAP measured unit shaft resistances were used as q_s in Equation (36). Then, using s_u of the corresponding layer, α-coefficients were back-calculated. This was followed by the regression analysis performed between the back-calculated α-coefficients and s_u values. A two-degree polynomial model was the best fit describing the relationship between α and s_u with a coefficient of determination (R^2) of 0.94 and an adjusted R^2 of 0.90, as shown in Figure 30.

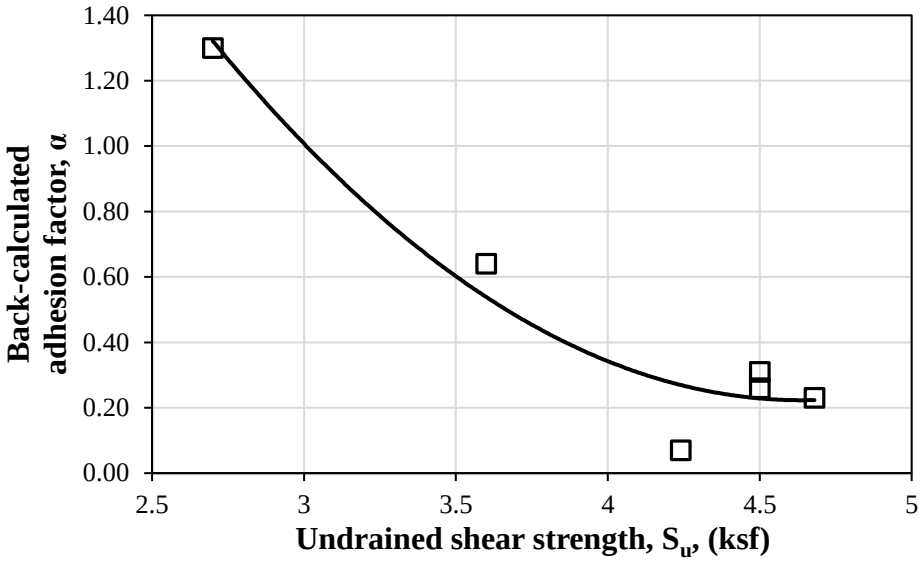

Source: Gebreslasie (2018)

Figure 30. Relationship between back-calculated adhesion factor and undrained shear strength for driven piles in IGM-soils (Gebreslasie 2018).

The regression model for the adhesion factor ($\hat{\alpha}$) in IGM-soils is given by

$$\hat{\alpha} = 0.292 s_u{}^2 - 2.7092 s_u + 6.5077 \quad (37)$$

5.4.1.2 Calibration of the bearing capacity factor, N_c

Because of the very small sample size of two, the N_c factor could not be calibrated for the estimation of end bearing in IGM-soils.

5.4.1.3 Calibration of the β coefficient

The unit shaft resistance (q_s) of a pile in cohesionless IGM-soils can be estimated using the β-method given as Equation (38).

$$q_s = \beta \times \sigma_v' \quad (38)$$

where,

σ_v' is the vertical effective geotechnical stress (ksf) prior to pile installation.

There were 16 IGM-soil layers applicable to β-method. β-coefficients were back-calculated using the CAPWAP measured unit shaft resistances and the vertical effective stresses of the corresponding IGM-soil layers. In order to relate the β-coefficients to the geomaterial properties, firstly a scatterplot was created between the back-calculated β-coefficients and the friction angle, ϕ before regression analysis. However, no relationship was observed from the scatterplot (Gebreslasie 2018). One of the possible reasons might be due to the uncertainties in the friction

angles that were not lab measured values but rather referred from WYDOT in-house tables established based on past test data.

5.4.1.4 Calibration of the bearing capacity factor, N_t

The unit end bearing (q_p) of a pile in IGM-soils can be estimated using β-method given as Equation (39).

$$q_p = N_t \times p_t \tag{39}$$

where,

p_t is the effective overburden stress at the pile tip.

There were total six bearing layers in IGM-soils which were analyzed using β-method. Firstly, N_t was back-calculated using Equation (39) where CAPWAP measured unit end bearing was taken as q_p. Scatterplot was then created to visually inspect the relationship between the back-calculated N_t and ϕ. However, no relationship was observed between N_t and ϕ (Gebreslasie 2018).

5.4.2 Calibration of design coefficients for IGM-rocks

The calibration of the design coefficients of the α- and the β-methods for the determination of shaft resistance and end bearing in IGM-rocks was described in the following subsections.

5.4.2.1 Calibration of the adhesion factor, α- coefficient

The unit shaft resistance (q_s) of a pile in a cohesive IGM-rock can be estimated using α- method given by Equation (40)

$$q_s = \alpha \times q_u \tag{40}$$

The s_u has been replaced by uniaxial compressive strength (q_u) in case of IGM-rocks as q_u is normally measured in laboratory to represent the strength property of IGM-rocks. There were a total of 12 IGM-rock layers. However, one IGM-rock layer was eliminated from regression analysis as it had comparatively higher q_u value than the other layers. Firstly, α-coefficients were back-calculated from Equation (40) using CAPWAP measured unit shaft resistances and the corresponding q_u values. Then the regression analysis was performed to describe the relationship between the back-calculated α-coefficients and the q_u values in ksf. A power model given by Equation (41) was found best describing the relationship with an R^2 of 0.60 and an adjusted R^2 of 0.555 in Figure 31.

$$\hat{\alpha} = \frac{64.63 \times q_u^{-0.656}}{100} \tag{41}$$

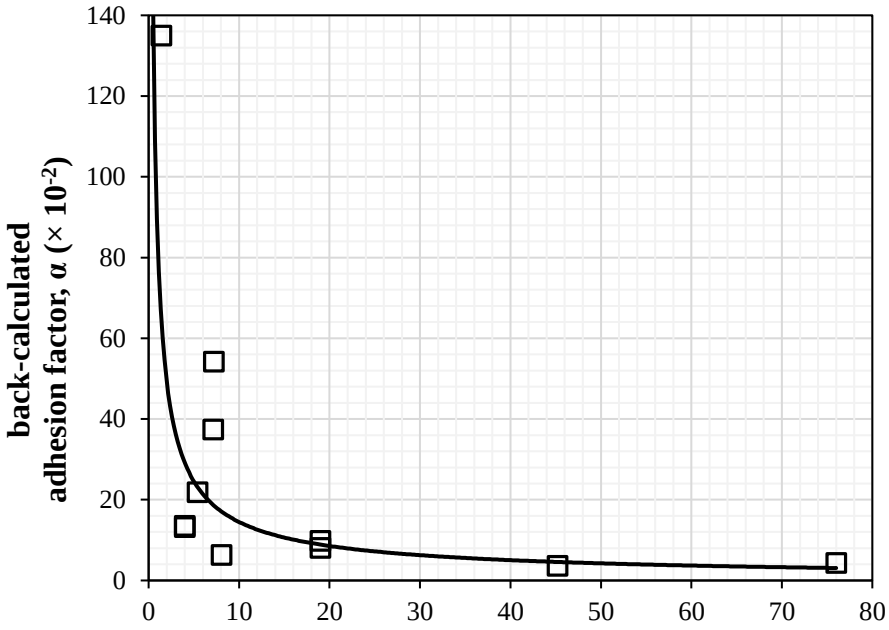

Source: Gebreslasie (2018)

Figure 31. Relationship between back-calculated α-coefficient and uniaxial compressive strength for driven piles in IGM-rocks (Gebreslasie 2018).

5.4.2.2 Calibration of the bearing capacity factor, N_c

The unit end bearing of a pile in cohesive IGM-rocks can be estimated using α-method given by Equation (42)

$$q_p = N_c \times q_u \tag{42}$$

There were 12 bearing layers consisting of IGM-rocks that were analyzed using the α- method. Using CAPWAP measured unit end bearing as q_p and the respective q_u of the IGM-rock layer, N_c was back-calculated for each pile. Then, the regression analysis was performed to relate the back-calculated N_c with q_u. Diagnostic plots of residuals were generated to assess the fitted model. On observing the diagnostic plots, two of the data points were excluded as one point exhibited extreme residual and the other showed high leverage value (Gebreslasie 2018). Thus, the regression analysis was reconducted on remaining data points after eliminating these two data points. A power model given by Equation (43) was the best fit for the expected N_c in terms of q_u with an R^2 of 0.719 and an adjusted R^2 of 0.684 as shown in Figure 32.

$$\widehat{N_c} = 39.8 \times q_u^{-0.635} \tag{43}$$

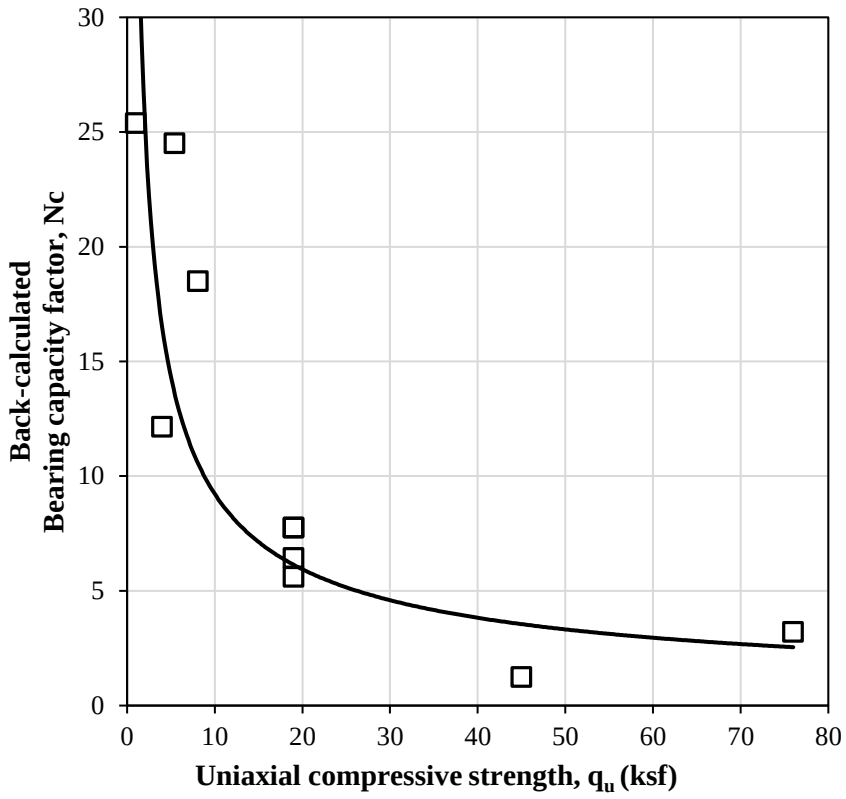

Source: Gebreslasie (2018)

Figure 32. Relationship between back-calculated Nc factor and uniaxial compressive strength for driven piles in IGM-rocks (Gebreslasie 2018).

5.4.2.3 Calibration of the β-coefficient

The unit shaft resistance in cohesionless IGM-rocks was calculated similarly as in IGM-soils by using Equation (38). There were 13 piles in IGM-rock layers that were analyzed using the β-method. Using the CAPWAP measured unit shaft resistance as q_s and the corresponding vertical effective stress, the β coefficient was back-calculated in IGM-rocks from Equation (38). Then, the regression analysis was performed to determine the relationship between back-calculated β-coefficient and the angle of friction, ϕ. A two-degree polynomial model given by Equation (44) was best fitted for the expected β-coefficient with an adjusted R^2 of 0.875, as shown in Figure 33.

$$\hat{\beta} = 0.0098\,\phi^2 - 0.75\phi + 14.63 \quad (44)$$

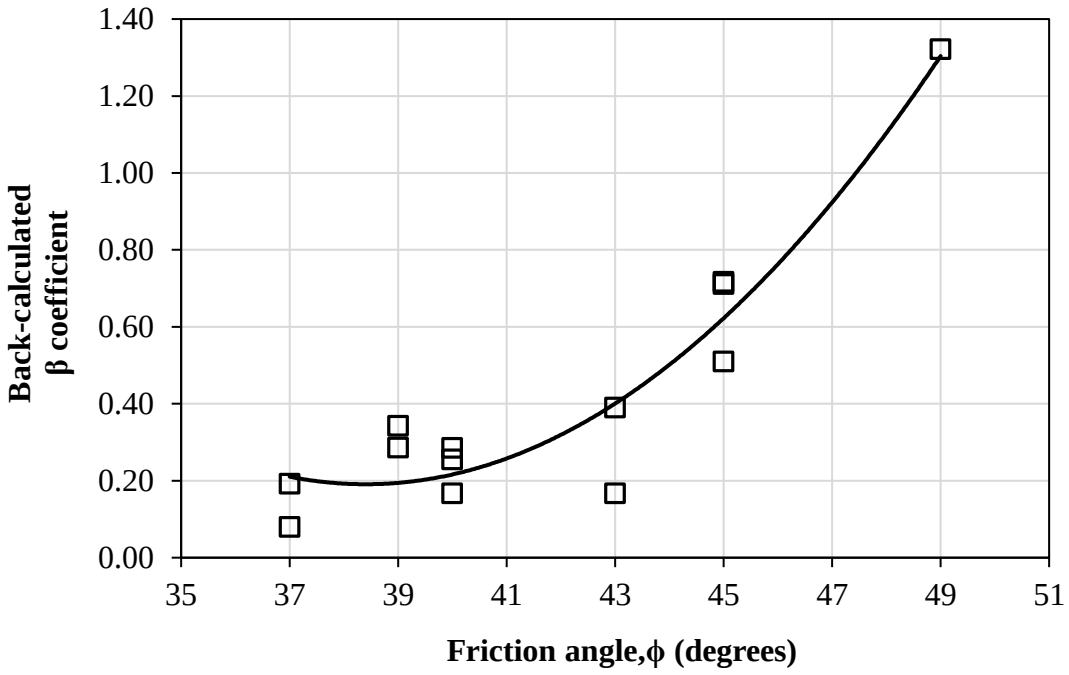

Source: Gebreslasie (2018)

Figure 33. Relationship between the back-calculated β coefficient and friction angle for driven piles in IGM-rocks (Gebreslasie 2018).

5.4.2.4 Calibration of the bearing capacity factor, N_t

Following the same procedure as described in Section 5.4.1.4 for the calibration of the bearing capacity factor, N_t in IGM-soils, the calibration was carried out for IGM-rocks. There were 13 piles in IGM-rocks bearing layers analyzed using the β-method. A two-degree polynomial model given by Equation (45) was the best fit between the back-calculated N_t and ϕ with a R^2 of 0.785 and an adjusted R^2 of 0.742 as shown in Figure 34.

$$\widehat{N_t} = 0.907\,\phi^2 - 71.399\phi + 1428.546 \quad (45)$$

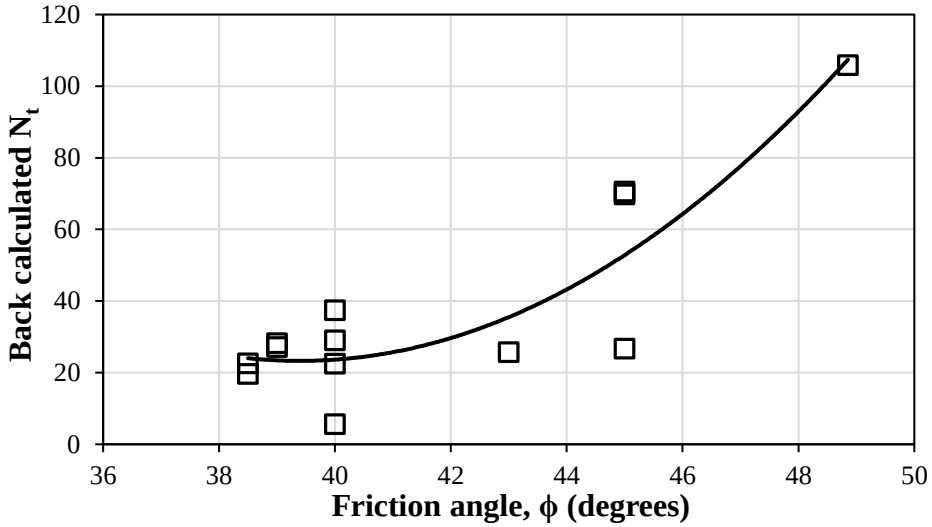

Source: Gebreslasie (2018)

Figure 34. Relationship between the back-calculated N_t and friction angle for driven piles in IGM-rocks (Gebreslasie 2018).

5.4.3 Summary of the calibrated α- and β-methods

The summary of the regression analyses performed by Gebreslasie (2018) for the calibration of design coefficients, is presented in Table 30.

Table 30. Summary of calibrated α- and β-methods for steel H-piles in IGMs (after Gebreslasie (2018)).

Static Analysis Method	**Unit Shaft Resistance (q_s)**	
	IGM-soil	**IGM-rock**
α-method	$\hat{\alpha} = 0.292 s_u{}^2 - 2.7092 s_u + 6.5077$ q_s (ksf) = $\hat{\alpha} \times s_u$; where, s_u is in ksf	$\hat{\alpha} = \frac{64.63 \times q_u^{-0.656}}{100}$ q_s (ksf) = $\hat{\alpha} \times q_u$; where, q_u is in ksf
β-method	NA[1]	$\hat{\beta} = 0.0098\,\phi^2 - 0.75\phi + 14.63$ q_s (ksf) = $\hat{\beta} \times \sigma'_v$ where, ϕ is in degree and σ'_v is in ksf
Static Analysis Method	**Unit End Bearing (q_p)**	
	IGM-soil	**IGM-rock**
α-method	NA[*]	$\widehat{N_c} = 39.8 \times q_u^{-0.635}$ q_p (ksf) = $\widehat{N_c} \times q_u$; where, q_u is in ksf
β-method	NA[1]	$\widehat{N_t} = 0.907\,\phi^2 - 71.399\phi + 1428.546$ q_p (ksf) = $\widehat{N_t} \times p_t$ where, ϕ is in degree and p_t is in ksf

s_u- undrained shear strength; q_s- unit shaft resistance; q_u- unconfined compressive strength; σ'_v- effective overburden stress at mid of soil layer; q_p- unit end bearing; p_t- effective overburden stress at pile tip; NA–not available; [1]–regression analyses revealed no relationships between variables, [*]– due to small sample size.

5.5 Validation using Pile Data from Literature

The calibrated α- and β-methods presented in previous section were assessed using pile load test data collected from available literature. Pile data collected by Brooks (2008), from Montana Department of Transportation (MDT), Long (2016), from Wisconsin Department of Transportation (WisDOT), and Larounis and Nop (2016), from Iowa DOT, were firstly evaluated for their usability. The data from Colorado Department of Transportation (CDOT) was also assessed.

Brooks (2008) assessed the performance of pile capacity determination methods consisting of DRIVEN, GRLWEAP, FHWA Gates driving formula, WSDOT Gates driving formula, and an empirical method used by the CDOT, in which the allowable axial pile capacity is limited to 25percent of material yield strength. Pile data, subsurface data, and CAPWAP results were obtained from nine bridge projects conducted by MDT. However, only eight projects were analyzed, as the Swan River Project (4288) was aborted because of counter-intuitive CAPWAP results. IGMs were categorized into cohesive and cohesionless IGMs where cohesive IGMs consisted of rocks like shale, claystone, siltstone, and sandstone, and cohesionless IGMs consisted of dense sandy gravels with high silt content. Twenty-one pile data were available, and 12 piles were open-ended pipe piles, five were steel H-piles, and the remaining four were close-ended pipe piles. Thirteen piles were driven into IGM-rocks, and the remaining eight piles were driven into dense sand and gravel (classified as IGM-soils). The subsurface profiles were available for the eight projects, and the CAPWAP results were reported in terms of total pile resistance, shaft resistance, and end bearing. However, the shaft resistance per geomaterial layer, especially the IGM layer, was not reported. Thus, the CAPWAP data in terms of total shaft resistance could not be used in validating our calibrated methods for determining shaft resistances in IGM-soil and IGM-rock. The CAPWAP data was used in validating calibrated methods for determining the end bearing in IGMs. Only 12 pile data were considered usable with some information for validating calibrated methods on end bearing in IGM-rocks. Calibrated β-method was used for estimating end bearing in sandstones and calibrated α-method was used for claystones and shales. However, as the required geomaterial properties and the information on pile plugging were missing, the following considerations were made in the end bearing calculations:

- Based on the observed friction angles for sandstones from Wyoming data, the minimum angle of 37° and the maximum angle of 45° were considered in the calculation. All the piles driven on sandstones were open-ended pipe piles whose diameters ranged from 406 mm to 762 mm. As box toe area was considered for determining unit end bearing in H-piles, the first combination of a friction angle of 37° and a closed toe area (considering plugged condition) was considered to yield the upper limit of the end bearing. The second combination consisting of actual cross-sectional steel area (unplugged) and a friction angle of 45° was considered to yield the lower limit of the end bearing.
- The missing UCS values of claystones from project 4329 were assumed as 27 ksf based on the average UCS of claystone from Wyoming data.
- Piles driven on claystones and shales were assumed a plugged toe area.

The pile data assembled by Long (2016) were also assessed to investigate if they could be used for validating the calibrated methods. Soil profiles, seven static load test results, and more than

200 dynamic load test results conducted on production piles driven in IGM-soils were reported. However, as the CAPWAP depthwise shaft resistance was absent, the calibrated methods for shaft resistances in IGMs could not be validated. Although the production piles were bearing on IGM-soils, calibrated methods were not developed for end bearing in IGM-soils, and these data can be used for future studies.

The data from Iowa DOT, presented in Larounis and Nop (2016), consisted of steel H-piles driven in IGM-rocks with 43 bents in shale, 36 in limestone, nine in sandstone, and one in siltstone. However, the data were non-usable as neither the CAPWAP nor static load test results were available. Similarly, the data from Colorado DOT were also non-usable due to the absence of CAPWAP results.

5.6 Discussion on Validation from Montana Data

The calculations of end bearing and resistance biases for the calibrated β- and α-methods are presented in Table 31 and Table 32, respectively. The predicted end bearing using calibrated methods and measured end bearing using CAPWAP are compared, in Figure 35 and Figure 36. Five data points in sandstones and seven in claystones were used from Mokwa and Brooks (2008) for validating the end bearing. In the absence of friction angles and plugging conditions for sandstones, their combinations were assumed to yield the upper and lower limits of end bearing, as shown in Table 31. The first combination of 37° friction angle with a closed toe area highly overestimated the end bearing with the mean resistance bias of 0.45 and resistance biases ranging from 0.19 to 0.69. The second combination of 45° and steel toe area highly underestimated the end bearing with the mean resistance bias of 4.40 and resistance biases ranging from 1.68 to 6.09. From Figure 35, the data points from both the combinations were highly deviated from the line of equity. From Table 32, the resistance biases obtained using calibrated α-method for estimating end bearing in cohesive IGM-rocks (claystones and shales) ranged from 0.45 to 2.39. The mean resistance bias of seven resistance biases from calibrated α-method was 1.47 with COV of 0.47. The discrepancy in end bearings of sandstones and cohesive IGM-rocks (claystones and shales) estimated from calibrated β- and α-methods, respectively might be due to several possible reasons. First possible reason might be the difference in the pile type used during calibration and validation. Steel H-piles were used for calibration while open-ended pipe piles were used for validation. Second reason might be the uncertainties in the friction angles and mobilized pile toe areas used for sandstones. The mobilized pile toe areas could be either fully plugged or unplugged. The discrepancy observed in Figure 36 between the predicted and measured end bearing might be attributed to the uncertainties in the UCS of claystones from project 4329.

Table 31. Determination of end bearing in sandstones using calibrated β-method and data from Montana DOT

Project Name	Pile Location	Pile Type	Pile Size (in)	Plugged Area (ft^2)	Toe Steel Area (ft^2)	N_t		Q_p (kips)		Q_{pm} (kips)	Resistance Bias	
						ϕ = 37°	ϕ = 45°	ϕ = 37° & plugged area	ϕ = 45° and unplugged area		ϕ = 37° & plugged area	ϕ = 45° and unplugged area
3417	O1	OP	16	1.40	0.19	28.47	52.27	528.59	59.77	286.8	0.54	4.80
	O2	OP	24	3.12	0.09	28.47	52.27	1045.87	118.06	198	0.19	1.68
	O3	OP	16	1.40	0.25	28.47	52.27	559.26	63.24	385.3	0.69	6.09
	B2	OP	30	4.95	0.25	28.47	52.27	1829.89	165.89	904.3	0.49	5.45
	B3	OP	30	4.95	0.09	28.47	52.27	1857.4	168.39	673.3	0.36	4.00
Mean											0.45	4.40
Std.											0.19	1.71
COV											0.42	0.39

COV- Coefficient of Variation of resistance biases; OP- Open-ended pipe pile; Q_p- Predicted end bearing; Q_{pm}- Measured end bearing from CAPWAP; Std.- Standard deviation of the resistance biases.

Table 32. Determination of end bearing in claystone and shale using calibrated α-method and data from Montana DOT

Project Name	Pile Location	Pile Type	Pile Size (in)	Bearing Layer	q_u(ksf)	Plugged Area (ft^2)	N_c	Q_p (kips)	Q_{pm} (kips)	Resistance Bias
3417	B4	OP	16	Claystone	16.27	1.40	6.77	153.51	127.76	0.83
2144	B1	CP	20	Shale	4.31	2.15	15.75	147.96	247.36	1.67
	B3	CP	20	Shale	1.96	2.15	25.92	111.09	134.19	1.21
	O1	OP	20	Shale	4.66	2.15	14.98	152.26	68.70	0.45
4329	B1	HP	12×84	Claystone	27.00*	1.08	5.94	137.10	214.58	1.56
	B2	CP	16	Claystone	27.00*	1.40	5.94	184.69	441.39	2.39
	B4	HP	12×84	Claystone	27.00*	1.08	5.94	138.81	303.72	2.19
Mean										1.47
Std.										0.70
COV										0.47

COV- Coefficient of Variation of resistance biases; OP- Open-ended pipe pile; CP- Closed-ended pipe pile; q_u- Uniaxial compressive strength; Q_p- Predicted end bearing; Q_{pm}- Measured end bearing from CAPWAP; Std.- Standard deviation of the resistance biases; *- assumed based on average UCS of claystones from Wyoming data.

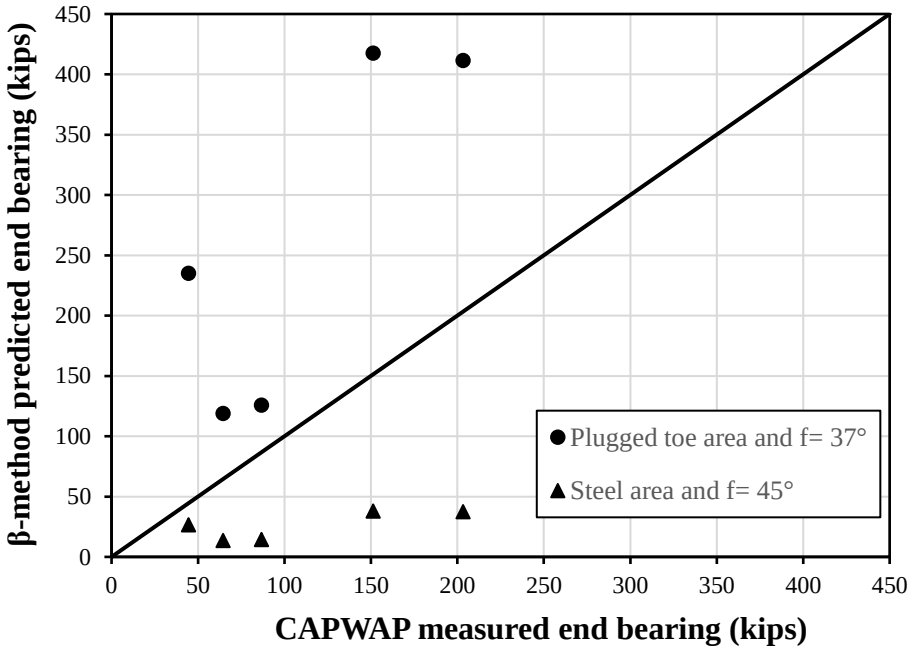

Source: Adhikari (2019)

Figure 35. Comparison of predicted vs. measured end bearing in sandstones.

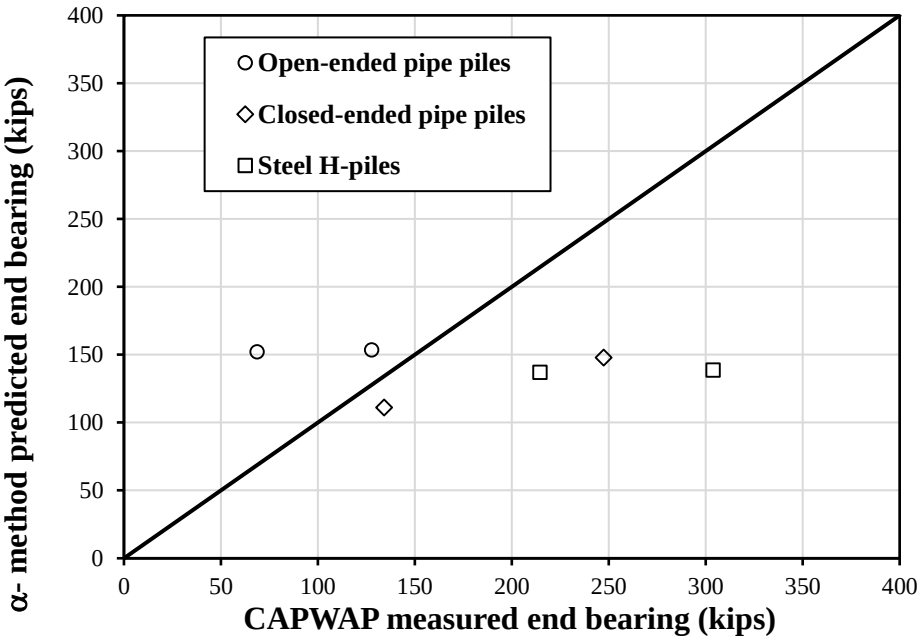

Source: Adhikari (2019)

Figure 36. Comparison of predicted vs. measured end bearing in claystones and shales.

5.7 Validation using Additional pile data from WYDOT

Since enough pile data were not available from literature to validate the calibrated methods for IGM-soils and IGM-rocks, additional nine pile data summarized in Table 33 were obtained from WYDOT.

Table 33. Summary of additional pile data obtained from WYDOT for validation.

S. No.	Project	Test pile no.	County	Pile size	L (ft)	Hammer	EOD blow counts (bpf)	Q_{tm} (kips)	Q_{sm} (kips)	Q_{em} (kips)
1	Laramie Streets	122N	Albany	12 × 53	28.7	APE D19-52	160	665	125	540
2	Laramie Streets	119O	Albany	12 × 53	27.8	APE D19-52	131	640	115	525
3	Laramie Streets	9S	Albany	12 × 53	15.3	APE D19-52	144	525.4	155.4	370
4	Laramie Streets	11S	Albany	12 × 53	15.3	APE D19-52	168	534.4	149.9	384.5
5	PB Marginal EBL (PS)	A-1 P-4	Laramie	12 × 53	73.2	APE D30-32	32	333	258	75
6	PB Marginal EBL (PS)	A-2 P-3	Laramie	12 × 53	70.0	APE D30-32	35	325	183	142
7	PB Marginal EBL (BS)	A-1 P-2	Laramie	12 × 53	51.0	APE D30-32	30	306	176	130
8	PB Marginal EBL (BS)	A-2 P-2	Laramie	12 × 53	41.0	APE D30-32	35	332	113	219
9	Woods Wardell	Pi-2 P-1	Sublette	12 × 53	23.0	APE D19-42	128	449.9	209.6	240.3

A-Abutment; EOD- End of Driving; L- Pile penetration; PB- Pine Bluffs; PS- Parson Streets; BS- Beech Street; Pi-Pier; P- Pile; Q_{tm}- CAPWAP measured total capacity; Q_{sm}- CAPWAP measured shaft capacity; Q_{em}- CAPWAP measured end bearing.

The description of the geomaterials along with their classification and design parameters, such as s_u, q_u, and ϕ, have been indicated in Table 34. IGM-rocks were categorized as cohesive and cohesionless geomaterials based on their parent geomaterials. For example, the parent geomaterial of sandstone is sand grain, which is a cohesionless geomaterial. Hence, sandstone was categorized as a cohesionless geomaterial while claystone was categorized as cohesive geomaterial. The design parameters were obtained from the boring logs. If they were not reported in the boring logs, they were either determined using the in-house reference tables developed by WYDOT or calculated using correlations from literature as described in Gebreslasie (2018). The approaches by which the design parameters were obtained are indicated by superscripts and footnotes in Table 34.

After obtaining the design parameters, α- and β- method were applied to estimate shaft resistances and end bearing in cohesive and cohesionless IGM-rocks, respectively. However, only α-method was applied to estimate shaft resistance in cohesive IGM-soils as calibration

could not be performed for end bearing estimation in IGM-soils, and shaft resistance estimation in cohesionless IGM-soils (Table 30) (Gebreslasie 2018). The nine pile data from three different projects were categorized in terms of geomaterials, pile resistance components, and the application of respective calibrated methods. The data available for validating each calibrated method in estimating each pile resistance component were reduced after categorization. Only three observations in IGM-soils and two observations in IGM-rocks were available for validating calibrated α-method in shaft resistance estimation. For validating calibrated α-method in end bearing estimation, only one observation was available. Four and five observations were available for validating calibrated β-method in shaft resistance and end bearing estimation, respectively in IGM-rocks. The calculated shaft resistances biases are presented in Table 35, and the calculated end bearing biases are presented in Table 36. The calibrated α-method had the mean resistance biases of 1.03 and 1.43 for shaft resistance estimation in IGM-soils and IGM-rocks, respectively. The calibrated β-method in IGM-rocks had the mean resistance biases of 1.28 and 1.61 for shaft resistance and end bearing estimation, respectively. The performance of calibrated α-method on end bearing estimation could not be determined because of a single data. The coefficients of variations were not calculated due to the small sample sizes less than or equal to five.

The performances of the calibrated methods on shaft resistance and end bearing estimations, illustrated in Figure 37 and Figure 38. Figure 37, shows that the calibrated α-method for IGM-soils provided the best estimation with all three triangular points almost fall on the line of equity. Despite slight underestimation of shaft resistance estimation, the performance of calibrated α-method was relatively better than the calibrated β-method for shaft resistance estimation in IGM-rocks. The calibrated β-method did not result in satisfactory estimation of both the shaft resistance and end bearing in IGM-rocks as evidenced from Figure 37 and Figure 38.

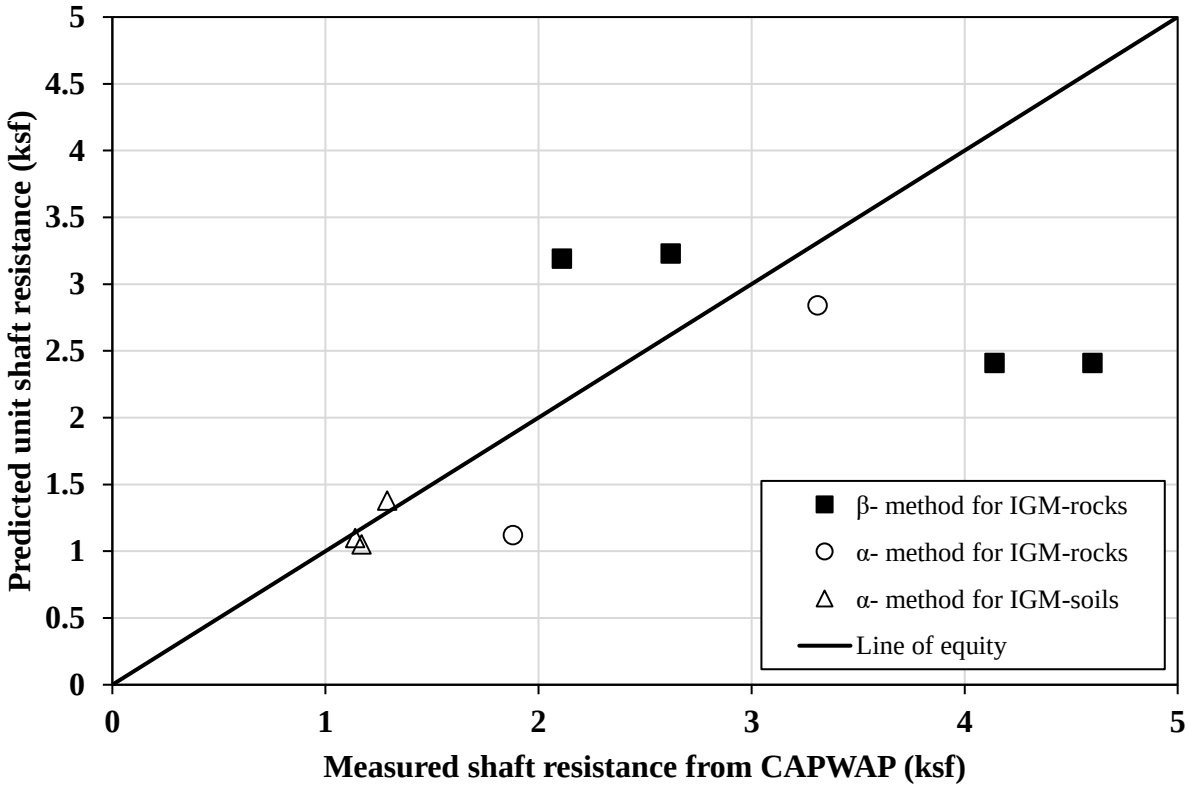

Source: Adhikari (2019)

Figure 37. Comparison of predicted unit shaft resistance using calibrated methods and the measured unit shaft resistance from CAPWAP.

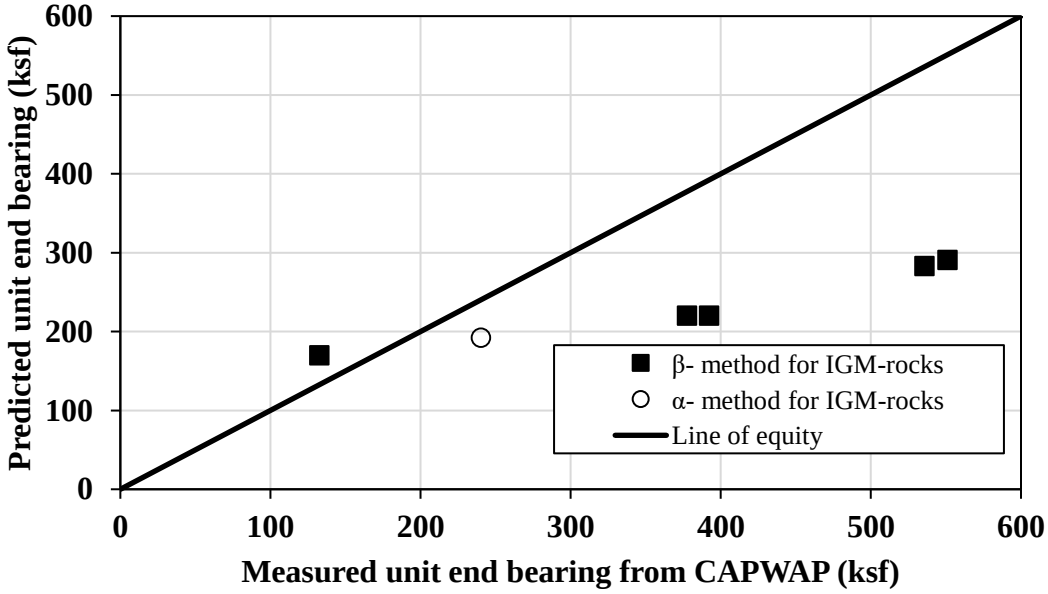

Source: Adhikari (2019)

Figure 38. Comparison of predicted unit end bearing using calibrated method and the measured unit end bearing from CAPWAP.

Table 34. Summary of geomaterial properties along the shafts and at bearing layers of additional test piles from WYDOT.

Project	Pile no.	Layer no.	Geomaterial Description	Layer Depth (ft)	$(N_1)_{60}$	γ (pcf)	RQD (%)	q_u (ksf)	c (psf)	ϕ (°)	s_u (ksf)	Classif-ication
Laramie Streets	122N	1	Lenticular-heterogenous silty-clayey sand with gravel, loose-medium dense, slightly moist saturated	18	15	117.6	NA	NA	850	26.7	1.36[#]	Soil
		2	Weathered siltstone with shale, slightly moist to dry	10.7	VH	138.75	57	80.8	NA	49[+]	NA	IGM-rock
Laramie Streets	119O	1	Lenticular-heterogenous silty-clayey sand with gravel, loose-medium dense, slightly moist saturated	18	15	117.6	NA	NA	850	26.7	1.36[#]	Soil
		2	Weathered siltstone with shale, slightly moist to dry	9.8	VH	138.75	57	80.8	NA	49[+]	NA	IGM-rock
Laramie Streets	9S	1	Lenticular-heterogenous silty-clayey sand with gravel, loose-medium dense, slightly moist saturated	11	63	117.6	NA	NA	850	26.7	1.36[#]	Soil
		2	Weathered siltstone with shale, slightly moist to dry	4.3	VH	138.75	57	80.8	NA	49.5[+]	NA	IGM-rock
Laramie Streets	11S	1	Lenticular-heterogenous silty-clayey sand with gravel, loose-medium dense, slightly moist saturated	11	63	117.6	NA	NA	850	26.7	1.36[#]	Soil
		2	Weathered siltstone with shale, slightly moist to dry	4.3	VH	138.75	57	80.8	NA	49.5[+]	NA	IGM-rock
PB Marginal EBL (PS)	A-1 P-4	1	Fill-slightly moist, medium dense, sandy silt with minor clay	16.39	37	128.9	NA	NA	500	32	1.38[$]	Soil
		2	Slightly moist, medium dense, silty sand & gravel	8	7	90[*]	NA	NA	321	37	0.53[#]	Soil
		3	Slightly moist, medium to very dense, sandy silt	48.81	21	108.3	NA	NA	NA	32	4[#]	IGM-soil
PB Marginal EBL (PS)	A-2 P-3	1	Fill-slightly moist, medium dense, sandy silt with minor clay	18.4	32	128.9	NA	NA	NA	NA	2.4[#]	Soil
		2	Slightly moist, medium dense, silty sand & gravel	15	9	120[*]	NA	NA	340	36.4	1.06[#]	Soil
		3	Slightly moist, medium to very dense, sandy silt	36.6	24	108.3	NA	NA	NA	NA	4.45[#]	IGM-soil

[*]- values taken from WYDOT table; [$]- calculated using WYDOT practice ($s_u = c + \sigma\tan\phi$); [#]- determined using Terzaghi's correlation between SPT N-values and s_u; NA- not available; [+]- recommended value for siltstones with very high SPT-N values based on Gebreslasie (2018); VH- very high equivalent SPT-N values exceeding 500; [1] – this lies at a depth within twice the pile size

Table 33. Summary of geomaterial properties along the shafts and at bearing layers of additional test piles from WYDOT (continue).

Project	Pile no.	Layer no.	Geomaterial Description	Layer Depth (ft)	$(N_1)_{60}$	γ (pcf)	RQD (%)	q_u (ksf)	c (psf)	ϕ (°)	s_u (ksf)	Classif-ication
PB Marginal EBL (BS)	A-1 P-2	1	Embankment-dry to slightly moist, medium dense, sandy silt with gravel	22.12	43	125*	NA	NA	NA	NA	2.40#	Soil
		2	Alluvium-dry to slightly moist, loose to dense, sandy silt with minor gravel	28.88	12	120*	NA	NA	NA	NA	1.67#	Soil
		3	Dry to slightly moist, dense to very dense, sandy silt to weak siltstone	0[1]	66	107.9	NA	NA	NA	40*	NA	IGM-rock
PB Marginal EBL (BS)	A-2 P-2	1	Embankment-dry to slightly moist, medium dense, sandy silt with gravel	20.77	43	125*	NA	NA	NA	NA	2.10#	Soil
		2	Alluvium-dry to slightly moist, loose to dense, sandy silt with minor gravel	20.23	44	120*	NA	NA	NA	NA	4.77#	IGM-soil
Woods Wardell	Pi-2 P-1	1	Hard, weathered siltstone & claystone bedrock, dry	18	68	128.45	NA	5	NA	NA	NA	IGM-rock
		2	Unweathered siltstone & claystone bedrock, very hard, dry	6.63	68	134.2	50	75	NA	NA	NA	IGM-rock

*- values taken from WYDOT table; $- calculated using WYDOT practice ($s_u = c + \sigma\tan\phi$); #- determined using Terzaghi's correlation between SPT N-values and s_u; NA- not available; +- recommended value for siltstones with very high SPT-N values based on Gebreslasie (2018); VH- very high equivalent SPT-N values exceeding 500; [1] –lies at a depth within twice the pile size

Table 35. Summary of shaft resistance biases in IGM-soils and IGM-rocks.

Shaft resistances in IGM-soils from α-method					
Project	**Pile no.**	**Layer no.**	**q_{sm}(ksf)**	**q_{sp}(ksf)**	**Resistance bias**
PB Marginal EBL (PS)	A-1 P-4	3	1.29	1.38	0.94
PB Marginal EBL (PS)	A-2 P-3	3	1.17	1.05	1.12
PB Marginal EBL (BS)	A-2 P-2	2	1.14	1.10	1.04
Shaft resistances in IGM-rocks from α-method					
Woods Wardell	Pi-2 P-1	1	1.88	1.12	1.68
		2	3.31	2.84	1.17
Shaft resistances in IGM-rocks from β-method					
Laramie Streets	122N	2	2.62	3.23	0.81
Laramie Streets	119O	2	2.11	3.19	0.66
Laramie Streets	9S	2	4.60	2.41	1.91
Laramie Streets	11S	2	4.14	2.41	1.72

q_{sm}- CAPWAP measured unit shaft resistance; q_{sp}- Predicted unit shaft resistance using calibrated equation.

Table 36. Summary of end bearing biases in IGM-rocks.

End bearing in IGM-rocks from β-method					
Project	**Pile no.**	**Layer no.**	**q_{em}(ksf)**	**q_{ep}(ksf)**	**Resistance bias**
Laramie Streets	122N	2	551.02	290.79	1.89
Laramie Streets	119O	2	535.71	283.26	1.89
Laramie Streets	9S	2	377.55	220.51	1.71
Laramie Streets	11S	2	392.35	220.51	1.78
PB Marginal EBL (BS)	A-1 P-2	3	132.65	170.02	0.78
End bearing in IGM-rocks from α-method					
Woods Wardell	Pi-2 P-1	2	240.3	192.43	1.27

q_{em}- CAPWAP measured unit end bearing; q_{ep}- Predicted unit end bearing using calibrated equation.

5.8 Change in Pile resistances

In order to investigate the change in pile resistances as a function of 24-hour restrike, the differences in the CAPWAP measured shaft resistances, and end bearing at the EOD and the BOR were quantified. As the restrikes for all pile cases were conducted the following day at approximately 24 hours after the EOD, the change in pile resistances presented here corresponds to the short-term pile response. Increase in pile resistance with time is known as pile setup while decrease in pile resistance with time is known as pile relaxation. The changes in unit end bearing and shaft resistance corresponding to geomaterials at the pile toe and pile shaft are presented as boxplots in Figure 39 and Figure 40, respectively.

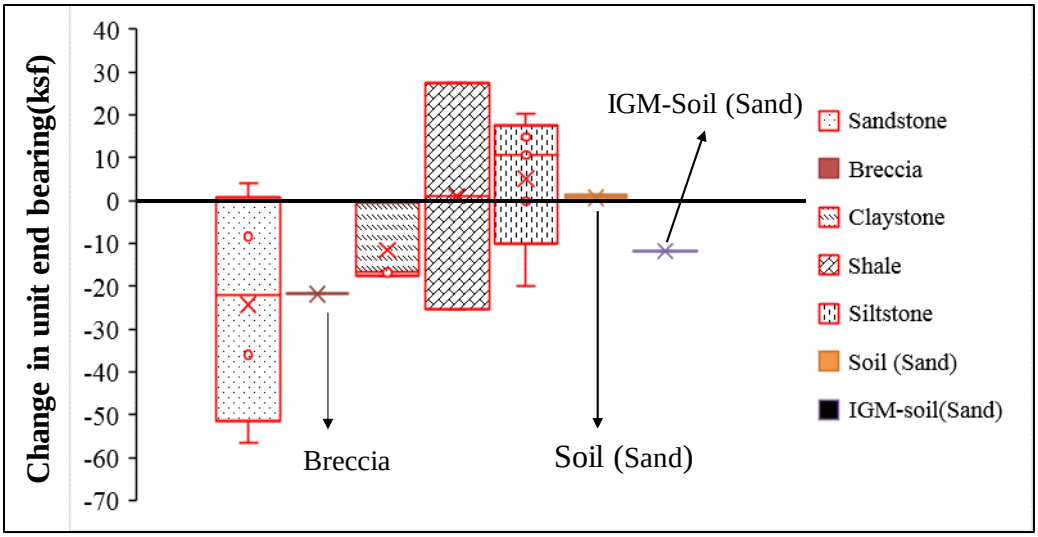

Source: Adhikari (2019)

Figure 39. Pile setup and relaxation observed in unit end bearing of different geomaterials.

Figure 39 shows that the IGM-rocks, such as sandstone, breccia, and claystones, exhibited pile relaxation. Sandstone exhibited the maximum relaxation of 57 ksf. One case of Breccia showed the relaxation of 22 ksf. However, some cases of piles bearing on IGM-rocks like shale, and siltstones showed both reduction and gain in unit end bearing. Of two pile cases on shales, one showed the relaxation of 25 ksf while the other showed pile setup of 28 ksf.

Figure 40 shows that majority of the geomaterials exhibited an increase in the unit shaft resistance with 24-hr restrike except dense sand and gravel (IGM-soil) and shale. Dense sand and gravel exhibited increase up to 0.6 ksf and decrease down to 1 ksf. Shale exhibited both increase and decrease in the unit shaft resistances. The increase was nearly as high as 1.25 ksf and the decrease was nearly down to 0.75 ksf. The decrease exhibited by other geomaterials was relatively insignificant.

The percentage change in unit end bearing with their respective $(N_1)_{60}$ for cohesionless IGM-rocks and q_u for cohesive IGM-rocks is presented in Figure 41 and Figure 42, respectively. Due to limited data points, relationship between percent change in unit end bearing and IGM properties could not be established.

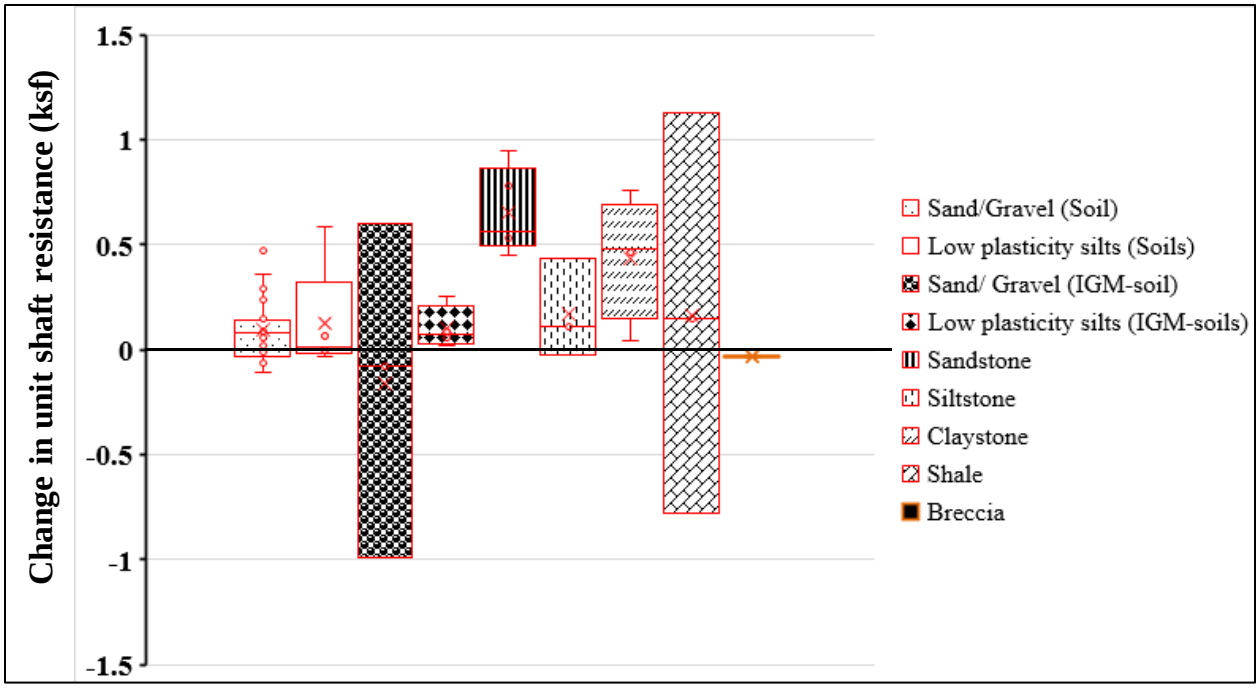

Source: Adhikari (2019)

Figure 40. Change in unit shaft resistance observed in different geomaterials.

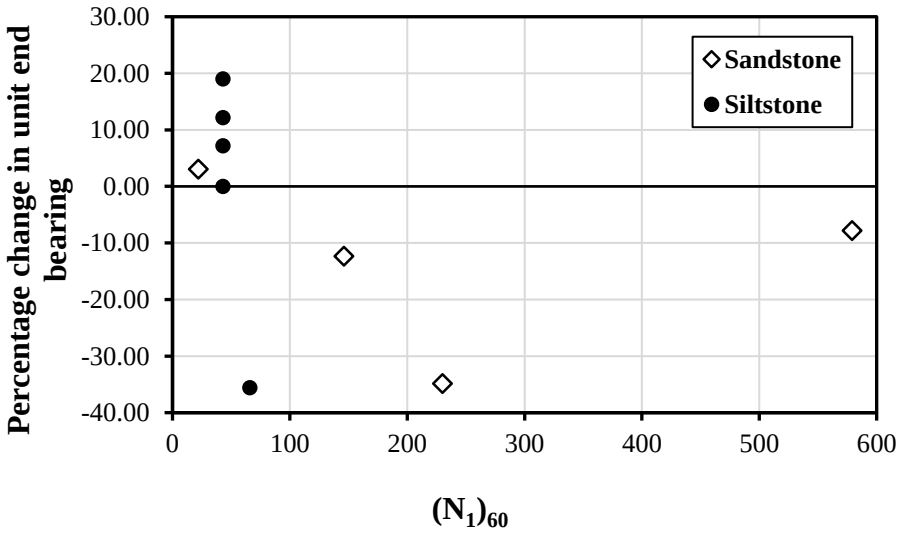

Source: Adhikari (2019)

Figure 41. Percentage change in unit end bearing with $(N_1)_{60}$ of sandstones and siltstones.

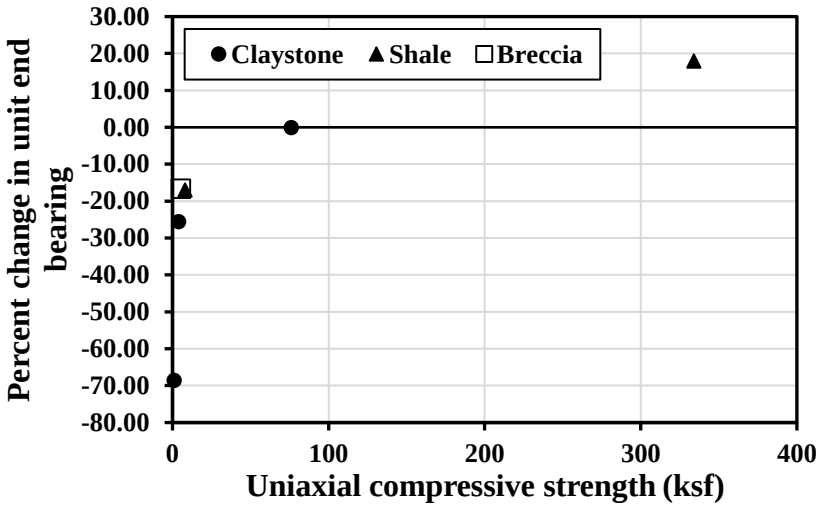

Source: Adhikari (2019)

Figure 42. Percentage change in unit end bearing with uniaxial compressive strength of claystone, shales, and breccia.

The percentage change in unit shaft resistances with $(N_1)_{60}$ values is presented in Figure 43, Figure 44, and Figure 45 for soils, IGM-soils, and IGM-rocks, respectively. As high as 180 percent increase in unit shaft resistance was observed in cohesionless soil. Few soils exhibited a decrease in shaft resistance with 51 percent being the maximum decrease. The percentage change in unit shaft resistance in cohesive soils was relatively lesser than cohesionless soils. For cohesive IGM-soils, only increase in unit shaft resistance was observed with maximum up to 20 percent. Only three cohesionless IGM-soils exhibited both the increase and decrease in unit shaft resistances. Unlike end bearing in IGM-rocks, increase in most of the unit shaft resistances was observed, in Figure 45.

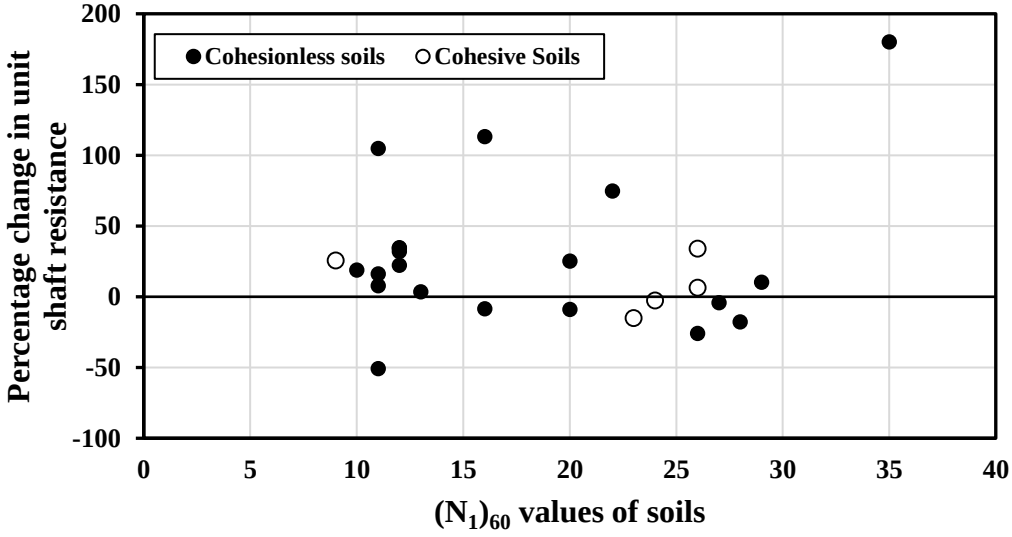

Source: Adhikari (2019)

Figure 43. Percentage change in unit shaft resistance with $(N_1)_{60}$ values of soils.

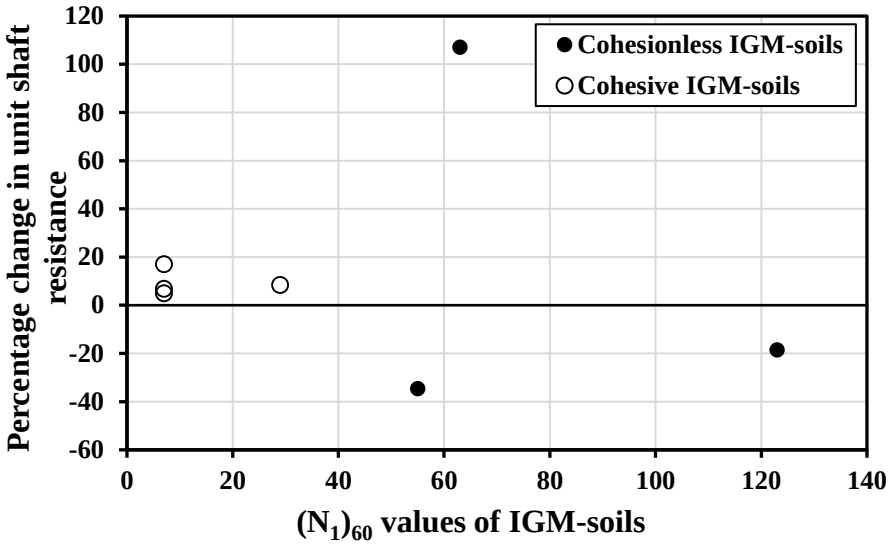

Source: Adhikari (2019)

Figure 44. Percentage change in unit shaft resistance with $(N_1)_{60}$ values of IGM-soils.

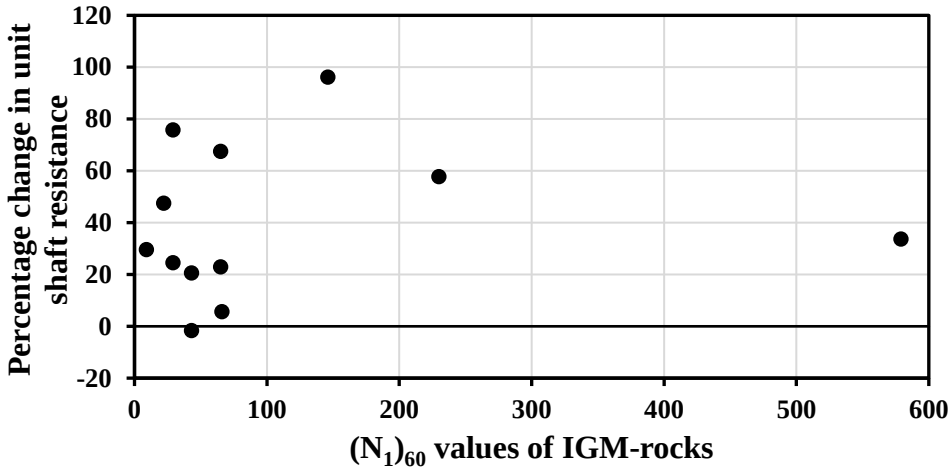

Source: Adhikari (2019)

Figure 45. Percentage change in unit shaft resistance with $(N_1)_{60}$ values of IGM-rocks.

From the assessment of change in unit end bearing and shaft resistances, unit end bearings decreased while unit shaft resistances increased in most cases. The combined effect of gain or loss in unit end bearing and shaft resistance influences the total pile capacity at BOR. The increase in shaft resistance may compensate the decrease in end bearing, resulting in no significant change in the total pile capacity.

5.9 Summary, Conclusions, and Recommendations

This chapter first evaluates the SA methods in different geomaterials in terms of statistical summaries, mean and COV of resistance biases. Then, the economic impact study of current pile design practice was made. The EOD and BOR records of 32 driven steel H-piles in IGM were

selected for the economic impact study. The assessment was performed based on the available CAPWAP results. Currently available SA methods developed for soils and used in the design of piles in IGM were shown to be inefficient as evidenced by the high COV. The economic study revealed that the current design procedures using the Nordlund and α-methods overestimated the pile resistances that ultimately lead to direct cost overruns associated with additional 0.84 lb and 3.86 lb of steel on average per kip load for both the EOD and BOR, respectively.

As the current pile design practice was proven to be inefficient, as characterized by high COV of static analysis methods, static analysis methods consisting of α- and β-methods were calibrated against IGM properties. Twelve pile data from MDT were utilized to evaluate the reliability of calibrated methods in the estimation of end bearing in IGM-rocks consisting of sandstones, claystones, and shale. However, an accurate end bearing prediction cannot be realized. The probable reasons are attributed to the following:

- Calibration was conducted based on steel H-piles; however, validation was conducted on mostly steel pipe piles.
- Since IGM friction angle and actual pile toe area were not reported, two combinations of internal friction angles and pile toe areas were adopted to yield the upper and lower limits of end bearing.
- Assumption on IGM UCS values was made based on the average UCS value observed from Wyoming report as IGM UCS values were not reported.

Additional and independent nine pile data from three projects provided by WYDOT were assembled and used for predicting shaft resistance and end bearing in IGM-rocks and shaft resistance in IGM-soils. The nine pile data were categorized based on the geomaterial (cohesive and cohesionless IGM-soils/ IGM-rocks), applicable calibrated method (α- and β methods), and pile resistance components (shaft resistance and end bearing), as shown in Table 35 and Table 36. After categorization, two and three data points were available for validating the α-method for IGM-rocks and IGM-soils respectively. Four and five data points were available for validating β-method in shaft resistance and end bearing estimation, respectively in IGM-rocks. However, only one data was available for validating α-method in end bearing estimation in IGM-rocks. The calibrated method could be validated if the mean resistance biases were approximately close to unity with lower COV of resistance biases. Nevertheless, COVs were not determined, due to small sample sizes of five or less. The evaluation showed that the α- method was relatively accurate in predicting the shaft resistance in IGM-soils with mean resistance bias of 1.03. Data were not enough to conclude the performance of calibrated α-method in IGM-rocks. The calibrated β-method did not yield accurate predictions of shaft resistance and end bearing estimations in IGM-rocks with mean resistance bias of 1.28 and 1.61, respectively. The poor performance might be due to the uncertainties in the determination of friction angles of the IGM-rocks that were used in the calibration and validation. All friction angles were not measured by in-situ and laboratory test methods, and they could not truly represent site conditions. Thus, the following recommendations are suggested to improve the pile resistance estimations in IGMs in future:

- IGM strength parameters should be measured and utilized in the calibration of design methods.
- Samples of IGMs should be tested to define their strength behaviors in terms of multiple material properties, rather than a single strength parameter. Incorporating multiple

material properties in the calibration can improve the efficiency of pile resistance estimation.

- More pile data in IGMs should be assembled to improve the calibration.
- The design coefficients should be formulated based on the fundamental behavior of pile-IGM interaction.

The time dependent study of piles driven on IGMs revealed decrease in the unit end bearing. All the IGM-soils and IGM-rocks exhibited decrease in unit end bearing on 24-hr restrike though some siltstones and shales exhibited some increase along with the decrease. The observed decrease in unit end bearing was as high as 70 percent in claystones, whereas the increase was minimal with 20percent in both the siltstone and shale. The decrease in unit end bearing may be due to the inability of the driving hammer to mobilize the end bearing on restrike and hence, may be apparent relaxation. Unlike end bearing, the time dependent study of shaft resistance of piles revealed mainly increase except in some shales and sand/gravel layers classified as IGM-soils. The gain in unit shaft resistance was as high as 180 percent for soils, 110 percent for IGM-soils, and nearly 100 percent for IGM-rocks. Few cases with decreased unit shaft resistances were observed in soils and IGM-soils. Thus, the gain or loss in total pile resistance is the combination of setup or relaxation in end bearing and shaft resistance. Relaxation of end bearing piles may lead to decrease in total pile resistance.

CHAPTER 6. WAVE EQUATION ANALYSIS OF DRIVEN PILES IN IGM

6.1 Introduction

AASHTO (2017) define IGMs as the materials whose strength and compressibility are transitional between rock and soil. Geotechnical engineering involves uncertainties arising from the inherent soil variability, measurement error, and transformation model (Kulhawy, 1992). These uncertainties are further aggravated when dealing with geomaterials that lie on the continuum between soils and rocks. IGMs can result either from the disintegration, weathering, shearing, and tectonization of hard rocks or from the consolidation and cementation process during lithification and diagenesis. Owing to the degree of transformation from rock to soil or vice-versa, IGMs exhibit greater variabilities in their engineering properties like density, hardness, and strength. Difficulties are often encountered in the identification, sampling, and quantification of engineering parameters representative of IGMs (Long and Horsfall, 2017). Although a large number of descriptive definitions exist for IGMs, they lack the consistent quantitative characterization for design and construction of driven piles. Designers often need to rely on correlations developed for soils to determine properties like unconfined compressive strength (UCS) and angle of internal friction from SPT N-values. Some difficulties associated with driven piles in IGMS are the determination of an adequate soil resistance to driving (SRD) profiles, selection of material parameters, and accurate modeling of the dynamic behavior during driving (Terente, et al., 2015). The pile penetrations into the IGMs are more unpredictable, and thus, relies greatly on the local experience and engineering judgment (Gannon, et al., 1999). Ng and Sullivan (2017b; 2016) and Ng et al. (2015) have illustrated the existing challenges of design and construction of driven piles in IGMs considering case studies of bridge projects in Wyoming.

The wave equation has been long applied to simulate a complex pile driving process by mathematical modeling of one-dimensional propagation of the wave in a pile. Smith (1960) provided the solution of the wave equation using a finite difference scheme. Using the mathematical model by Smith (1951; 1960), a computer program called WEAP was developed by Goble et al. (1976) and Hirsch et al. (1976) for dynamic analysis of piles during driving. The program models the hammer, driving system, pile, and soil (geomaterial) through a combination of lumped masses, springs, and dashpots. WEAP is a widely used dynamic analysis method today for the drivability analysis, static pile resistance estimation, determination of induced stresses in the pile, and assurance of pile integrity. It offers economic construction control measures including verification of the designed pile capacity in the field where static pile load tests are economically not feasible. The bearing graph is one of the important outputs of WEAP, which is for pile resistance determination.

The bearing graph analysis is influenced by the input parameters in the hammer model, driving system model, pile model, and soil model. For a fixed hammer with an observed stroke height and a fixed driving system for driving a pile, the bearing graph is only influenced by the soil (geomaterial) model. The geomaterial is modelled by a series of springs and dashpots attached to the lumped masses (pile segments) of a pile to represent the shaft resistance. A spring and a dashpot are also connected to the end pile segment to represent the toe resistance or end bearing. The spring models the static resistance, whereas the dashpot models the dynamic resistance of a geomaterial. The static resistance at any time on a pile segment (i) is dependent upon the ratio of

the spring displacement (u_i) to the quake value (q_i) and an ultimate static resistance (R_{ui}) in that pile segment as shown by Equations (46) and (47). Thus, q_i is an important spring model parameter, which corresponds to the displacement at which the elastic spring yields (Pile Dynamics, Inc. 2005). Moreover, the underlying equations in WEAP used for calculating R_{ui} were originally developed for soils. Hence, there is a need to investigate the performance of WEAP whose underlying equations for determining static geotechnical resistance are non-representative of IGMs.

$$R_{si} = \left(\frac{u_i}{q_i}\right) R_{ui} \text{ for } \frac{u_i}{q_i} \leq 1 \quad (46)$$

$$R_{si} = R_{ui} \text{ for } \frac{u_i}{q_i} > 1 \quad (47)$$

Due to the unavailability of static analysis methods specific to IGMs for the determination of unit shaft resistance and end bearing, users mostly rely upon default WEAP values. The equations and the limiting values used by WEAP for determination of unit shaft resistance and end bearing were originally developed for soils and are non-representative for IGMs. Furthermore, challenges are often encountered during the input of the IGMs in the geomaterial profile due to the maximum allowable SPT N-value of 60, and the selection of the dynamic parameters. Therefore, the study has been conducted to assess the performance of the WEAP based on an electronic database of steel H-piles driven in IGMs throughout Wyoming. Twenty-five piles driven in IGMs with the EOD records out of 35 were selected for the study as these contained all the required pile, subsurface, hammer and driving information. A bearing graph generated for each pile has been analyzed to assess the reliability of WEAP in determining axial pile resistance based on the observed blow counts during a pile driving process. The study presents research outcomes and recommendations to facilitate wave equation analysis of driven piles in IGMs. Resistance factors using FOSM, FORM, and Monte Carlo Simulation (MCS) have also been calibrated to achieve the required reliability during the application of WEAP in IGMs.

6.2 Challenges of Dealing with IGMs in WEAP

The major challenge for bearing graph analysis of piles driven in IGMs lies in the input of the geomaterial profile for static analysis. Two static analysis methods presented in WEAP are soil type based method (ST) and SPT N-value based method (SA^*). ST method allows qualitative, while SA^* method allows a quantitative description of the geomaterial. IGMs cannot be inputted into the program as a separate geomaterial, and they need to be modeled either as a very dense granular or hard cohesive soil when ST method is adopted. Although the geomaterial input considering rock or other geomaterial can be a possible way for inputting IGMs in SA^* method, the program does not generate the unit shaft and toe resistances, and the user needs to manually input these values. However, the manual input is impossible due to the lack of reliable static analysis methods for the determination of unit shaft resistance and end bearing of piles on IGMs. Recent studies by Adhikari et al. (2018) and Ng and Sullivan (2017a) confirmed that the current AASHTO (2017) provision of treating IGMs as soils for static analysis resulted in highly inconsistent estimation of pile resistances.

IGMs often have SPT N-values exceeding 60, which is the maximum value accepted by the SA^* method. Although other geomaterial properties like uniaxial compressive strength (UCS) and

friction angle (ϕ) can be used in place of SPT-N value in the SA* method to input IGMs, these parameters are rarely obtained from laboratory tests due to the difficulties in sampling and laboratory testing of IGMs. Additionally, the limiting unit shaft resistance (q_s) and end bearing (q_t) in the ST and SA* methods, as summarized in Table 37 and Table 38, may not be representative for IGMs. Often, the measured unit end bearing values from CAPWAP for IGMs are seen to be higher than these limiting values used in WEAP. This again necessitates the user-defined unit resistances for IGMs. However, lack of established static analysis methods to determine unit resistances in IGMs has compelled the users to rely on the available methods developed for soils in WEAP.

Table 37. Limiting unit shaft resistance and end-bearing of ST method in WEAP (Pile Dynamics, Inc., 2005).

Analysis method	Soil Type		Limit (ksf)		Soil Type		Limit (ksf)	
			q_s	q_t			q_s	q_t
ST	Non-cohesive soils	Very loose	0.5	50	Cohesive	Very soft	0.07	1.13
		Loose	1.0	100		Soft	0.22	3.38
		Medium	1.5	150		Medium	0.40	6.77
		Dense	2.0	200		Stiff	0.80	13.53
		Very dense	4.0	400		Very stiff	1.33	27.07
						Hard	1.61	36.09

q_s- limiting unit shaft resistance; q_t- limiting unit end bearing.

Table 38. Limiting unit shaft resistance and end-bearing of SA* method in WEAP (Pile Dynamics, Inc., 2005).

Analysis method	Soil Type	Limit (ksf)	
		q_s	q_t
SA*	Sand and gravel	5.22	250.62
	Clay	1.57	67.67
	Silts	5.22 (Non-cohesive) /1.57 (Cohesive)	125.31

q_s- limiting unit shaft resistance; q_t- limiting unit end bearing.

The selection of the dynamic parameters, like damping and quake values for IGMs, possess another challenge. However, the scope of the study encompasses only the assessment of the WEAP recommended toe quake values corresponding to dense soil and hard rocks in the bearing graph analysis as the IGMs present in the bearing layers were assumed to influence toe quake values. Toe damping values recommended in WEAP are independent of geomaterials because of which they were not included in the scope of the study. Toe quake values recommended by the GRLWEAP software version 2010-4, as presented in Table 39, are based on the geomaterial and pile type, whether displacement or non-displacement, which further depends upon the plugging condition as per the WEAP manual (Pile Dynamics, Inc., 2005). H-piles with a width less than 20 inches is considered as displacement piles in WEAP.

Table 39. WEAP recommended toe quake values from GRLWEAP software version 2010-4.

Geomaterial Type	Pile type	Quake (in)
All soil types, soft Rock	Non-displacement piles i.e. driving unplugged	0.1
Very dense or hard soils	Displacement Piles of diameter or width D	D/120
Soils which are not very dense or hard	Displacement Piles of diameter or width D	D/60
Hard Rock	All Types	0.04

6.3 Bearing Graph Analysis

Twenty-five of the 28 piles with the EOD records, which were driven in IGMs (Figure 29), were selected for the study. The project information, pile location and size, driving hammer, bearing layer and its properties, and EOD blow counts can be referred from Table 8 in chapter 3. Since the widths of all piles in the study are smaller than 20 inches and information regarding the plugging condition was not available, all piles were assumed as displacement piles for the selection of toe quake values.

For this study, the bearing IGM layers were categorized into IGM-rocks and IGM-soils to reduce the variation in the material behavior of IGMs ranging from rocks to soils. IGM-rocks refer to the IGMs, which are geologically defined as rocks but whose strengths are not high enough to induce structural failure of the pile. IGM-soils refer to the disintegrated geomaterials, which are stronger than soils. IGM-rocks in this study consist of sandstone, shale, claystone, siltstone, and breccia and IGM-soils consist of dense sand and gravels having $(N_1)_{60}$ greater than 50 and low plasticity silts having UCS greater than 2.7 ksf.

WEAP analysis begins with the input of the hammer data, driving system, pile data, and geomaterial information. The information about the hammer, driving system, pile properties, and subsurface profiles have been retrieved from the WyoPile database. Driving system data comprises of the helmet weight, pile cushion, and hammer cushion material. Since all test piles are steel H-piles, only the hammer cushion properties were required. The driving system data (helmet weight and cushion properties) provided in the reports were used for the analysis; otherwise, the manufacturer's recommended values were adopted. The analysis has been conducted based on the field driving records. Therefore, hammer stroke was fixed to the average hammer stroke during the last foot of driving. As SA^* method allows more comprehensive and quantitative input of geomaterials, the static soil resistance determination was facilitated by entering the geomaterial profile using the SA^* method.

6.3.1 SA^* Method

Due to the limitation of the WEAP in describing IGMs, the following steps were followed for geomaterial profile input in the SA^* method:

1) If $(N_1)_{60}$ values of the geomaterials are less than 60, $(N_1)_{60}$ and unit weight values are used.

2) If $(N_1)_{60}$ values of IGM-rocks, like sandstone and siltstone whose constituents are majorly cohesionless coarse-grained geomaterials, exceed 60, the angle of internal friction (ϕ) and unit weight values are used.
3) If $(N_1)_{60}$ values of IGM-rocks, like claystone and shale whose constituents consist mainly of cohesive geomaterials, exceed 60, UCS and unit weight values are used.
4) If $(N_1)_{60}$ values of IGM-soils, like dense sand and gravel and silts (cohesionless silts), exceed 60, the angle of internal friction and unit weight values were used.

Although the above-mentioned steps allowed an alternative way of IGM input for geomaterial profile in SA* method, it is important to note that the underlying equations for static geotechnical analysis in WEAP are for soils. Also, the default toe quake values assigned by the WEAP may not always correspond to the dense or stiff geomaterials when other properties, such as angle of internal friction, and UCS are used to define IGMs. Therefore, the analysis was conducted considering two different cases for the toe quake values as follows:

- Case I: Bearing graph analysis was conducted using program assigned toe quake values.
- Case II: Bearing graph analysis was conducted using toe quake values of D/120 for IGM-soils and 0.04 in for IGM-rocks, where D is a pile dimension.

Two shaft-damping values of 0.05 s/ft and 0.20 s/ft are recommended by WEAP for non-cohesive and cohesive soils respectively. The intermediate value of 0.10 s/ft is assigned by the program for silts. In the case of layered soils, a constant value, which the weighted average shaft-damping value with respect to the static resistance contributed by the layers to the total static resistance, is assigned throughout the shaft. The shaft quake and the toe damping are independent of geomaterial and pile types, and constant values of 0.1 in and 0.15 s/ft, respectively, are used in the analysis.

After all the required inputs were made, the drivability analysis was carried out. Since the drivability analysis was conducted based on observed blow counts at the EOD, the setup and the gain/loss factors were considered unity to assume no pile setup/relaxation. Using the shaft resistance percentage determined from the drivability analysis, bearing graph analysis was conducted to estimate the pile resistance based on the EOD blow counts.

6.4 Results

Pile resistances were determined for each test pile from bearing graph analysis in WEAP considering both the abovementioned cases for toe quake values. The estimated pile resistance from WEAP was compared to the respective measured pile resistance from CAPWAP and expressed in terms of a resistance bias. Resistance bias is a ratio of the measured pile resistance to the estimated pile resistance. Resistance bias greater than 1 indicates that the resistance predicted by WEAP is less than the measured capacity from CAPWAP. The comparison of the WEAP predicted resistance to CAPWAP measured resistance is shown in Figure 46 for both the cases. The statistical results of the resistance biases are summarized in Table 40.

Figure 46 shows that most of the points lie close to one-to-one (bias=1) line and within the range of bias lines from 0.75 to 1.25, indicating that WEAP predictions are approximately close to

CAPWAP values. However, there are few points whose biases are smaller than 0.75 and larger than 1.25. The two circles out of three, lying above the bias line of 0.75 are for two piles in BNSF Torrington Project with relatively long pile penetration lengths of 100 ft and 139 ft. The remaining one belongs to the shortest pile with penetration length of 19.5 ft of Hunter Creek project. The pile resistances of these two longer piles and a shortest pile seem to be highly overestimated by WEAP. The square points above the bias line of 0.75 are attributed to the overestimation of pile resistances resulting from the reduction in the toe quake values from D/60 to D/120 or 0.04 in for IGMs. Table 40 indicates that the number of piles whose resistances have been overestimated increased from 13 to 16 as the toe quake values change from Case I to Case II.

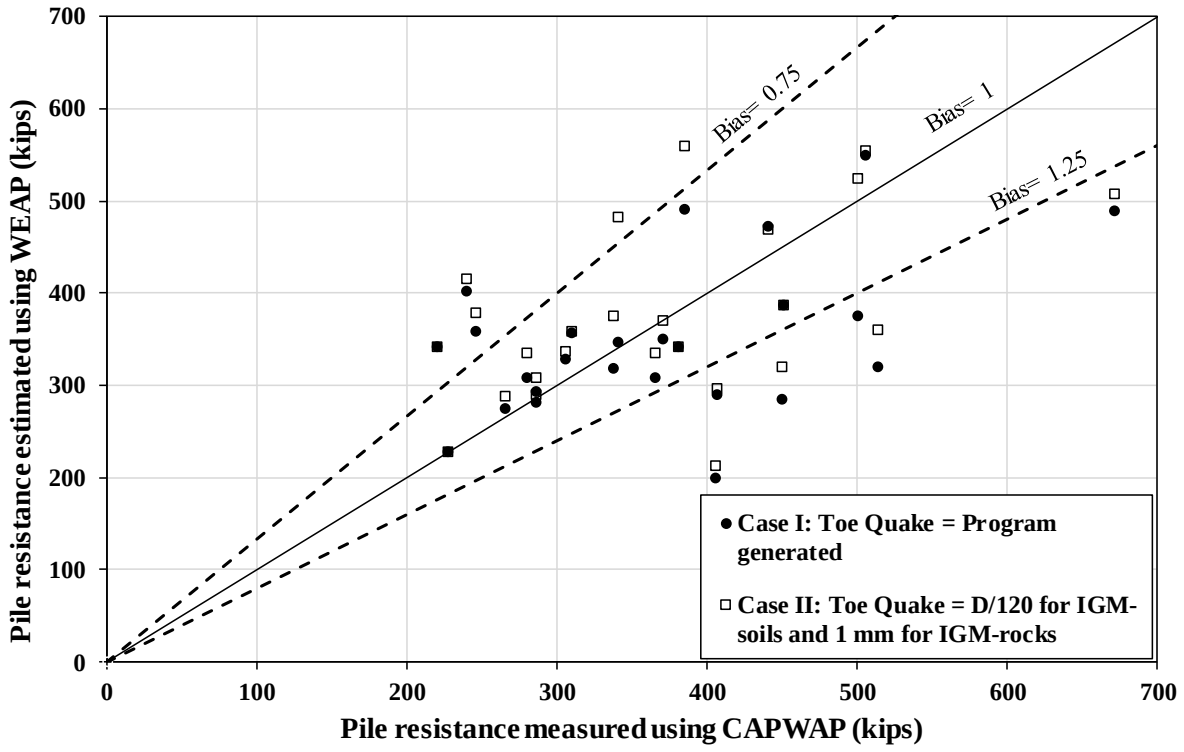

Source: Adhikari (2019)

Figure 46. WEAP predicted resistances vs. CAPWAP measured resistances.

Table 40. Summary of statistical results of two cases

Statistical Parameters	Case I	Case II
Number of data (n)	25	25
Mean Bias, λ_R	1.06	1.01
Standard deviation	0.33	0.30
Coefficient of Variation (COV)	0.31	0.30
Maximum Bias	2.02	1.90
Minimum Bias	0.59	0.58
Number of pile cases overestimated	13	16

Case I- Program generated toe quake value; Case II – Toe quake is 0.04 in for IGM-rocks and D/120 for IGM-soils.

6.5 Resistance Factors

To satisfy the LRFD, a resistance factor (φ) is applied to a nominal pile resistance to yield a factored pile resistance. Resistance factors currently recommended by AASHTO (2017) for IGMs were originally developed for soils. The target reliability indices (β_T) used in the calibration of resistance factors are 2.33 and 3.09 for redundant and non-redundant pile groups, respectively (Paikowsky et al., 2004). Applying the recommended resistance factors to IGMs which were developed for soils, will not ascertain these target reliability indices. Thus, it is important to calibrate the resistance factors to reflect the reliability of pile resistance estimation pertaining to IGMs. This study aims at calibrating resistance factors for the bearing graph analysis of WEAP for IGMs. The FOSM, FORM, and MCS were used for the determination of resistance factors. The fitted distributions of the biases for both cases are shown in Figure 47.

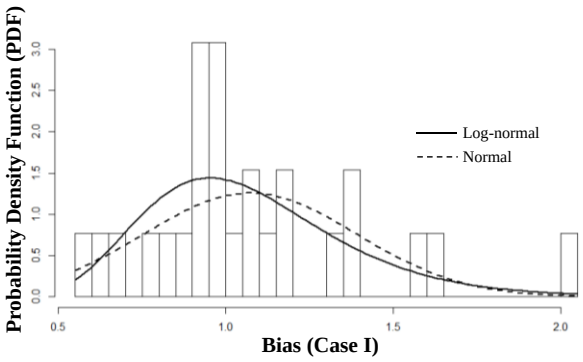

Source: Adhikari (2019)

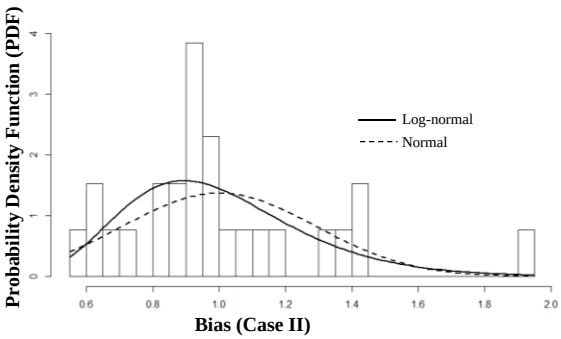

Source: Adhikari (2019)

Figure 47. Fitted distribution curves of biases in case I and case II respectively.

From Shapiro-Wilk normality test, the p-values of the Case I biases were 0.04 and 0.80 for normal and lognormal distribution, respectively. Similarly, the p-values from Shapiro-Wilk test for Case II biases are 0.02 and 0.58 for normal and lognormal distribution. As the p-values were greater than the significance level of 0.05 for lognormal distributions, lognormal distributions were confirmed. Also, the fitted distributions, as shown in Figure 47, confirm lognormal distributions for both cases. Using the closed form equation of FOSM, as given by Equation (23), preliminary resistance factors were firstly determined using FOSM for both cases. The statistical parameters of the loads required for the calculation of resistance factors were selected from Paikowsky et al. (2004), which are summarized in Table 7. Dead load to live load ratio was taken as two. Then, the resistance factors were determined using FORM and MCS. The detailed procedures on FORM and MCS are explained in sections 2.7.6 and 2.7.7, respectively. The resistance factors for Cases I and II corresponding to β_T of 2.33 and 3.00 from all three FOSM, FORM, and MCS are given in Table 41. Number of simulations considered in MCS was 1 million. Resistance factors for the Case I was slightly greater than that for Case II because the pile resistances based on the default program generated toe quake values were relatively underestimated resulting in a higher mean bias of 1.06. The FORM and MCS resistance factors were almost equal for both the target reliability indices. The FORM and MCS resistance factors were approximately 13 percent higher than FOSM resistance factors on average for reliability index 2.33. However, for reliability index 3.00, MCS and FORM resistance factors were 14 percent and 17 percent higher than FOSM resistance factors. On increasing the reliability index to 3.00 from 2.33, the FOSM, FORM, and MCS resistance factors decreased by 22 percent, 19

percent, and 21 percent, respectively. Thus, decreasing the reliability index by 20 percent would be reasonable for non-redundant pile groups.

Table 41. Calibrated resistance factors from FOSM, FORM, and MCS.

Case	Statistical Summaries			Calibrated Resistance Factor (φ)					
				FOSM		FORM		MCS	
	λ_R	COV_R	N	β_T= 2.33	β_T= 3.00	β_T= 2.33	β_T= 3.00	β_T= 2.33	β_T= 3.00
I	1.08	0.29	25	0.60	0.47	0.68	0.55	0.68	0.54
II	1.01	0.30	25	0.55	0.43	0.62	0.50	0.62	0.49

Case I- Program generated toe quake value; Case II – Toe quake is 0.04 in for IGM-rocks and D/120 for IGM-soils.

6.6 Summary and Conclusions

Due to the limitations in describing the geomaterial profile consisting IGMs in WEAP and the absence of reliable static analysis methods for determination of unit shaft resistance and end bearing in IGMs, challenges are encountered in the design and construction of piles in IGMS. The assessment of the performance of WEAP in IGMs has become extremely important to evaluate the reliability of the method in verification of the designed pile capacity. Furthermore, the application of the AASHTO recommended resistance factors developed for soils on IGMs cannot assure the required target reliability in the design and construction of driven piles in IGMs.

This study was conducted based on 25 steel H-piles driven in IGMs retrieved from an electronic database (WyoPile) developed by the research team. Detailed methodology recommended for conducting the bearing graph analysis using WEAP for piles in IGMs is presented. The effects of Case I considering program generated default toe-quake values and Case II considering user-defined toe-quake values of D/120 and 0.04 in for IGM-soils and IGM-rocks on pile resistance estimations were assessed. The suggested steps on inputting properties of IGM in WEAP yield reliable pile resistance estimations with mean biases of 1.08 and 1.01 for Cases I and II, respectively with approximate COVs of 30 percent. The slightly higher mean bias of Case I indicates that the program generated toe-quake values are slightly conservative. Nevertheless, the difference is not significant, and the users can rely on the default program generated toe-quake values for the bearing graph analysis using WEAP.

As FOSM resistance factors were conservative, the average of FORM and MCS rounded down to nearest 0.05 are recommended. The resistance factor of 0.65 and 0.60 is recommended for the Cases I and II of WEAP with the target reliability index of 2.33 for redundant pile groups. The resistance factors can be decreased by 20 percent for target reliability index of 3.00 corresponding to non-redundant pile groups. These newly calibrated resistance factors for piles in IGMs are higher than the current AASHTO recommended resistance factor of 0.5. The uncertainties in these resistance factors have been assessed in section 7.6. Thus, using the procedures outlined above for piles in IGMs, higher resistance factors can be employed. Overall, the WEAP bearing graph analysis can be concluded as a reliable construction control method for pile capacity verification during construction.

CHAPTER 7. CALIBRATION OF RESISTANCE FACTORS FOR DESIGN OF DRIVEN PILES IN IGMS

7.1 Introduction

LRFD is a reliability-based design that considers uncertainties in loads and resistances separately using load and resistance factors to maintain a prescribed level of safety, measured in terms of reliability index, β. Resistance factors calibrated for driven piles in soils are currently recommended for designing driven piles in IGMs by the AASHTO (2017). These resistance factors incorporate various uncertainties associated with inherent material properties, design parameters, and design models to ensure a prescribed level of reliability in the design. However, the resistance factors calibrated based on pile databases in soils (Paikowsky et al. 2004) are unlikely to account for the uncertainties prevalent in IGMs. Consequently, reliable and economic pile design cannot be achieved in IGMs. This necessitates the quantification of uncertainties in the pile design specific to IGMs followed by the calibration of resistance factors.

This chapter presents the calibration of resistance factors for SA methods using three reliability models: FOSM, FORM, and MCS methods. The calibration was conducted by considering new geomaterial classification criteria for driven piles and Wyoming pile datasets formed after categorization of geomaterials under different SA methods for two pile resistance components (shaft resistance and end bearing). Resistance factors were calculated for the datasets formed after combining original 28 driven pile records at end of driving with the additional nine pile data from three different projects obtained for validation in chapter 5. Resistance factors were calculated for the existing and calibrated SA methods. Histograms along with fitted distribution curves for normal and log-normal distributions were presented for each group of geomaterial and SA method. Lognormal distribution was selected as the best fit distribution from the maximum likelihood method and the lognormality was further confirmed using normality tests by Shapiro and Wilk (1965) and Anderson and Darling (1952). Efficiency factors were calculated to compare existing and calibrated SA methods. Finally, SA methods and their respective resistance factors were recommended based on efficiency factors for the design of driven piles in IGMs.

7.2 Statistical parameters and Distribution of Resistance Biases for Calibration

Calibration of resistance factors requires statistical parameters, such as mean, standard deviation, and COV along with a best fit distribution for all random variables involved in a limit state function (Allen et al. 2005). The random variables involved in the limit state function for this study were pile resistance (R), dead load (DL), and live load (LL). For the calculation of reliability index, β, the statistical parameters should correspond to the statistics of measured R, DL, and LL, which are obtained by scaling of the bias as explained in section 2.7.6 of chapter 2. As the statistics of the bias corresponding to DL and LL were adopted from literature (Paikowsky et al. 2004) (Table 7), obtaining the statistics of the bias corresponding to resistance, known as resistance bias, formed the foremost task.

The SA methods to estimate axial pile resistances using α- method, β-method, λ-method, SPT method, and Nordlund method in three main geomaterials: soils, IGM-soils, and IGM-rocks, were conducted in chapter 5. The estimated shaft resistances and end bearings from each SA method in particular geomaterial were compared to the measured resistances from CAPWAP to

determine their resistance biases for each SA method and geomaterial. Then the statistical summaries in terms of mean ($\bar{x}$) and coefficient of variation (COV), calculated as a ratio of sample standard deviation to mean, of these resistance biases were calculated and can be referred from Table 42. Soils were excluded from the analysis as the existing resistance factors from AASHTO (2017) were based on comparatively large pile data on soils. The distributions of random variables involved in a limit state function are utilized during the probability based calibration of resistance factors. Lognormal distribution was selected as the best fit distribution for modeling resistance biases based on log likelihood values, and was further confirmed by tests by Shapiro and Wilk (1965) and Anderson and Darling (1952). The details on the selection of lognormal distribution can be referred from Adhikari (2019). The histograms along with fitted normal and log-normal distributions of shaft resistance and end bearing biases from existing SA methods are presented in Figures 48 to 51.

Table 42. Statistical summaries of existing SA methods.

Geo-material	**SA method**	**Statistical summaries for shaft resistance**		
		($\bar{x}$)	**COV**	**N**
IGM-soil	α-method	1.17	0.64	9
	β-method	1.45	1.73	16
	Nordlund	1.05	1.70	16
	SPT	2.41	1.38	16
	λ-method	0.67	0.93	14
IGM-rock	α-method	1.15	1.20	14
	β-method	1.05	0.98	17
	Nordlund	0.60	0.85	17
	SPT	1.35	0.52	17
	λ-method	0.38	1.17	25
Geo-material	**SA method**	**Statistical summaries for end bearing**		
		($\bar{x}$)	**COV**	**N**
IGM-soil	α-method	3.97	0.38	5
	β-method	1.07	0.95	6
	Nordlund	2.04	1.01	6
	SPT	0.24	0.59	6
IGM-rock	α-method	2.73	1.02	13
	β-method	0.36	0.62	18
	Nordlund	0.44	0.43	18
	SPT	1.22	1.87	18

$\bar{x}$- Sample mean of resistance biases; COV- Coefficient of variation of resistance biases; N- Sample size.

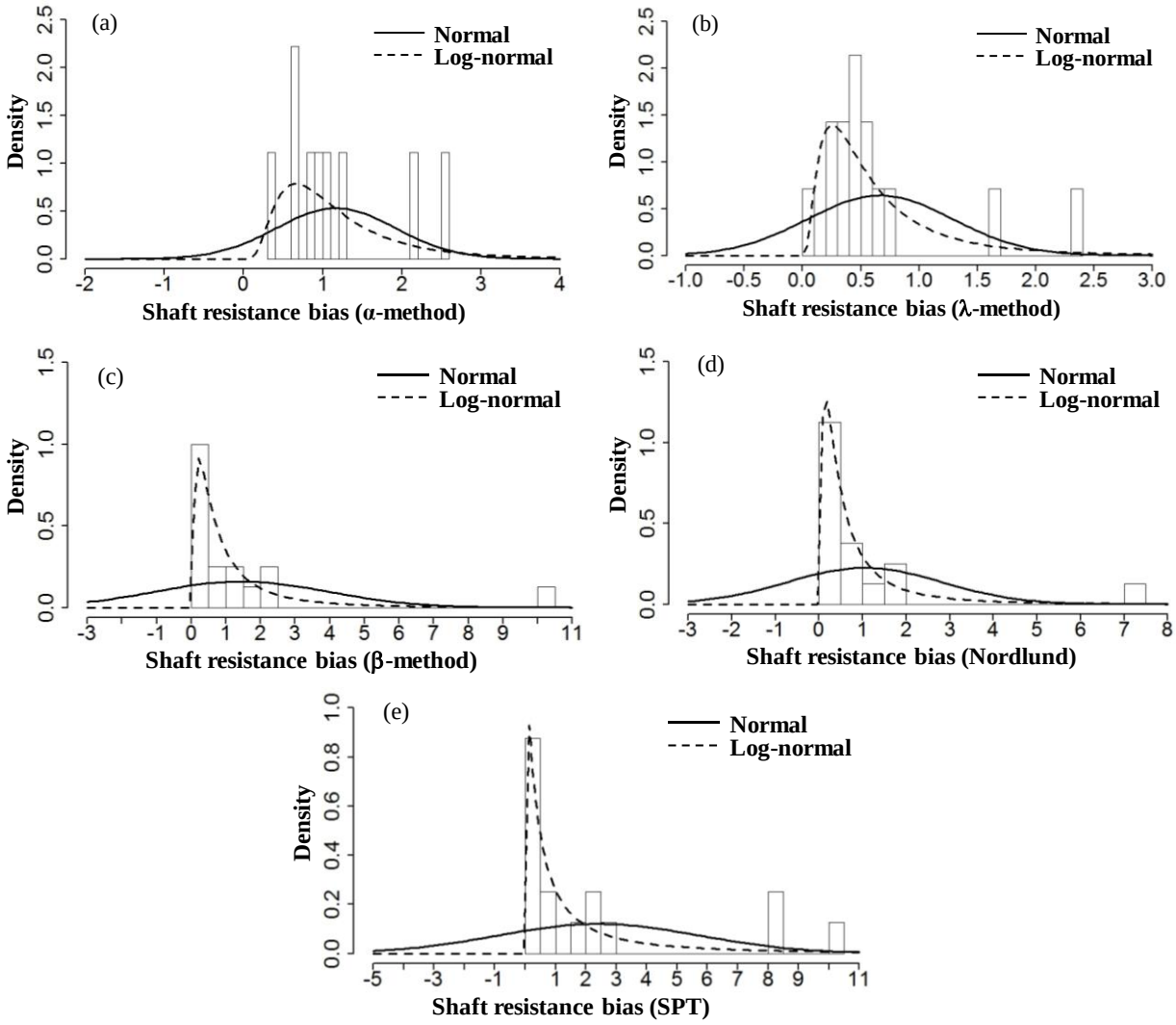

Source: Adhikari (2019)

Figure 48. Histograms and fitted distributions of shaft resistance biases in IGM-soils for esxisting (a) α-method (b) λ-method (c) β-method (d) Nordlund method (e) SPT method.

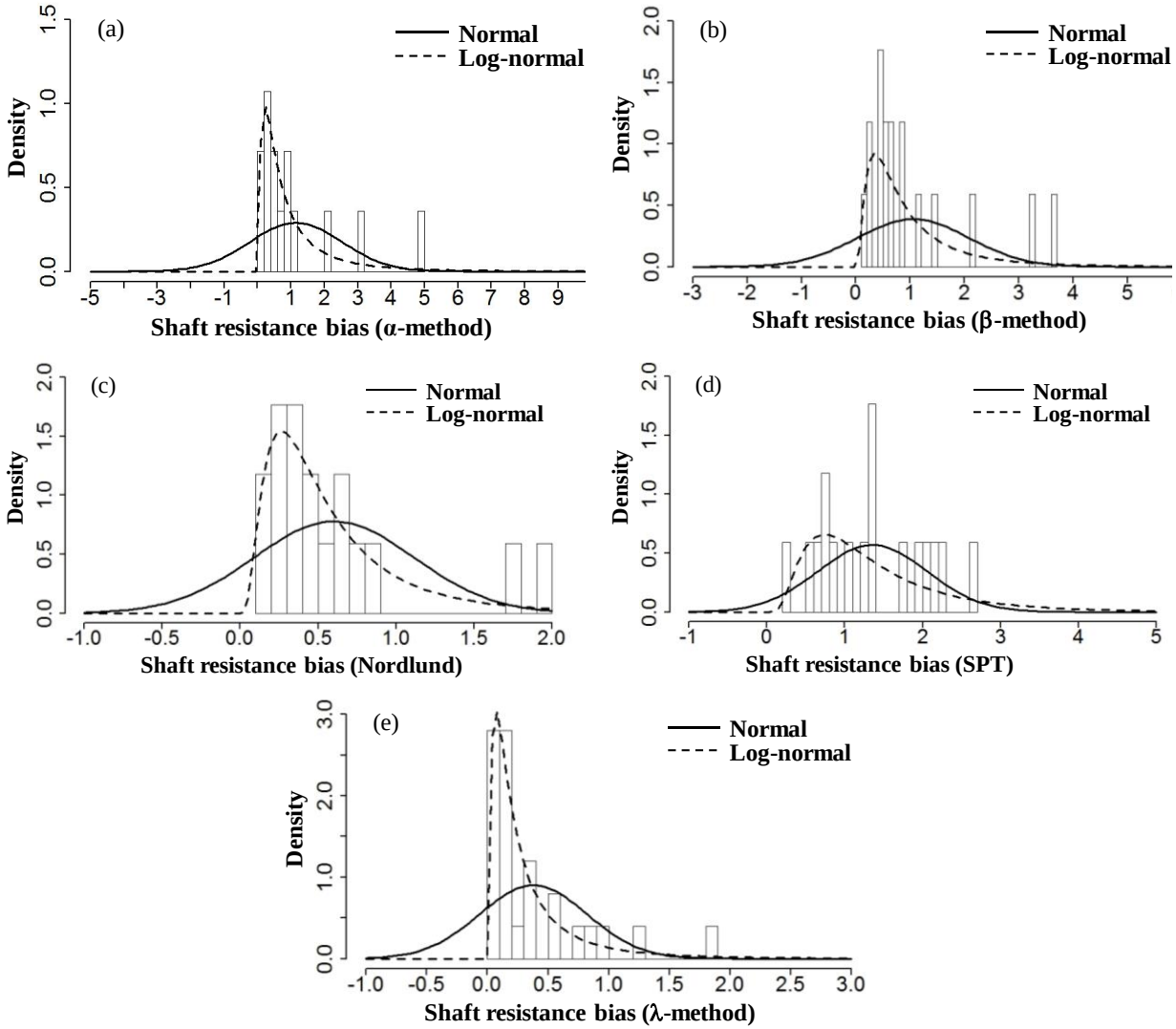

Source: Adhikari (2019)

Figure 49. Histograms and fitted distributions of shaft resistance biases in IGM-rocks for existing (a) α- method (b) β-method (c) Nordlund method (d) SPT method (e) λ-method.

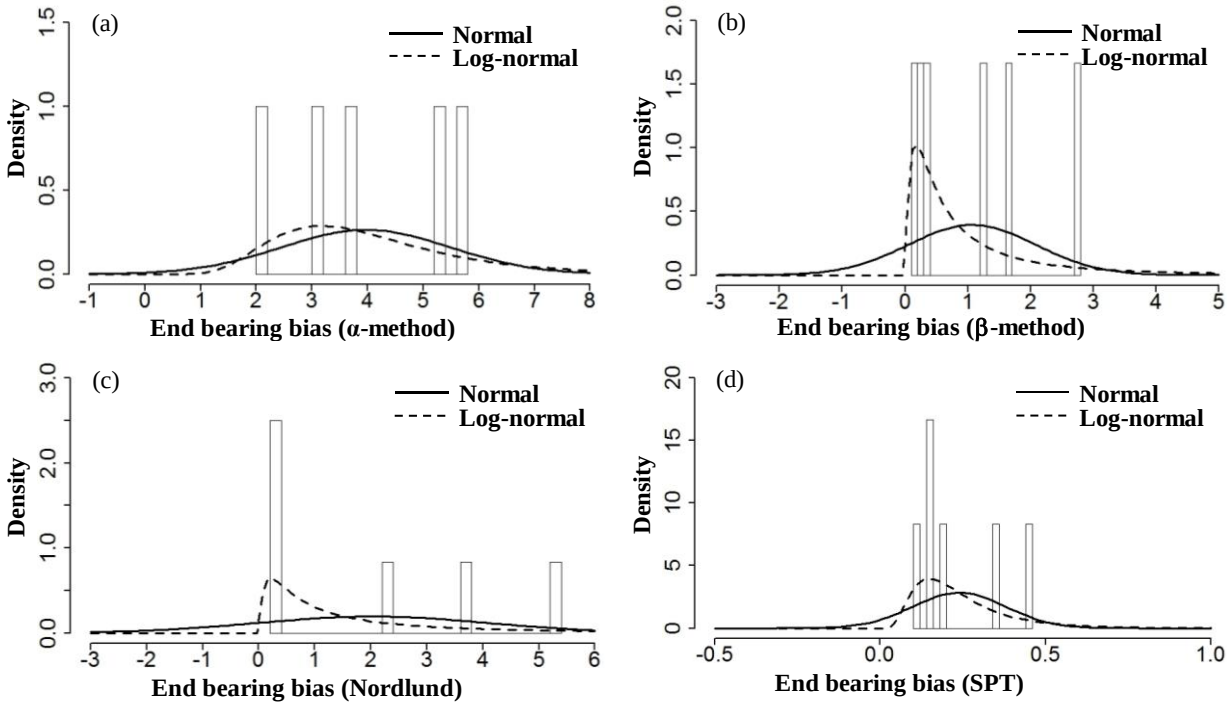

Source: Adhikari (2019)

Figure 50. Histograms and fitted distributions of end bearing biases in IGM-soils for existing (a) α-method (b) β-method (c) Nordlund method (d) SPT method.

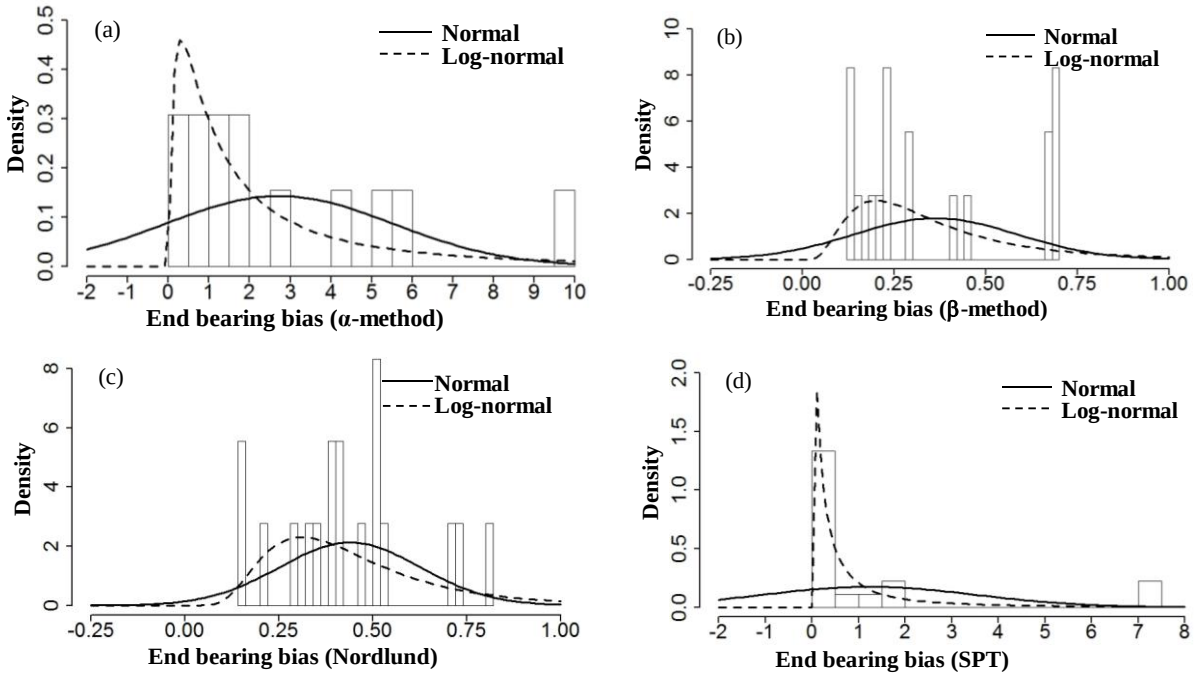

Source: Adhikari (2019)

Figure 51. Histograms and fitted distributions of end bearing biases in IGM-rocks for existing (a) α-method (b) β-method (c) Nordlund method (d) SPT method.

7.3 Resistance factors of Existing SA Methods

After confirming the lognormal distribution of the biases, resistance factors were calculated from FOSM, FORM, and MCS incorporating the additional data for the target reliability indices (β_T) of 2.33 and 3.00. Resistance factors presented in Table 43 were calculated without removing outliers. Comparison of resistance factors from all three reliability-based methods is presented in Figure 52. The relatively high resistance factors due to high mean resistance bias of 3.97 and low COV of 0.38 of α-method for end-bearing in IGM-soils was excluded in the comparison study presented in Figure 52.

Table 43. Resistance factors of existing SA methods.

For shaft resistance										
Geo-material	**SA met.**	**Statistical summaries**			**FOSM resistance factor (φ)**		**FORM resistance factor (φ)**		**MCS resistance factor (φ)**	
		($\bar{x}$)	**COV**	**N**	**β_T=2.33**	**β_T= 3.00**	**β_T= 2.33**	**β_T= 3.00**	**β_T= 2.33**	**β_T=3.00**
IGM-soil	α-met.	1.17	0.64	9	0.307	0.202	0.326	0.219	0.325	0.207
	β-met.	1.45	1.73	16	0.06	0.03	0.059	0.030	0.061	0.025
	Nord.	1.05	1.70	16	0.04	0.02	0.046	0.021	0.046	0.019
	SPT	2.41	1.38	16	0.16	0.08	0.167	0.083	0.166	0.075
	λ-met.	0.67	0.93	14	0.097	0.056	0.101	0.059	0.102	0.055
IGM-rock	α-met.	1.15	1.20	14	0.103	0.054	0.106	0.056	0.106	0.052
	β-met.	1.05	0.98	17	0.139	0.079	0.144	0.083	0.144	0.078
	Nord.	0.60	0.85	17	0.102	0.061	0.106	0.064	0.106	0.060
	SPT	1.35	0.52	17	0.460	0.321	0.495	0.353	0.493	0.336
	λ-met.	0.38	1.17	25	0.036	0.019	0.037	0.019	0.037	0.018
For end bearing										
Geo-material	**SA method**	**Statistical summaries**			**FOSM resistance factor (φ)**		**FORM resistance factor (φ)**		**MCS resistance factor (φ)**	
		($\bar{x}$)	**COV**	**N**	**β_T=2.33**	**β_T=3.00**	**β_T= 2.33**	**β_T= 3.00**	**β_T= 2.33**	**β_T=3.00**
IGM-soil	α-met.	3.97	0.38	5	1.832	1.375	2.025	1.565	2.016	1.508
	β-met.	1.07	0.95	6	0.15	0.09	0.156	0.091	0.156	0.084
	Nord.	2.04	1.01	6	0.26	0.14	0.265	0.150	0.265	0.138
	SPT	0.24	0.59	6	0.07	0.05	0.075	0.051	0.075	0.049
IGM-rock	α-met.	2.73	1.02	13	0.335	0.187	0.348	0.196	0.346	0.182
	β-met.	0.36	0.62	18	0.099	0.065	0.105	0.071	0.105	0.067
	Nord.	0.44	0.43	18	0.182	0.133	0.199	0.150	0.198	0.144
	SPT	1.22	1.87	18	0.042	0.018	0.043	0.018	0.043	0.017

met.- Method; Nord.- Nordlund; $\bar{x}$- Sample mean of resistance biases; COV- Coefficient of variation of resistance biases; N- Sample size; β_T- Target reliability index.

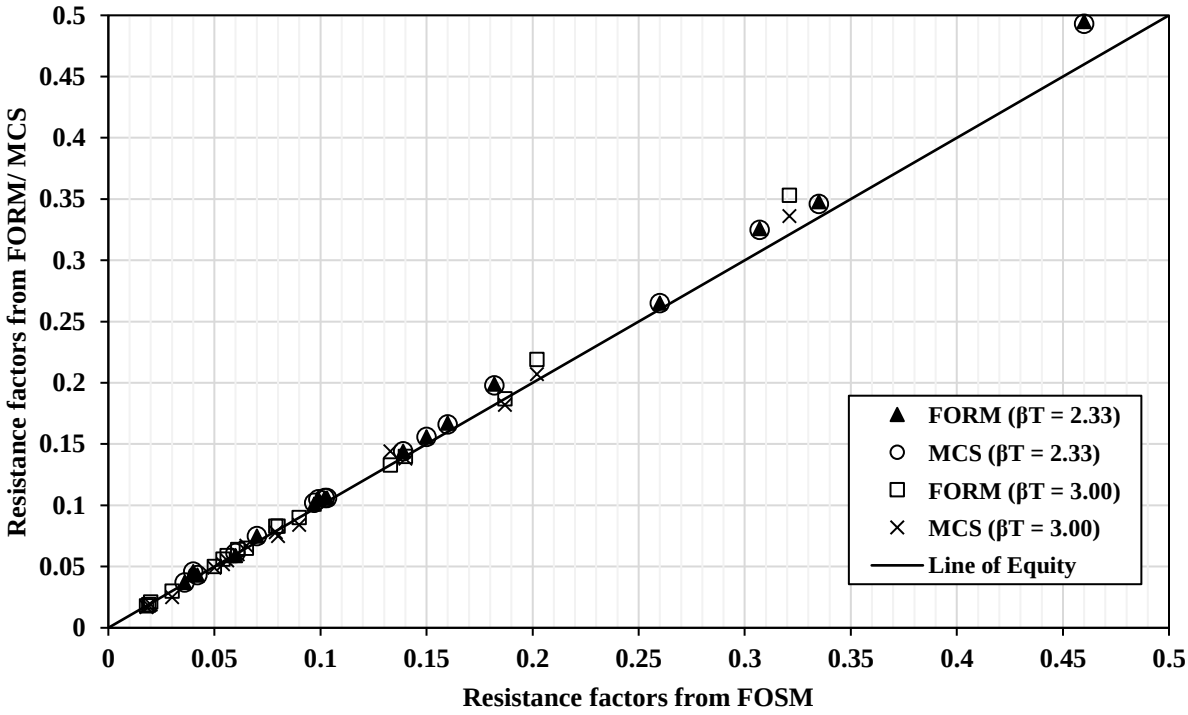

Source: Adhikari (2019)

Figure 52. Comparison of resistance factors from FOSM, FORM, and MCS.

Figure 52 shows that the resistance factors from FORM and MCS for β_T= 2.33 were similar as indicated by overlapping triangles and circles. However, the MCS resistance factors were slightly lower than the FORM resistance factors for β_T= 3.00. Except some MCS resistance factors corresponding to β_T= 3.00, all FORM and MCS resistance factors were higher than the FOSM resistance factors. The percentage increase in FORM and MCS resistance factors with respect to FOSM resistance factors for β_T= 2.33 ranged from 2 percent to 9 percent averaging to 5 percent. For β_T= 3.00, increase in FORM resistance factors with respect to FOSM ranged from 0 percent to 10 percent with an average of 3 percent. However, for β_T= 3.00, percentage increase in MCS resistance factors ranged from -17 percent to 8 percent with -2.43 percent decrease on average.

7.4 Resistance factors of Calibrated SA methods

In order to improve the design efficiency of piles driven into IGMs, α- and β-methods were calibrated and validated using Wyoming pile data on both the cohesive and cohesionless IGMs as described in chapter 5. However, calibration could not be achieved for shaft resistance estimation in cohesionless IGM-soils and end bearing in cohesive and cohesionless IGM-soils either due to small sample size or no correlation between design coefficients and IGM properties (Gebreslasie 2018). This section presents the resistance factors of calibrated α- and β-methods (known as calibrated SA methods in this study). As for existing methods, lognormal distributions were confirmed as best distribution model for resistance biases from calibrated SA methods. The histograms of the biases from calibrated SA methods along with fitted normal and lognormal

distributions, are shown in Figure 53 to Figure 55. The statistical summaries of the resistance biases and the resistance factors of the calibrated SA methods are presented in Table 44.

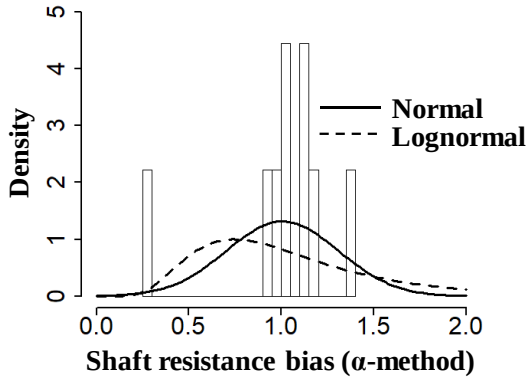

Source: Adhikari (2019)

Figure 53. Histograms and fitted distributions of shaft resistance biases from calibrated α-method in IGM-soils.

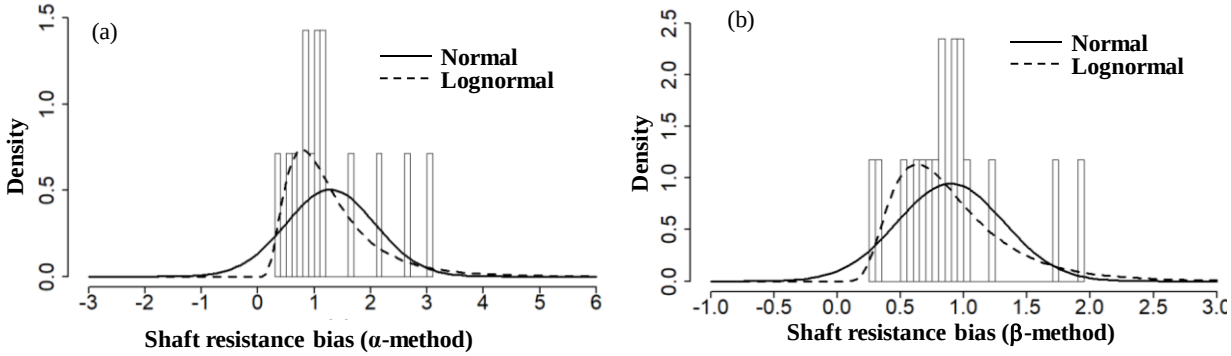

Source: Adhikari (2019)

Figure 54. Histograms and fitted distributions of shaft resistance biases from calibrated (a) α-method and (b) β- method in IGM-rocks.

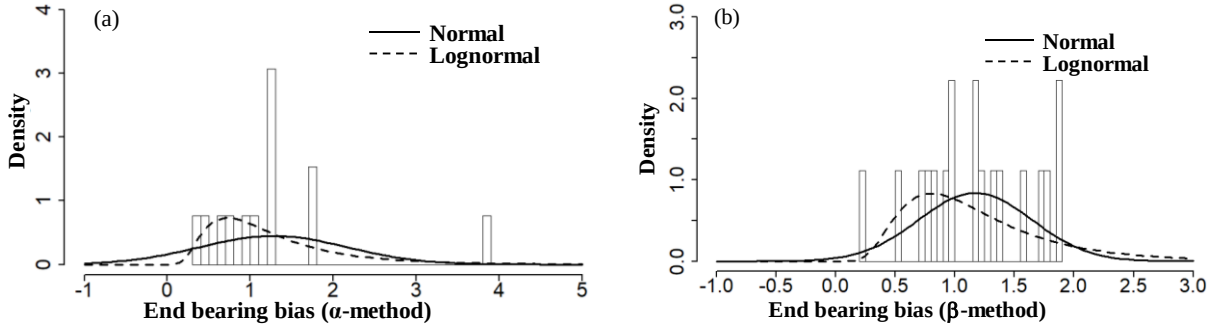

Source: Adhikari (2019)

Figure 55. Histograms and fitted distributions of end bearing biases from calibrated (a) α-method and (b) β- method in IGM-rocks.

Table 44. Statistical summaries and resistance factors of calibrated static analysis methods.

For shaft resistance										
Geomaterial	**Calibrated SA method**	**Statistical summaries**			**FOSM resistance factor (φ)**		**FORM resistance factor (φ)**		**MCS resistance factor (φ)**	
		($\bar{x}$)	**COV**	**N**	**β_T=2.33**	**β_T=3.00**	**β_T=2.33**	**β_T=3.00**	**β_T=2.33**	**β_T=3.00**
IGM-soil	α-met.	1.01	0.30	9	0.547	0.428	0.622	0.505	0.620	0.489
IGM-rock	α-met.	1.29	0.61	14	0.358	0.238	0.385	0.262	0.383	0.251
	β-met.	0.90	0.47	17	0.341	0.244	0.371	0.273	0.370	0.263
For end bearing										
Geomaterial	**Calibrated SA method**	**Statistical summaries**			**FOSM resistance factor (φ)**		**FORM resistance factor (φ)**		**MCS resistance factor (φ)**	
		($\bar{x}$)	**COV**	**N**	**β_T=2.33**	**β_T=3.00**	**β_T=2.33**	**β_T=3.00**	**β_T=2.33**	**β_T=3.00**
IGM-rock	α-met.	1.28	0.70	13	0.297	0.190	0.312	0.203	0.312	0.191
	β-met.	1.17	0.41	18	0.512	0.379	0.555	0.422	0.553	0.407

met.- Method; Nord.- Nordlund; $\bar{x}$- Sample mean of resistance biases; COV- Coefficient of variation of resistance biases; N- Sample size; β_T- Target reliability index.

Comparisons of the resistance factors of calibrated and existing SA methods for shaft resistance and end bearing estimations are presented in Figure 56 and Figure 57, respectively. Figure 56 shows that the resistance factors of the calibrated SA methods are higher than that of existing SA methods in both IGM-soils and IGM-rocks. The resistance factors of calibrated SA methods for shaft resistance estimation are also higher than the current AASHTO (2017) recommended resistance factors of 0.35 for α-method and 0.25 for β-method. However, the resistance factors of existing SA methods determined based on Wyoming data are lower than the current AASHTO (2017) resistance factors. Thus, using AASHTO (2017) resistance factors for IGM dominant Wyoming geology will not ensure the target reliability.

Figure 57 shows that the resistance factors of calibrated α-method are comparatively less than the resistance factors of existing α-method based on Wyoming pile data in end bearing estimation. Contrarily, the resistance factors of calibrated β-method are higher than the resistance factors of existing β-method. The resistance factors for calibrated α-method are even less than the current AASHTO (2017) recommended resistance factor of 0.35. However, resistance factors alone cannot reveal the efficiency of the methods in resistance estimation. Thus, the SA methods are compared in terms of efficiency factors in the next Section 7.5.

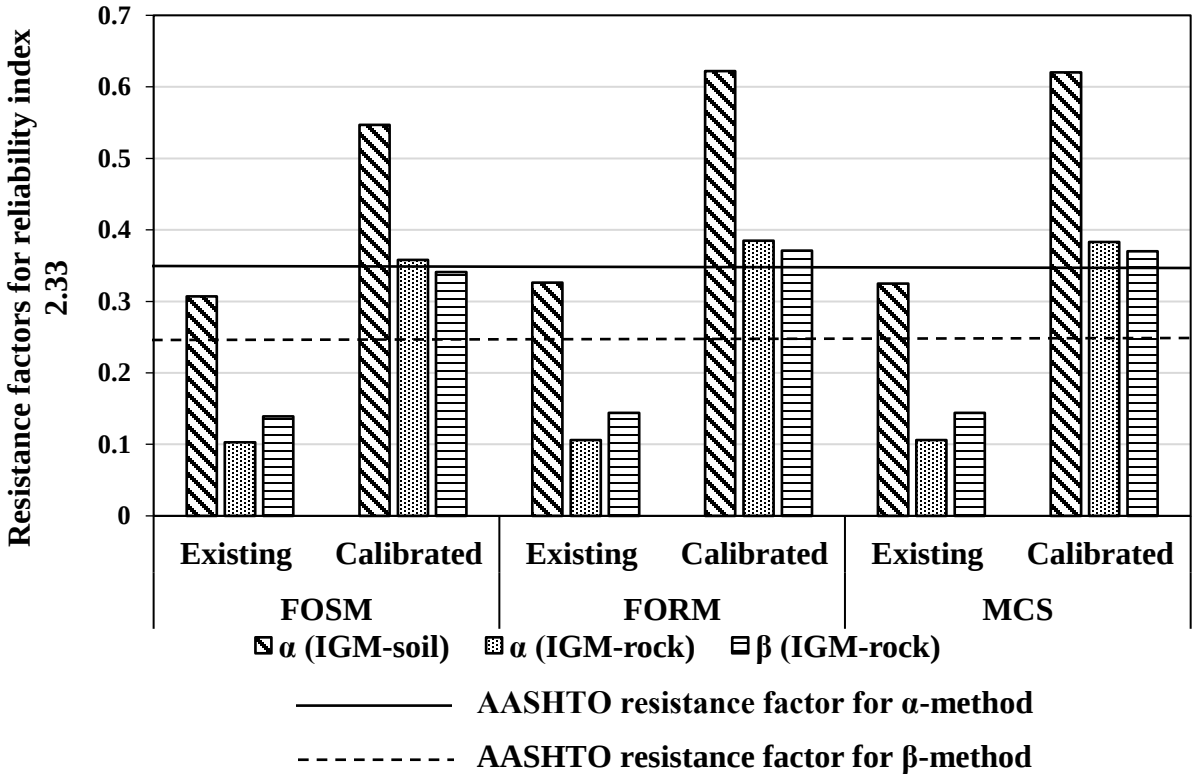

Source: Adhikari (2019)

Figure 56. Comparison of resistance factors of calibrated and existing SA methods for shaft resistance estimation.

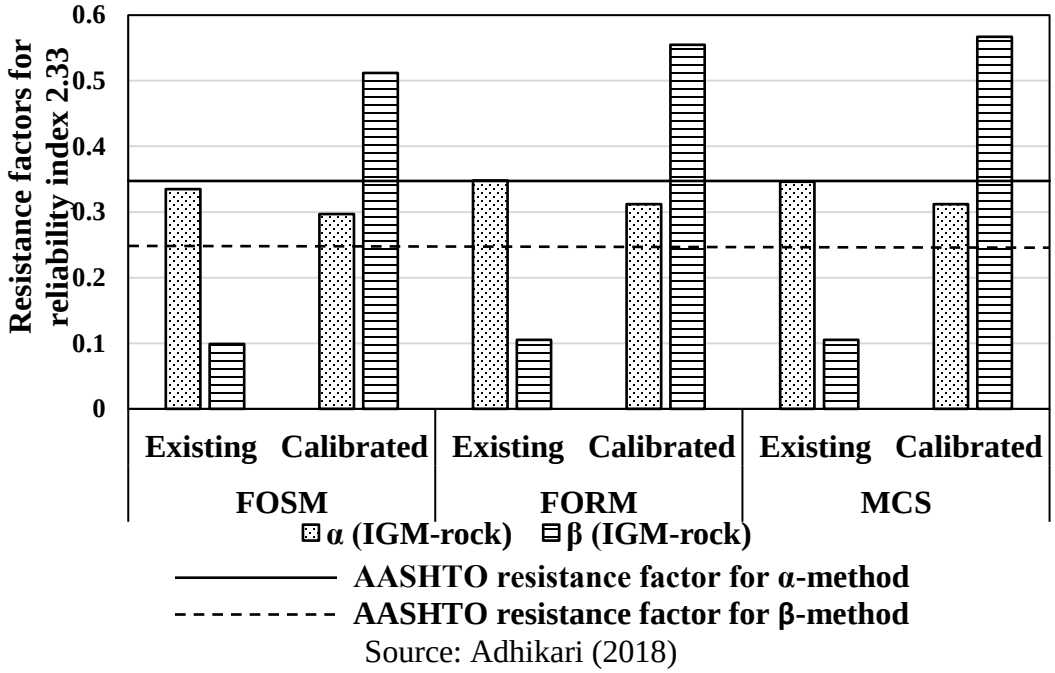

Source: Adhikari (2018)

Figure 57. Comparison of resistance factors of calibrated and existing SA methods for end bearing estimation.

7.5 Comparison of SA Methods in Terms of Efficiency Factors

McVay et al. (2000) indicated that the economic performance can be determined by the efficiency factor, which is the ratio of resistance factor to the mean resistance bias ($\varphi/\bar{x}$). Thus, efficiency factors provide a basis for selecting SA method for the design of piles driven into IGMs. As FOSM resistance factors were conservative and slightly different from FORM and MCS, the MCS resistance factors were selected for the calculation of efficiency factors. The efficiency factors of existing and calibrated SA methods have been presented in Table 45 and Table 46 for shaft resistance and end bearing estimations, respectively.

Table 45 shows that the efficiency factors of calibrated α-method (IGM-soil), α-method (IGM-rock), and β-method (IGM-rock) for shaft resistance estimation were higher than that of the existing methods. For reliability index 2.33, the calibrated α-method had the highest efficiency factor of 0.61 for shaft resistance estimation in IGM-soils followed by the calibrated β-method for end bearing estimation in IGM-rocks with efficiency factor of 0.48. This implies that a more economic pile design can be achieved using the calibrated methods and their resistance factors. However, comparison could not be made on the Nordlund, SPT, and λ-methods on which calibration was not conducted. The efficiency factors of SPT methods were relatively higher than that of Nordlund methods for both IGM-soils and IGM-rocks.

Table 45. Efficiency factors of existing and calibrated SA methods for shaft resistance estimation.

Geomaterial	SA method	Efficient factor			
		Existing SA method		Calibrated SA method	
		β_T= 2.33	β_T= 3.00	β_T= 2.33	β_T= 3.00
IGM-soil	α-method	0.28	0.18	0.61	0.48
	β-method	0.04*	0.02*	NA[1]	NA[1]
	Nordlund	0.04*	0.02*	NA	NA
	SPT	0.07*	0.03*	NA	NA
	λ-method	0.15	0.08	NA	NA
IGM-rock	α-method	0.09	0.05	0.30	0.19
	β-method	0.14	0.07	0.41	0.29
	Nordlund	0.18	0.10	NA	NA
	SPT	0.37	0.25	NA	NA
	λ-method	0.10	0.05	NA	NA

*- Additional pile data did not increase the sample size; [1]- Not applicable as calibration did not result in any correlation; NA- Not applicable as calibration was not conducted; β_T-Target reliability index.

Table 46 shows that the efficiency factors of calibrated α- and β-methods were higher than the existing methods for end bearing estimation in IGM-rocks. Comparing the existing SA methods for cohesionless IGM-soils, the β-method had relatively higher efficiency than Nordlund and SPT methods.

Table 46. Efficiency factors of existing and calibrated SA methods for end bearing estimation.

Geomaterial	SA method	Efficiency factor			
		Existing SA method		Calibrated SA method	
		β_T= 2.33	β_T= 3.00	β_T= 2.33	β_T= 3.00
IGM-soil	α-method	0.51	0.38	NA[#]	NA[#]
	β-method	0.11[*]	0.06[*]	NA[1]	NA[1]
	Nordlund	0.10[*]	0.06[*]	NA	NA
	SPT	0.05[*]	0.02[*]	NA	NA
IGM-rock	α-method	0.13	0.07	0.24	0.15
	β-method	0.29	0.19	0.48	0.35
	Nordlund	0.45	0.33	NA	NA
	SPT	0.04	0.01	NA	NA

[*]- Additional pile data did not increase the sample size; [1]- Not applicable as calibration did not result in any correlation; [#]- Not calibrated due to small sample size; NA- Not applicable as calibration was not conducted; β_T- Target reliability index.

7.6 Recommendation

The recommended static analysis methods and their respective resistance factors for the estimation of shaft resistance and end bearing in IGMs are presented in Table 47. Calibrated methods with higher efficiency factors are recommended over the existing methods. The recommended resistance factors for calibrated methods are taken as the average of FORM and MCS resistance factors rounded down to the nearest 0.05. FOSM resistance factors were not considered as they were relatively conservative. As the resistance factor for calibrated α-method is comparatively high and is based on small sample size, the resistance factor of 0.5 is recommended for reliability index 2.33. This resistance factor is the lower bound resistance factor. For reliability index 3, 0.4 is recommended.

The average of FORM and MCS resistance factors of existing β- and Nordlund methods for shaft resistance estimation in IGM-soils (Table 43) are extremely low as 0.05. Thus, the resistance factors for these two existing β- and Nordlund methods are recommended as 0.15 and 0.10 (Table 48) respectively for reliability index 2.33. For reliability index 2.33, the resistance factor for SPT method for shaft resistance estimation in IGM-soils based on Wyoming data (Table 43) is recommended as 0.15. Although these resistance factors are lower than the AASHTO (2017) recommended resistance factors of 0.25, 0.45, and 0.30 for β-, Nordlund, and SPT methods respectively, AASHTO (2017) recommendations cannot satisfy the target reliability index for shaft resistance estimation in IGM-soils. For end bearing estimation in cohesive IGM-soils, the extremely high resistance factor of 2.02, for existing α-method (Table 43) due to very small sample size of five, is not recommended. Until more pile data become available for calibration, AASHTO (2017) resistance factor of 0.35 is suggested for the existing α-method and should be used with caution. The average of FORM and MCS resistance factors of existing β- and Nordlund for end bearing estimation in IGM-soils, as determined from Wyoming data (Table 43), are recommended as 0.15 and 0.25 respectively for reliability index 2.33. For SPT methods for end bearing estimation determined from Wyoming data (Table 43) is as low as 0.07. Therefore, 0.1 is recommended for SPT method (Table 48) for end bearing estimation in IGM-soil.

Table 47. Recommended SA methods for pile resistance estimation in IGMs

Resistance	Geomaterials		SA method	Resistance factor for β_T= 2.33 (φ)	Resistance factor for β_T= 3.00 (φ)
Shaft resistance	IGM-soils	Cohesive	Calibrated α-method	0.50	0.40
		Cohesionless[$]	Existing β-method/	0.15	0.10
			Existing Nordlund	0.10	0.05
			Existing SPT method	0.15	0.10
	IGM-rocks	Cohesive	Calibrated α-method	0.35	0.25
		Cohesionless	Calibrated β-method	0.35	0.25
End bearing	IGM-soils	Cohesive[$]	Existing α-method	0.35*	0.28[#]
		Cohesionless[$]	Existing β-method/	0.15	0.10[1]
			Existing Nordlund	0.25	0.15[1]
			Existing SPT method	0.10	0.05
	IGM-rocks	Cohesive	Calibrated α-method	0.30	0.20[1]
		Cohesionless	Calibrated β-method	0.55	0.40

β_T- Target reliability index; [$]-Calibrated SA method cannot be developed in this study; [1]- rounded up as the average was 0.01 less to the closest 0.05. *- From AASHTO (2017); [#]- AASHTO (2017) was reduced by 20%.

7.7 Assessing Uncertainty in Resistance Factors of SA Methods and WEAP

The resistance factors determined were based on small sample sizes. Thus, assessing the uncertainties in resistance factors would be necessary. To assess the uncertainties, firstly a number of sets (nset) were generated using MCS based on the statistical parameters of best fit (lognormal) distribution of resistance bias. Each set consists of number of randomly generated resistance biases (nsamp). Secondly, mean and standard deviation of each set were determined for the lognormal distribution. Then, MCS was conducted with 100,000 simulations in each set as described in Section 2.7.7 to determine a resistance factor from that set. This ultimately results in 'nset' number of resistance factors. A flowchart summarizing these steps is presented in Figure 58. To assess the required number of resistance factor sets, the mean and standard deviation of the resistance factors were generated for 10, 100, 200, and 300 sets with each set consisting of 18 samples corresponding to the calibrated β-method for end bearing estimation in IGM-rocks. The mean of the resistance factors ranged from 0.55 to 0.58 and the uncertainty measured in terms of standard deviation ranged from 0.096 (for 200 sets) to 0.133 (for 10 sets). As the mean resistance factors from both 200 and 300 sets were equal to 0.571, 300 sets were selected to repeat the analysis for all the calibrated SA methods. However, studies can be conducted in future to determine the optimum number of sets required for each calibrated SA method. The statistical summary consisting of mean, standard deviation and 95 percent confidence interval of the resistance factors for calibrated and existing SA methods are presented in Table 48.

Table 48. Uncertainties in resistance factors of SA methods and WEAP for reliability index, $\beta_T = 2.33$.

SA method for shaft resistance						
Geomaterial	**SA methods**	**N**	**RF from MCS (Table 43 & Table 44)**	**Mean of RF**	**SD of RF**	**95% CI of RF**
IGM-soil	C. α-met.	9	0.620	0.642	0.116	0.450-0.885
	E. β- met.	16	0.061	0.146	0.08	0.048-0.336
	E. Nord.	16	0.046	0.104	0.05	0.003-0.22
	E. SPT- met.	16	0.166	0.312	0.142	0.109-0.630
IGM-rock	C. α-met.	14	0.383	0.440	0.131	0.221-0.752
	C. β-met.	17	0.370	0.396	0.090	0.234-0.752
SA methods for end bearing						
Geomaterial	**Calibrated SA method**	**N**	**RF from MCS (Table 43 & Table 44)**	**Mean of RF**	**SD of RF**	**95% CI of RF**
IGM-soil	E. β- met.	6	0.156	0.258	0.129	0.09-0.566
	E. Nord.	6	0.265	0.472	0.252	0.133-1.081
	E. SPT- met.	6	0.075	0.09	0.034	0.037-0.167
IGM-rock	α-method	13	0.312	0.381	0.126	0.178-0.665
	β-method	18	0.553	0.571	0.110	0.383-0.831
WEAP for total resistance						
Geomaterial	**WEAP**	**N**	**RF from MCS (Table 41)**	**Mean of RF**	**SD of RF**	**95% CI of RF**
IGM	Bearing graph (Case I)	25	0.68	0.69	0.08	0.55-0.84
IGM	Bearing graph (Case II)	25	0.62	0.63	0.07	0.49-0.78

E- Existing; C- Calibrated; met.- method; N- Sample size (nsamp used in R-code); RF- Resistance factor; SD- Standard deviation; CI- Confidence Interval.

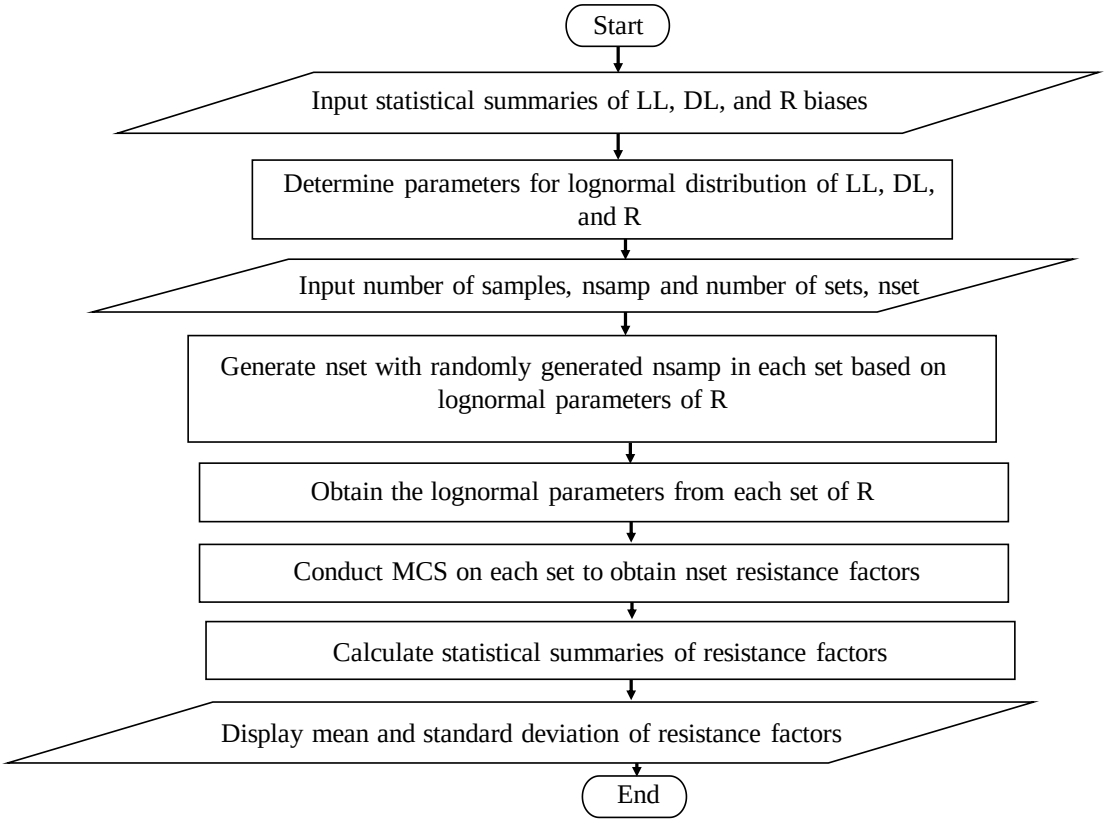

Source: Adhikari (2019)

Figure 58. Flowchart summarizing the procedures adopted for assessing uncertainties in resistance factors.

The mean of resistance factors determined considering 'nset' sets of resistance factors are slightly greater, 0.07 on average, than the resistance factors calculated using single MCS, as evident from Table 48. The sample sizes of all the calibrated and existing SA methods are less than 20, and the uncertainties ranged from 0.03 to 0.25. The average uncertainty was calculated as 0.11. To assess the change in the uncertainties along with the sample sizes, the above-mentioned procedure was repeated for the calibrated β-method on end bearing estimation in IGM-rock by varying sample sizes for 18, 30, 50, 100, 200, 300, and 500. For fast computation, only 100 sets were considered for each sample size. The results of resistance factors in terms of mean values (μ) and the range within one standard deviation (σ) are plotted in Figure 59.

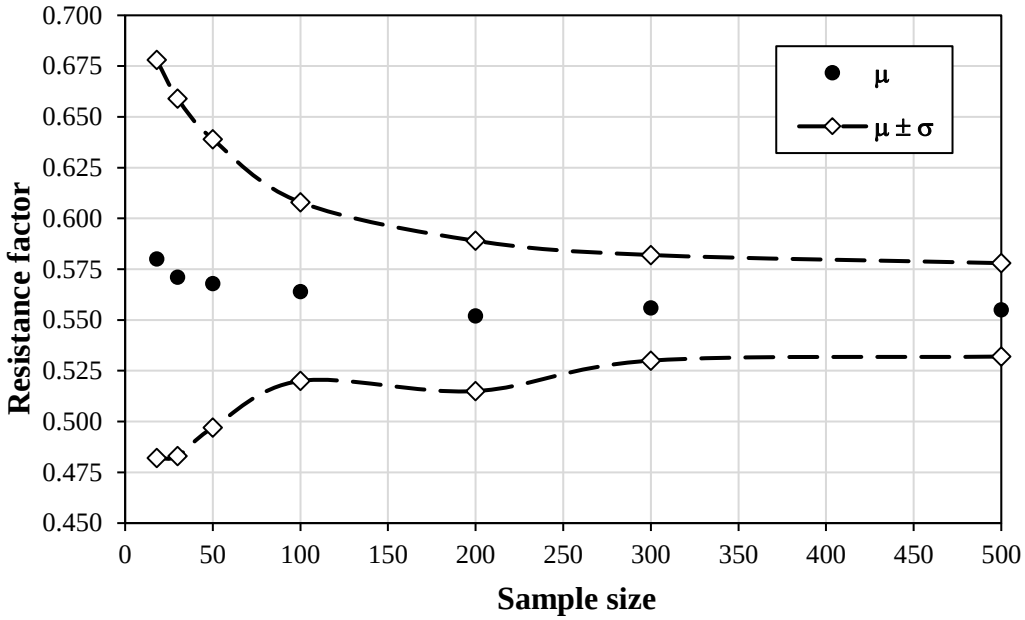

Source: Adhikari (2019)

Figure 59. Variation in the mean resistance factors with sample sizes for the calibrated β-method on end bearing estimation in IGM-rock.

Figure 59 shows that the band of one standard deviation above and below the mean resistance factors gets narrower when the sample size increases. The uncertainty measured in terms of standard deviation decreases from 0.1 to 0.02 when sample size increased from 18 to 500. The uncertainty at 100 samples is approximately 0.05. The width of uncertainty band remains almost same from 300 to 500 samples. Thus, the number of samples has direct influence on the uncertainty of the resistance factors. Though the calculated uncertainties also depend upon the mean and COV of resistance biases used to generate random samples, this is important to understand how the uncertainties can be decreased with sample sizes.

7.8 Conclusion

Resistance factors were calibrated using Wyoming pile data for different geomaterials, SA methods, and pile resistance components. Efficiency factors were determined to establish the recommendation for the existing and calibrated SA methods and their respective resistance factors. Based on the results, the following conclusions are drawn:

- The resistance factors from FOSM are relatively conservative when compared to the resistance factors from FORM and MCS.
- The FORM and MCS resistance factors are similar for β_T= 2.33. However, MCS resistance factors are relatively lower than FORM resistance factors for β_T= 3.00.
- The MCS and FORM resistance factors decrease by almost 40 percent, on average, when the reliability index increases from 2.33 to 3.00.
- The MCS and FORM resistance factors are approximately larger than FOSM resistance factors by 5 percent, on average, for β_T= 2.33. However, some MCS resistance factors are found to be smaller than the FOSM resistance factors for β_T= 3.00.

- The calibrated SA methods are concluded to be more efficient than the existing SA methods for the determination of shaft resistance and end-bearing in IGM-rocks. For IGM-soils, the calibrated α-method, which is more efficient than the existing α-method, is recommended for shaft resistance estimation in IGM-soils. Existing SA methods with resistance factors calibrated based on Wyoming pile data are recommended for estimating end bearing in IGM-soils and estimating shaft resistance in cohesionless IGM-soils.
- The resistance factor of 0.5 was recommended for calibrated α-method in estimating shaft resistance in IGM-soils. The resistance factor of 0.35 was recommended for both calibrated α- and β- methods in estimating shaft resistance in IGM-rocks. The resistance factors of 0.30 and 0.55 were recommended for calibrated α- and β- methods in estimating end bearing in IGM-rocks. However, due to the small sample sizes of less than 20, uncertainties of nearly 0.1 is expected in these resistance factors. Thus, verification of these resistance factors is required prior to the application.
- Uncertainties in the resistance factors were dependent upon the sample sizes. The uncertainty measured in terms of standard deviation decreases from 0.1 to 0.02 when sample size increased from 18 to 500 for calibrated β-method in IGM-rock for end bearing estimation. Thus, it is necessary to have representative sample size to produce reliable resistance factors.

CHAPTER 8. SUMMARY, CONCLUSIONS, AND RECOMMENDATIONS

8.1 Summary

The overall goal of the research project was to develop locally calibrated LRFD procedures for driven piles in IGMs, in Wyoming. The objectives of the study are to determine efficient and reliable SA methods for pile design and dynamic procedures for construction control. Using the historical pile data obtained from WYDOT that were compiled in an electronic database (WyoPile), as described in chapter 3, geomaterial classification criteria were developed in chapter 4 to establish a standard quantitative delineation between soils, IGM-soils, and IGM-rocks. Utilizing this proposed geomaterial classification criteria, current SA methods were evaluated for their reliability in the estimation of pile resistances in IGMs, in chapter 5. Economic implications of using current SA methods for the design of driven piles were assessed. New SA methods were calibrated and validated using an independent set of additional pile data in Wyoming to improve the estimation of pile resistances in IGMs. Furthermore, the gain and loss in pile resistances with time were studied. Chapter 6 presents the recommended procedures for performing the WEAPand evaluated the uncertainties in pile resistance estimation to ensure a prescribed reliability in pile construction control. Chapter 7 presents the results of the calibration of resistance factors, a comparative study of existing and calibrated SA methods in terms of efficiency factors, and the effect of sample sizes on the uncertainties of resistance factors.

8.2 Conclusions

The conclusions obtained from the study are described below:

1) An extensive literature review found inconsistent definitions of IGMs and hard rocks. Currently available SA methods developed for soils and used in the design of piles in IGM were shown to be inefficient as evidenced by the high COVs (Table 27).
2) Also, low resistance factors were determined for SA methods in comparison to the current AASHTO (2017) recommendations, justifying the assumption that the target reliability indices cannot be achieved during the design using the current design procedures.
3) The economic study revealed that the current design procedures using the Nordlund and α-methods overestimated the pile resistances which ultimately lead to direct cost overruns with additional 0.84 lb and 3.86 lb of steel on average per kip load for both the EOD and BOR conditions, respectively.
4) The time dependent study revealed general relaxation of end bearing of piles driven on IGMs. All the IGM-soils and IGM-rocks exhibited decrease in unit end bearing on 24-hr restrike though some siltstones and shales exhibited both setup and relaxation in the unit end bearing. The observed decrease in unit end bearing was as high as 70 percent in claystones, whereas the increase was minimal with 20 percent in both the siltstone and shale.
5) The time dependent study revealed general setup of shaft resistance of piles driven in IGMs. The gain in unit shaft resistance was as high as 180 percent for soils, 110 percent for IGM-soils, and nearly 100 percent for IGM-rocks. Only a few cases of relaxation in unit shaft resistances were observed in dense sand/gravel (IGM-soils) and shales. Dense sand and gravel exhibited an increase in the unit shaft resistance up to 0.6 ksf and

decrease to 1 ksf. Shale exhibited an increase up to 1.25 ksf and a decrease nearly down to 0.75 ksf.

6) Owing to the limitation of inputting IGM properties in WEAP, two procedures, denoted as Case I and Case II, were proposed to input IGM properties for bearing graph analysis. With these IGM input procedures, the effects of Case I considering program generated default toe-quake values and Case II considering user-defined toe-quake values of D/120 and 0.04 in for IGM-soils and IGM-rocks on pile resistance estimations were assessed. The suggested steps on inputting IGM properties in WEAP yield reliable pile resistance estimations with mean biases of 1.06 and 1.01 for Cases I and II, respectively, and with nearly the same COVs of 30 percent. The slightly higher mean bias of Case I indicates that the program generated toe-quake values are slightly conservative. Nevertheless, the difference is not significant, and users can rely on the default-generated toe-quake values for the bearing graph analysis using WEAP.
7) Additional nine pile data obtained from three different projects in Wyoming were used in the validation of the calibrated SA methods. The evaluation showed that the calibrated α-method was relatively accurate in predicting the shaft resistance in IGM-soils with a mean resistance bias of 1.03. Data were not enough to conclude the performance of the calibrated α-method in IGM-rocks. The calibrated β-method did not yield accurate predictions of shaft resistance and end bearing estimations in IGM-rocks with mean resistance bias of 1.28 and 1.61, respectively. The poor performance might be due to the uncertainties in the determination of friction angles of the IGM-rocks which were used in the calibration and validation.
8) The MCS and FORM resistance factors are larger than FOSM resistance factors by 5percent, on average, for β_T= 2.33. The MCS and FORM resistance factors decrease by almost 40 percent, on average, when the reliability index increases from 2.33 to 3.00.
9) The calibrated SA methods are concluded to be more efficient than the existing SA methods for the determination of shaft resistance and end-bearing in IGM-rocks. The calibrated α-method is recommended for shaft resistance estimation in IGM-soils. Existing SA methods with resistance factors calibrated based on Wyoming pile data are recommended for estimating end bearing in IGM-soils and shaft resistance in cohesionless IGM-soils.
10) Uncertainties in the resistance factors were dependent upon the sample sizes. The uncertainty of the resistance factor measured in terms of standard deviation decreases from 0.1 to 0.02 when sample size increased from 18 to 500 for the calibrated β-method in IGM-rock for end bearing estimation.

8.3 Recommendations from the Study

In order to improve the pile resistance estimations using SA methods and pile construction control using WEAP, the following recommendations are suggested:

1) IGMs can be categorized into IGM-soils and IGM-rocks to reduce the uncertainties in pile resistance estimation in IGMs ranging from hard soils to soft rocks. Soil-based and rock-based geomaterials can be classified based upon the geological description of the geomaterials. Criteria for separating IGM-soils from soils and IGM-rocks from hard rocks are recommended. Geomaterials can be classified following the criteria presented in a flowchart (Figure 28) for the purpose of driven pile design.

2) The criterion using $(N_1)_{60}$ of 50 is established for differentiating cohesionless soils from IGM-soils based on the performance of the existing β-method and Nordlund method in predicting the pile resistances. Cohesionless soil-based geomaterials having $(N_1)_{60}$ greater than 50 are recommended as IGM-soils.
3) The classification criterion to differentiate cohesive soils and IGM-soils is established based on the unit CAPWAP shaft resistance of 1 ksf that corresponds to an undrained shear strength (s_u) of 2.7 ksf. Hence, cohesive soil-based geomaterials with s_u values greater than 2.7 ksf are recommended as IGM-soils.
4) Boundary UCS values to separate IGM-rocks from hard rocks were obtained by back-calculation on equating the geotechnical resistance to the compressive strength of the pile. These UCS values are presented in charts in appendices to facilitate the classification of IGM-rocks from hard rocks for commonly used Grade 50 HP14×89, HP14×73, HP12×74, HP12×53, and HP10×42. However, the methodology adopted can be extended to other pile types to develop similar charts. Rock types, intact and fractured rocks are considered during the preparation of charts. RMR is used to distinguish intact and fractured rocks. Since not all parameters are available for the RMR calculation, a modified procedure utilizing only measured UCS and RQD values with maximum ratings of remaining parameters is recommended for the RMR calculation.
5) When measured shear strength properties and corrected SPT N-values of geomaterials are not available, they can be approximated from the catalogs developed for the shaft resistance and end bearing estimations using Table 11 and Table 12, respectively.
6) Based on comparative analysis of existing and calibrated SA methods, the complete recommended static analysis method of driven piles with the corresponding resistance factor is presented in Table 49. The resistance factors for two geomaterial input procedures (Case I and Case II described in Section 6.3) using WEAP are presented in
7) Table 50. The resistance factors presented in Table 50 are the lower bound resistance factors obtained by reducing the uncertainties in resistance factors from Chapter 6.
8) Equations of calibrated SA methods for the determination of shaft resistance and end bearing in IGM-soils and IGM-rocks are presented in Table 51. The resistance factors calibrated based on the target reliability index (β_T) of 2.33 are applicable to redundant pile group with a pile size greater than or equal to four. The resistance factors calibrated based on the β_T of 3.00 are for nonredundant pile group with a pile size less than four.

Table 49. Recommendation of SA methods and resistance factors.

Resistance	Geomaterials		SA method	Resistance factor for β_T= 2.33 (φ)	Resistance factor for β_T= 3.00 (φ)
Shaft resistance	IGM-soils	Cohesive	Calibrated α-method	0.50	0.40
		Cohesionless	Existing β-method	0.15	0.10
			Existing Nordlund	0.10	0.05
			Existing SPT method	0.15	0.10
	IGM-rocks	Cohesive	Calibrated α-method	0.35	0.25
		Cohesionless	Calibrated β-method	0.35	0.25
End bearing	IGM-soils	Cohesive	Existing α-method	0.35	0.28
		Cohesionless	Existing β-method	0.15	0.10
			Existing Nordlund	0.25	0.15
			Existing SPT method	0.10	0.05
	IGM-rocks	Cohesive	Calibrated α-method	0.30	0.20
		Cohesionless	Calibrated β-method	0.55	0.40

Table 50. Recommended resistance factors for bearing graph analysis of WEAP.

Resistance	Case	Resistance Factor (φ)	
		β_T= 2.33	β_T= 3.00
Total pile resistance from bearing graph	Case I- Program generated toe quake value	0.60	0.48
	Case II – Toe quake is 0.04 in for IGM-rocks and D/120 for IGM-soils	0.55	0.45

Table 51. Calibrated SA methods (Gebreslasie 2018).

Static Analysis Method	Unit Shaft Resistance	
	IGM-soil	**IGM-rock**
α-method	$\hat{\alpha} = 0.29 s_u^{\,2} - 2.71 s_u + 6.51$ q_s (ksf) = $\hat{\alpha} \times s_u$ where, s_u is in ksf	$\hat{\alpha} = \frac{64.63 \times q_u^{-0.66}}{100}$ q_s (ksf) = $\hat{\alpha} \times q_u$ where, q_u is in ksf
β-method	NA[1]	$\hat{\beta} = 0.01\phi^2 - 0.75\phi + 14.63$ q_s (ksf) = $\hat{\beta} \times \sigma'_v$ where, ϕ is in degree and σ'_v is in ksf
Shaft resistance, $R_s = q_s \times A_s$, where, A_s is surface area of pile. A_s= 2× (flange width + web depth) × embedment length		
Static Analysis Method	**Unit End Bearing**	
	IGM-soil	**IGM-rock**
α-method	NA[*]	$\widehat{N_c} = 39.8 \times q_u^{-0.64}$ q_p (ksf) = $\widehat{N_c} \times q_u$ where, q_u is in ksf
β-method	NA[1]	$\widehat{N_t} = 0.91\,\phi^2 - 71.4\phi + 1428.55$ q_p (ksf) = $\widehat{N_t} \times p_t$ where, ϕ is in degree and p_t is in ksf
End bearing, $R_p = q_p \times A_p$, where A_p is box cross sectional area of pile. A_s= flange width × web depth		

s_u- undrained shear strength; q_s- unit shaft resistance; q_u- unconfined compressive strength; σ'_v- effective overburden stress at mid of soil layer; q_p- unit end bearing; p_t- effective overburden stress at pile tip; NA–not available; [1]–regression analyses revealed no relationships between variables, [*]– due to small sample size.

8.4 Recommendations to Current WYDOT Manuals

To improve the driven pile performance in the State of Wyoming, conclusions drawn from this research were proposed as recommendations to current WYDOT application and construction manuals. Several recommendations to the current WYDOT Bridge Applications Manual Chapter 4, Sections 4.04 and 4.06 (WYDOT, 2008) are provided in Table 52. Recommendations to the current pile construction practices are provided in Table 53 with respected to the WYDOT Standard Specifications for Road and Bridge Construction Manual (2010) and in Table 54 for the WYDOT Construction Manual (2019). To facilitate the implementation of the research outcomes in future pile design using the SA methods and a construction control using WEAP in Wyoming, a LRFD pile design example, is presented in Appendix C.

Table 52. Recommendations to current WYDOT Bridge Applications Manual (2008).

Section	Current Specifications	Recommendation
4.04: Substructure Types-Steel Piling	Steel piling is used when footings cannot be founded on rock or competent soils within a reasonable depth.	Intermediate Geomaterials can be included in this statement.
4.04: General Design and Detail Information-Pile Points	When piles are driven through material that may damage or deflect the end of the piles, PILE POINTS may be required. These will be recommended by the Geology Program. The detailer must choose the correct PILE POINT DETAIL based on the size of the piling.	It is important to note that piles driven into Intermediate Geomaterials could experience pile relaxation after the end of driving. Pile points are recommended for piles in IGMs.
4.06: Explanation of Geology Report-General	Included in the GENERAL information are the geologic and hydrologic history of the region, description of existing structures, ground water elevation, material suitable for riprap, and a general description of the foundation materials encountered.	Each foundation geomaterial should be described in a Geology Report as soil, IGM-soil, IGM-rock or hard rock following the recommended classification criteria.
4.06: Explanation of Geology Report-Recommendations	Included in the RECOMMENDATIONS are the basic substructure types - footings, piling, and drilled shaft foundations. Allowable values shown include the AASHTO required factors of safety.	Replace the sentence to "Allowable pile resistances shown include the AASHTO required resistance factors for soils and calibrated resistance factors for IGMs."
4.06: Explanation of Geology Report-Piling	Recommendations for PILING include desired pile tip elevations at which driving refusal and design refusal are reached, skin friction and uplift values, the necessity for pile points, preboring, and pile dynamic analyzer (PDA) testing.	Allowable skin friction and end bearing in IGMs should be estimated using the recommended static analysis methods and LRFD procedures. Construction control using a signal matching technique (i.e., PDA with CAPWAP analysis) should be recommended to confirm the performance of piles in IGMs.

Table 53. Recommendations to current WYDOT Standard Specifications for Road and Bridge Construction Manual (2010).

Section	Recommendation
504.3.1.1	It is recommended to use a large pile driving equipment to install steel piles into Intermediate Geomaterials to fully mobilize the skin friction and end bearing prior to reaching the pile refusal while satisfying the allowable pile stresses of 90 percent of the minimum yield strength for steel piles.
504.4.3 and 504.4.4	Recommended LRFD procedure for wave equation analysis should be considered.
504.4.4	Soil Resistance Piling: Replace the "a safety factor" with "a resistance factor"
504.4.4	Dynamic Load Test: Construction control using a signal matching technique (i.e., PDA with CAPWAP analysis) should be recommended at the end of driving and 24-hour restrike to confirm the performance of piles in IGMs.

Table 54 Recommendations to current WYDOT Construction Manual (2019).

Section	Recommendation
504	Inspection: Ensure the pile hammer is warmed before performing the 24-hour restrike on piles driven into Intermediate Geomaterials. Hammer blow counts should be recorded in driving logs during driving and 24-hour strike.

8.5 Recommendations for Future Works

Recommendations for future research works are suggested to improve the limitations in this study and advance the knowledge pertaining to driven piles in IGMs.

1) The contribution of the surrounding soil to the bracing of a driven pile has not yet been fully investigated. In this study, piles were assumed fully embedded in the soil, and the unbraced length (L) was assumed zero. However, nonzero unbraced length in fully embedded geomaterials can be investigated in the future by considering depth to fixity in addition to laterally unsupported length for unbraced length determination.
2) The classification criteria developed for cohesive soil-based geomaterials were based on only 10 samples. Thus, further investigations and verifications are needed to improve the criterion on more cohesive soil-based geomaterials. The cohesive soil-based geomaterial used in the present study was limited to low plasticity soils.
3) Samples of IGMs should be comprehensively tested to determine their strength behaviors in terms of multiple material properties, rather than a single strength parameter. Incorporating multiple material properties in the calibration of SA methods can improve the efficiency of pile resistance estimation.
4) Due to the availability of limited lab measured strength parameters, most of the strength parameters were either correlated, or adopted from WYDOT tables. Using geomaterial properties from various sources incorporated many uncertainties in the geomaterial properties, which might have aggravated the resistance biases. Thus, SA methods may be further improved using lab measured geomaterial parameters.
5) As the current resistance factors suffer from high uncertainties due to limited sample sizes, resistance factors need to be recalibrated with the availability of additional data.

REFERENCES

AbdelSalam, S. S., Ng, K. W., Sritharan, S., Suleiman, M. T., and Roling, M. (2012). *Development of LRFD procedures for bridge pile foundations in Iowa-Volume III: Recommended Resistance Factors with Consideration of Construction Control and Setup* (No. IHRB Projects TR-584). Institute for Transportation, Iowa State University,Ames, IA. https://intrans.iastate.edu/app/uploads/2018/03/tr-584_lrfd_vol_iii_w_cvr1.pdf

Abu-Hejleh, N. M., O'Neill, M. W., Hanneman, D., and Attwoll, W. J. (2005). Improvement of the Geotechnical Axial Design Methodology for Colorado's Drilled Shafts Socketed in Weak Rocks. *Journal of the Transportation Research Board*, 1936(1), pp. 100-107. http://dx.doi.org/10.3141/1936-12

Abu-Hejleh, N., Kramer, W. M., Mohamed, K., Long, J. H., and Zaheer, M. A. (2013). *Implementation of AASHTO LRFD design specifications for driven piles*. FHWA-RC-13-001. FHWA Resource Center, Matteson, IL. https://www.fhwa.dot.gov/resourcecenter/teams/geohydraulics/lrfdpilespecs.pdf

Abu-Hejleh, N.M., Abu-Farsakh, M., Suleiman, M.T., and Tsai, C., 2015. Development and Use of High-Quality Databases of Deep Foundation Load Tests. *Transportation Research Record: Journal of the Transportation Research Board*, No. 2511, Transportation Research Board, Washington, D.C., pp. 27-36. https://doi.org/10.3141/2511-04

Adhikari, P. (2019). *Load and resistance factor design and construction control of driven piles in intermediate geomaterials*. Ph.D. Thesis. University of Wyoming, Laramie, WY.

Adhikari, P., Gebreslasie, Z.Y., Ng, K.W., Wulff, S.S., and Sullivan, T., (2018). Static and dynamic analysis of steel H-piles in soft rocks considering LRFD using a recently developed electronic database. IFCEE 2018, Geotechnical Special Publication 294, ASCE, Orlando, FL, pp. 83-92. https://doi.org/10.1061/9780784481578.009

Akai, K. (1997). "Testing Methods for Indurated Soils and Soft Rocks Interim Report." *Geotechnical Engineering of Hard Soils-Soft Rocks: Proceedings of an International Symposium for ISSMFE, IAEG and ISRM.* Athens, Greece, September 1993, pp.1707--1737.

American Association of State Highway and Transportation Officials. (2017). *AASHTO LRFD Bridge Design Specifications*, Eighth Edition, U.S. Customary Units, Washington, D.C.

Allen, T. M. (2005). *Development of the WSDOT Pile Driving Formula and Its Calibration for Load and Resistance Factor Design (LRFD)*. Final Report No. WA-RD 610.1. Prepared for Washington State Department of Transportation and in cooperation with U.S. Department of Transportation, Federal Highway Administration. https://www.wsdot.wa.gov/research/reports/fullreports/610.1.pdf

Allen, T.M., Nowak, A.S., and Bathurst, R.J. (2005). *Calibration to determine load and resistance factors for geotechnical and structural design*. Transportation Research E-Circular, (E-C079). http://onlinepubs.trb.org/onlinepubs/circulars/ec079.pdf

Anderson, T. W., and Darling, D. A. (1952). Asymptotic theory of certain" goodness of fit" criteria based on stochastic processes. *The annals of mathematical statistics*, 23(2), pp. 193-212. https://projecteuclid.org/download/pdf_1/euclid.aoms/1177729437

Baecher, G.B., and J.T. Christian. (2003). *Reliability and Statistics in Geotechnical Engineering*. J. Wiley, Chichester, West Sussex, England.

Becker, D., and Moore, I. (2006). Canadian foundation engineering manual.

British Standards Institution. (1981). BS5930: *Code of Practice for Site Investigations*, BSI, London.

Brooks, H. M. (2008). *Axial Capacity of Piles Supported on Intermediate Geomaterials.* Masters Thesis, Montana State University, Bozeman, MT. http://citeseerx.ist.psu.edu/viewdoc/download?doi=10.1.1.427.8227&rep=rep1&type=pdf

Carter, J.P. and Kulhawy, F.H. (1988). *Analysis and Design of Drilled Shaft Foundations Socketed into Rock.* Report EL-5918, Electric Power Research Institute, Palo Alto, CA.; Cornell University, Geotechnical Engineering Group, Ithaca, NY.

Cherubini, C., and Vessia, G. (2007). "Reliability approach for the side resistance of piles by means of the total stress analysis (α method)." *Canadian Geotechnical Journal*, *44*(11), pp. 1378-1390. https://doi.org/10.1139/T07-061

Clarke, B.G, and Smith, A. (1992). "Self-boring pressuremeter tests in weak rocks." *Construction and Building Materials*, 6(2), pp. 91-96. https://doi.org/10.1016/0950-0618(92)90057-6

Clayton, C R I. (1995). *The Standard Penetration Test (SPT): Methods and Use.* CIRIA, London.

Colorado Department of Transportation (CDOT). (2018). *CDOT Bridge Design Manual*. CDOT, CO.

Cornell, C. A. (1969). Structural Safety Specification Based on Second-Moment Reliability Analysis. In Final Report, *Symp on Concepts of Safety of Structures and Methods of Design*, Zurich, IABSE, London. http://doi.org/10.5169/seals-5948

Davisson, M., 1972. High Capacity Piles. *In Proceedings, Soil Mechanics Lecture Series on Innovations in Foundation Construction*, ASCE, IL Section, Chicago, IL, pp. 81-112.

de Freitas, H. (1993). Introduction to Session 1.2: Weak Arenaceous Rock. *The Engineering Geology of Weak Rock: Proceedings of the 26th Annual Conference of the Engineering Group Geological Society*, Leeds, UK, September 1990, 115123.

Du, X. (2005). First Order and Second Reliability Methods. *Probabilisitc Engineering Design.* pp.1-33. http://web.mst.edu/~dux/repository/me360/ch7.pdf

Esrig, M.E., and Kirby, R.C. (1979). Advances in General Effective Stress Method for the Prediction of Axial Capacity for Driven Piles in Clay. In Proc., *11th Annual Offshore Technology Conference*, pp. 437–449. https://doi.org/10.2118/8553-PA

Fellenius, B. H., (1991). Pile foundations. *In Foundation engineering handbook* (pp. 511-536). Springer, Boston, MA.

Florida Department of Transportation (FDOT). (2016). *Soils and Foundations Handbook*. State Materials Office, Gainesville, FL.

Gannon, J. A., Masterton, G. G., Wallace, W. A., and Wood, D. M. (1999). *Piled Foundations in Weak Rock.* Construction Industry Research and Information Association, London, UK.

Gebreslasie, Y. Z. (2018). Static Analysis Methods for Estimating the Capacity of Driven Piles in Intermediate Geomaterials (IGM). Master Thesis, University of Wyoming, Laramie, WY.

Goble, G. G. and Rausche, F. (1976). *Wave equation analysis of pile driving -WEAP Program Manual*. U.S. Department of Transportation, Vol. 1–4, Report No. FHWA IP-76-14.1 through IP-76-14.4.

Green, D.,Ng, K.W., Dunker, K.F., Sritharan, S., and Nop, M. (2012). *Development of LRFD Procedures for Bridge Piles in IOWA - Volume IV: Design Guide and Track Examples.* Iowa Highway Research Board, Iowa.

Haberfield, C. M., and I. W. Johnston. (1993). Factors influencing the interpretation of pressuremeter tests in soft rock. *Geotechnical Engineering of Hard Soils- Soft Rocks.* Balkema, Rotterdam, pp. 525-531.

Hacking, I. (1975). *The Emergence of Probability*. Cambridge University Press, Cambridge.

Hannigan, P. J., Goble, G. G., Likins, G. E., & Rausche, F. (2006). *Design and construction of driven pile foundation, vol I. US Department of Transportation*, Federal Highway Administration, publication no. FHWA NHI-05-042.

Hartle, R. A., Wilson, K. E., Amrhein, W. A., Zang, S. D., Bouscher, J. W., and Volle, L. E. (2003). *LRFD Design Example for Steel Girder Superstructure Bridge*. Report No. FHWA NHI -04-041, Federal Highway Administration, Arlington, Virginia.

Hasofer, A. M., and Lind, N. C. (1974). Exact and invariant second-moment code format. *Journal of the Engineering Mechanics division*, 100(1), pp. 111-121.

Hirsch, T.J.Jr., Carr, L., and Lowery, L.L.Jr., (1976). *Pile Driving Analysis Wave Equation User's Manuals – TTI Program*. Vol. 1-4, Report No. FHWA IP- 76-13.1 through IP-76-13.4.

Hoek, E. and E.T. Brown. (1988). The Hoek–Brown Failure Criterion—A 1988 Update. *Proceedings 15th Canadian Rock Mechanics Symposium*, *Rock Engineering for Underground Excavations*, October 3-4, Toronto, ON, Canada, pp. 31–38.

Illinois Department of Transportation (IDOT). (2009). *All Geotechnical Manual Users (AGMU) Memo 10.2- Geotechnical Pile Design*. Illinois Department of Transportation, Division of Highways, Springfield, IL.

Illinois Department of Transportation (IDOT). (2012). *Bridge Manual* . Illinois Department of Transportation, Bureau of Bridges and Structures, Division of Highways, Springfield, IL.

ISRM, (1981). Basic Geotechnical Description of Rock Masses. ISRM Commission on Classification of Rocks and Rock Masses. *Int. J. Rock Mech. Min. Sci. & Geomech. Abstr.* 18, pp. 85-110.

ISSMFE, (1989). *Report of the Technical Committee on soft rocks and indurated soils*. Japanese Society of Soil Mechanics.

Johnston, I. W. (1989). Discussion Leaders Report: Material Properties of Weak Rock. *Proceedings of the International Conference on Soil Mechanics and Foundation Engineering*, Montreal, Canada, pp. 2831-2833.

Johnston, I. W. (1994). Soil Mechanics, Rock Mechanics and Soft Rock Technology. *Proceedings of the Institution of Civil Engineers. Geotechnical engineering.* 107 (1), pp. 3-9.

Jowers, R. and Bennett, G. (2016). *Tennessee Department of Transportation (TDOT) Geotechnical Manual*. Geotechnical Engineering Section, Nashville, TN.

Kalavar, S., and Ealy, C., 2000. FHWA deep foundation load test database. *New technological and design developments in deep foundations*, pp. 192-206. https://doi.org/10.1061/40511(288)14

Kulhawy, F. H. (1992). On the evaluation of static soil properties. Edited by R. B. Seed and R. W. Boulanger. *Stability and Performance of slopes and embankments II* (GSP). New York: American Society of Civil Engineers, pp. 95-115.

Kulhawy, F.H. (1996). From Casagrande's 'Calculated Risk' to Reliability-based Design in Foundation Engineering. *Civil Engineering Practice* 11(2), pp. 43–56.

Kulhawy, F. H., and Mayne, P. W. (1990). *Manual on Estimating Soil Properties for Foundation Design* (No. EPRI-EL-6800). Electric Power Research Inst., Palo Alto, CA (USA); Cornell Univ., Ithaca, NY (USA). Geotechnical Engineering Group.

Lai, P.W. (2012). An Introduction to the Design Methodology of FB-Deep. In Design Training and Expo. FDOT Structures Design Office, State Geotechnical Engineering Section, FL. (Presentation slides) https://fdotwww.blob.core.windows.net/sitefinity/docs/default-source/content/geotechnical/documents/fb-deep.pdf?sfvrsn=bf6bf0c1_0

Larounis, N., and Nop, M. (2016). *Further Evaluation of Steel H-piles Driven to Bedrock*. Iowa Department of Transportation.

Long, J.H. (2016). *Static Pile Load Tests on Driven Piles into Intermediate-Geo Materials*. Report No. WHRP 0092-12-08. Department of Civil Engineering, University of Illinois at Urbana/ Champaign, Urbana, IL. https://wisconsindot.gov/documents2/research/0092-12-08-final-report.pdf

Long, J., and Anderson, A. (2014). *Improvement of Driven Pile Installation and Design in Illinois: Phase 2*. Department of Civil and Environmental Engineering, University of Illinois at Urbana-Champaign, Illinois Department of Transportation. http://hdl.handle.net/2142/50310

Long, J., and Horsfall, J., 2017. *Static pile load tests on driven piles in intermediate geo materials*. Project 0092-12-08, Research Brief, Wisconsin Highway Research Program, February, Madison, WI. https://wisconsindot.gov/documents2/research/0092-12-08-final-report.pdf

Long, J. H., Hendrix, J., and Baratta, A. (2009). *Evaluation/Modification of IDOT Foundation Piling Design and Construction Policy*. Illinois Department of Transportation, University of Illinois at Urbana-Champaign.Urbana, IL. http://hdl.handle.net/2142/13791

Long, J. and Horsfall, J. (2017). Static Pile Load Tests on Driven Piles in Intermediate Geo-Materials. Project 0092-12-08, Research Brief, Wisconsin Highway Research Program, February, Madison, WI.

Maine Department of Transportation (MaineDOT). (2014). Bridge Design Guide. MaineDOT, Augusta, ME.

Mayne, P. W., Christopher, B. R., Berg, R., & DeJong, J. (2002). Subsurface investigations—geotechnical site characterization. *Publication Number FHWA-NHI-01-031, National Highway Institute, Federal Highway Administration, Washington, DC.*

Meyerhof, G. (1976). Bearing Capacity and Settlement of Pile Foundations. American Society of Civil Engineers. *Journal of the Geotechnical Engineering Division*, Vol. 102, No. 3, March, pp. 195–228.

Minnesota Department of Transportation (MnDOT). (2016). *LRFD Bridge Design Manual*. Bridge Office, MnDOT. Oakdale, MN.

Mokwa, R. and Brooks, H. (2008). *Axial Capacity of Piles Supported on Intermediate Geomaterials.* Final Report No. FHWA/MT-08-008/8117-32, Montana State University, Western Transportation Institute, Bozeman, MT. https://www.mdt.mt.gov/other/webdata/external/research/docs/research_proj/axial/final_report.pdf

Mokwa, R.L. and Brooks, H., (2009). Driven Pile Capacity in Intermediate Geomaterial Formations. *In Contemporary Topics in Deep Foundations*, (GSP 185), ASCE, March 15-19, Orlando, FL, pp. 263-270. https://doi.org/10.1061/41021(335)33

Montana Department of Transportation (MDT). (2008). *MDT Geotechnical Manual*. MDOT, Helena, MT.

Ng, K. W. (2011). *Pile Setup, Dynamic Construction control and Load and Resistance Factor Design of Vertically Loaded Steel H-Piles*. Ph.D. Dissertation, Iowa State University of Science and Technology, Ames, IA.

Ng, K. and Sullivan, T., 2017a. Recent development of Load and Resistance Factor Design (LRFD) for driven piles on Soft Rock. *Geotechnical Special Publication* No. 283, GeoRisk 2017, ASCE, Denver, CO, pp. 307-316. https://doi.org/10.1061/9780784480700.030

Ng, K.W., and Sullivan, T., 2017b. Challenges and recommendations for piles driven in soft rock. *Geotechnical Engineering Journal of SEAGS-AGSSEA*, Special Issue on Research & Practice in Foundations & Deep Ground Improvement Techniques, 48(3), September, pp. 1-10.

Ng, K.W., and Sullivan, T., 2016. Demonstrating challenges of driven piles in rock using two case studies in Wyoming, USA. *Proceedings of 19th Southeast Asian Geotechnical Conferenc*e, Subang Jaya, Malaysia.

Ng, K.W., Yasrobi, S.Y., and Sullivan, T.A. (2015). Current Limitations and Challenges with Estimating Resistance of Driven Piles on Rock as Demonstrated Using Three Case Studies in Wyoming. *Proceedings of International Foundations Congress & Equipment Exposition*, Geotechnical Special Publication No. 256, San Antonio, TX, pp. 500-517. https://ascelibrary.org/doi/pdf/10.1061/9780784479087.048

Nordlund, R.L. (1963). "Bearing Capacity of Piles in Cohesionless Soils." *Journal of Soil Mechanics and Foundation Division*, ASCE, Vol. 89, SM 3, pp. 1-36.

North Carolina Department of Transportation. (2014). *LRFD Driven Pile Foundation Design Policy*. 6th Update. North Carolina Department of Transportation, Raleigh, NC.

Oliveira, R. (1993). "Weak rock materials." *The Engineering Geology of Weak Rock*. Balkema, Rotterdam: A.A. Balkema Publishers, Old Post Road, pp. 5-15.

O'Neil, M. W., and Reese, L. C. (1999). *Drilled Shafts: Construction Procedures and Design Methods*. No. FHWA-IF-99-025, Federal Highway Administration, Washington, D.C.

Oregon Department of Transportation (ODOT). (2015). *Geotechnical Design Manual.* ODOT, Salem, OR.

Paikowsky, S. G., B. Birgisson, M. McVay, T. Nguyen, C. Kuo, G. Baecher, B. Ayyub, K. Stenersen, K.O'Malley, L. Chernauskas, and, M. O'Neill., (2004). *NCHRP Report 507: Load and Resistance Factor Design (LRFD) for Deep Foundations*. Transportation Research Board of the National Academies, Washington, D.C.

Paikowsky, S. G., Marchionda C. M., O'Hearn, C. M., and, Canniff, M. C., (2009). *Developing a Resistance Factor for Mn/DOT's Pile Driving Formula*. Minnesota Department of Transportation, St. Paul, Minnesota.

Pennsylvania Department of Transportaion (PennDOT). (2015). *Design Manual, Part 4*. PennDOT, Harrisburg, PA.

Petek, K., Mitchell, R., and Ellis, H.,(2016). *FHWA Deep Foundation Load Test Database Version 2.0 User Manual*. No. FHWA-HRT-17-034, Federal Highway Administration, McLean, VA.

Phoon, K.K. and Kulhawy, F. H. (1999). Characterization of geotechnical variability. *Canadian Geotechnical Journal*, 36(4), pp. 612-624. https://doi.org/10.1139/t99-038

Pile Dynamics, Inc. (2000). *CAPWAP for Windows Manual*. Pile Dynamics, Inc., Cleveland, OH.

Rackwitz, R., & Fiessler, B. (1978). Structural reliability under combined load sequence. *Computer & Structures*, 9, pp. 489-494.

Rausche, F., and Goble, G. (1979). Determination of Pile Damage by Top Measurements. In *Behavior of Deep Foundations*. American Society for Testing and Materials. Philadelphia, PA.

Rocha, M. (1971). A method of integral sampling of rock masses. *Rock Mechanics*, 3, pp 1-12.

Rohde, J., and Feng. H. (1990). Analysis of the Variability of Unconfined Compression Tests of Rock. *Rock Mechanics and Rock Engineering* (Springer-Verlag), 23, pp. 231-236.

Roling, M. J., Sritharan, S., and Suleiman, M. T., (2011). Introduction to PILOT database and establishment of LRFD resistance factors for the construction control of driven steel H-piles. *Journal of Bridge Engineering*, 16(6), pp. 728-738. https://doi.org/10.1061/(ASCE)BE.1943-5592.0000247

Rosenblueth, E., and Esteva, L. (1972). *Reliability Basis for Some Mexican Codes.* ACI Publication SP-31. American Concrete Institute, Detroit, MI.

Rowe, R.K., and Armitage, H.H. (1987). A Design Method for Drilled Piers in Soft Rock. *Canadian Geotechnical Journal*, 24(1), pp. 126–142.

Sandford, T., & Stuart, C. (2014). *Development and Evaluation of Pile "High Strain Dynamic Test Database" to Improve Driven Capacity Estimates: Phase II Report*. (No. ME 14-01 Phase 2). University of Maine, Orono, ME. https://www.maine.gov/mdot/research/docs/reports/BrdgRsch_14-01p2.pdf

Santi, P.M. and Doyle, B.C. (1997). The locations and engineering characteristics of weak rock in the US: In Santi, PM and Shakoor, A. *Characterization of Weak and Weathered Rock Masses*, Association of Engineering Geologists Special Publication 9, Association of Engineering Geologists, Denver, CO, pp.1-22.

Shapiro, S. S., & Wilk, M. B. (1965). An analysis of variance test for normality (complete samples). *Biometrika*, 52(3/4), pp. 591-611. https://www.jstor.org/stable/2333709

Smith, E. A. L. (1951). Pile driving impact. Proceedings, *Industrial Computation Seminar*, September 1950, International Business Machines Corp., New York, N.Y., p. 44.

Smith, E. A. L. (1960). Pile driving analysis by the wave equation. American Society of Civil Engineers, *ASCE Journal for Soil Mechanics and Foundation Engineering*, Vol. 86, SM4 pp.35-61.

Smith, E. A. L. (1962). Pile-Driving Analysis by the Wave Equation. *American Society of Civil Engineers Transactions*. 127, pp. 1145-1193.

Smith, T., A. Banas, M. Gummer, and J. Jin., (2010). *Recalibration of the GRLWEAP LRFD Resistance Factor for Oregon DOT*. OR-RD-98-00. Research Unit, Oregon Department of Transportation, Salem, OR. https://ntlrepository.blob.core.windows.net/lib/36000/36100/36116/GRLWEAP_LRFD.pdf

South Carolina Department of Transportation (SCDOT) (2010). *SCDOT geotechnical design manual*. South Carolina Department of Transportation. Columbia, SC.

Stark, T. D., Long, J. H., & Assem, P. (2013). *Improvement for Determining the Axial Capacity of Drilled Shafts in Shale in Illinois.* Research Report No. FHWA-ICT-13-017. Illinois Center for Transportation, Department of Civil and Environmental Engineering, University of Illinois at Urbana-Champaign, Urbana, IL. http://hdl.handle.net/2142/45762

Terente, V., Irvine, J., Comrie, R., and Crowley, J. (2015). Pile Driving and Pile Installation Risk in Weak Rock. *In Proceedings of Frontiers in Offshore Geotechnics III*, Edited by V. Meyer, Taylor & Francis Group, UK, pp. 569-574.

Thompson, C.D. and Thompson, D.E. (1985). Real and Apparent Relaxation of Driven Piles. *Journal of Geotechnical Engineering*, ASCE, 111 (2), pp.225-237.

Tomlinson, M.J. (1987). *Pile Design and Construction Practice*. Viewpoint Publication, p. 415.

Tschebotarioff, G.P. (1973). *Foundations, Retaining, and Earth Structures*. 2nd Edition, McGraw-Hill.

Turner, J. P. (2006). *Rock-Socketed Shafts for Highway Structure Foundations.* NCHRP Synthesis 360. Transportation Research Board, Washington, D.C. http://www.geotechnicaldirectory.com/publications/Drilled-Shafts/nchrp_syn_360.pdf

Vesic, A. S. (1977). Design of pile foundations. *NCHRP synthesis of highway practice*, (42).

Vijayvergiya, V.N., and Focht, J.A., (1972). A New Way to Predict the Capacity of Piles in Clay. *In Proc., 4 the Annual Offshore Technology Conference*, Vol. 2, Houston, TX, pp. 865–87.

Washington State Department of Transportation (WSDOT). (2015). *WSDOT Geotechnical Design Manual.* WSDOT, Olympia, WA. https://www.wsdot.wa.gov/publications/manuals/fulltext/M46-03/Geotech.pdf

Withiam, J.L., Voytko, E.P., Barker, R.M., Duncan, J.M., Kelly, B.C., Musser, S.C., and Elias, V., (1998). *Load and Resistance Factor Design (LRFD) for Highway Bridge Substructures*, FHWA HI-98-032, Federal Highway Administration, Washington, D.C.

APPENDIX A. DESIGN CHARTS FOR q_{usi}

The charts showing boundary Uniaxial Compressive Strength (UCS) values, q_{usi}, separating intact IGM-rocks from hard rocks are presented below.

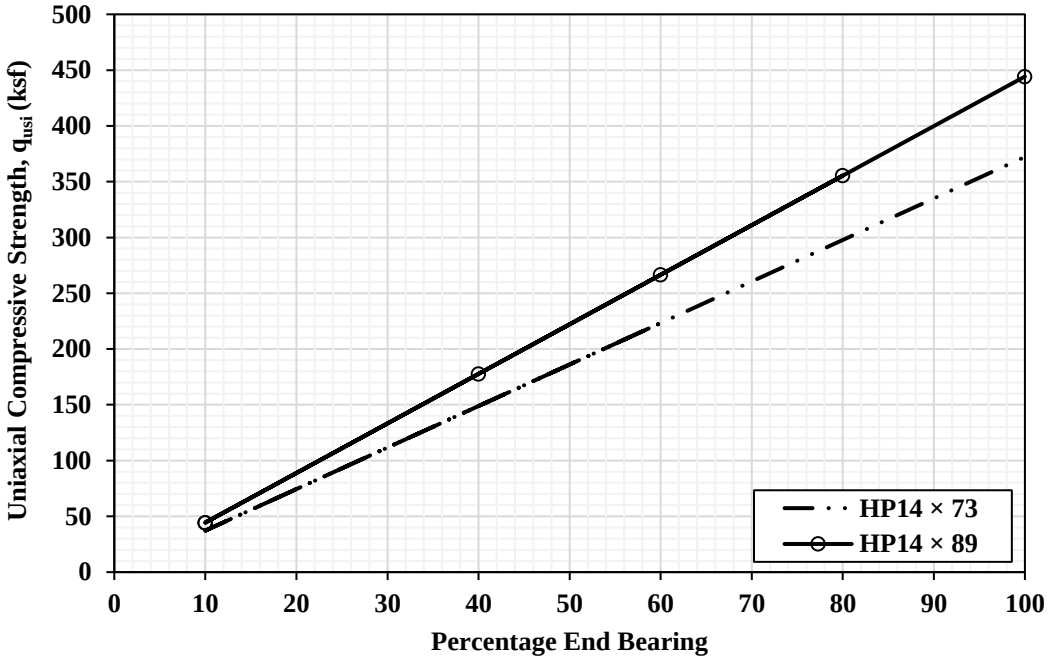

Source: Adhikari (2019)

Figure 60. Calculated q_{usi} values for intact IGM-rocks or hard rocks for Grade 50 HP14×89 and HP14×73 piles.

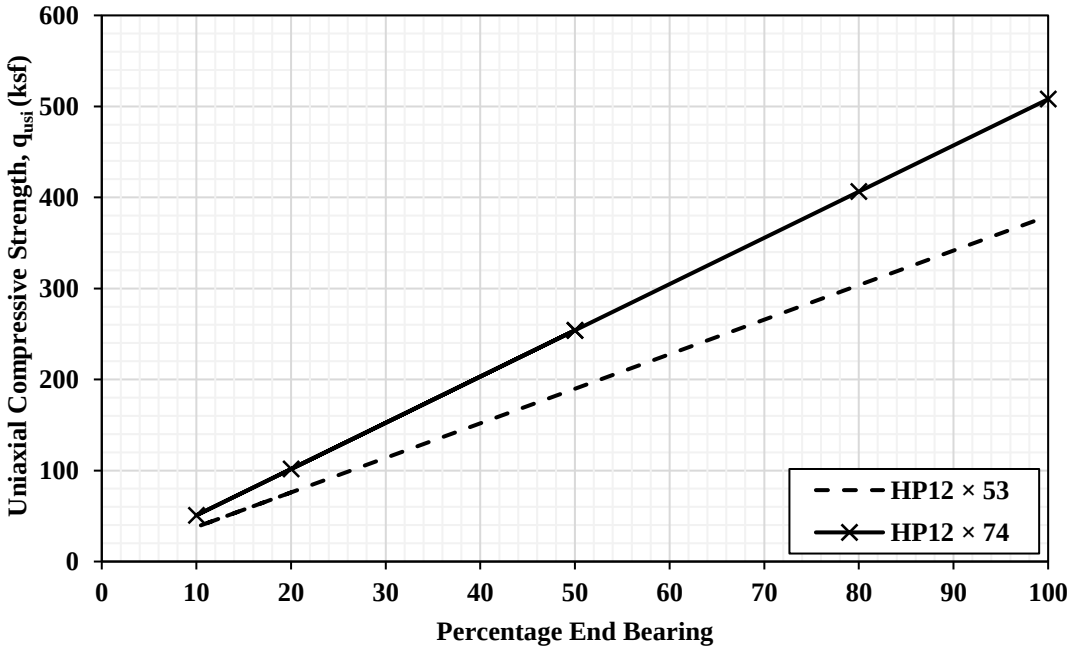

Source: Adhikari (2019)

Figure 61. Calculated q_{usi} values for intact IGM-rocks or hard rocks for Grade 50 HP12×74 and HP12×53 piles.

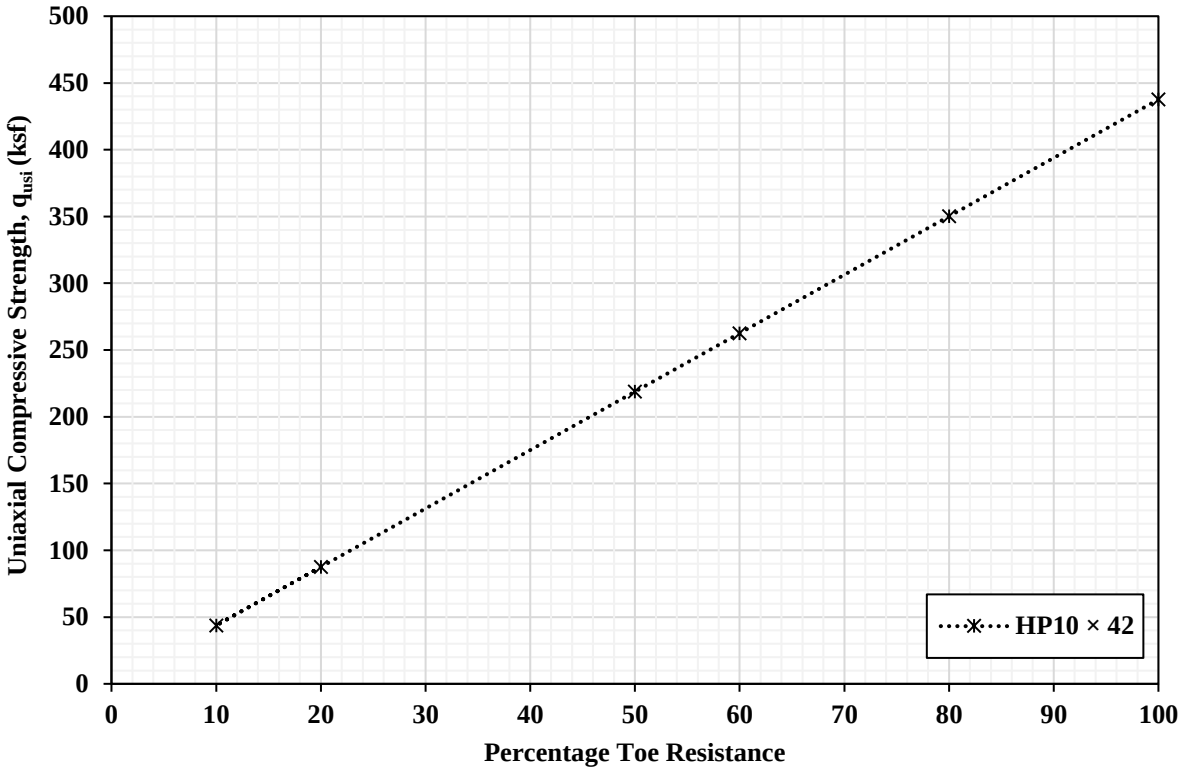

Source: Adhikari (2019)

Figure 62. Calculated q_{usi} values for intact IGM-rocks or hard rocks for Grade 50 HP10×42 piles.

APPENDIX B. DESIGN CHARTS FOR q_{usf}

The charts showing boundary Uniaxial Compressive Strength (UCS) values, q_{usf}, separating fractured IGM-rocks from hard rocks are presented below.

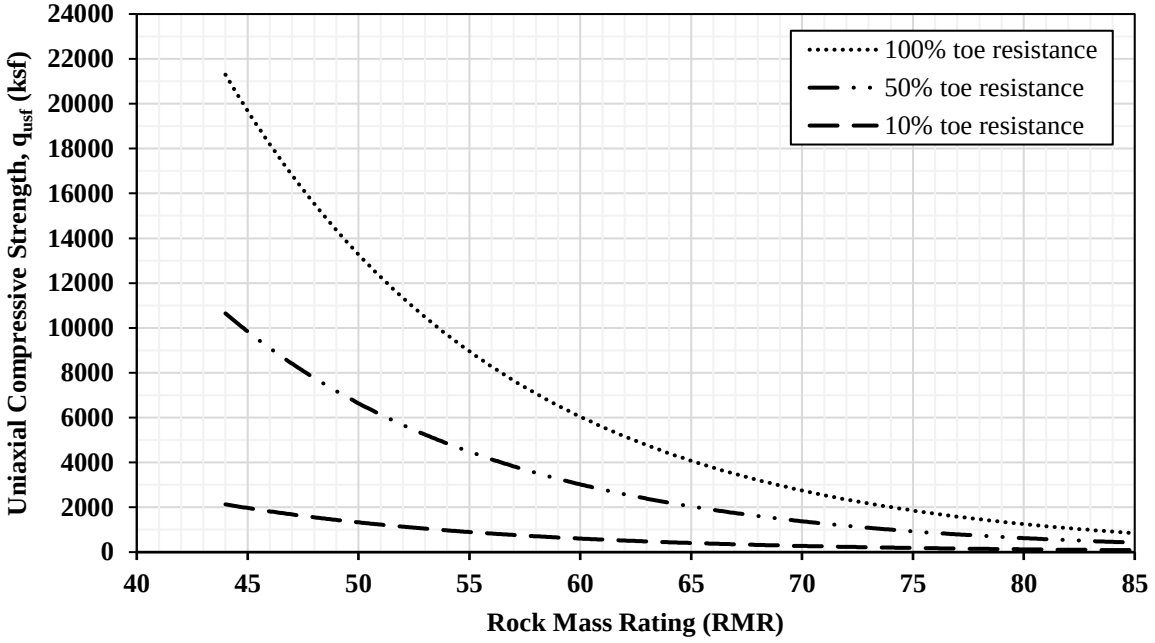

(a) Argillaceous Rocks

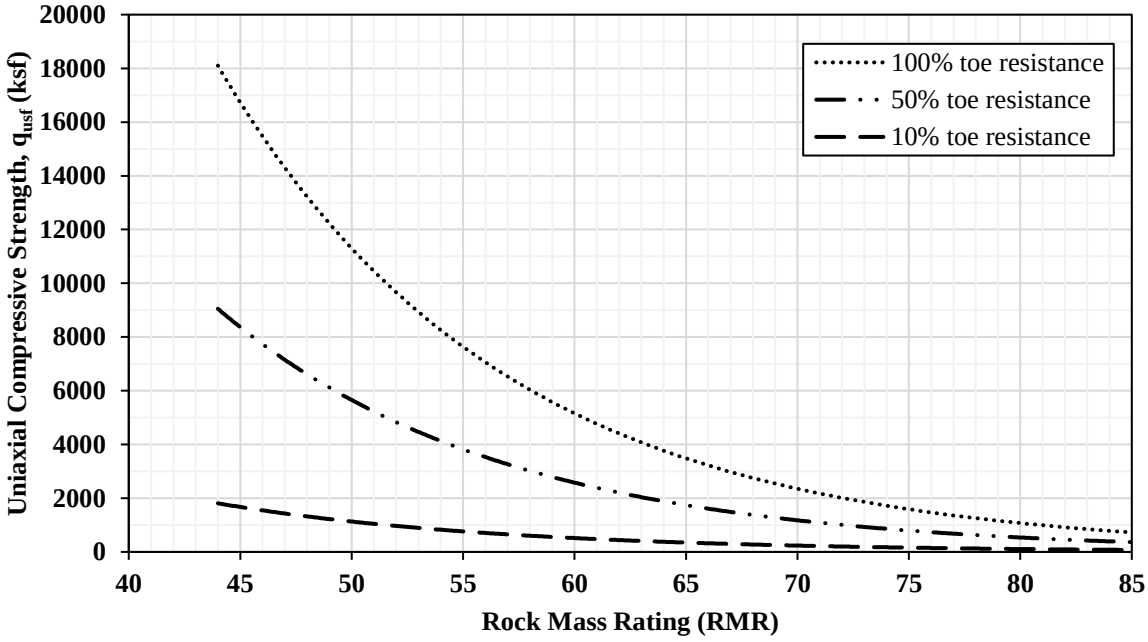

(b) Aranaceous Rocks
Source: Adhikari (2019)

Figure 63. Calculated q_{usf} values for Grade 50 HP14×89 pile for two rock types.

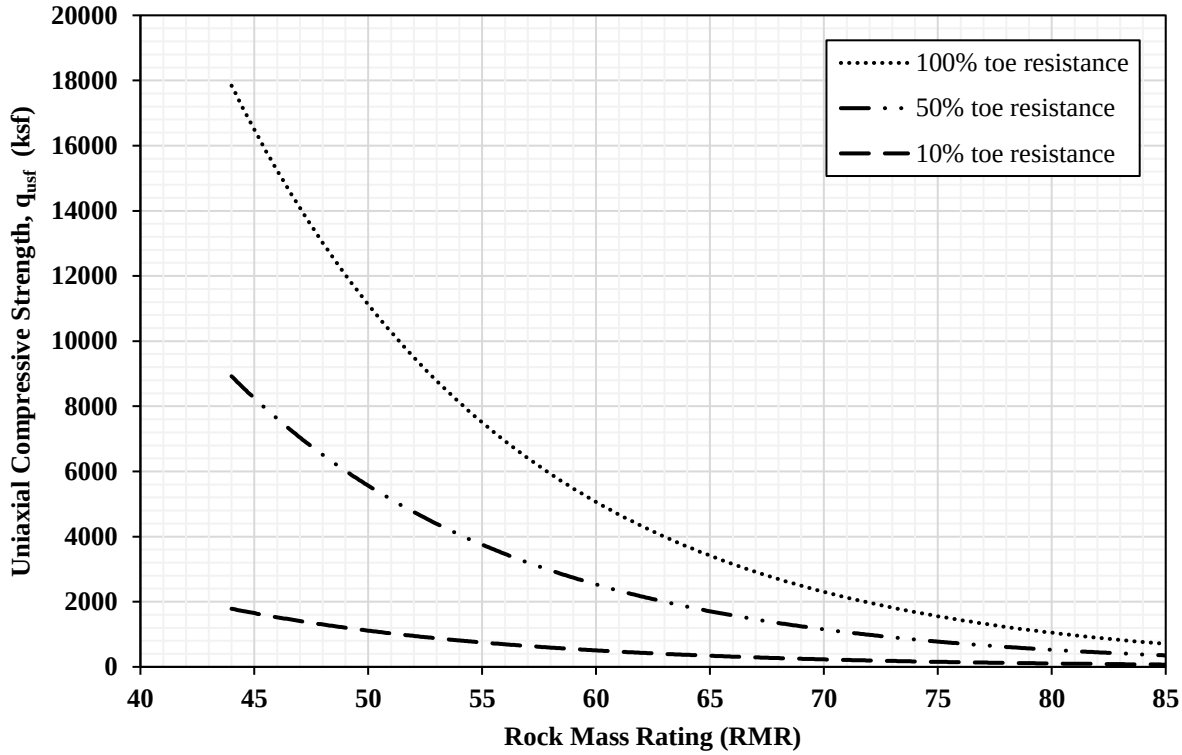

(a) Argillaceous Rocks

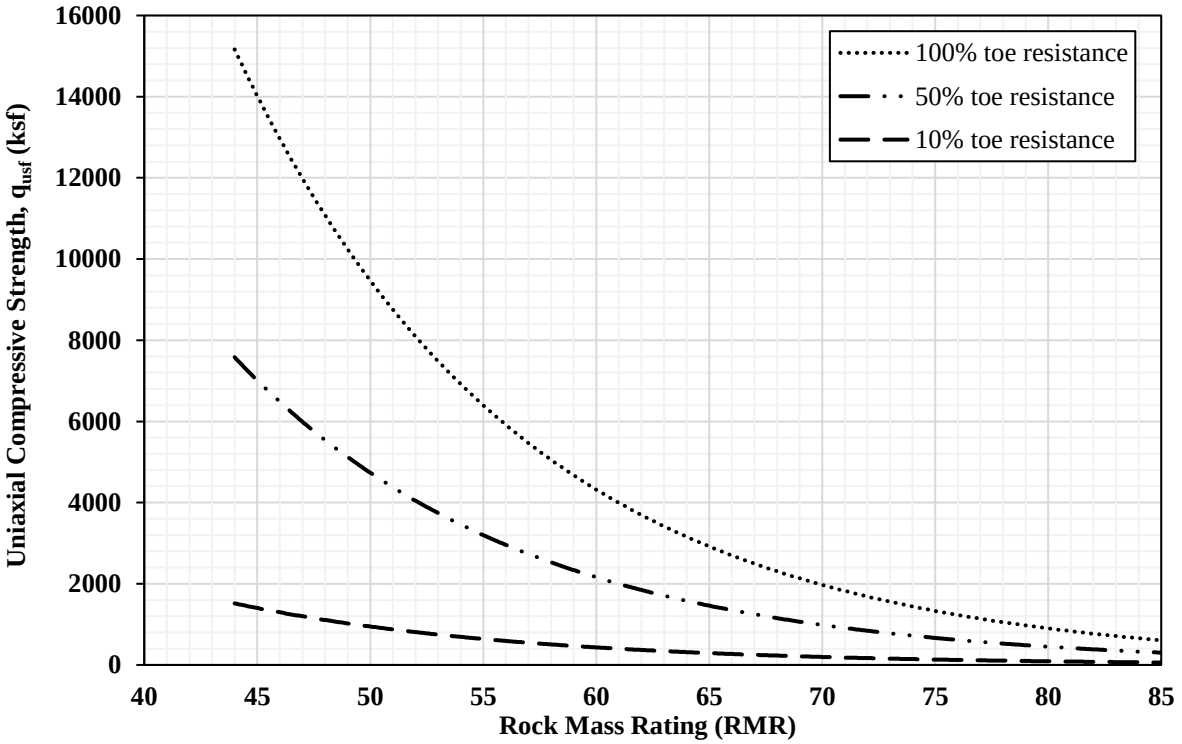

(b) Aranaceous Rocks

Source: Adhikari (2019)

Figure 64. Calculated q_{usf} values for Grade 50 HP14×73 pile for two rock types.

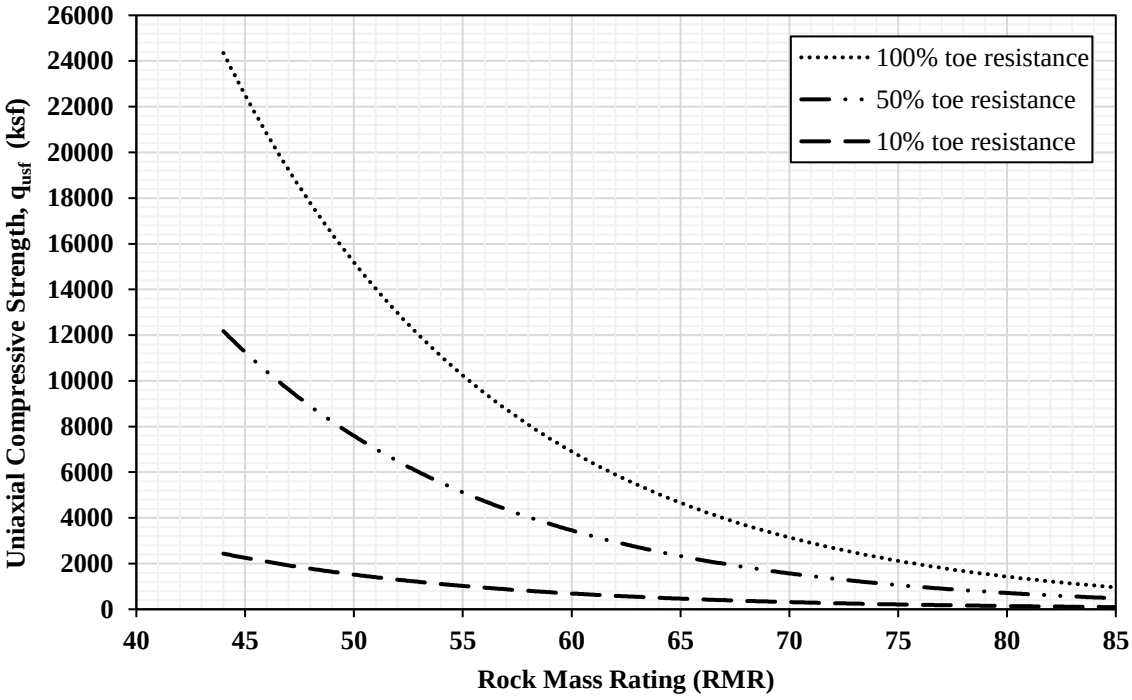

(a) Argillaceous Rocks

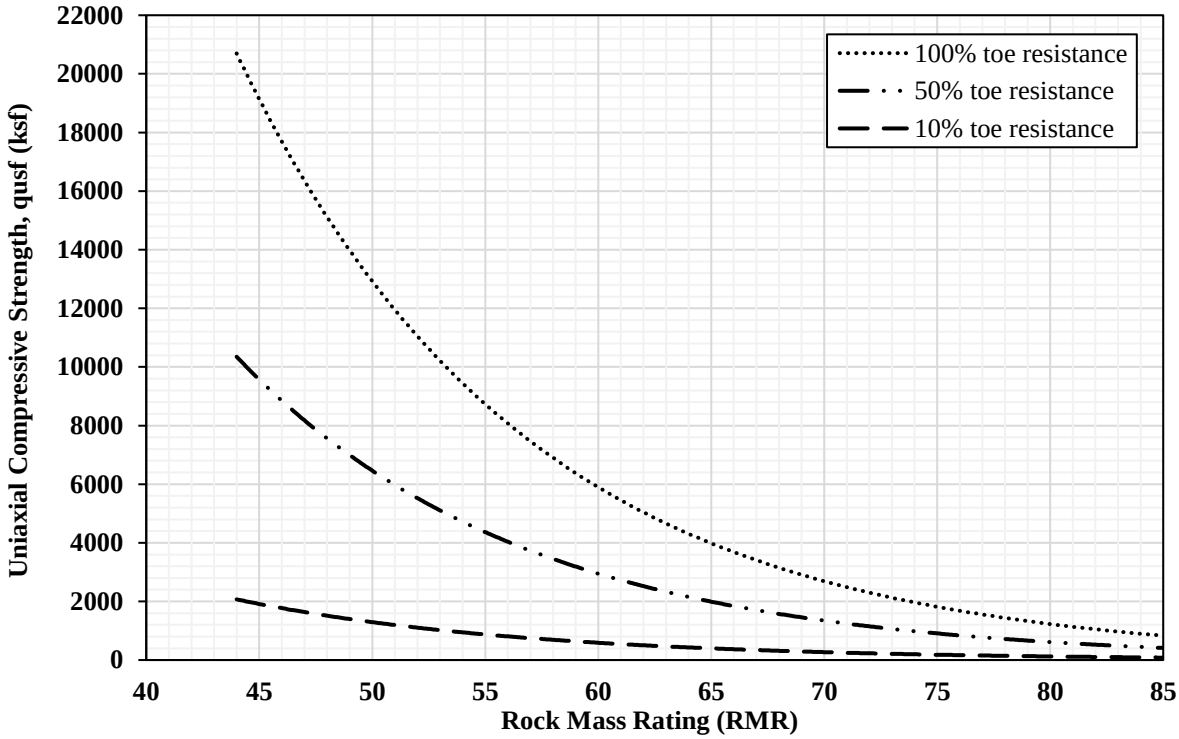

(b) Aranaceous Rocks

Source: Adhikari (2019)

Figure 65. Calculated q_{usf} values for Grade 50 HP12×74 pile for two rock types.

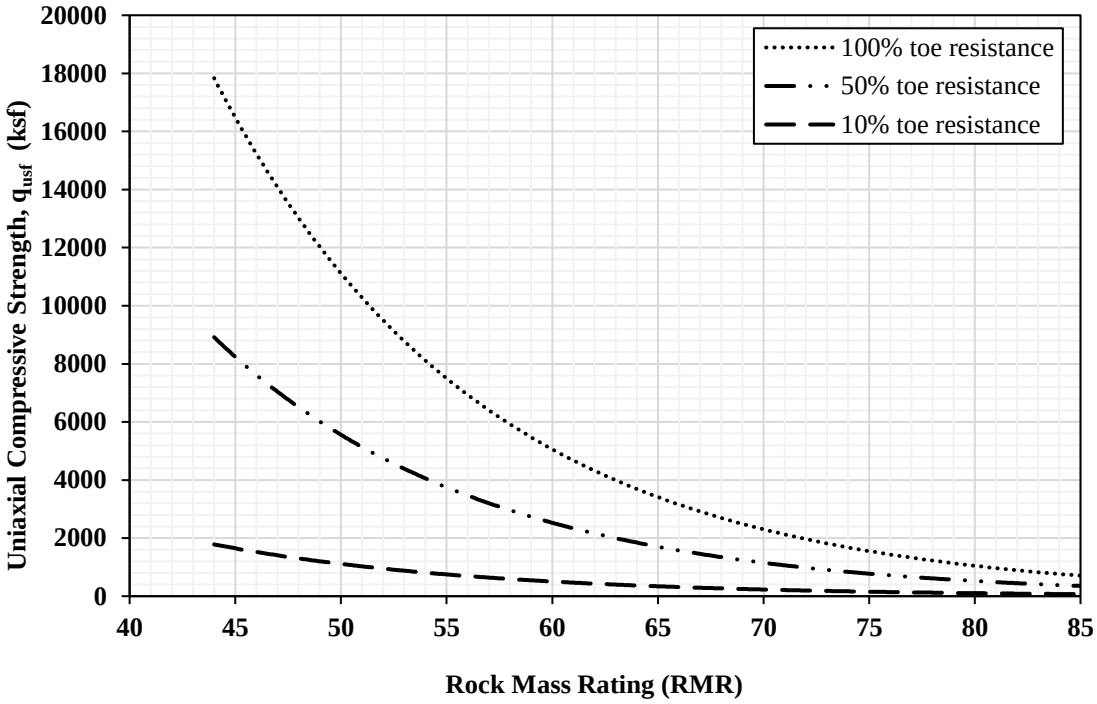

(a) Argillaceous Rocks

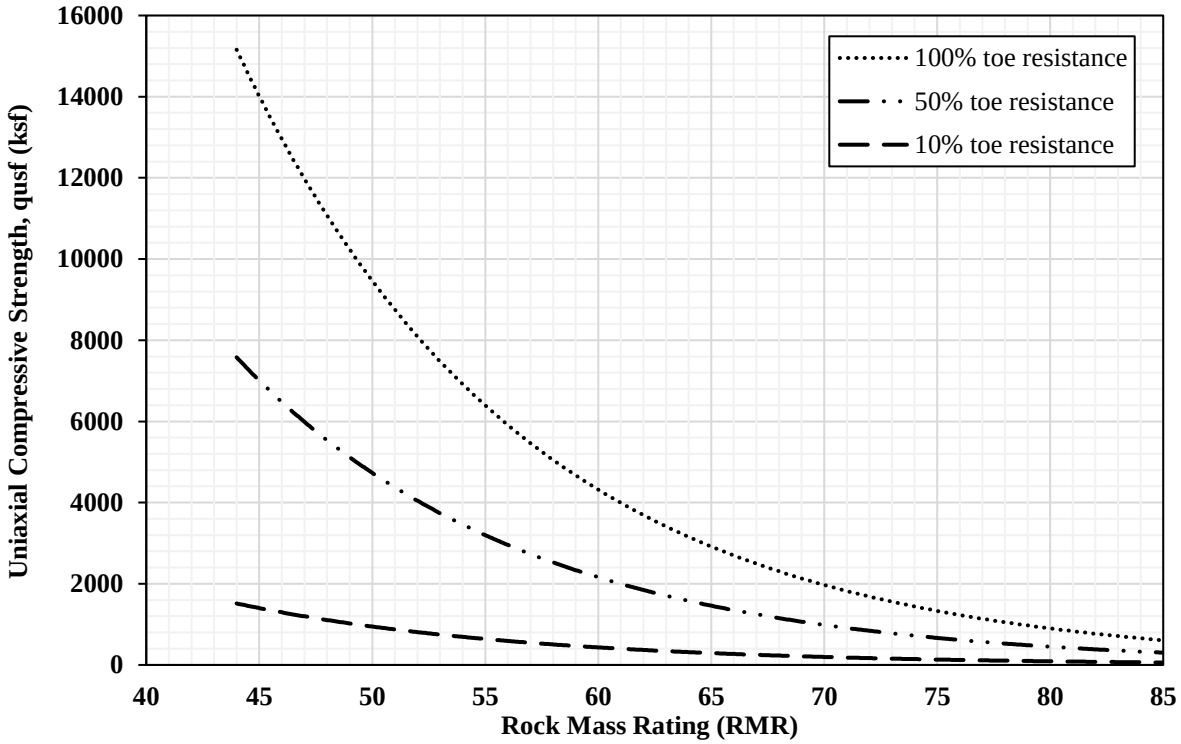

(b) Aranaceous Rocks

Source: Adhikari (2019)

Figure 66. Calculated q_{usf} values for Grade 50 HP12×53 pile for two rock types.

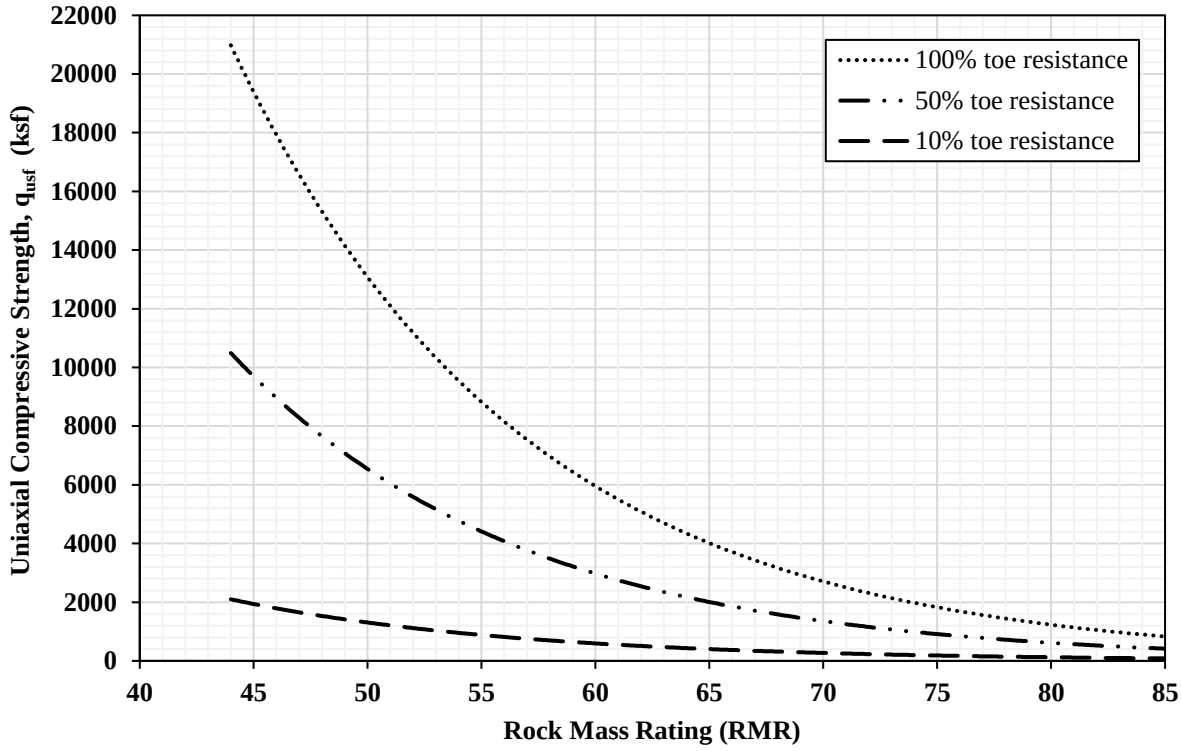

(a) Argillaceous Rocks

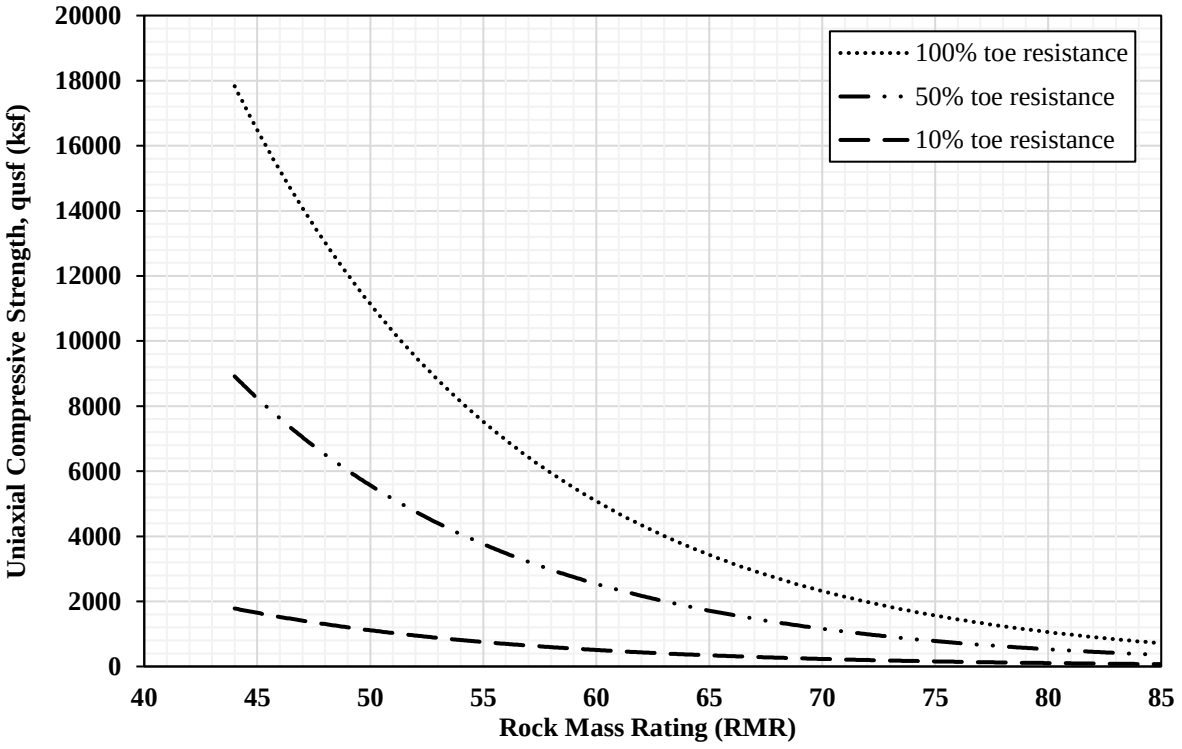

(b) Aranaceous Rocks

Source: Adhikari (2019)

Figure 67. Calculated q_{usf} values for Grade 50 HP10×42 pile for two rock types.

APPENDIX C. LRFD PILE DESIGN EXAMPLE

This appendix presents a LRFD pile design example to illustrate the application of the proposed geomaterial classification, the static analysis methods, and the construction control procedure using WEAP on a Grade 50, HP12×53 steel pile driven at the Abutment No. 1 (West) of bridge project located in Pine Bluff Parson Street, Laramie County, WY. The design example was divided into two parts: pile design using static analysis methods and pile construction control using WEAP. The design example was developed based only on axial load. Other governing factors, such as downdrag, scour and lateral load, should be considered when applicable. The factored load per pile was reported as 188 kips, and hence, the total factored load for the abutment consisting of five piles is 940 kips. The subsurface profile at the test pile location is shown in Figure 68. The properties of the four geomaterial layers are summarized in Table 55. Groundwater was not encountered during the geotechnical investigation.

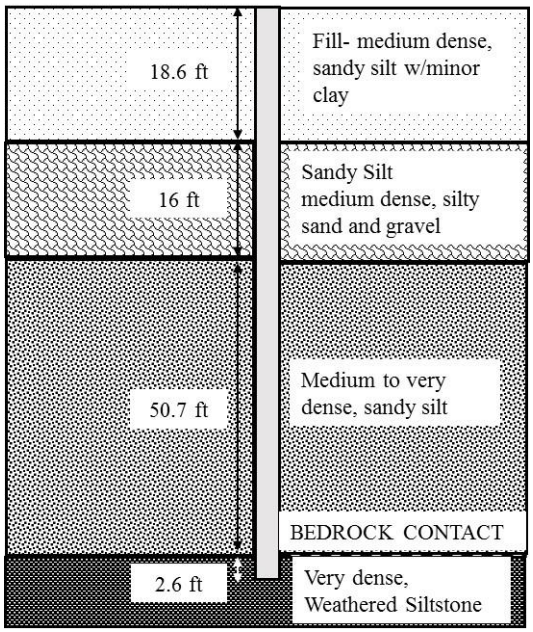

Figure 68. Subsurface profile at the test pile location of Pine Bluff Parson Street bridge project, Laramie County, WY.

Table 55. Properties of geomaterial layers at the test pile location.

Layer no.	Geomaterial description	Pile embed-ment (ft)	USCS classification	PI	Unit weight, γ (pcf)	$(N_1)_{60}$	s_u /[q_u] (ksf)	ϕ (°)	RQD
1	Fill-medium dense, sandy silt w/minor clay	18.6	ML	5	125	24	0.93	36.2	NA
2	Sandy silt, medium dense, silty sand and gravel	16	SC-SM	4	112	7	4.24	33.7	NA
3	Medium to very dense, sandy silt	50.7	ML	5	110	29	4.68	36.8	NA
4	Very dense, weathered siltstone	2.6	NA	NA	112	66	[45.2]	40	59%

s_u- undrained shear strength; ϕ- friction angle; q_u – uniaxial compressive strength; ML- Low plasticity silt; NA- Not available; SC-SM-Silty and clayey sand; $(N_1)_{60}$-Corrected SPT N-value; and RQD-Rock Quality Designation.

Pile Design Using Static Analysis Methods

The following eight steps are presented to illustrate the pile design process:

1) Classify the geomaterials in Step 1 as cohesive or cohesionless soils and/or IGMs in accordance to the proposed geomaterial classification flowchart presented in Figure 28.
2) Determine the nominal shaft resistance and end bearing following Steps 2 and 3 using static analysis methods recommended in Table 49.. Refer to Table 5 and respective subsections for existing static analysis methods. Refer to Table 51 for the calibrated static analysis methods.
3) Determine factored shaft resistance and end bearing in Steps 4 and 5 by multiplying the nominal shaft resistance and end bearing obtained in Steps 2 and 3 by the corresponding resistance factors of SA methods recommended in Table 49.Determine the total factored pile resistance in Step 6.
4) Verification of the IGM rock classification is conducted in Step 7.
5) Contract pile length and pile group size are determined in Step 8.

Geomaterial Classification (Step 1) (Refer Figure 28)

1) Based on the geomaterial description, the upper three layers are soil-based geomaterial, and the fourth layer is rock-based geomaterial.
2) Soil-based geomaterials are categorized as cohesionless or cohesive based on USCS classification. All the three soil-based layers are categorized as cohesive geomaterials for static analysis. Though the classification system developed did not include SC-SM for layer 2, it is classified as cohesive as both the low plasticity silts, ML and clayey silty sand, SC-SM, have nearly the same plasticity indices.
3) Layer 1 is classified as soil since the undrained shear strength is less than 2.7 ksf. Layers 2 and 3 are classified as IGM-soil as their undrained shear strengths are greater than 2.7 ksf.
4) For rock-based geomaterial in layer 4, the modified RMR is calculated as illustrated in Table 56 using the lab measured uniaxial compressive strength and observed RQD along with maximum ratings for the remaining three parameters. (Refer Section 8.3, No. 4)

Table 56. Determination of RMR value for geomaterial classification purpose.

Parameter	Parameter value	Relative rating
Uniaxial compressive strength	45.2 ksf	0
RQD	59%	13
Spacing of joints	NA	30*
Condition of joints	NA	25*
Ground water conditions	NA	10*
RMR (Uncorrected)		78

NA- Not available; *- maximum ratings considered.

5) Since RMR obtained from Table 56 is less than 85, the q_{usf} is determined using Figure 66(a) for siltstone considered as an argillaceous rock. The q_{usf} values range from 200 ksf to 1200 ksf for percentage toe resistances ranging from 10 percent to 100 percent. Based on the 25 historical piles driven in IGMs in Wyoming, the percentage of end bearing ranges from 16 percent to 83 percent with an average of 52 percent. Considering a lower percent end bearing would result in a more conservative q_{usf} value and since the measured uniaxial compressive strength of 45.2 ksf is lesser than the lower q_{usf} of 200 ksf, the siltstone (layer 4) is reasonably assumed as IGM-rock. On the other hand, the percent end bearing can be estimated using Equation (35) and the calculation is shown as follows:

$((N_1)'_{60}) = (18.6 \text{ ft} \times 24 + 16 \text{ ft} \times 7 + 50.7 \text{ ft} \times 29 + 2.6 \text{ ft} \times 66)/(87.9 \text{ ft}) = 25$
Percentage end bearing = $13.61 - 0.004 \text{ (pile length)}^2 + 12.80 \ln ((N_1)'_{60})$
Percentage end bearing = $13.61 - 0.004 (87.9 \text{ ft})^2 + 12.80 \ln (25)$
Percentage end bearing = 24%

For 24 percent end bearing and RMR of 78, the q_{usf} determined from Figure 66(a) exceeds the q_u of 45.2 ksf. On the other hand, the q_{usf} can be calculated using equations discussed in Section 4.5 as shown in the following calculations:

$P_e = \frac{\pi^2 E}{\left(\frac{KL}{r_s}\right)^2} A_g = \frac{\pi^2 \times 29000 \text{ ksi}}{\left(\frac{1.2 \times 0.008 \times 12 \text{ in}}{2.86 \text{ in}}\right)^2} 21.8 \text{ in}^2 \approx$ very large

$P_o = QF_yA_g = 1 \times 50 \text{ ksi} \times 21.8 \text{ in}^2 = 1{,}090$ kips

As P_e is very large, $\frac{P_e}{P_o} \geq 0.44$

$P_n = \left[0.658^{\left(\frac{P_o}{P_e}\right)}\right] P_o \approx P_o$ [As, $0.658^{\left(\frac{P_o}{P_e}\right)} \approx 1$]

$P_n = 1{,}090$ kips

For RMR 78 and argillaceous rocks,
m = 2; s ≈ 0 (from Hoek and Brown 1988)
Using Equation (33),

$$q_{usf} = \frac{\text{percent toe resistance} \times P_n \times 0.6}{\left[\sqrt{s} + \sqrt{(m\sqrt{s}+s)}\right] \times 0.5 \times \text{Box toe area}} = \frac{0.24 \times 1090 \times 0.6}{\left[\sqrt{0} + \sqrt{(2\sqrt{0}+0)}\right] \times 0.5 \times 0.98} = 320.33 \text{ ksf}$$

Hence, siltstone can be reasonably classified as IGM-rock. The verification of the IGM-rock material can be performed in Step 7.

Determination of nominal shaft resistance (Step 2)

For Layer 1:

For cohesive soil, existing α-method given by Equation (2) is used. For S_u of 0.93 ksf and steel H-pile, α value of 0.8 can be approximated from Figure 1. The unit shaft resistance and nominal shaft resistance of layer 1 are determined as follows:

$q_{s1} = \alpha \times S_u = 0.8 \times 0.93 = 0.74$ ksf

$R_{s1} = q_{s1} \times 2 \times$ (flange width + web depth) × pile embedment = 0.74 ksf × 2 × ((11.80 in + 12 in)/12 in per foot) × 18.6 ft

$R_{s1} = 54.60$ kips

For Layer 2:

For cohesive IGM-soil, calibrated α-method is used (Table 49 and Table 51). The calibrated α-coefficient is calculated as

$$\hat{\alpha} = 0.29 s_u^{\,2} - 2.71 s_u + 6.51$$

$\hat{\alpha} = 0.29\ (4.24\ \text{ksf})^2 - 2.71\ (4.24\ \text{ksf}) + 6.51 = 0.27$

The unit shaft resistance is calculated as

$q_{s2} = \hat{\alpha} \times s_u = 0.27 \times 4.24$ ksf $= 1.15$ ksf

The nominal shaft resistance is calculated as

$R_{s2} = q_s \times 2 \times$ (flange width + web depth) × pile embedment = 1.15 × 2 × ((11.80 in + 12 in)/12 in per foot) × 16 ft

$R_{s2} = 72.99$ kips

For Layer 3:

For cohesive IGM-soil, calibrated α-method is used (Table 49 and Table 51). The calibrated α-coefficient is calculated as

$$\hat{\alpha} = 0.29 s_u^{\,2} - 2.71 s_u + 6.51$$

$\hat{\alpha} = 0.29\ (4.68\ \text{ksf})^2 - 2.71\ (4.68\ \text{ksf}) + 6.51 = 0.23$

The unit shaft resistance is calculated as

$q_{s3} = \hat{\alpha} \times s_u = 0.23 \times 4.68 = 1.05$ ksf

The nominal shaft resistance is calculated as

$R_{s3} = q_s \times 2 \times$ (flange width + web depth) × pile embedment = 1.05 ksf × 2 × ((11.80 in + 12 in)/12 in per foot) × 50.7 ft

$R_{s3} = 211.17$ kips

For Layer 4:

For cohesive IGM-rock, calibrated α-method is used (Table 49 and Table 51). The calibrated α-coefficient is calculated as

$$\hat{\alpha} = \frac{64.63 \times q_u^{-0.66}}{100}$$

$$\hat{\alpha} = \frac{64.63 \times 45.2\text{ksf}^{-0.66}}{100} = 0.053$$

The unit shaft resistance is calculated as

$q_{s4} = \hat{\alpha} \times q_u = 0.053 \times 45.2$ ksf $= 2.40$ ksf

The nominal shaft resistance is calculated as
$R_{s4} = q_s \times 2 \times$ (flange width + web depth) $\times$ pile embedment = 2.40 ksf $\times 2 \times$ ((11.80 in + 12 in)/12 in per foot) $\times$ 2.6 ft
R_{s4} = 24.75 kips

Determination of nominal end bearing (Step 3)
For Layer 4:
For cohesive IGM-rock, calibrated α-method is used (Table 49 and Table 51). The calibrated end bearing factor is calculated as
$\widehat{N_c} = 39.8 \times q_u^{-0.64}$
$\widehat{N_c} = 39.8 \times 45.2\text{ksf}^{-0.64} = 3.54$
The unit end bearing is calculated as
$q_p = \widehat{N_c} \times q_u$ = 3.54 × 45.2 ksf = 160 ksf
$R_p = q_p \times$ (flange width × web depth) = 160 ksf × (11.80 in × 12 in)/144 in^2 per ft^2) = 157.33 kips

Determination of factored shaft resistance (Step 4)
The summation of all factored shaft resistance along the pile embedded length is given by
$\varphi R_s = \varphi_1 R_{s1} + \varphi_2 R_{s2} + \varphi_3 R_{s3} + \varphi_4 R_{s4}$
where, φ_1, φ_2, φ_3, and φ_4 are the resistance factors corresponding to the static analysis methods used. For a redundant pile group with a target reliability index (β_T) of 2.33, the resistance factor φ_1 of 0.35 for the existing α-method for the cohesive soil is obtained from the AASHTO LRFD Bridge Design Specifications (2017). The resistance factors φ_2, φ_3, and φ_4 are taken from . for IGMs based on a redundant pile group.
φR_s = (0.35 × 54.60 kips) + (0.5 × 72.99 kips) + (0.5 × 211.17 kips) + (0.35 × 24.75 kips)
φR_s = 169.85 kips

Determination of factored end bearing (Step 5)
The factored end bearing is calculated by multiplying the resistance factor obtained from Table 49 with the nominal end bearing determined from Step 3.
$\varphi R_p = 0.30 \times 157.29$ kips = 47.19 kips

The percent end bearing is calculated based on factored resistances as
Percent end bearing = $\frac{\varphi R_p}{\varphi R_p + \varphi R_s} \times 100\% = \frac{47.19\text{ kips}}{47.19\text{ kips} + 169.85\text{ kips}} \times 100\%$ = 22%

Determination of total factored pile resistance (Step 6)
Total factored pile resistance = $\varphi R_s + \varphi R_p$ = 169.85 kips + 47.19 kips = 217 kips

The estimated factored pile resistance is close to the factored CAPWAP resistance of 201.37 kips at the end of driving. This is only for a demonstration of the proposed LRFD design procedure since PDA/CAPWAP will not be available during the design state.

Important Note: All resistance factors are selected based on a target reliability index of 2.33 for a redundant pile group (pile size equals or greater 4). However, the factored resistances should be recalculated using the resistance factors corresponding to the target reliability index of 3.00 if a non-redundant pile group is recommended in Step 8.

Verification of bearing layer geomaterial classification (Step 7)
For 22 percent end bearing and RMR of 78, the q_{usf} determined from Figure 66(a) again exceeds the q_u of 45.2 ksf. Hence, siltstone is reasonably classified as IGM-rock. On the other hand the q_{usf} can be calculated as shown in Step 1 following the procedure presented in Section 4.5.

Determination of contract pile length and pile group (Step 8)
According to WYDOT practice, the depth of a pile driven into the IGM bearing layer can be determined from a drivepoint result (typically a pile refusal depth is estimated at 100 drivepoint blows per one inch penetration). The embedded pile length is determined to be 87.9 ft. The pile length including an assumed 2 ft embedment in the footing and a 1 ft allowance for cutoff due to driving damage is estimated as

Pile length = 87.9 + 2 + 1 = 90.9 ft

If the length for steel H-piles is specified in 5 ft increments, the contract pile length of 95 ft is recommended.
The pile size of the Abutment No. 1 can be determined as

$$\text{Pile size} = \frac{\text{Total Factored Load per Abutment or Pier}}{\text{Total Factored Resistance per Pile from}} = \frac{940 \text{ kips}}{217 \text{ kips}} = 4.33 \approx 5$$

Hence, five piles are needed at the Abutment No. 1 to satisfy the LRFD strength limit state. Since, this is a redundant pile group, the resistance factors used in the calculation of the factored pile resistance in Steps 4, 5 and 6 are adequate. If a redundant pile group is resulted from this calculation, the factored pile resistance calculation has to be revised accordingly.

Pile Construction Control Using WEAP
After the bridge contract is let and prior to start of pile driving, the contractor should provide the pile hammer information for the construction control consideration using WEAP. The pile hammer information should include the cap (helmet) number and hammer identification information with details, hammer cushion, and pile cushion (where required), as well as pile size, pile length, and estimated pile driving resistance.

For this design example, the hammer was Delmag D 16-32 with a hammer cushion thickness of 6 in, helmet weight of 3.08 kips, and area of 416 in^2. The analysis was carried by fixing the observed stroke of 7.5 ft. The geomaterials input into the WEAP is described in the next section. Since same resistance factors were recommended for both Cases 1 and II described in Section 6.3, the WEAP analysis was performed using the default toe quake value generated by WEAP, which is the proposed Case I procedure.

Geomaterial Input in WEAP

1) As the $(N_1)_{60}$ values of the upper three layers are less than 60, the $(N_1)_{60}$ values and unit weights summarized in Table 55 are used. The geomaterials are input as cohesionless silt as they have low plasticity indices.
2) As the $(N_1)_{60}$ value of the siltstone is greater than the maximum allowed 60, friction angle and unit weights summarized in Table 55 are used. The siltstone was modelled as cohesionless silt.

3) Since groundwater table was not encountered during the geotechnical investigation, it is assumed to be 100 ft which is deeper than the pile tip.
4) The geomaterial profile input for the static analysis is shown in Figure 69.

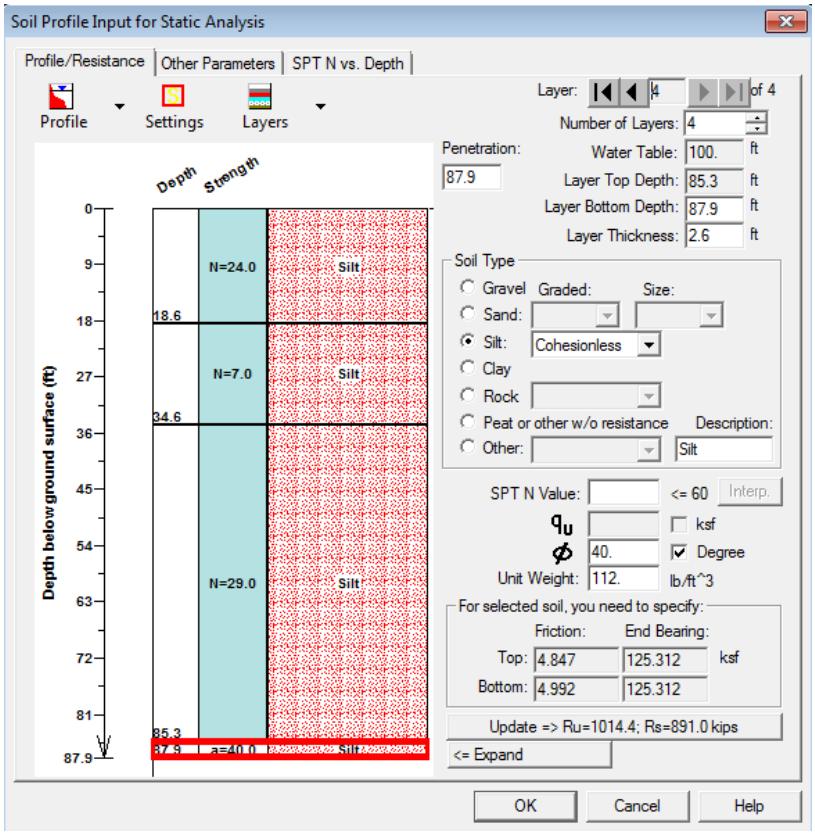

Figure 69. Screenshot of soil profile input screen for static analysis in GRLWEAP 2010.

Driveability Analysis

After the geomaterial input, drivability analysis is performed to determine the percentage shaft resistance and the adequacy of the proposed pile hammer. Figure 70 shows the output from the driveability analysis. The result indicates that the pile driving refusal at 120 blows per foot will occur at about 42 ft of the pile penetration. The analysis suggests that the hammer may not have sufficient energy to drive the pile through the IGM layers.

Bearing Graph Analysis

The determined percentage shaft resistance is used in the bearing graph analysis. The outputs from the bearing graph analysis are shown in Figure 71 and Figure 72.

AASHTO LRFD Bridge Design Specifications (2017)

Considering the current resistance factor of 0.5 for WEAP recommended in the AASHTO LRFD Bridge Design Specifications (2017), the target nominal pile driving resistance is $R_{driving\text{-}target}$ = 188/0.5 = 376 kips

Interpolating from Figure 72, target blow counts required for the target nominal pile driving resistance of 376 kips is 251 blows per foot which greatly exceeds the pile refusal blow count of 120 blows per foot. This outcome aligned with that from the driveability analysis at which pile refusal or hard driving is expected during construction.

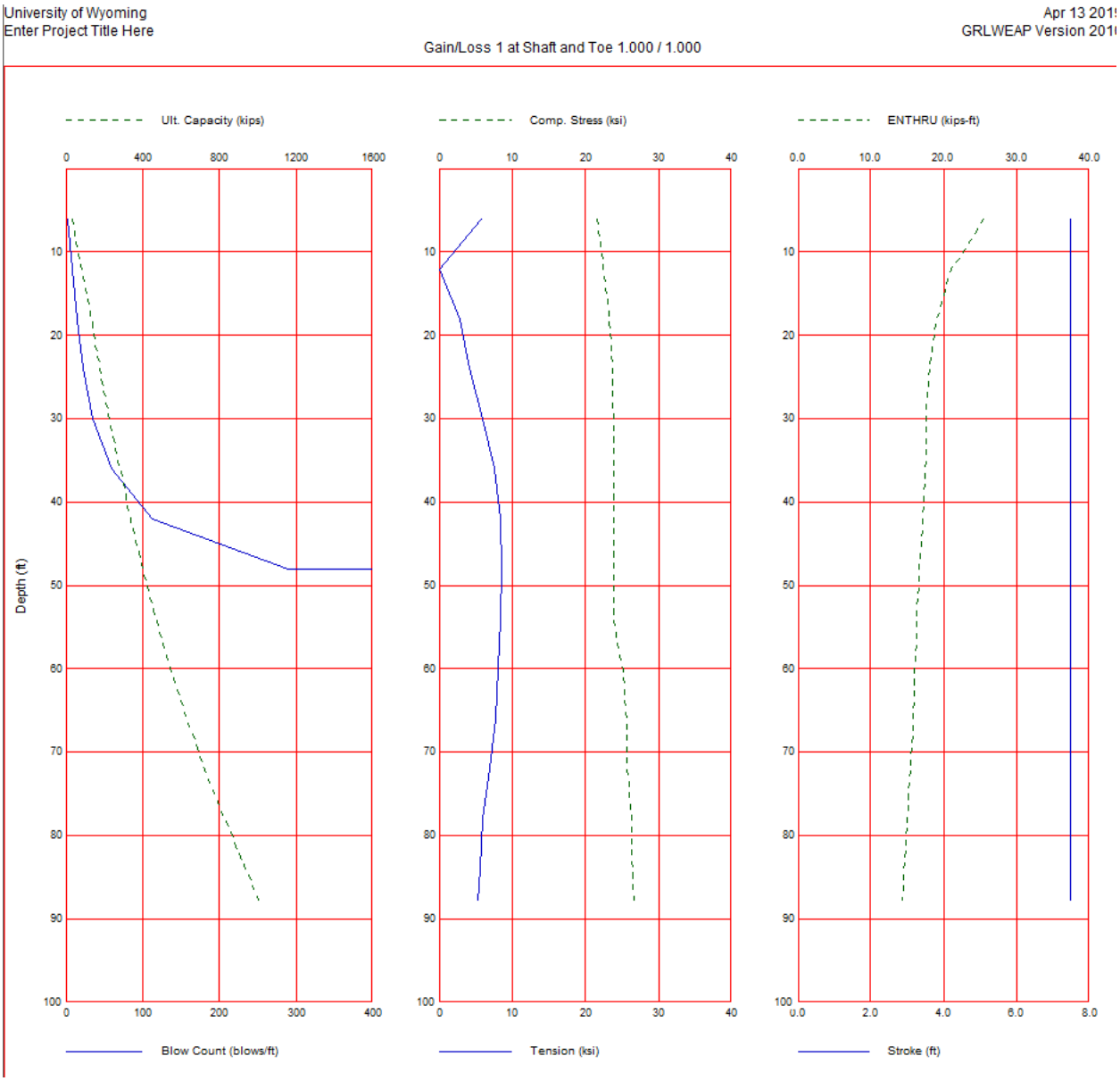

Figure 70. Driveability analysis output from GRLWEAP 2010.

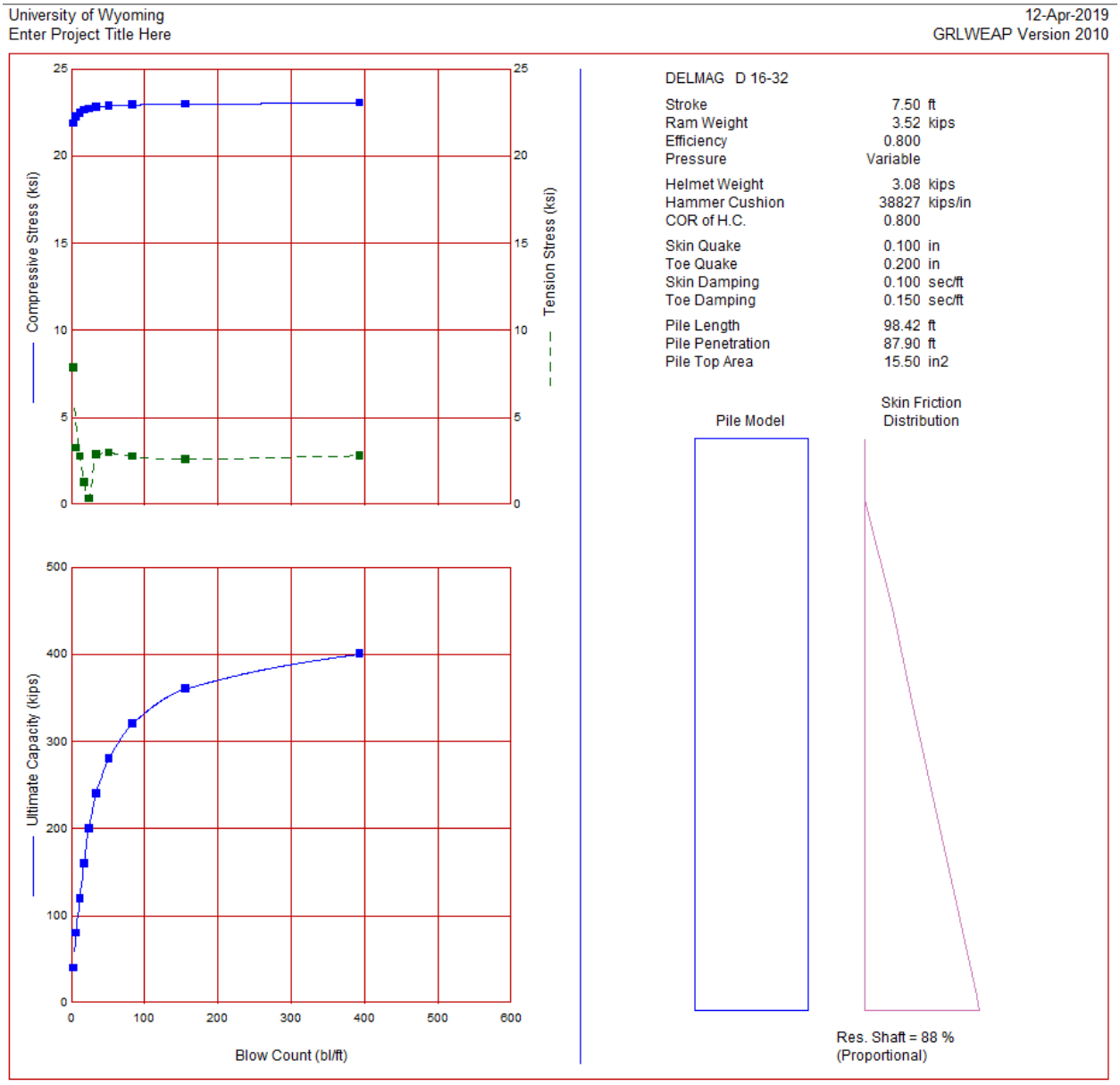

Figure 71. Bearing graph output from GRLWEAP 2010.

University of Wyoming 12-Apr-2019
Enter Project Title Here GRLWEAP Version 2010

Ultimate Capacity kips	Maximum Compression Stress ksi	Maximum Tension Stress ksi	Blow Count bl/ft	Stroke ft	Energy kips-ft
40.0	21.86	7.86	2.9	7.50	24.74
80.0	22.24	3.25	6.9	7.50	20.66
120.0	22.45	2.75	12.4	7.50	18.59
160.0	22.61	1.28	17.7	7.50	17.14
200.0	22.69	0.35	24.3	7.50	16.52
240.0	22.77	2.88	34.4	7.50	16.09
280.0	22.86	2.98	51.4	7.50	15.85
320.0	22.91	2.77	83.9	7.50	15.68
360.0	22.97	2.60	156.1	7.50	15.54
400.0	23.02	2.81	393.3	7.50	15.50

Figure 72. Bearing graph output in tabular form from GRLWEAP 2010.

LRFD Recommendations from this Research

Considering the resistance factor of 0.6 for WEAP (Case I) recommended in this study, the target nominal pile driving resistance is

$R_{driving\text{-}target}$ = 188/0.6 = 313.33 kips

Interpolating from Figure 72, target blow counts required for the target nominal pile driving resistance of 313.33 kips is 79 blows per foot. The estimated hammer blow count of 79 is relatively lower than the actual blow count of 164 bpf observed at the end of driving during the construction. This is just an illustration how the recommendation obtained from this research study improves the construction control process.

Inspector Chart Analysis

Since stroke height of the single acting diesel hammer will vary during construction, an inspector chart analysis can be performed for the target nominal pile driving resistance (e.g. 341.8 kips based on the LRFD recommendation from the research). Figure 73 shows the output of the inspector chart that relates the hammer stroke height to the hammer blow count. The result indicates a minimum hammer stroke height of 7.5 ft is needed to avoid a pile refusal.

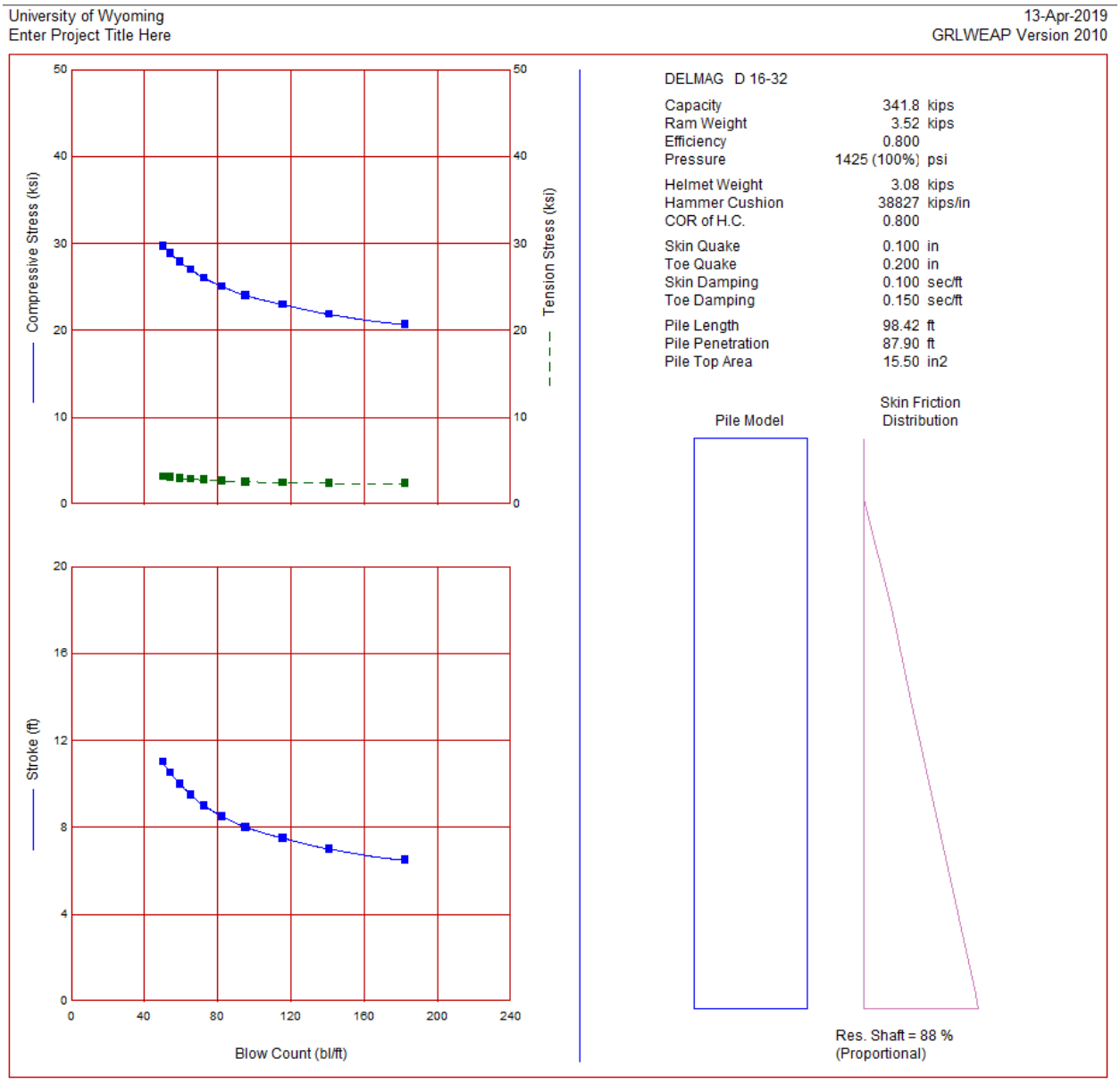

Figure 73. Inspector chart output from GRLWEAP 2010.